Dissertation zur Erlangung des Doktorgrades

der Fakultät für Chemie und Pharmazie

der Ludwig-Maximilians-Universität München

Phosphorus Nitrides at Extreme Conditions

Sebastian Vogel

aus

Lindenfels, Deutschland

2019

Erklärung

Diese Dissertation wurde im Sinne von § 7 der Promotionsordnung vom 28. November 2011 von Herrn Prof. Dr. Wolfgang Schnick betreut.

Eidesstattliche Versicherung

Diese Dissertation wurde eigenständig und ohne unerlaubte Hilfe erarbeitet.

München, den 06.01.2020

.....

Sebastian Vogel

Dissertation eingereicht am:	22.10.2019
1. Gutachter:	Prof. Dr. Wolfgang Schnick
2. Gutachter:	Prof. Dr. Hubert Huppertz
Mündliche Prüfung am:	16.12.2019

Für meine Familie.

Viele verfolgen hartnäckig den Weg, den sie gewählt haben,

aber nur wenige das Ziel.

Friedrich W. Nietzsche

Danksagung

Ich danke Herrn Prof. Dr. Wolfgang Schnick herzlichst für die Betreuung meiner Dissertation sowie für die zahlreichen Ratschläge, Hilfestellungen und Fachgespräche während meiner Zeit in seinem Arbeitskreis. Zudem bedanke ich mich für die bereitgestellten Mittel und für die freie Themenwahl, welche mich zur Anfertigung dieser Arbeit motiviert hat.

Herrn Prof. Dr. Hubert Huppertz danke ich ganz herzlich für die Übernahme des Koreferats dieser Arbeit.

Ferner bedanke ich mich bei Prof. Dr. Leonid Dubrovinsky, Prof. Dr. Konstantin Karaghiosoff, PD Dr. Constantin Hoch und Prof. Dr. Hans-Christian Böttcher für ihre Bereitschaft als Mitglieder der Prüfungskommission meiner mündlichen Prüfung zur Verfügung zu stehen.

Frau Dr. Stefanie Kiefer danke ich an dieser Stelle stellvertretend für den Verband der Chemischen Industrie e.V. für die Verleihung eines Promotionsstipendiums durch den Fonds der Chemischen Industrie e.V sowie für die Betreuung während meiner Zeit als Stipendiat.

Mein besonderer Dank gilt meinen Vorgängern Dr. Dominik Baumann und Dr. Alexey Marchuk. Bei Dominik Baumann bedanke ich mich für die soliden Vorarbeiten und die erfolgreiche Kooperation im Rahmen des PON-Projekts. Alexey Marchuk danke ich ganz herzlich für die ausführliche Einarbeitung zu Beginn meiner Zeit im Arbeitskreis Schnick. Seine Einführungen zur Hochdruckpresse und Röntgenstrukturanalyse sowie Inspirationen zur Themenfindung haben die Grundlage für alle meine weiteren Arbeiten gelegt. In diesem Kontext möchte ich auch Dr. Simon Kloß ganz besonders dafür danken, dass er stets sein Wissen und seine Erfahrung mit mir geteilt hat und durch viele inspirierende Diskussionen zum Entstehen dieser Arbeit beigetragen hat. Bei PD Dr. Constantin Hoch bedanke ich mich herzlich für die stets offene Tür sowie für die zahlreichen fachlichen Gespräche und Hilfestellungen.

Vielen herzlichen Dank an alle meine internen, wie externen Kooperationspartner, welche mich in verschieden thematischen Bereichen mit ihrer fachlichen Expertise unterstützt haben. So danke ich Prof.

Dr. Oliver Oeckler, Dr. Lukas Neudert und Dr. Robin Niklaus für die Unterstützung im Rahmen des PON-Projekts und darüber hinaus.

My special thanks go to Prof. Dr. Natalia Dubrovinskaia, Prof. Dr. Leonid Dubrovinsky, Dr. Elena Bykova, and Dr. Maxim Bykov for the fruitful collaboration over the course of my PhD. I am very grateful that Natalia Dubrovinskaia and Leonid Dubrovinsky welcomed me as a trainee in high-pressure sciences and shared their resources and time with me during my stays at the BGI Bayreuth. Here, I further thank Dr. Irina Chuvashova, Dr. Alexander Kurnosov, Dr. Stella Chariton, Egor Koemets, and Timofey Fedotenko for their local support during the preparations of diamond anvil cells. I give all my thanks to Leonid Dubrovinsky, Natalia Dubrovinskaia, Elena Bykova, and Maxim Bykov for sharing their expertise and knowledge with me and supporting my projects prior, during, and after beamtimes at the ESRF and DESY facility. It was a real pleasure to learn from you and to work with you. This thesis is greatly enhanced by the results of this productive cooperation, which I really appreciate. Furthermore, I thank Dr. Anna Pakhomova and Dr. Volodimyr Svitlyk for their local support at the DESY and ESRF facility, respectively.

Mein herzlicher Dank gilt zudem Dr. Christina Schneider für die angenehme und inspirierende Zusammenarbeit im Fachgebiet der Präbiotik. Diese Kooperation hat mir einen interessanten Blick über den Tellerrand hinaus ermöglicht und war eine willkommene Abwechslung zum heat-and-beat der Festkörperchemie.

Meinen Praktikanten Sebastian Ambach, Amalina Buda und Christoph Gross danke ich für ihre Unterstützung bei meinen Forschungsprojekten sowie für ihre Neugierde an der Festkörperchemie.

Meinen Arbeitskollegen aus dem Labor D2.110 und dessen Umfeld möchte ich ganz herzlich für die angenehme Atmosphäre in den vergangenen Jahren danken. Danke, dass statt Konkurrenz und Wettbewerb stets die Zusammenarbeit und das gemeinsame Lösen von Problemen im Vordergrund standen. Mein besonderer Dank gilt diesbezüglich Dr. Simon Kloß, Dr. Matthias Wörsching, Dr. Christian Maak, Dr. Eva Bertschler, Dr. Philipp Bielec, Dr. Frank Tambornino, Sebastian Wendl, Mathias Mallmann, Tobias Giftthaler und Stefanie Schneider. Danke für die vielen inspirierenden sowie amüsanten Gespräche im Labor, während den gemeinsamen Kaffeepausen sowie an unseren Laborabenden. Ich freue mich zudem

sehr darüber, dass mit Sebastian Ambach und Reinhard Pritzl bereits ambitionierte Doktoranden in den Startlöchern stehen, um das P/N-Thema weiterzuführen.

Bei Dr. Thomas Bräuniger, Otto Zeman und Christian Minke bedanke ich mich sehr für die Durchführung zahlreicher NMR-Experimente und für die anschließende gemeinsame Diskussion der Ergebnisse. Dr. Christian Maak, Christian Minke und Lisa Gamperl danke ich ferner für die vielen REM- und EDX-Untersuchungen im Rahmen dieser Arbeit. Für die Aufnahme von Einkristalldatensätzen bedanke ich mich bei Dr. Peter Mayer und Daniel Beck. Frau Sokol und Dr. Fabian Keßler gilt ferner mein Dank für die Aufnahme von FTIR-Spektren. Für das Bereitstellen einer funktionierenden Infrastruktur sowie für die Hilfestellungen bei zahlreichen organisatorischen Angelegenheiten bedanke ich mich besonders bei Olga Lorentz, Wolfgang Wünschheim, Dr. Dieter Rau und Thomas Miller. Schließlich danke ich allen Kollegen aus den Arbeitskreisen Schnick, Johrendt und Lotsch für das angenehme und kollegiale Arbeitsklima im 2. OG von Haus D.

Während meiner Zeit als Student und Doktorand durfte ich mich nicht nur fachlich sondern auch persönlich weiterentwickeln. Dafür bedanke ich mich herzlich bei meinen engsten Freunden in München und im Odenwald, die mich während dieser Zeit unterstützt haben.

Noch wichtiger als gute Freunde ist eine gesunde und glückliche Familie, bei der ich mich abschließend ganz herzlich bedanke. Vielen Dank Melanie, dass du deine Begeisterung für die Wissenschaft und die Forschung in vielen inspirierenden Gesprächen mit mir geteilt hast. Du bist mir privat wie beruflich immer ein Vorbild. Bei meinen Großeltern Toni und Sebastian sowie Herta und Peter bedanke ich mich herzlich für ihre Unterstützung und ihr stetiges Interesse an meinem Werdegang. Danke, dass ihr immer an mich denkt und glaubt. Bei dir Alice bedanke ich mich ganz herzlich für die vielen schönen Stunden, die wir gemeinsam im Odenwald, in München und ganz besonders auf unseren Reisen rund um die Welt verbringen. Danke, dass du auch in stressigen Zeiten immer für mich da bist, mir stets den Rücken stärkst und mich bedingungslos liebst. Mama und Papa, bei euch kann ich mich gar nicht genug bedanken. Vielen herzlichen Dank, dass ich mich in jeder Lebenslage auf euch verlassen kann und dass ihr mich auf meinem Lebensweg immer uneingeschränkt unterstützt. Ihr habt mich zu dem gemacht, der ich heute bin und dafür werde ich euch immer dankbar sein.

Sebastian Vogel

Table of Contents

United in nitride: Unprecedented boron phosphorus nitride BP_3N_6 with entire fourfold coordination of B and P blends structural motifs of both, α-P_3N_5 and c-BN. It was prepared from reactive precursors in a one-step high-pressure high-temperature reaction, demonstrating an innovative access to mixed non-metal nitrides.

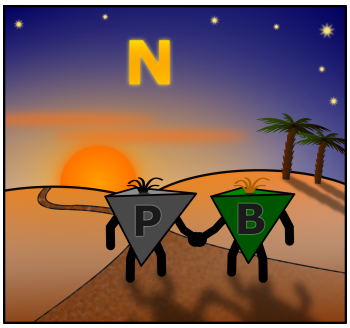

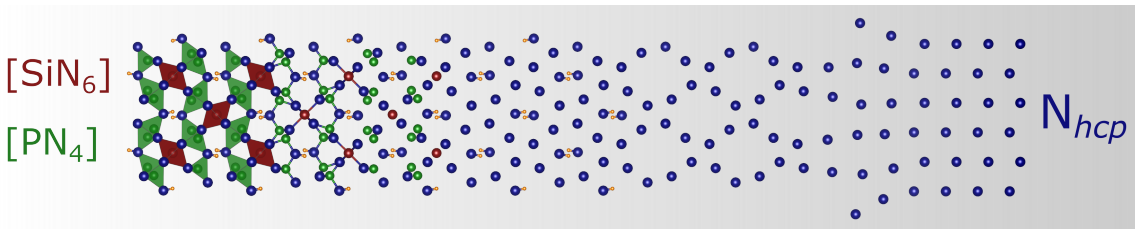

Under pressure: The silicon phosphorus nitride imide SiP_2N_4NH was synthesized in a high-pressure high-temperature reaction, using HCl as a mineralizer. Its highly condensed structure is built up from SiN_6 octahedra and PN_4 tetrahedra and can be derived from a significantly distorted hexagonal close-packing of nitride anions.

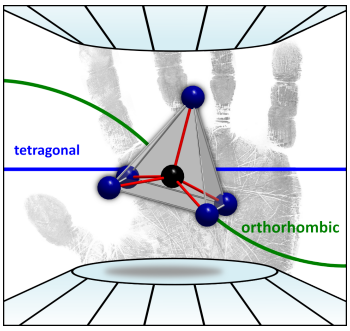

Phosphorus gives high five: The phase diagram of phosphorus oxonitride (PON) was extended by a post-coesite form of PON, in which P is fivefold coordinated by O and N, which has not been reported for any PON form before. Post-coesite PON adopts a stishovite-related structure and suggests an unexhausted polymorphism including sixfold coordinated P in PON structures.

Under pressure: α-BP_3N_6 was investigated in situ upon cold compression to a maximum pressure of 42 GPa, at which laser-heating induced a phase transition into its high-pressure polymorph β-BP_3N_6. β-BP_3N_6 is the first nitride to contain PN_6 octahedra, representing a much sought-after structural motif in fundamental research on non-metal nitrides.

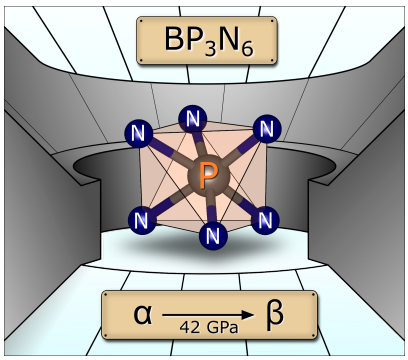

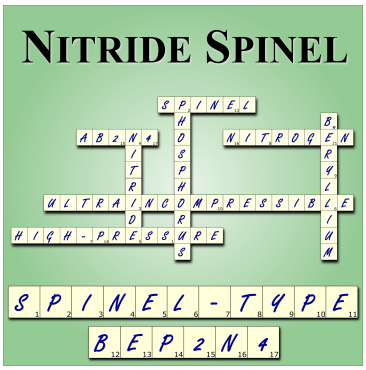

Nitride spinel: At 47 GPa and 1800 K phenakite-type BeP_2N_4 was transformed into the spinel-type form of BeP_2N_4 using a laser-heated diamond anvil cell. Its crystal structure was investigated using pressure-dependent in situ synchrotron XRD measurements and its isothermal bulk modulus was determined to >300 GPa, which renders spinel-type BeP_2N_4 an ultraincompressible material.

1. Introduction

1.1. A Brief Homage on Nitrides

A deep breath and billions of trillions of gas molecules flood our lungs, providing us properly dosed oxygen vital for life. The main components of the Earth's atmosphere are nitrogen (N_2, 78.08 vol-%, 75.52 wt-%), oxygen (O_2, 20.95 vol-%, 23.14 wt-%), and argon (Ar, 0.93 vol-%, 1.29 wt-%) besides trace gases and aerosols such as CO_2 and H_2O.[1] Paradoxically, in the Earth's crust, oxygen is considered to be the most abundant element (46.60 wt-%) besides a very low nitrogen level (0.0056 wt-%).[2,3] Why does our Earth feature those contrary ratios of oxygen and nitrogen? And why is this relevant to this thesis?

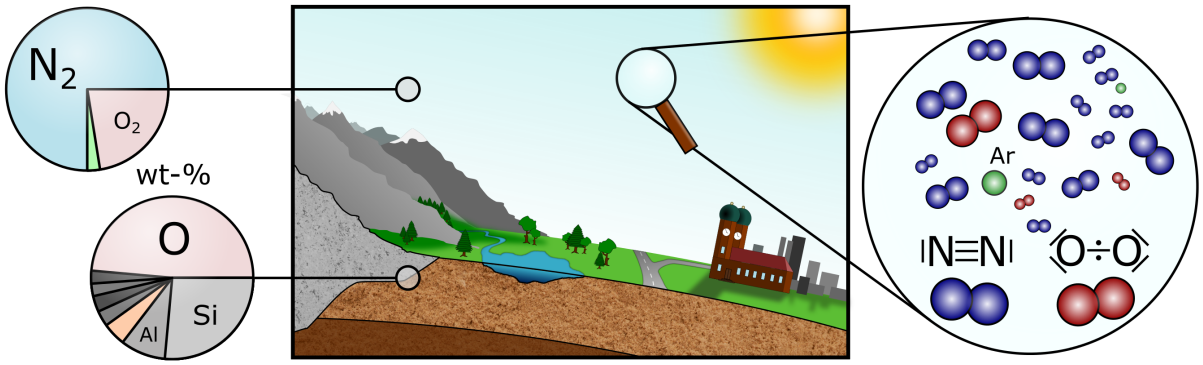

Figure 1.1.: Elemental nitrogen is the major component of the Earth's atmosphere, whereas oxygen is the most abundant element in the Earth's crust. This fact is attributable to the different chemical behavior of the reactive O_2 and the inert N_2 molecule.

Elemental oxygen is consumed by all living creatures and formed within plants during the process of photosynthesis. The oxygen level of the Earth's atmosphere is thus maintained by a continuous cycle of consumption and recreation. The predominant state of elemental oxygen is the diradical form

that features a nominal double bond with a bonding energy of 498 kJ·mol^{-1} (Figure 1.1).[4] This double bond can be readily activated by moderate heat or enzymes, which makes oxygen a reactive species. Moreover, owing to its high redox potential (E^0 = +1.229 V; $O_{2(g)}$, $H^+/H_2O_{(l)}$),[5] oxygen is easily reduced to the oxidation state −II and therefore acts as a strong oxidizer, which is in line with its high electron affinity (−1.46 eV) and electronegativity (3.5).[4,6] In contrast, elemental nitrogen features a triple bond (941 kJ·mol^{-1}, Figure 1.1) that is almost twice as stable as the oxygen double bond.[4] Owing to the positive electron affinity of nitrogen (+0.07 eV) and its negative redox potential (E^0 = −0.736 V; $N_{2(g)}$, NH_3/OH^-), it does not form stable isolated anions.[5,7] Therefore, N_2 may be classified as an inert gas rather than as a reactive species. That is why the Earth's atmosphere is enriched with unreactive molecular nitrogen, whereas the Earth's crust is mainly composed of oxide (O^{2-}) materials. Herein, oxo(alumo)silicates appear as the most abundant constituents, while the trace amounts of nitrogen predominantly exist in the form of the ammonium ion NH_4^+.[2] Nitride (N^{3-}) minerals, such as Qingsongite (BN),[8] Sinoite (Si_2N_2O),[9] Nierite (Si_3N_4),[10] Osbornite (TiN),[11] Siderazot (Fe_5N_2),[12] Carlsbergite (CrN),[13] or Roaldite (Fe_4N),[14] however, are very rare and mostly located within meteorites.[15,16]

Synthetic nitrides, however, are extensively investigated by modern solid-state chemistry, as they feature intriguing materials properties, such as wide band gap semiconductivity, thermal, chemical, and mechanical resilience, as well as ion conductivity. Therefore, synthetic nitrides are applied in numerous state-of-the-art technologies, such as solid-state LED lighting (GaN-based semiconductors and nitridosilicate-based phosphors),[17–23] 4th/5th generation of mobile communications (4G/5G, GaN-based semiconductors),[24–26] and high-performance ceramics (e. g. Si_3N_4, BN).[27–29] Furthermore, nitride materials are discussed to rise to one of today's most urgent challenges, namely the future supply and storage of renewable and clean energy.[30–38] The preparation of nitrides in laboratories, however, is challenging, considering the inert character of elemental nitrogen and its positive electron affinity, as briefly outlined above. Besides the strict exclusion of moisture and oxygen, the key challenge of nitride synthesis is the unfavored reduction of elemental nitrogen to the nitride oxidation state (−III) and the subsequently stabilization of the nitride ion N^{3-} against untoward oxidation. The success story of nitride materials, therefore, is the particular merit of decades of fundamental research, from which various preparative techniques have been developed.

Nitridosilicates and nitridophosphates are considered to be two of the best examined classes of nitrides, as they feature an immense structural and elemental diversity.[39–41] Their fundamental investigations

have repeatedly been pioneering in the emerging field of nitride solid-state chemistry, especially in the terms of preparative techniques, considering advanced synthetic approaches such as high-pressure high-temperature techniques[41–43] or ion exchange reactions, for instance.[44] Just as the oxosilicate class of compounds is derived from silicon dioxide SiO_2, silicon nitride Si_3N_4 and phosphorus nitride P_3N_5 appear as the parent compounds of nitridosilicates and nitridophosphates, respectively. Thus far, three Si_3N_4 polymorphs (α-, β-, and γ-Si_3N_4) were reported, which all have extensively been investigated at ambient and high pressures in terms of their structural, elastic, and materials properties.[27,45–48] In contrast, phosphorus nitrides appear rather sparsely examined in terms of their materials properties and structural behavior at high pressures. Within this thesis, the term *phosphorus nitrides* is deemed to describe not only the binary compound P_3N_5 itself, but the whole collective of all P/N compounds that form neutral covalent networks, including multinary compounds such as phosphorus oxide nitrides (PON, P_4N_6O),[49,50] phosphorus nitride imides (PNNH, P_4N_6NH),[51,52] as well as double nitrides,* such as $SiPN_3$ and BeP_2N_4.[54,55]

It is apparent that phosphorus nitrides are a highly diverse class of compounds, although their fundamental examination has been restricted by challenging syntheses, and their high-pressure behavior has mostly been discussed on the basis of theoretical studies, previously. This thesis therefore strives to remedy the deficiencies in fundamental research on phosphorus nitrides in terms of their preparation and high-pressure behavior. Within the following sections the present state of research of phosphorus nitrides is briefly outlined, commenting their structural chemistry (Section 1.2), established preparative techniques (Section 1.3), as well as their high-pressure polymorphism (Section 1.4), in order to finally frame the strategic objective of this thesis that involves the development of a new synthesis strategy and structural in situ investigations at high pressures (Section 1.5).

*Liebau introduced the term *double oxide* to describe ternary silicon oxides with the second cation having a similar electronegativity than Si (e. g. $ZnSiO_3$).[53] Referring to Liebau's definition, the term *double nitride*, however, is used to describe ternary nitrides, in which the cations feature the same coordination polyhedra rather than a similar electronegativity (e. g. BeP_2N_4, $SiPN_3$).[54,55]

1.2. The Structural Chemistry of Phosphorus Nitrides

The basic research on P/N compounds may be distinguished into molecular, polymeric, and solid-state chemistry, though all of these branches of chemistry are also to some degree intertwined. Numerous molecular and polymeric P^{V} and P^{III} derivates of phosphorus amides as well as phosphazanes and phosphazenes (e. g. $(PNCl_2)_3$, Figure 1.2a)[56,57] were reported, of which an overview is provided in literature.[58,59] Moreover, the diatomic molecule $P^{III}N$ was prepared and investigated on its spectroscopic and thermal stability.[60,61] Within the field of solid-state chemistry, in turn, structures of PN, PN_2, PN_3, P_2N_3, and P_3N_4 were investigated by theoretical studies,[62–64] and phosphorus oxide nitride glasses were experimentally examined.[65,66] The preparation of crystalline solid-state P/N compounds has been focused on phosphorus nitrides and nitridophosphates, thus far. The binary nitride P_3N_5 was initially synthesized in 1903 through ammonolysis of P_4S_{10} as formally described in Equation 1.1.[67] The crystal structure of α-P_3N_5, however, was first solved in 1997 from a sample that was crystallized by a gentle thermal decomposition of $[P(NH_2)_4]I$ at 825 °C (Equation 1.2), since previously only disordered mixtures of α- and β-P_3N_5 had been obtained.[52,68]

$$3\,P_4S_{10} + 20\,NH_3 \longrightarrow 4\,P_3N_5 + 30\,H_2S \tag{1.1}$$

$$3\,[P(NH_2)_4]I \longrightarrow \alpha\text{-}P_3N_5 + 3\,NH_4I + 4\,NH_3 \tag{1.2}$$

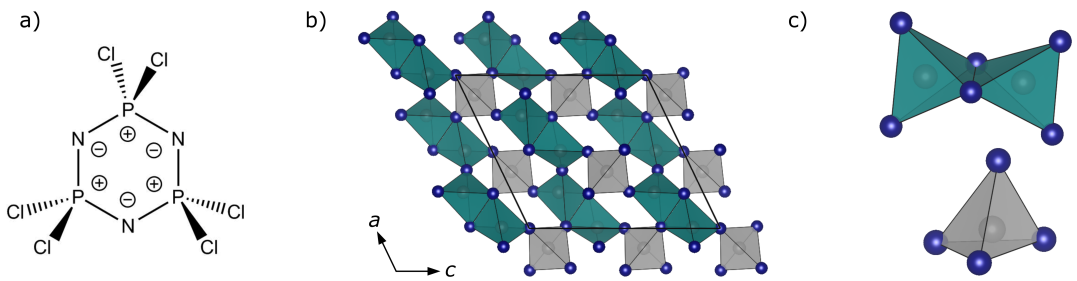

Figure 1.2.: Hexachloro-*cyclo*-triphosphazene $(PNCl_2)_3$ is a molecular compound that has been used as a precursor in phosphorus nitride synthesis (a).[56,57] The unique crystal structure of α-P_3N_5 (b) is built up from edge-sharing (cyan) and all-side vertex-sharing PN_4 tetrahedra (gray, c).[52] P: gray, N: blue.

α-P_3N_5 crystallizes in a unique structure type that is built up from chains of edge-sharing PN_4 tetrahedra, which are interconnected by all-side vertex-sharing PN_4 tetrahedra (Figure 1.2b, c). The PN_4 tetrahedron is therefore considered the fundamental building unit of phosphorus nitrides, reminiscent of SiO_2 structures. Phosphorus nitrides, however, may also feature edge-sharing PN_4 tetrahedra (Figure 1.2 and 1.3),[52,69] which in silicates is only controversially discussed for fibrous silica.[70] This may be due to nitrogen featuring a higher valence than oxygen, which enforces a higher degree of condensation in nitride structures, as discussed below.[71] Moreover, owing to similar energies of the 3p(P) and 2p(N) orbitals,[72] the P–N bond has a highly covalent character, which reduces the effective charges and thus, the electrostatic repulsion between two tetrahedra centers.

Tetrahedra-based structures can be classified by their degree of condensation κ that describes the ratio of tetrahedra centers (T) to tetrahedra corners (X): $\kappa = \mathrm{n}(T)/\mathrm{n}(X)$. The degree of condensation of a binary phase T_xX_y is predefined by its chemical formula, as all constituents can be regarded as either tetrahedra centers or tetrahedra corners. Thus, κ is determined by the formal charge of the T and X ions (Figure 1.3a). For a certain anion X (e. g. N^{-III}), κ increases with decreasing charges of T, as illustrated by the series P_3N_5 (T^{V}, $\kappa = 0.6$), Si_3N_4 (T^{IV}, $\kappa = 0.75$), BN (T^{III}, $\kappa = 1.0$), and Be_3N_2 (T^{II}, $\kappa = 1.5$). In contrast, κ decreases for a certain cation T (e. g. P^{V}), with higher oxidation states of X as illustrated by P_3N_5 (X^{-III}, $\kappa = 0.6$) and P_2O_5 (X^{-II}, $\kappa = 0.4$). For tetrahedra-based structures, κ is bound at the low end to 0.25, corresponding to non-condensed tetrahedra as illustrated for molecular POF_3 ($X^{-II/-I}$, $\kappa = 0.25$).

The degree of condensation of tetrahedra networks, therefore, correlates with the coordination number of the anions X, as briefly discussed for POF_3, P_2O_5, PON, P_3N_5, $SiPN_3$, and BeP_2N_4 below and illustrated in Figure 1.3c. While non-condensed POF_3 tetrahedra solely feature terminal $X^{[1]}$ (X = O, F) sites,[73,74] the lowly condensed structure of adamantane-like P_2O_5 ($\kappa = 0.4$) is built up from P_4O_{10} units that feature terminal ($X^{[1]}$) and twofold coordinated O sites ($X^{[2]}$).[75] The condensed structure of cristobalite-type PON, in contrast, solely features all-side vertex-sharing $P(O/N)_4$ tetrahedra with twofold coordinated O and N sites ($X^{[2]}$).[49] In highly condensed tetrahedra-based networks with $\kappa > 0.5$, however, threefold coordinated X sites ($X^{[3]}$) are mandatory, and thus are observed in P_3N_5, $SiPN_3$, and BeP_2N_4.[52,54,55] Structures with $\kappa \geq 1.0$ even feature four-, five-, or sixfold coordinated X sites, as realized by BN, $BeSiN_2$, and Be_3N_2, for instance.[76–78]

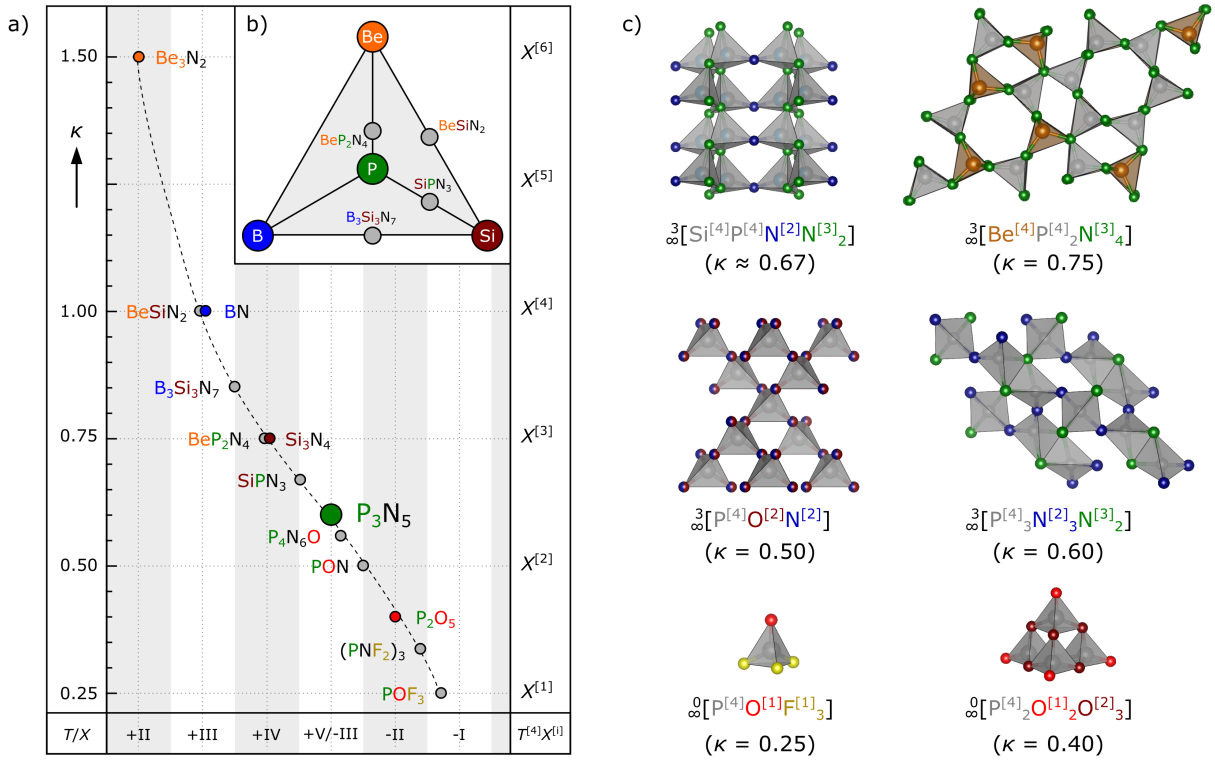

Figure 1.3.: The degree of condensation (κ) describes the ratio of tetrahedron centers (T = P, Si, B, Be) and tetrahedron corners (X = N, O, F) and is predefined by the chemical formula of a certain compound. Thus, it is affected by the formal charges of the T and X ions and may be tuned by mixed occupation sites, as apparent from phosphorus oxide nitrides and mixed covalent nitrides (a, b). An increase in κ, therefore, necessitates an increasing coordination number of the terminal/linking anions X as illustrated for POF_3, P_2O_5, PON, P_3N_5, $SiPN_3$, and BeP_2N_4 (c). Referring to the formalism introduced by Niggli and further developed by Lima-de-Faria et al., the coordination number of a certain atom is given in superscripted square brackets within this thesis. $P^{[4]}$ thus, refers to a fourfold coordinated P, for instance, and the P/N network of the α-P_3N_5 structure is expressed by the systematic formula ${}^{3}_{\infty}\left[P^{[4]}{}_3N^{[2]}{}_3N^{[3]}{}_2\right]$. Herein, the dimensionality of the network is given by the superscript number of dimensions, in which a structural unit has an infinite extension (here: ${}^{3}_{\infty}[\ldots]$).[79,80]

It is therefore apparent that the structural chemistry of phosphorus nitrides is closely related to the degree of condensation, which can be tuned by the substitution of P and N leading to mixed phosphorus nitrides (e. g. $SiPN_3$, BeP_2N_4) and phosphorus oxide/imide nitrides (e. g. PON, PNNH), for instance.[†] Starting from phosphorus nitride P_3N_5 ($\kappa = 0.6$), κ is decreased when O^{2-} or isolobal NH^{2-} functionality is introduced into the P/N network, which may formally be considered as a hydrolysis or ammonolysis of

[†]By the incorporation of electropositive metal cations M^{m+} a decrease in κ is mandatory, opening the compound class of nitridophosphates $M_xP_yN_z$. For those anionic P_yN_z networks, κ is limited to a minimum value of 0.25, corresponding to non-condensed tetrahedra (e.g. Li_7PN_4),[81] and its maximum value is limited to $\kappa < 0.6$. A detailed overview of the preparative and structural chemistry of nitridophosphates is provided in literature.[41]

P_3N_5 (Figure 1.3a). Reported representatives of phosphorus oxide nitrides and phosphorus imide nitrides are P_4N_6O ($\kappa \approx 0.57$),[50] PON ($\kappa = 0.5$, Figure 1.3c),[49] P_4N_6NH ($\kappa \approx 0.57$),[69] and PNNH ($\kappa = 0.5$),[51] as well as the nitridic clathrate $P_4N_4(NH)_4(NH_3)$ ($\kappa = 0.5$)[82] and the phosphorus imide oxide nitride $P_8O_8N_6(NH)_3$ ($\kappa \approx 0.47$).[83]

In contrast, κ can be increased by the incorporation of lower charged network forming elements such as Si^{4+}, B^{3+}, or Be^{2+}, which corresponds to a formal combination of variable amounts of the respective binary nitrides, yielding mixed covalent nitrdes. This strategy was successfully used for the preparation of $SiPN_3$ ($\kappa \approx 0.67$)[54] and BeP_2N_4 ($\kappa = 0.75$) already (Equation 1.3 and 1.4), with their structures illustrated in Figure 1.3c.[55] Likewise, the double nitrides $BeSiN_2$ ($\kappa = 1.0$)[77] and $Si_3B_3N_7$ ($\kappa \approx 0.86$)[84,85] can be interpreted, as shown in Equation 1.5 and 1.6.

$$\frac{1}{3}\,Si_3N_4 + \frac{1}{3}\,P_3N_5 \equiv SiPN_3 \tag{1.3}$$

$$\frac{1}{3}\,Be_3N_2 + \frac{2}{3}\,P_3N_5 \equiv BeP_2N_4 \tag{1.4}$$

$$\frac{1}{3}\,Be_3N_2 + \frac{1}{3}\,Si_3N_4 \equiv BeSiN_2 \tag{1.5}$$

$$Si_3N_4 + 3\,BN \equiv Si_3B_3N_7 \tag{1.6}$$

There are, however, only few known double nitrides within the Be/B/Si/P/N system (Figure 1.3b), which is most likely owed to the fact that the formal reaction of two binary nitrides appears highly unfavored, if not inoperable, considering the acid-base concept of oxides by Lux and Flood.[86,87] If this concept is transferred to nitride materials, BN, Si_3N_4, and P_3N_5 are assigned an acid character, as they likely act as nitride acceptors within a acid base reaction. Considering further the refractory character of BN and Si_3N_4, as well as the thermal instability of P_3N_5, the preparation of double nitrides, in particular of mixed phosphorus nitrides, has ever since been a challenging issue, as will be explained in the following section.

1.3. The Synthesis of Phosphorus Nitrides

The synthesis of nitrides is generally complicated by the fact that the targeted compounds may be prone to decomposition and elimination of N_2. This is owed to the positive electron affinity of nitrogen (+0.07 eV)[7] and the large stability of the nitrogen triple bond in N_2 (941 kJ·mol^{-1}), as outlined above.[4] Hence, preparative methods and reaction conditions have to be carefully considered in order to stabilize the nitride ion N^{3-} against oxidation. In the case of phosphorus nitrides, however, P^{V} may readily act as a redox partner, as it can be reduced to oxidation states +III, 0, or −III, usually forming amorphous PN, elemental phosphorus, or phosphides. This central problem may be best illustrated by the incremental thermal decomposition of P_3N_5 above 850 °C (Equation 1.7).[68,82]

$$P_3^{V}N_5^{-III} \longrightarrow 3\,P^{III}N^{-III} + N_2^{0} \longrightarrow 3\,P^{0} + {}^{5}/_{2}\,N_2^{0} \tag{1.7}$$

Owing to small inter diffusion coefficients and high lattice energies, however, the (re)formation of chemical bonds usually hardly proceeds at temperatures < 1000 °C in solid-state materials, which discloses the dilemma of preparative P/N chemistry: *The crystallization temperature of phosphorus nitrides usually exceeds their decomposition temperature.* In the recent years, however, preparative techniques have been developed that circumvent this issue by either decreasing the crystallization temperature or increasing the decomposition temperature.

The crystallization temperature of phosphorus nitrides can be decreased by the employment of mineralizers, such as ammonium halides (e. g. NH_4I) or hydrogen halides (e. g. HCl), which were used during the syntheses and crystallization of α-P_3N_5 and α-P_4N_6NH, for instance (Equation 1.2, 1.8, and 1.9).[52,68,69]

$$(PNCl_2)_3 + 2\,NH_4Cl \xrightarrow{775\,^{\circ}C} \alpha\text{-}P_3N_5 + 8\,HCl \tag{1.8}$$

$$4\,P_3N_5 + NH_4Cl \xrightarrow{820\,^{\circ}C} 3\,P_4N_6NH + HCl \tag{1.9}$$

It is assumed that mineralizers facilitate the reversible cleavage and (re)formation of the highly covalent P–N bonds at moderate temperatures. This conception is based on findings from the molecular and polymer chemistry of P/N compounds that are thoroughly summarized in literature.[59] Accordingly, the P–N bond is easily cleaved under hydrous,[88,89] and anhydrous acidic conditions,[90,91] employing

hydrogen halides, for instance. Moreover, HCl was found to be an excellent leaving group during the condensation of (R)P–Cl and H–N(R') species, as exemplarily illustrated by the formation of $(PNCl_2)_3$ (Equation 1.10).[56,57] Thus, a reversible cleavage and (re)formation of (R)P–N(R') bonds may be assumed in solid-state chemistry as well, with (R)P–Cl and H–N(R') appearing as plausible intermediate species during the polycondensation of phosphorus nitrides (Equation 1.11). Herein, the rests (R) and (R') may refer to H/N/Cl in the case of molecular species and to (macro)molecular P/N fragments in the case of solid-state compounds.

$$3\,NH_4Cl + 3\,PCl_5 \longrightarrow (PNCl_2)_3 + 12\,HCl \tag{1.10}$$

$$(R)P{-}Cl + H{-}N(R') \rightleftharpoons (R)P{-}N(R') + HCl \tag{1.11}$$

Another approach to bypass high reaction temperatures is the condensation of reactive molecular precursors, as this enables a kinetically controlled reaction rather than the formation of thermodynamic products (e. g. N_2) and the decomposition of the targeted products. For instance, this approach was employed for the preparation of the mixed silicon phosphorus nitride $SiPN_3$.[54] Here, the unfavored direct reaction of the two Lux-Flood acids Si_3N_4 and P_3N_5 (Equation 1.12) was bypassed by the gentle ammonolysis of molecular $Cl_3SiNPCl_3$ at −78 °C and a subsequent pyrolysis of the intermediate product at 800 °C in a flow of dry NH_3, which yielded a partially crystalline, but highly disordered product (Equation 1.13).[54] The crystallization of $SiPN_3$ was finally realized at 900 °C (24 h) in an evacuated sealed quartz tube, using minor amounts of NH_4Cl as a mineralizer. Amorphous $Si_3B_3N_7$ was likewise prepared by ammonolysis of molecular $Cl_2BNHSiCl_3$ and pyrolysis at 1400 °C in N_2 atmosphere,[84,85] and the usage of more versatile monomeric molecular precursors, such as $OP(NH_2)_3$, $SP(NH_2)_3$, and hydrogenphosphates enabled the preparation of amorphous PON and numerous (oxo)nitridophosphates.[41,49,83,92–94]

$$\text{"}Si_3N_4 + P_3N_5 \longrightarrow 3\,SiPN_3\text{"} \tag{1.12}$$

$$Cl_3SiNPCl_3 \xrightarrow[NH_{3(l)}]{-78\,^\circ C} \text{“}SiPN(NH)(NH_2)_4\text{”} \xrightarrow[NH_3]{800\,^\circ C} SiPN_3 \xrightarrow[NH_4Cl]{900\,^\circ C} SiPN_{3(crystalline)} \tag{1.13}$$

Instead of decreasing the crystallization temperature of phosphorus nitrides by mineralizers or gentle reaction pathways, their decomposition temperature is increased by the employment of high-pressure

high-temperature (HP/HT) techniques, which have been emerged to the most established synthetic approach in today's preparative P/N chemistry. Following Le Chatelier's principle, the heat-induced elimination of N_2 can be suppressed by applying external pressures in the gigapascal range (GPa) that are achieved with large volume presses. Reaction temperatures of up to 2000 °C were reported, without causing decomposition of P/N compounds or the release of N_2.[42] Using this HP/HT approach, numerous nitridophosphates ($M_xP_yN_z$) have been prepared at high pressures, employing the belt and the multianvil technique.[41,42,95] Metal azides, metal nitrides, and metal halides, as well as P_3N_5 and $LiPN_2$ have been established as the most common starting materials, and additional amounts of NH_4Cl were shown to facilitate single-crystal growth.[96–98] A detailed overview on the preparative access to nitridophosphates is provided in literature.[41]

The HP/HT approach, however, was also used for the preparation of phosphorus nitrides, as illustrated by the synthesis of the double nitride BeP_2N_4 at 5 GPa and 1500 °C, in which the binary nitrides Be_3N_2 and P_3N_5 were used as starting materials (Equation 1.14).[55] Moreover, the unique nitridic clathrate $P_4N_4(NH)_4(NH_3)$ (Equation 1.15) and the first phosphorus imide oxide nitride $P_8O_8N_6(NH)_3$ were prepared at 11 and 12 GPa, starting from P_3N_5 and NH_4N_3, and amorphous PON, respectively.[82,83]

$$Be_3N_2 + 2\,P_3N_5 \xrightarrow[1500\,^\circ C]{5\,GPa} 3\,BeP_2N_4 \tag{1.14}$$

$$16\,P_3N_5 + 21\,NH_4N_3 \xrightarrow[600\,^\circ C]{11\,GPa} 12\,P_4N_4(NH)_4(NH_3) + 28\,N_2 \tag{1.15}$$

Besides for the synthesis of highly condensed mixed phosphorus nitrides, the HP/HT technique was used for the structural investigations of the (pseudo) binary compounds P_3N_5, PNNH, P_4N_6NH, and PON at high pressures. From that, numerous high-pressure polymorphs have been characterized, attesting phosphorus nitrides a remarkable polymorphism, reminiscent of that of SiO_2 and Si_3N_4. A brief overview of experimental and theoretical studies on the high-pressure behavior of phosphorus nitrides is provided below.

1.4. Phosphorus Nitrides at High Pressures

Phosphorus nitrides have been investigated at high-pressures for over 20 years, and various experimental and theoretical studies show that their structural chemistry follows the generalized behavior of inorganic solids at high pressures, as described by the high-pressure rules.[99,100] In contrast to the high-pressure behavior of BN and Si_3N_4 that have been extensively investigated by experiments up to the megabar range (> 100 GPa),[46,47,76,101–103] respective studies on phosphorus nitrides had been very rare in number, prior to this thesis.[104,105]

Due to the distinct polymorphism of SiO_2, isoelectronic PON has been investigated at high pressures, early on.[105] At ambient pressure, PON crystallizes in the β-cristobalite-type structure (cri), which is transformed at elevated temperatures into moganite- and α-quartz-type polymorphs at 2.5 and 4.5 GPa, respectively.[49,106–108] Moreover, upon cold compression of cri-PON a displacive phase transition has been observed at pressures > 13 GPa.[104,105] Heating PON at 12 GPa further yielded an unprecedented PON polymorph (δ-PON) with a structure that had been suggested for a SiO_2 polymorph from theoretical studies, before (Figure 1.4a).[109,110] Moreover, PON was shown to adopt a coesite-type structure at 15.5 GPa, in line with the polymorphism of SiO_2.[111] All these previously reported forms of PON are exclusively built up from $P(O/N)_4$ tetrahedra (Figure 1.4a), but high-pressure polymorphs with an increased coordination number of P appear plausible, considering high-pressure phases of $TiPO_4$, $AlPO_4$, and $CaBe_2P_2O_8$ that feature five- or even sixfold O-coordinated P.[112–114] With regard to the close relation between SiO_2 and PON, a stishovite-analog rutile-type form of PON may therefore be conceivable at sufficiently high pressures.[115] Prior to this thesis, high-pressure investigations on PON, however, have mainly been limited to about 16 GPa, with only few exceptions of cold compression experiments.[104,105]

Besides examinations on PON, the structural chemistry of phosphorus nitrides was further investigated by screening the phase diagrams of P_3N_5, PNNH, and P_4N_6NH for high-pressure polymorphs in multianvil presses up to a maximum pressure of 14 GPa. The high-pressure polymorphs β-PNNH and β-P_4N_6NH have been prepared at 6 GPa and are built up from all-side vertex-sharing PN_4 tetrahedra.[96,116] γ-P_3N_5, that was prepared from α-P_3N_5 at 11 GPa, in contrast, is the first phosphorus nitride, for which the rare motif of fivefold N-coordinated P was observed.[117] Its unique structure can be expressed by the Niggli formula ${}^{3}_{\infty}\left[P^{[4]}P^{[5]}{}_2N^{[2]}N^{[3]}{}_4\right]$ and features chains of edge-sharing square PN_5 pyramids that are interconnected by all-side vertex-sharing PN_4 tetrahedra (Figure 1.4b). Likewise, a second high-

pressure form of P_4N_6NH was prepared at 14 GPa (γ-P_4N_6NH) that is built up from trigonal PN_5 bipyramids and all-side vertex-sharing PN_4 tetrahedra in a 1 : 1 ratio, as described by the Niggli formula ${}^{3}_{\infty}\left[P^{[4]}{}_2P^{[5]}{}_2N^{[2]}{}_3N^{[3]}{}_4H\right]$ and illustrated in Figure 1.4c.[118]

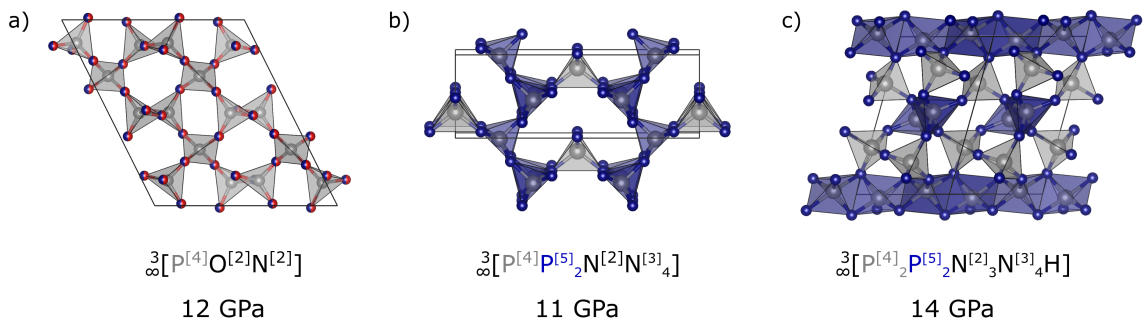

Figure 1.4.: Crystal structures of δ-PON (a), γ-P_3N_5 (b), and γ-P_4N_6NH (c) with respective Niggli formulas and synthesis pressures.[109,117,118] $P(O,N)_4$ and PN_4 tetrahedra are illustrated in gray and PN_5 polyhedra are drawn in blue. P: gray, O: red, N: blue.

Although phosphorus nitrides have been investigated in a rather limited pressure range previously, they were shown to feature a highly diverse structural chemistry at elevated pressures that is based on interconnected PN_4 and PN_5 polyhedra. This posed the question, whether a PN_6 coordination polyhedron, as it is observed in hexaazidophosphates $P(N_3)_6^-$,[119] may also be energetically favored in phosphorus nitrides at sufficiently high pressures. Therefore, numerous theoretical studies on the high-pressure behavior of various phosphorus nitrides were performed prior to this thesis.

At pressures exceeding 43 GPa, a kyanite-type form of P_3N_5 (δ-P_3N_5) that features four- and sixfold N-coordinated P is proposed.[120] It is further predicted that pressure quenching leads to a structural distortion at about 34 GPa, resulting in another polymorph, which is built up from PN_4, PN_5, and PN_6 units and denoted as δ'-P_3N_5. Subsequent DFT calculations confirm that octahedrally N-coordinated P is presumable in P_3N_5 at high pressures, but suggest a V_3O_5-type form as the thermodynamically stable phase at pressures >35.5 GPa.[64] Furthermore, theoretical studies on the high-pressure behavior of β-P_4N_6NH suggest a regular contraction of the β-P_4N_6NH structure up to 110 GPa, at which the formation of PN_6 octahedra is stated.[121] With respect to γ-P_4N_6NH that was prepared at 14 GPa, this as-predicted high-pressure polymorph is denoted δ-P_4N_6NH within this thesis.

Investigating the high-pressure polymorphism of mixed phosphorus nitrides, the highly condensed double nitride BeP_2N_4 has been discussed as a promising candidate for sixfold N-coordinated P all along. BeP_2N_4 is isoelectronic with Si_3N_4 and crystallizes in the phenakite structure type that is homeotypic with β-Si_3N_4.[55] It is known that the spinel-type form (γ-Si_3N_4) is the stable polymorph of Si_3N_4 at pressures > 13 GPa.[46,122,123] Therefore, a spinel-type polymorph of BeP_2N_4 that features BeN_4 and PN_6 polyhedra was investigated by numerous DFT calculations, which suggest it as the stable polymorph at pressures exceeding 14–24 GPa.[55,124–126] Moreover, the phase diagrams of $LiPN_2$ and $CuPN_2$ were recently screened by theoretical studies that predict high-pressure polymorphs with sixfold N-coordinated P.[127,128] Accordingly, two NaCl-related $LiPN_2$ polymorphs (hR4 and cF64) are proposed to form at 44 and 136 GPa, respectively, and a NiAs-related structure (oP8) is predicted the stable $LiPN_2$ phase at pressures > 259 GPa.[127] $CuPN_2$, in turn, is proposed to undergo phase transition at 34 GPa into a hR4 or oC16 structure that features PN_6 octahedra and linear N-coordinated Cu. At pressures > 120 GPa, however, the NaCl-related hR4' polymorph is predicted as the stable $CuPN_2$ phase.[128] An overview of phosphorus nitrides that have been investigated at high pressures by experimental and/or theoretical studies is provided in Figure 1.5.

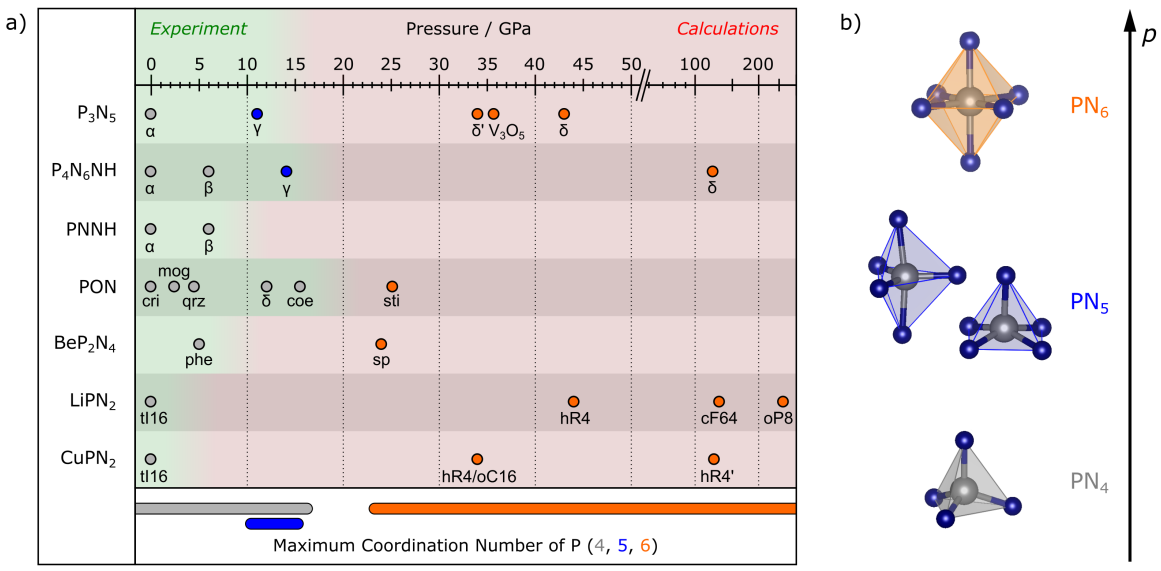

Figure 1.5.: Overview of experimentally and theoretically investigated polymorphs of various phosphorus nitrides. In line with the pressure coordination rule,[99,100] the coordination number of P increases with pressure from tetrahedrally coordinated $P^{[4]}$ to fivefold coordinated $P^{[5]}$, as reported for γ-P_3N_5 and γ-P_4N_6NH.[117,118] Sixfold N-coordinated $P^{[6]}$ is suggested for high-pressure forms of P_3N_5,[64,120] P_4N_6NH,[121] PON,[115] BeP_2N_4,[55,124–126] $LiPN_2$,[127] and $CuPN_2$,[128] but has not been observed experimentally, prior to this thesis.

Beyond the high-pressure polymorphism of phosphorus nitrides, the presented theoretical investigations provide information on their elastic properties, such as their compressibility (bulk modulus K_0) and Vickers hardness (H_V). Herein, α-P_3N_5 (K_0 = 87–99 GPa), γ-P_3N_5 (K_0 = 103–116 GPa) and β-P_4N_6NH (K_0 = 66 GPa) appear as rather compressible materials, while δ'-P_3N_5 (K_0 = 240 GPa) is proposed to be quite incompressible.[120,121] The calculated elastic properties of spinel-type BeP_2N_4 (K_0 = 263–291 GPa, H_V = 45 GPa),[55,124–126] moreover, suggest it as an very incompressible and superhard material, which appears plausible when compared to γ-Si_3N_4 (K_0 = 290–317 GPa, H_V = 30–43 GPa).[46,47,103,123,129,130] Prior to this thesis, experimental investigations on the elastic properties of phosphorus nitrides, however, have solely been limited to cri-PON and α-PNNH, whose bulk moduli were determined with K_0(cri-PON) = 80(5) GPa and K_0(α-PNNH) = 102(2) GPa.[104,105]

Recapitulating, phosphorus nitrides were shown to feature a diverse high-pressure polymorphism from experimental ex situ studies at pressures < 16 GPa. Moreover, numerous theoretical investigations on various phosphorus nitrides suggest an even enriched structural diversity at elevated pressures, as a PN_6 motif may be likely observed in high-pressure polymorphs of P_3N_5, P_4N_6NH, BeP_2N_4, $LiPN_2$, and $CuPN_2$. Hence, the high-pressure behavior phosphorus nitrides appears inadequately investigated, when compared to other covalent nitrides, such as BN and Si_3N_4, for instance, that have extensively been examined at high-pressure conditions by in situ and ex situ studies.[46,47,76,101–103]

1.5. Scope of this Thesis

Today's state of research on phosphorus nitrides poses two central issues for fundamental progression. On the one hand, the elemental diversity of phosphorus nitrides is constrained by the preparative chemistry, as there is no systematic access to mixed covalent nitrides of Be, B, Si, and P, which restricts structural investigations on highly condensed nitride networks. On the other hand, the high-pressure behavior of phosphorus nitrides appears inadequately investigated in terms of their high-pressure polymorphism and elastic properties, considering numerous theoretical studies that propose various phases with intriguing materials properties. Therefore, this thesis is concerned with both, the development of an innovative access to mixed phosphorus nitrides, as well as with the expansion of the experimental pressure range, in which phosphorus nitrides are systematically investigated.

The first part of this thesis strives to design a novel synthetic strategy for the preparation of mixed phosphorus nitrides that combines various established synthetic approaches. The over-all challenge of the preparative chemistry of phosphorus nitrides is to balance their decomposition and crystallization temperature, as they are prone to the heat-induced elimination of N_2. Thus, some phosphorus nitride syntheses use reactive precursors, such as P_4S_{10}, $[P(NH_2)_4]I$, $(PNCl_2)_3$, NH_3, and NH_4N_3, in order to circumvent high thermal activation barriers. It was further shown that hydrogen halides (e.g. HCl) facilitate the reversible cleavage and (re)formation of the highly covalent P–N bonds, which is essential for the formation of new compounds. As exemplified by the syntheses of BeP_2N_4 and $P_4N_4(NH)_4(NH_3)$, moreover, high-pressure high-temperature (HP/HT) conditions can be used for the preparation of phosphorus nitrides, at which the employment of mineralizers, such as NH_4Cl or LiF, can facilitate the formation of single-crystals.

Recapitulating, one can deduce four factors that may grant a successful synthesis of phosphorus nitrides, as there are (*i*) the employment of reactive precursors, (*ii*) the reversible cleavage and (re)formation of P–N bonds, (*iii*) high pressures and temperatures, and (*iv*) the use of mineralizers. Considering these factors of success, one now can draft an explorative strategy to screen for unprecedented preparative approaches. Accordingly, $(PNCl_2)_3$ and NH_4N_3 may be reacted at HP/HT conditions to formally produce P_3N_5, N_2, and HCl (Equation 1.16).

$$\text{"}2\,(PNCl_2)_3 + 3\,NH_4N_3 \xrightarrow{\text{HP/HT}} 2\,P_3N_5 + 4\,N_2 + 12\,HCl\text{"} \tag{1.16}$$

Herein, in situ formed HCl likely facilitates the reversible cleavage and (re)formation of P–N bonds, which enables an atomic rearrangement during synthesis. Adding a mineralizer such as NH_4Cl may further support the growth of single-crystals, without introducing any additional elements into the reaction. Be, B, or Si may further be introduced into the system by adding precursors, such as $BeCl_2$, $(BNHCl)_3$, or $Si(NH)_2$, in order to obtain highly condensed mixed phosphorus nitrides within the Be/B/Si/P/N system. However, it turns out that even refractory BN and Si_3N_4 can serve as starting materials, which thus is used as a starting point for the further development of an innovative preparative access to mixed phosphorus nitrides that grants the initial syntheses of α-BP_3N_6 and SiP_2N_4NH, as presented in Chapter 3 and 4.

The second part of this thesis is concerned with in situ and ex situ investigations on the high-pressure behavior of phosphorus nitrides. As described earlier in this chapter, elevated pressures are commonly

used in the preparative chemistry of P/N compounds. May be that is why the search for high-pressure phases of phosphorus nitrides has been associated with their preparation early on. Prior to this thesis, numerous high-pressure phases of PON, P_3N_5, PNNH, and P_4N_6NH were prepared in large volume presses at pressures < 16 GPa, certifying phosphorus nitrides a divers high-pressure polymorphism. It was further shown that the coordination number of phosphorus can be increased by high pressures, as illustrated by PN_5 polyhedra that have been reported for the γ-P_3N_5 and γ-P_4N_6NH structures. Moreover, the phase diagrams of P_3N_5, P_4N_6NH, BeP_2N_4, $LiPN_2$, and $CuPN_2$ were investigated by DFT calculations previously, some of them even within the megabar range (> 100 GPa). These theoretical studies provide information on the elastic properties of phosphorus nitrides and propose the formation of numerous high-pressure polymorphs that likely feature sixfold N-coordinated P as a structural motif within the pressure range of approximately p = 25–50 GPa. Such a PN_6 motif, however, has not been observed in any nitride material before, and thus is considered the missing link in structural chemistry of phosphorus nitrides.

Pressures > 25 GPa are easily accessible with diamond anvil cells that have been established as the gold standard method for in situ high-pressure investigations up to 150 GPa, with advanced setups even reaching maximum pressures > 1000 GPa, as briefly outlined in Chapter 2.[131] Moreover, sample heating and in situ microfocus single-crystal X-ray diffraction are possible, when diamond anvil cells are used in combination with laser-heating setups and 3rd generation synchrotron facilities. To examine the pressure-dependent behavior of phosphorus nitrides and to further accomplish the formation of the sought-after PN_6 motif, thus, laser-heated diamond anvil cells are used for in situ investigations up to a maximum pressure of about 50 GPa within this thesis. Besides the binary nitride P_3N_5 itself, silica-analog PON, unprecedented BP_3N_6 and Si_3N_4-related BeP_2N_4 appear as the most promising candidates, as outlined below.

PON is isoelectronic with SiO_2 and forms cristobalite-, moganite-, α-quartz- and coesite-analog phases up to a maximum pressure of 15.5 GPa. Considering this close structural relation, a stishovite-type form of PON that features $P(O/N)_6$ octahedra may be the most plausible PON phase at pressures > 16 GPa. Moreover, a stishovite-type PON may feature intriguing materials properties, as stishovite was considered the world's hardest oxide for quite some time.[132,133] Therefore, the phase diagram of PON is screened for a post-coesite polymorph at pressures up to 20 GPa in a large volume press, and the structural and elastic properties of this post-coesite PON are investigated in situ up to 40 GPa using a diamond anvil cell and synchrotron radiation, as presented in Chapter 5.

The development of an innovative preparative technique led to the preparation of the unprecedented α-BP_3N_6 (Chapter 3). The α-BP_3N_6 structure blends structural motifs of α-P_3N_5 and superhard c-BN,[134,135] raising the question on its structural and physical properties at high-pressures. Moreover, α-BP_3N_6 is considered to be a promising candidate to form a high-pressure polymorph that features sixfold N-coordinated of P, as the PN_6 motif is proposed at about 35–45 GPa in P_3N_5,[64,120] whereas an increased coordination number of B in BN may not be realized at pressures < 850 GPa.[136–138] The elastic properties of α-BP_3N_6 are therefore investigated in a diamond anvil cell up to a maximum pressure of about 42 GPa, at which further the formation of the high-pressure polymorph β-BP_3N_6 is induced by laser-heating. β-BP_3N_6 is the first phosphorus nitride that features sixfold N-coordinated P as a structural motif, as is presented in Chapter 6.

BeP_2N_4 crystallizes in the phenakite structure and thus, is isoelectronic and homeotypic with β-Si_3N_4. Similar to the spinel-type γ-Si_3N_4, phenakite-type BeP_2N_4 is considered to form a high-pressure phase with the regular spinel structure by numerous DFT calculations. This spinel-type BeP_2N_4 has further been predicted to show outstanding material properties that are comparable to those of γ-Si_3N_4. Chapter 7 is therefore attended to the preparation of spinel-type BeP_2N_4 and its pressure-dependent in situ investigation using laser-heated diamond anvil cells and synchrotron radiation.

In summary, the first part of this thesis addresses the development of a preparative high-pressure high-temperature technique that enables the synthesis of the mixed phosphorus nitrides BP_3N_6 (Chapter 3) and SiP_2N_4NH (Chapter 4). Subsequently, the high-pressure investigations of PON (Chapter 5), BP_3N_6 (Chapter 6), and BeP_2N_4 (Chapter 7) are presented, which provide unprecedented insights into the elastic and structural behavior of phosphorus nitrides. Finally, the reported results are summarized in Chapter 8 and discussed within their scientific context in Chapter 9. As the employment of high-pressure conditions is an essential approach of this thesis, however, a brief overview of state-of-the-art high-pressure techniques is priorly provided within the next Chapter.

1.6. References

[1] N. Wiberg, E. Wiberg, A. F. Holleman, *"Lehrbuch der anorganischen Chemie"*, Gruyter, Berlin, 101th Ed., **1995**.

[2] G. Markl, *"Minerale und Gesteine"*, Springer Berlin Heidelberg, Berlin, Heidelberg, **2015**.

[3] R. L. Rudnick, S. Gao in *Treatise on Geochemistry*, Elsevier, **2003**.

[4] E. Riedel, C. Janiak, *"Anorganische Chemie"*, De Gruyter, Berlin, New York, 8th Ed., **2011**.

[5] S. G. Bratsch, *"Standard Electrode Potentials and Temperature Coefficients in Water at 298.15 K"*, *J. Phys. Chem. Ref. Data* **1989**, *18*, 1.

[6] C. Blondel, *"Recent experimental achievements with negative ions"*, *Phys. Scr.* **1995**, *T58*, 31.

[7] J. Mazeau, F. Gresteau, R. I. Hall, A. Huetz, *"Energy and width of $N^-(^3P)$ from observation of its formation by dissociative attachment to N_2 and NO"*, *J. Phys. B: At. Mol. Phys.* **1978**, *11*, L557.

[8] L. F. Dobrzhinetskaya, R. Wirth, J. Yang, H. W. Green, I. D. Hutcheon, P. K. Weber, E. S. Grew, *"Qingsongite, natural cubic boron nitride: The first boron mineral from the Earth's mantle"*, *Am. Mineral.* **2014**, *99*, 764.

[9] K. Keil, C. A. Andersen, *"Occurrences of Sinoite, Si_2N_2O, in Meteorites"*, *Nature* **1965**, *207*, 745.

[10] M. R. Lee, S. S. Russell, J. W. Arden, C. T. Pillinger, *"Nierite (Si_3N_4), a new mineral from ordinary and enstatite chondrites"*, *Meteoritics* **1995**, *30*, 387.

[11] F. A. Bannister, *"Osbornite, meteoritic titanium nitride"*, *Mineral. Mag. J. Mineral. Soc.* **1941**, *26*, 36.

[12] O. Silvestri, *"Das Vorkommen des Stickstoffeisens unter den Fumarolen-Producten des Aetna und künstliche Darstellung dieser Verbindung"*, *Ann. Phys. Chem.* **1876**, *233*, 165.

[13] H. J. Axon, J. Kinder, C. W. Haworth, J. W. Horsfield, *"Carlsbergite, CrN, in troilite, FeS, of the Sikhote Alin meteoritic iron"*, *Mineral. Mag.* **1981**, *44*, 107.

[14] H. P. Nielsen, V. F. Buchwald, *"Roaldite, a new nitride in iron meteorites"*, *Lunar Planet. Sci.* **1982**, *12*, 1343.

[15] W. H. Baur, *"Occurrence of Nitride Nitrogen in Silicate Minerals"*, *Nature* **1972**, *240*, 461.

[16] J. W. Anthony, R. A. Bideaux, K. W. Bladh, M. C. Nichols, *"Handbook of Mineralogy"*, http://www.handbookofmineralogy.org/ (last visit: 10/05/2019).

[17] N. M. AB, *"The Nobel Prize in Physics 2014"*, https://www.nobelprize.org/prizes/physics/2014/summary/ (last visit: 10/05/2019).

[18] R.-J. Xie, N. Hirosaki, *"Silicon-based oxynitride and nitride phosphors for white LEDs—A review"*, *Acta Crystallogr. Sect. A: Found. Adv.* **2007**, *8*, 588.

[19] H. X. Jiang, J. Y. Lin, *"Nitride micro-LEDs and beyond–a decade progress review"*, *Opt. Express* **2013**, *21*, A475.

[20] X. L. Nguyen, T. N. N. Nguyen, V. T. Chau, M. C. Dang, *"The fabrication of GaN-based light emitting diodes (LEDs)"*, *Adv. Nat. Sci.: Nanosci. Nanotechnol.* **2010**, *1*, 25015.

[21] R. Mueller-Mach, G. Mueller, M. R. Krames, H. A. Höppe, F. Stadler, W. Schnick, T. Juestel, P. Schmidt, *"Highly efficient all-nitride phosphor-converted white light emitting diode"*, *Phys. Status Solidi A* **2005**, *202*, 1727.

[22] P. Pust, V. Weiler, C. Hecht, A. Tücks, A. S. Wochnik, A.-K. Henß, D. Wiechert, C. Scheu, P. J. Schmidt, W. Schnick, *"Narrow-band red-emitting $Sr[LiAl_3N_4]:Eu^{2+}$ as a next-generation LED-phosphor material"*, *Nat. Mater.* **2014**, *13*, 891.

[23] P. Pust, P. J. Schmidt, W. Schnick, *"A revolution in lighting"*, *Nat. Mater.* **2015**, *14*, 454.

[24] T. J. Flack, B. N. Pushpakaran, S. B. Bayne, *"GaN Technology for Power Electronic Applications: A Review"*, *J. Electron. Mater.* **2016**, *45*, 2673.

[25] K. Yuk, G. R. Branner, C. Cui in 60th International Midwest Symposium on Circuits and Systems, IEEE, Piscataway, NJ, **2017**.

[26] B. Kim, V. Z.-Q. Li in Compound Semiconductor Integrated Circuit Symposium, IEEE, Piscataway, NJ, **2017**.

[27] F. L. Riley, *"Silicon Nitride and Related Materials"*, *J. Am. Ceram. Soc.* **2000**, *83*, 245.

[28] J. Eichler, C. Lesniak, *"Boron nitride (BN) and BN composites for high-temperature applications"*, *J. Eur. Ceram. Soc.* **2008**, *28*, 1105.

[29] J. Kopac, P. Krajnik, *"High-performance grinding—A review"*, *J. Mater. Process. Technol.* **2006**, *175*, 278.

[30] F. K. Keßler, Y. Zheng, D. Schwarz, C. Merschjann, W. Schnick, X. Wang, M. J. Bojdys, *"Functional carbon nitride materials – design strategies for electrochemical devices"*, *Nat. Rev. Mater.* **2017**, *2*, 17030.

[31] F. Podjaski, J. Kröger, B. V. Lotsch, *"Toward an Aqueous Solar Battery: Direct Electrochemical Storage of Solar Energy in Carbon Nitrides"*, *Adv. Mater.* **2018**, *30*, 1705477.

[32] X. Wang, K. Maeda, A. Thomas, K. Takanabe, G. Xin, J. M. Carlsson, K. Domen, M. Antonietti, *"A metal-free polymeric photocatalyst for hydrogen production from water under visible light"*, *Nat. Mater.* **2009**, *8*, 76.

[33] J. Wen, J. Xie, X. Chen, X. Li, *"A review on γ-C_3N_4-based photocatalysts"*, *Appl. Surf. Sci.* **2017**, *391*, 72.

[34] A. Zakutayev, *"Design of nitride semiconductors for solar energy conversion"*, *J. Mater. Chem. A* **2016**, *4*, 6742.

[35] W. Schnick, J. Lücke, *"Lithium ion conductivity of $LiPN_2$ and Li_7PN_4"*, *Solid State Ionics* **1990**, *38*, 271.

[36] S. Zhao, Z. Fu, Q. Qin, *"A solid-state electrolyte lithium phosphorus oxynitride film prepared by pulsed laser deposition"*, *Thin Solid Films* **2002**, *415*, 108.

[37] E.-M. Bertschler, C. Dietrich, J. Janek, W. Schnick, *"$Li_{18}P_6N_{16}$ – A Lithium Nitridophosphate with Unprecedented Tricyclic $P_6N_{16}^{18-}$ Ions"*, *Chem. – Eur. J.* **2017**, *23*, 2185.

[38] E.-M. Bertschler, C. Dietrich, T. Leichtweiß, J. Janek, W. Schnick, *"Li^+ Ion Conductors with Adamantane-Type Nitridophosphate Anions β-$Li_{10}P_4N_{10}$ and $Li_{13}P_4N_{10}X_3$ with X = Cl, Br"*, *Chem. – Eur. J.* **2018**, *24*, 196.

[39] W. Schnick, *"Nitridosilicates, oxonitridosilicates (sions), and oxonitridoaluminosilicates (sialons)"*, *Int. J. Inorg. Mater.* **2001**, *3*, 1267.

[40] M. Zeuner, S. Pagano, W. Schnick, *"Nitridosilicates and oxonitridosilicates: from ceramic materials to structural and functional diversity"*, *Angew. Chem. Int. Ed.* **2011**, *50*, 7754; *Angew. Chem.* **2011**, *123*, 7898.

[41] S. D. Kloß, W. Schnick, *"Nitridophosphates: A Success Story of Nitride Synthesis"*, *Angew. Chem. Int. Ed.* **2019**, *58*, 7933; *Angew. Chem.* **2019**, *131*, 8015.

[42] K. Landskron, E. Irran, W. Schnick, *"High-Temperature High-Pressure Synthesis of the Highly Condensed Nitridophosphates NaP_4N_7, KP_4N_7, RbP_4N_7, and CsP_4N_7 and Their Crystal-Structure Determinations by X-ray Powder Diffraction"*, *Chem. – Eur. J.* **1999**, *5*, 2548.

[43] S. D. Kloß, W. Schnick, *"Rare-earth-metal nitridophosphates through high-pressure metathesis"*, *Angew. Chem. Int. Ed.* **2015**, *54*, 11250; *Angew. Chem.* **2015**, *127*, 11402.

[44] P. Bielec, W. Schnick, *"Increased Synthetic Control-Gaining Access to Predicted $Mg_2Si_5N_8$ and β-$Ca_2Si_5N_8$"*, *Angew. Chem. Int. Ed.* **2017**, *56*, 4810; *Angew. Chem.* **2017**, *129*, 4888.

[45] D. Hardie, K. H. Jack, *"Crystal Structures of Silicon Nitride"*, *Nature* **1957**, *180*, 332.

[46] A. Zerr, R. Riedel, G. Miehe, G. Serghiou, M. Schwarz, E. Kroke, H. Fueß, P. Kroll, R. Boehler, *"Synthesis of cubic silicon nitride"*, *Nature* **1999**, *400*, 340.

[47] J. Z. Jiang, F. Kragh, D. J. Frost, K. Ståhl, H. Lindelov, *"Hardness and thermal stability of cubic silicon nitride"*, *J. Phys.: Condens. Matter* **2001**, *13*, L515.

[48] S. Hampshire, *"Silicon nitride ceramics–review of structure, processing and properties"*, *J. Achiev. Mater. Manuf. Eng.* **2007**, *24*, 43.

[49] L. Boukbir, R. Marchand, Y. Laurent, P. Bacher, G. Roult, *"Preparation and time-of-flight neutron diffraction study of the cristobalite-type PON phosphorus oxynitride"*, *Ann. Chim. Fr.* **1989**, *14*, 475.

[50] J. Ronis, B. Bondars, A. Vitola, T. Millers, J. Schneider, F. Frey, *"Crystal Structure of the Phosphorus Oxynitride P_4ON_6"*, *J. Solid State Chem.* **1995**, *115*, 265.

[51] W. Schnick, J. Lücke, *"Darstellung, Kristallstruktur und IR-spektroskopische Untersuchung von Phosphor(V)-nitrid-imid, HPN_2"*, *Z. Anorg. Allg. Chem.* **1992**, *610*, 121.

[52] S. Horstmann, E. Irran, W. Schnick, *"Synthesis and Crystal Structure of Phosphorus(V) Nitride α-P_3N_5"*, *Angew. Chem. Int. Ed. Engl.* **1997**, *36*, 1873; *Angew. Chem.* **1997**, *109*, 1938.

[53] F. Liebau, *"Structural Chemistry of Silicates: Structure, Bonding, and Classification"*, Springer Berlin Heidelberg, Berlin, Heidelberg, **1985**.

[54] H.-P. Baldus, W. Schnick, J. Lücke, *"Silicon Phosphorus Nitride, the First Ternary Compound in the Silicon-Phosphorus-Nitrogen System"*, *Chem. Mater.* **1993**, *5*, 845.

[55] F. J. Pucher, S. R. Römer, F. W. Karau, W. Schnick, *"Phenakite-type BeP_2N_4 – a possible precursor for a new hard spinel-type material"*, *Chem. – Eur. J.* **2010**, *16*, 7208.

[56] J. Liebig, *"Nachtrag der Redaction, Briefwechsel mit F. Wöhler"*, *Ann. Pharm.* **1834**, *11*, 139.

[57] H. N. Stokes, *"Ueber Chlorphosphorstickstoff und zwei seiner homologen Verbindungen"*, *Ber. Dtsch. Chem. Ges.* **1895**, *28*, 437.

[58] T. N. Miller, A. V. Vitola, *"Neorganicheskie soedineniia fosfora s azotom (Inorganic Compounds of Phosphorus with Nitrogen)"*, Zinatne, **1986**.

[59] D. Corbridge, *"Phosphorus - An Outline of its Chemistry, Biochemistry and Technology"*, Elsevier, Amsterdam, Oxford, New York, Tokyo, 3rd Ed., **1990**.

[60] O. M. Uy, F. J. Kohl, K. D. Carlson, *"Dissociation energy of PN and other thermodynamic properties for the vaporization of P_3N_5"*, *J. Phys. Chem.* **1968**, *72*, 1611.

[61] R. Ahlrichs, M. Bär, H. S. Plitt, H. Schnöckel, *"The stability of PN and $(PN)_3$. Ab initio calculations and matrix infrared investigations"*, *Chem. Phys. Lett.* **1989**, *161*, 179.

[62] S. Ma, C. He, L. Z. Sun, H. Lin, Y. Li, K. W. Zhang, *"Stability of two-dimensional PN monolayer sheets and their electronic properties"*, *Phys. Chem. Chem. Phys.* **2015**, *17*, 32009.

[63] Z. Raza, I. Errea, A. R. Oganov, A. M. Saitta, *"Novel superconducting skutterudite-type phosphorus nitride at high pressure from first-principles calculations"*, *Sci. Rep.* **2014**, *4*, 5889.

[64] J. Dong, A. A. Kinkhabwala, P. F. McMillan, *"High-pressure polymorphism in phosphorus nitrides"*, *Phys. Status Solidi B* **2004**, *241*, 2319.

[65] B. C. Bunker, D. R. Tallant, C. A. Balfe, R. J. Kirkpatrick, G. L. Turner, M. R. Reidmeyer, *"Structure of Phosphorus Oxynitride Glasses"*, *J. Am. Ceram. Soc.* **1987**, *70*, 675.

[66] M. R. Reidmeyer, D. E. Day, *"Phosphorus oxynitride glasses"*, *J. Non-Cryst. Solids* **1995**, *181*, 201.

[67] A. Stock, B. Hoffmann, *"Die Einwirkung von Ammoniak auf Phosphorpentasulfid und der Phosphorstickstoff, P_3N_5"*, *Ber. Dtsch. Chem. Ges.* **1903**, *36*, 314.

[68] W. Schnick, J. Lücke, F. Krumeich, *"Phosphorus Nitride P_3N_5: Synthesis, Spectroscopic, and Electron Microscopic Investigations"*, *Chem. Mater.* **1996**, *8*, 281.

[69] S. Horstmann, E. Irran, W. Schnick, *"Phosphorus(V) Nitride Imide HP_4N_7: Synthesis from a Molecular Precursor and Structure Determination with Synchrotron Powder diffraction"*, *Angew. Chem. Int. Ed. Engl.* **1997**, *36*, 1992; *Angew. Chem.* **1997**, *109*, 2085.

[70] A. Weiss, A. Weiss, *"Über Siliciumchalkogenide. VI. Zur Kenntnis der faserigen Siliciumdioxyd-Modifikation"*, *Z. Anorg. Allg. Chem.* **1954**, *276*, 95.

[71] R. Marchand, F. Tessier, A. Le Sauze, N. Diot, *"Typical features of nitrogen in nitride-type compounds"*, *Int. J. Inorg. Mater.* **2001**, *3*, 1143.

[72] J. B. Mann, T. L. Meek, L. C. Allen, *"Configuration Energies of the Main Group Elements"*, *J. Am. Chem. Soc.* **2000**, *122*, 2780.

[73] T. Moritani, K. Kuchitsu, J. Morino, *"Molecular structures of phosphoryl fluoride, phosphoryl chloride, and thiophosphoryl chloride studied by gas electron diffraction"*, *Inorg. Chem* **1971**, *10*, 344.

[74] M. Feller, K. Lux, A. Kornath, *"Crystal Structure and Spectroscopic Investigations of POF_3"*, *Z. Anorg. Allg. Chem.* **2014**, *640*, 53.

[75] H. C. J. de Decker, C. H. Mac Gillavry, *"Die Krystallstruktur des Flüchtigen Metastabilen Phosphorpentoxyds"*, *Recl. Trav. Chim. Pays-Bas* **1941**, *60*, 153.

[76] R. H. Wentorf, *"Cubic Form of Boron Nitride"*, *J. Chem. Phys.* **1957**, *26*, 956.

[77] P. Eckerlin, *"Die Kristallstruktur von $BeSiN_2$"*, *Z. Anorg. Allg. Chem.* **1967**, *353*, 225.

[78] M. v. Stackelberg, R. Paulus, *"Untersuchungen über die Kristallstruktur der Nitride und Phosphide zweiwertiger Metalle"*, *Z. Phys. Chem.* **1933**, *22B*, 305.

[79] J. Lima-de-Faria, E. Hellner, F. Liebau, E. Makovicky, E. Parthé, *"Nomenclature of inorganic structure types. Report of the International Union of Crystallography Commission on Crystallographic Nomenclature Subcommittee on the Nomenclature of Inorganic Structure Types"*, *Acta Crystallogr. Sect. A: Found. Adv.* **1990**, *46*, 1.

[80] U. Müller, *"Anorganische Strukturchemie"*, Vieweg + Teubner, Wiesbaden, 6th Ed., **2008**.

[81] W. Schnick, J. Lücke, *"Synthesis and crystal structure of lithium phosphorus nitride Li_7PN_4: The first compound containing isolated PN_4-tetrahedra"*, *J. Solid State Chem.* **1990**, *87*, 101.

[82] F. Karau, W. Schnick, *"A nitridic clathrate: $P_4N_4(NH)_4(NH_3)$"*, *Angew. Chem. Int. Ed.* **2006**, *45*, 4505; *Angew. Chem.* **2006**, *118*, 4617.

[83] S. J. Sedlmaier, V. R. Celinski, J. Schmedt auf der Günne, W. Schnick, *"High-pressure synthesis and structural investigation of $H_3P_8O_8N_9$: a new phosphorus(V) oxonitride imide with an interrupted framework structure"*, *Chem. – Eur. J.* **2012**, *18*, 4358.

[84] H.-P. Baldus, M. Jansen, *"Novel High-Performance Ceramics—Amorphous Inorganic Networks from Molecular Precursors"*, *Angew. Chem. Int. Ed. Engl.* **1997**, *36*, 328; *Angew. Chem.* **1997**, *109*, 338.

[85] M. Jansen, J. C. Schön, L. van Wüllen, *"The route to the structure determination of amorphous solids: a case study of the ceramic $Si_3B_3N_7$"*, *Angew. Chem. Int. Ed.* **2006**, *45*, 4244; *Angew. Chem.* **2006**, *118*, 4350.

[86] H. Lux, *""Säuren" und "Basen" im Schmelzfluss: Die Bestimmung der Sauerstoffionen-Konzentration"*, *Z. Elektrochem. Angew. Phys. Chem.* **1939**, *45*, 303.

[87] H. Flood, T. Förland, *"The acidic and basic properties of oxides"*, *Acta Chem. Scand.* **1947**, *1*, 592.

[88] A. W. Garrison, C. E. Boozer, *"The acid-catalyzed hydrolysis of a series of phosphoramidates"*, *J. Am. Chem. Soc.* **1968**, *90*, 3486.

[89] T. A. Modro, D. H. Graham, *"Phosphoric Amides. 3.1 Acidic Cleavage of the Phosphorus-Nitrogen Bond in Acyclic and Cyclic Phosphoramidates"*, *J. Org. Chem.* **1981**, *46*, 1923.

[90] R. Greenhalgh, J. R. Blanchfield, *"The Cleavage of Phosphorus to Nitrogen Bonds with Hydogen Fluoride"*, *Can. J. Chem.* **1965**, *44*, 501.

[91] Z. Skrowaczewska, P. Mastalerez, *"O dzialaniu chlorowcowodorów na wiazanie P–N niektórych amidów pochodnych kwasu fosforowego (The action of hydrogen halides upon the P–N bond of some derivates of phosphoric acid)"*, *Roczniki Chem.* **1955**, *29*, 415.

[92] S. J. Sedlmaier, E. Mugnaioli, O. Oeckler, U. Kolb, W. Schnick, *"SrP_3N_5O: a highly condensed layer phosphate structure solved from a nanocrystal by automated electron diffraction tomography"*, *Chem. – Eur. J.* **2011**, *17*, 11258.

[93] S. Correll, O. Oeckler, N. Stock, W. Schnick, *"$Li_xH_{12-x-y+z}P_{12}O_yN_{24-y}Cl_z$ – An Oxonitridophosphate with a Zeolite-like Framework Structure Composed of 3-Rings: NPO"*, *Angew. Chem. Int. Ed.* **2003**, *42*, 3549; *Angew. Chem* **2003**, *115*, 3674.

[94] S. J. Sedlmaier, M. Döblinger, O. Oeckler, J. Weber, J. Schmedt auf der Günne, W. Schnick, *"Unprecedented zeolite-like framework topology constructed from cages with 3-rings in a barium oxonitridophosphate: NPT"*, *J. Am. Chem. Soc.* **2011**, *133*, 12069.

[95] H. Huppertz, *"Multianvil high-pressure / high-temperature synthesis in solid state chemistry"*, *Z. Kristallogr.* **2004**, *219*, 330.

[96] A. Marchuk, F. J. Pucher, F. W. Karau, W. Schnick, *"A high-pressure polymorph of phosphorus nitride imide"*, *Angew. Chem. Int. Ed.* **2014**, *53*, 2469; *Angew. Chem.* **2014**, *126*, 2501.

[97] A. Marchuk, V. R. Celinski, J. Schmedt auf der Günne, W. Schnick, *"$MH_4P_6N_{12}$ (M = Mg, Ca): new imidonitridophosphates with an unprecedented layered network structure type"*, *Chem. – Eur. J.* **2015**, *21*, 5836.

[98] S. Vogel, W. Schnick, *"SrP_3N_5NH: A Framework-Type Imidonitridophosphate Featuring Structure-Directing Hydrogen Bonds"*, *Chem. – Eur. J.* **2018**, *24*, 14275.

[99] A. Neuhaus, *"Structural Behavior, and Valence State of Inorganic Matter in the Realm of Higher and Highest Pressure"*, *Chimia* **1964**, *18*, 93.

[100] W. Kleber, K.-T. Wilke, *"Synthese und Kristallchemie anorganischer Stoffe bei hohen Drücken und Temperaturen"*, *Krist. Techn.* **1969**, *4*, 165.

[101] C. Cazorla, T. Gould, *"Polymorphism of bulk boron nitride"*, *Sci. Adv.* **2019**, *5*, eaau5832.

[102] B. Kiefer, S. R. Shieh, T. S. Duffy, T. Sekine, *"Strength, elasticity, and equation of state of the nanocrystalline cubic silicon nitride γ-Si_3N_4 to 68 GPa"*, *Phys. Rev. B: Condens. Matter Mater. Phys.* **2005**, *72*, 14102.

[103] A. Zerr, M. Kempf, M. Schwarz, E. Kroke, M. Göken, R. Riedel, *"Elastic Moduli and Hardness of Cubic Silicon Nitride"*, *J. Am. Ceram. Soc.* **2002**, *85*, 86.

[104] K. J. Kingma, R. E. G. Pacalo, P. F. McMillan, *"High-Pressure Stability of the Cristobalite Framework in PON and PN(NH)"*, *Eur. J. Solid State Inorg. Chem.* **1997**, *34*, 679.

[105] K. J. Kingma, R. E. Gerald Pacalo, P. F. McMillan in *Properties of the earth and planetary materials at high pressure and temperature*, Geophysical monograph, American Geophysical Union, Washington, **1998**.

[106] C. Chateau, J. Haines, J.-M. Léger, A. LeSauze, R. Marchand, *"A moganite-type phase in the silica analog phosphorus oxynitride"*, *Am. Mineral.* **1999**, *84*, 207.

[107] J. Haines, C. Chateau, J.-M. Léger, A. Le Sauze, N. Diot, R. Marchand, S. Hull, *"Crystal structure of moganite-type phosphorus oxynitride: Relationship to other twinned-quartz-based structures"*, *Acta Cryst.* **1999**, *55*, 677.

[108] J.-M. Léger, J. Haines, L. S. de Oliveira, C. Chateau, A. Le Sauze, R. Marchand, S. Hull, *"Crystal structure and high pressure behaviour of the quartz-type phase of phosphorus oxynitride PON"*, *J. Phys. Chem. Solids* **1999**, *60*, 145.

[109] D. Baumann, S. J. Sedlmaier, W. Schnick, *"An unprecedented AB_2 tetrahedra network structure type in a high-pressure phase of phosphorus oxonitride (PON)"*, *Angew. Chem. Int. Ed.* **2012**, *51*, 4707; *Angew. Chem.* **2012**, *124*, 4784.

[110] A. Le Bail, *"Databases of virtual inorganic crystal structures and their applications"*, *Phys. Chem. Chem. Phys.* **2010**, *12*, 8521; (entry no. 3102887).

[111] D. Baumann, R. Niklaus, W. Schnick, *"A high-pressure polymorph of phosphorus oxonitride with the coesite structure"*, *Angew. Chem. Int. Ed.* **2015**, *54*, 4388; *Angew. Chem.* **2015**, *127*, 4463.

[112] M. Bykov, E. Bykova, M. Hanfland, H.-P. Liermann, R. K. Kremer, R. Glaum, L. S. Dubrovinsky, S. van Smaalen, *"High-Pressure Phase Transformations in $TiPO_4$: A Route to Pentacoordinated Phosphorus"*, *Angew. Chem. Int. Ed.* **2016**, *55*, 15053; *Angew. Chem.* **2016**, *128*, 15277.

[113] J. Pellicer-Porres, A. M. Saitta, A. Polian, J. P. Itie, M. Hanfland, *"Six-fold-coordinated phosphorus by oxygen in $AlPO_4$ quartz homeotype under high pressure"*, *Nat. Mater.* **2007**, *6*, 698.

[114] A. Pakhomova, G. Aprilis, M. Bykov, L. Gorelova, S. S. Krivovichev, M. P. Belov, I. A. Abrikosov, L. Dubrovinsky, *"Penta- and hexa-coordinated beryllium and phosphorus in high-pressure modifications of $CaBe_2P_2O_8$"*, *Nat. Commun.* **2019**, *10*, 768.

[115] D. Baumann, *"Novel Phosphorus (Oxo)Nitrides at Extreme Conditions"*, Dissertation, Ludwig-Maximilians-Universität, Munich, **2015**.

[116] D. Baumann, W. Schnick, *"High-pressure polymorph of phosphorus nitride imide HP_4N_7 representing a new framework topology"*, *Inorg. Chem.* **2014**, *53*, 7977.

[117] K. Landskron, H. Huppertz, J. Senker, W. Schnick, *"High-Pressure Synthesis of γ-P_3N_5 at 11 GPa and 1500 °C in a Multianvil Assembly: A Binary Phosphorus(V) Nitride with a Three-Dimensional Network Structure from PN_4 Tetrahedra and Tetragonal PN_5 Pyramids"*, *Angew. Chem. Int. Ed.* **2001**, *40*, 2643, *Angew. Chem.* **2001**, *113*, 2713.

[118] D. Baumann, W. Schnick, *"Pentacoordinate phosphorus in a high-pressure polymorph of phosphorus nitride imide $P_4N_6(NH)$"*, *Angew. Chem. Int. Ed.* **2014**, *53*, 14490; *Angew. Chem.* **2014**, *126*, 14718.

[119] H. W. Roesky, *"Preparation of Hexaazidophosphates"*, *Angew. Chem. Int. Ed. Engl.* **1967**, *6*, 637; *Angew. Chem.* **1967**, *79*, 651.

[120] P. Kroll, W. Schnick, *"A Density Functional Study of Phosphorus Nitride P_3N_5: Refined Geometries, Properties, and Relative Stability of α-P_3N_5 and γ-P_3N_5 and a Further Possible High-Pressure Phase δ-P_3N_5 with Kyanite-Type Structure"*, *Chem. – Eur. J.* **2002**, *8*, 3530.

[121] A. Morales-García, E. del Corro, *"Revealing the local properties of β-HP_4N_7, a promising candidate for high pressure synthesis of new materials"*, *Mater. Res. Express* **2015**, *2*, 45904.

[122] M. Schwarz, G. Miehe, A. Zerr, E. Kroke, B. T. Poe, H. Fueß, R. Riedel, *"Spinel-Si_3N_4: Multi-Anvil Press Synthesis and Structural Refinement"*, *Adv. Mater.* **2000**, *12*, 883.

[123] N. Nishiyama, J. Langer, T. Sakai, Y. Kojima, A. Holzheid, N. A. Gaida, E. Kulik, N. Hirao, S. I. Kawaguchi, T. Irifune, Y. Ohishi, *"Phase relations in silicon and germanium nitrides up to 98 GPa and 2400 °C"*, *J. Am. Ceram. Soc.* **2019**, *102*, 2195.

[124] W. Y. Ching, S. Aryal, P. Rulis, W. Schnick, *"Electronic structure and physical properties of the spinel-type phase of BeP_2N_4 from all-electron density functional calculations"*, *Phys. Rev. B* **2011**, *83*, 155109.

[125] Y.-C. Ding, B. Xiao, *"Electronic Structure, Mechanical Properties and Intrinsic Hardness of a New Superhard Material BeP_2N_4"*, *Acta Phys.-Chim. Sin.* **2011**, *27*, 1621.

[126] M. Zhang, H. Yan, Y. Zhao, Q. Wei, *"Mechanical properties and atomistic deformation mechanism of spinel-type BeP_2N_4"*, *Comput. Mater. Sci.* **2014**, *83*, 457.

[127] J. Lv, X. Yang, D. Xu, Y.-X. Huang, H.-B. Wang, H. Wang, *"High-pressure polymorphs of $LiPN_2$: A first-principles study"*, *Front. Phys.* **2018**, *13*, 9592.

[128] D. Xu, B. Li, T. Iitaka, Q. Cui, H. Wang, H. Wang, *"Exotic high-pressure behavior of double nitride $CuPN_2$"*, *Comput. Mater. Sci.* **2018**, *152*, 217.

[129] N. Nishiyama, R. Ishikawa, H. Ohfuji, H. Marquardt, A. Kurnosov, T. Taniguchi, B.-N. Kim, H. Yoshida, A. Masuno, J. Bednarcik, E. Kulik, Y. Ikuhara, F. Wakai, T. Irifune, *"Transparent polycrystalline cubic silicon nitride"*, *Sci. Rep.* **2017**, *7*, 44755.

[130] I. Tanakaa, F. Oba, T. Sekine, E. Ito, A. Kubo, K. Tatsumi, H. Adachi, T. Yamamoto, *"Hardness of cubic silicon nitride"*, *J. Mater. Res.* **2002**, *17*, 731.

[131] N. Dubrovinskaia, L. Dubrovinsky, N. A. Solopova, A. Abakumov, S. Turner, M. Hanfland, E. Bykova, M. Bykov, C. Prescher, V. B. Prakapenka, S. Petitgirard, I. Chuvashova, B. Gasharova, Y.-L. Mathis, P. Ershov, I. Snigireva, A. Snigirev, *"Terapascal static pressure generation with ultrahigh yield strength nanodiamond"*, *Sci. Adv.* **2016**, *2*, 1.

[132] J.-M. Léger, J. Haines, M. Schmidt, J. P. Petitet, A. S. Pereira, J. A. H. da Jornada, *"Discovery of hardest known oxide"*, *Nature* **1996**, *383*, 401.

[133] L. S. Dubrovinsky, N. A. Dubrovinskaia, V. Swamy, J. Muscat, N. M. Harrison, R. Ahuja, B. Holm, B. Johansson, *"Materials science. The hardest known oxide"*, *Nature* **2001**, *410*, 653.

[134] F. Datchi, A. Dewaele, Y. Le Godec, P. Loubeyre, *"Equation of state of cubic boron nitride at high pressures and temperatures"*, *Phys. Rev. B: Condens. Matter Mater. Phys.* **2007**, *75*, 127.

[135] M. T. Yeung, R. Mohammadi, R. B. Kaner, *"Ultraincompressible, Superhard Materials"*, *Annu. Rev. Mater. Res.* **2016**, *46*, 465.

[136] R. M. Wentzcovitch, M. L. Cohen, P. K. Lam, *"Theoretical study of BN, BP, and BAs at high pressures"*, *Phys. Rev. B* **1987**, *36*, 6058.

[137] N. E. Christensen, I. Gorczyca, *"Optical and structural properties of III-V nitrides under pressure"*, *Phys. Rev. B: Condens. Matter Mater. Phys.* **1994**, *50*, 4397.

[138] L. Hromadová, R. Martoňák, *"Pressure-induced structural transitions in BN from ab initio metadynamics"*, *Phys. Rev. B: Condens. Matter Mater. Phys.* **2011**, *84*, 241252.

2. High-Pressure Techniques: State of the Art

High-pressure is a potent approach for the synthesis and structural examination of phosphorus nitrides. Although, the high-pressure methodology is not further developed or improved in this thesis, a brief digression on high-pressure techniques is provided below, summarizing the current state of the art, as well as briefly illustrating the specific setups that were used over the course of this PhD project.

The development of high-pressure techniques originates from the desire to understand processes in the Earth's interior, and thus, the methodology is the particular merit of scientists working in the fields of earth and planetary sciences, mineralogy, and materials sciences.[1] High-pressure, however, is a versatile tool in chemistry, as well. Considering simple thermodynamics, synthetic chemists are limited by three variables when screening the energy hypersurface, namely temperature, mole fraction, and pressure. Despite being seldom used in explorative chemistry in the past, high-pressure techniques gain more traction nowadays, because it allows control of the third thermodynamic parameter, *pressure*.[2–4] Within this thesis, high-pressure conditions are used to facilitate unprecedented chemical reactions and to examine the pressure-dependent structural behavior and polymorphism of phosphorus nitrides in situ.

By the basic physical principle, a pressure p is generated by a force F that is applied upon an area A (Equation 2.1, Figure 2.1a). Therefore, the pressure increases for high forces and small areas, illustrating the two fundamental ideas behind the generation of high pressures, namely the maximization of the force F, and the minimization of the area A.

$$p = F/A \tag{2.1}$$

In everyday life, pressures are usually quantified in bar. Taking the SI unit system as a basis, however, the pressure is given in Newton (N) per square meter (m^2) that equals one Pascal (Pa). Within high-pressure sciences, gigapascal (GPa) has been established the most common unit of pressure, with 1 GPa corresponding to 10^4 bar, as illustrated in Figure 2.1b.

There are multiple methods that use elevated pressures for chemical reactions and phase transitions.* While pressure ampoules reach small gas pressures of several bar, autoclaves and hot isostatic presses are used for the generation of moderate pressures, but are still limited to several tenths of 1 GPa. To generate high static pressures (> 1 GPa) large volume presses and diamond anvil cells are the established techniques in high-pressure sciences. Within the last decades, successive improvements and the development of new setups have repeatedly pushed the boundary of the maximum pressure that can be realized by large volume presses and diamond anvil cells.[5,6] Today's high-end techniques, therefore, enable maximum pressures of > 100 GPa in large volume presses[7,8] and about 1000 GPa in diamond anvil cells (Figure 2.1b).[9] Routine large volume presses, however, usually operate below 40 GPa, and diamond anvil cells are commonly used up to 150 GPa in standard experiments. Both, large volume presses and diamond anvil cells have been used over the course of this PhD project and thus, are separately outlined in more detail below.

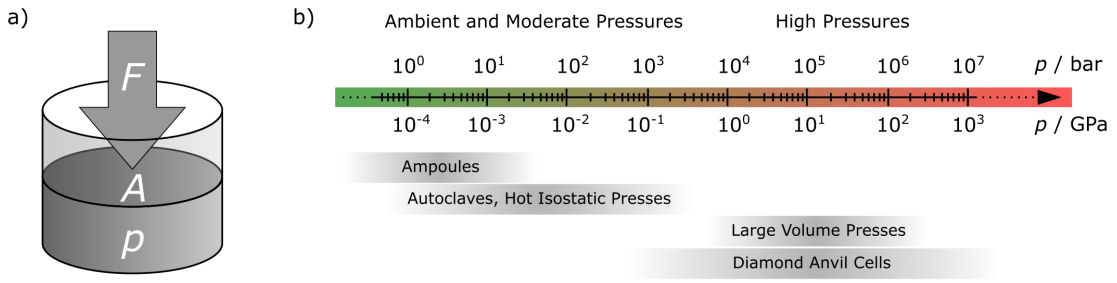

Figure 2.1.: A schematic illustration of the physical description of pressure $p = F/A$ (a) and the logarithmic pressure scale in bar and GPa with pressure ranges of ambient-, moderate-, and high-pressure techniques (b).

In the history of *large volume presses* many techniques for high-pressure generation have been developed, such as the Piston cylinder, the Belt apparatus, the Paris-Edinburgh press, and the multianvil technique. The achievable force that a large volume press can provide scales with its hydraulic system, which usually limits the maximum load to about 1000–3000 t, corresponding to a maximum force of about 10–30 MN. Advanced setups, however, can also provide loads of 5000–8000 t (50–80 MN),[10,11] and even a 50 000 t press had been used for high-pressure research.†[5] The maximum sample pressure,

*Within this thesis, only static pressure techniques are discussed and employed. Dynamic pressures, however, may be considered, when a comprehensive overview is attended.

†Even higher loads are obtained by forging presses that, however, may not be discussed in the context of high-pressure sciences.

however, is strongly affected by the compression geometry and the sample size. State-of-the-art large volume presses commonly employ the Kawai-type multianvil technique that uses an octahedron-within-cubes payload for the generation of quasi-hydrostatic pressures (Figure 2.2c, d).[12] Here, the uniaxial pressure of a downstroke hydraulic press is distributed to six first stage anvils by guiding steel components, creating a cubic compression space, as exemplary shown for a modified Walker module in Figure 2.2b.[13] Eight cubes with truncated edges further serve as second stage anvils that compress an octahedron, which contains the sample and an internal resistance heating system. These assemblies are characterized by the octahedron edge length (OEL) and the truncated edge length (TEL) of the second stage anvils. Typical assemblies are 25/17, 18/11, 14/8, 10/5, and 8/3 (OEL/TEL in millimeter), but even smaller assemblies can be used for maximum pressure generation.[14] While the octahedron is commonly made out of Cr_2O_3-doped MgO, the second stage anvils may consist of sintered tungsten carbide (WC) or sintered diamond (SD), affecting the pressure performance of the large volume press.

Using tapered second stage anvils of WC and a 5.7/1.5 assembly, the maximum pressure in a Kawai-type multianvil press was recently expanded from 40–50 GPa[15,16] to about 65 GPa,[17] and pressures > 100 GPa could be realized, using SD anvils and a 4.1/1.0 assembly.[7] It was further shown that even pressures of about 125 GPa can be generated in large volume presses, when a set of third stage anvils (nano-polycrystalline diamond, NPD) is introduced into the octahedron.[8] These advanced setups, though pushing the benchmark of maximum pressures, impaired the sample size to $\ll 1\,\mathrm{mm}^3$, which does not meet the demand of preparative chemistry. Suitable sample amounts, however, are accessible employing routine Kawai-type multianvil setups that grant sample volumes of several $1\,\mathrm{mm}^3$ at maximum pressures of about 25 GPa.[18] These samples are commonly analyzed ex situ at ambient conditions after pressure-quenching. Advanced large volume press setups that are compatible with in situ techniques, however, are installed at the synchrotron facilities ESRF (ID6),[19] APS (GSECARS),[20] Soleil (PSICHÉ),[21] and DESY (P61B, under construction),[22] for instance.

Within this thesis two identically constructed large volume presses (Voggenreiter, Mainleus, Germany) were used that had been installed in the Schnick group in 1999 and 2007.[18] Using one hydraulic cylinder, each of these downstroke presses can generate a maximum load of 1000 t, corresponding to a uniaxial force of almost 10 MN (Figure 2.2a). A modified Walker module was used to enable a Kawai-type octahedron-within-cubes compression assembly, as illustrated in Figure 2.2b, c.[12,13] The maximum pressure of this setup is about 25 GPa, 16 GPa, and 10 GPa for the 10/5, the 14/8, and the 18/11 assembly,

respectively, and the electronic resistance heating system uses graphite furnaces for the generation of a maximum temperature of about 1500 °C.[18] Owing to a successive conversion into diamond, the employment of graphite is limited to about 10 GPa and 1500 °C, but $LaCrO_3$ can serve as a furnace material for more extreme conditions.[18] More detailed information on the assembly preparation and the execution of high-pressure high-temperature syntheses is provided in literature,[2,18] as well as in the Supporting Information within this thesis (Chapters A–E).

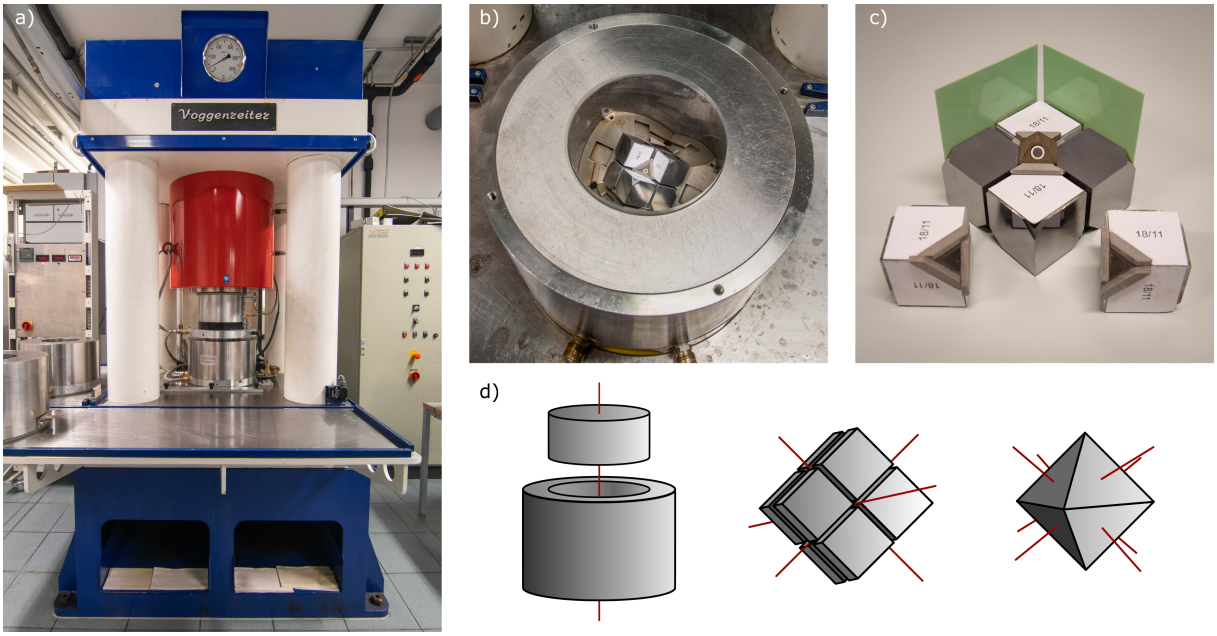

Figure 2.2.: Exemplary illustration of a 1000 t (10 MN) large volume press that is used for high-pressure high-temperature reactions up to a maximum pressure of about 25 GPa (a). A modified Walker module with the Kawai-type octahedron-within-cubes payload (b, c) grants the generation of quasi-hydrostatic pressures by an equal pressure distribution along various spatial axes (d, red lines).

Today's highest static pressures can be generated by *diamond anvil cells*, which have been developed and improved for more than half a century.[6] A detailed overview of the design and the operation of diamond anvil cells is provided in literature.[23,24] This section, therefore, focuses on recent developments and improvements, and briefly describes the diamond anvil cell that was used for in situ studies over the course of this PhD project.

Diamond anvil cells are commonly used for the generation of static pressures in the range of 0.1–150 GPa, with advanced setups even reaching the terapascal boundary.[6,9] In contrast to the sophisticated

octahedron-within-cubes payload of multianvil presses, the basic design of diamond anvil cells is rather simple, but preparation and operation are complicated due to the small dimensions of the setup. The simplest setups use two diamond anvils with flat 100–500 µm culets that are mounted on loadable seats, typically made out of tungsten carbide (WC). The diamonds are separated by a drilled-thru metallic gasket that forms the pressure chamber, which usually contains the sample, an internal pressure standard, and a pressure transmitting medium. Here, ruby spheres commonly serve as the pressure standard,[25–27] but also elements or simple compounds such as Ne, Au, Pt, or NaCl can be used.[28] To increase pressure, the two opposed diamond anvils are driven towards each other by an external membrane- or screw-induced force, compressing the sample chamber between the culets (Figure 2.3a).

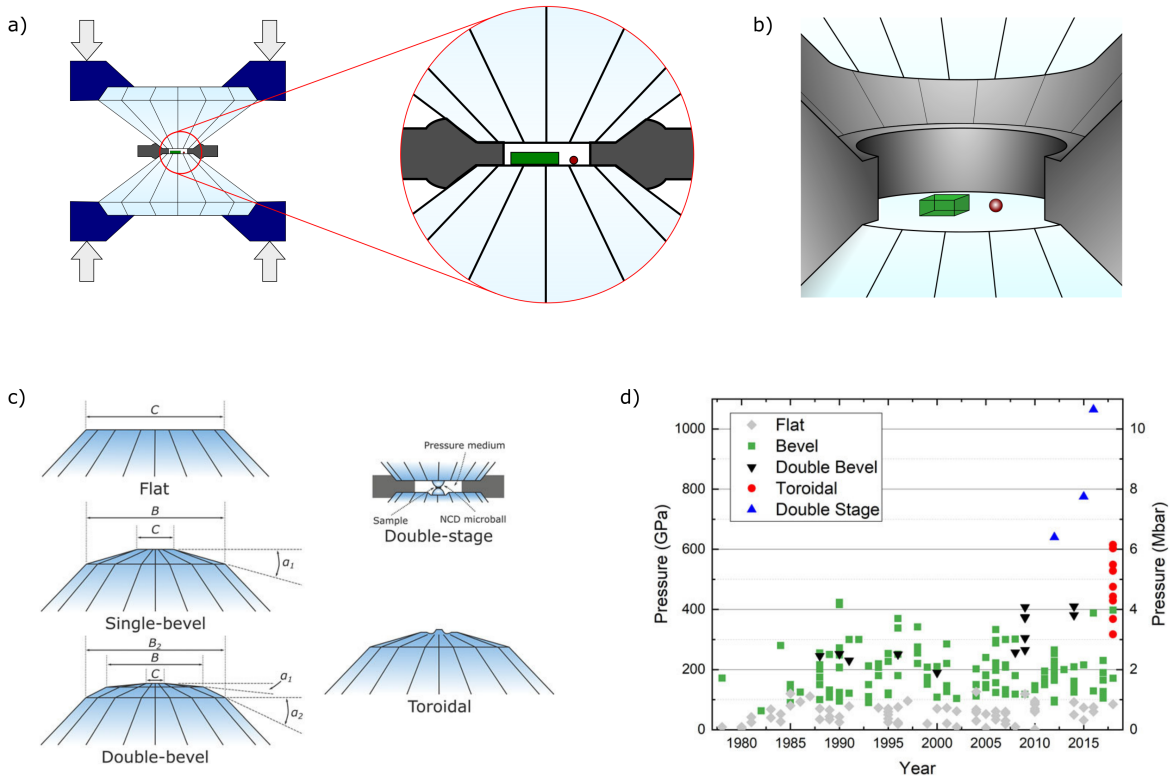

Figure 2.3.: Schematic illustration of a diamond anvil cell with flat diamond anvils in light blue, seats in dark blue, metallic gasket in gray, sample in green and ruby sphere in red (a, b). The development of advanced diamond anvil designs (c) repeatedly pushed the boundary of the maximum pressure in diamond anvil cells (d). Partially adapted with permission from Reference [29].

Considering Equation 2.1, the pressure in a diamond anvil cell can be maximized by either decreasing the culet area or increasing the external force. The maximum force, however, is restricted by the mechanical strength of the seats and the diamond anvils, and may not exceed 10 kN.[23,30] Therefore, recent developments focused on the design of the diamond anvils, accomplishing the balance between the miniaturization of the culet and the stabilization of the sample.[29] Using diamond anvils with flat culets, the maximum pressure is limited to about 150 GPa, while the employment of single- or double-beveled diamond anvils grant pressures up to 400 GPa (Figure 2.3c, d).[30,31] The highest pressures, however, have been generated using focused ion beam milled toroidal diamond anvils,[32,33] or double-stage diamond anvil cells,[34] with the latter breaking the 1000 GPa benchmark for the first time.[9]

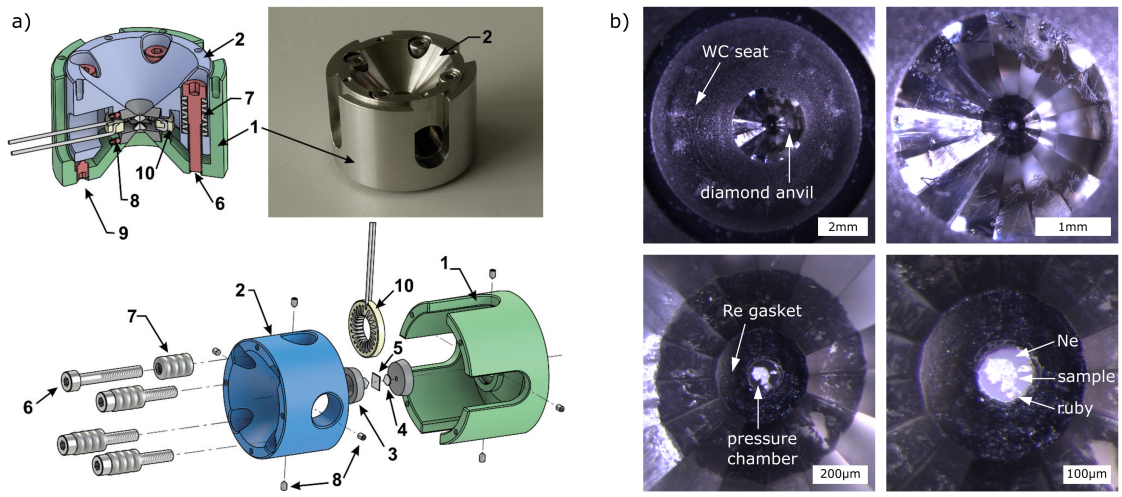

Figure 2.4.: A sketch of a BX90 diamond anvil cell with inner and outer steel components (1, 2), WC seats (3), diamond anvils (4), metallic gasket (5), screws (6), conical spring washers (7), setscrews for diamond alignment (8), safety screw (9), and optional resistive heater (10), as adapted with permission from Reference [35] (a) and microphotographs taken through a BX90 cell that is loaded with a polycrystalline sample, ruby spheres and Ne (b).

Despite of the high static pressure range (0.1–1000 GPa),[6,9] an additional advantage of diamond anvil cells is the transparency of diamond in a broad electromagnetic spectrum, which enables the in situ usage of preparative and analytic techniques, as well as the optical visualization of the sample. Sample heating, for instance, is a quite routine procedure, which can be performed using a resistive heating system[36] or a laser heating setup,[37,38] but also internal-resistive heated diamond-anvil cells have recently been developed.[39] Moreover, advanced analytic techniques, such as Raman spectroscopy,[40,41] synchrotron

Mössbauer spectroscopy,[42–45] NMR spectroscopy,[46–48] and laser-ultrasonics,[49] as well as electrical and magnetic measurements[50–52] have been adapted for the use in diamond anvil cells. The most powerful achievement, however, is the development of in situ single-crystal X-ray diffraction at high-pressure conditions, which is usually performed at synchrotron facilities, as discussed below.[35,53–58]

The high-pressure experiments in diamond anvil cells and the in situ synchrotron XRD investigations over the course of this PhD project were performed in collaboration with the working groups of Natalia Dubrovinskaia and Leonid Dubrovinsky, involving particular contributions of Elena Bykova and Maxim Bykov. BX90 diamond anvil cells and flat Boehler-Almax-type diamond anvils were employed, as illustrated in Figure 2.4a.[35,53] Herein, culets of 250 µm deemed sufficient for the generation of pressures up to about 50 GPa, and a wide opening angle ($2\theta = 40°$) granted a high resolution in synchrotron XRD experiments.

Quite a lot routine in situ XRD experiments in diamond anvil cells investigate molecular crystals. These studies are usually performed at moderate pressures and thus, provide sample amounts that can be probed at in-house diffractometers, at which the cell is mounted on a standard goniometer.[59,60] It is, however, apparent that the miniaturization of the pressure chamber at high pressures causes a miniaturization of the sample, which necessitates X-ray radiation of small focus and high brilliance. Therefore, in situ XRD studies at high- and ultra-high-pressure conditions are performed at 3rd generation synchrotrons that are currently considered the world's most brilliant photon sources. The synchrotron facilities further provide specialized extreme conditions beamlines that support diamond anvil cell setups and specific sample environments, such as heating systems, magnetic fields, or cryostats. Respective beamlines are, for instance, P02.2 at PETRA III, DESY (Hamburg, Germany),[61,62] ID27 at the ESRF (Grenoble, France),[63] I15 at the Diamond Light Source (Didcot, UK),[64] 12.2.2 at the ALS (Berkeley, USA),[65,66] 13-ID-D at the APS (Argonne, USA),[67] and PSICHÉ at Soleil (Gif-sur-Yvette Cedex, France).[21] The capabilities and the advantages of such extreme conditions beamlines are briefly outlined below. As most of the in situ experiments of this thesis were performed at P02.2 (PETRA III, DESY), this setup will be used as an example (Figure 2.5).[38,61,62]

PETRA III is a 3rd generation light source that operates at 6–8 GeV and the extreme conditions beamline P02.2 uses a high-energy undulator U23 for the generation of synchrotron radiation within an energy range of 25.6–60.0 keV, corresponding to wavelengths between 0.484 and 0.207 Å, respectively.[61] The beam can be focused by a Kirkpatrick–Baez mirror system to about $2\times2\,\mu m^2$ and even a submicron

beam has been established at P02.2, recently.[62] The diamond anvil cell is mounted in front of a fast 2D detector (Perkin Elmer, XRD1621) and single-crystal datasets can be collected by omega step scans (rotation around one axis). Moreover, P02.2 provides multiple-purpose optics that grant on-line laser heating from both sides (200 W NIR laser), on-line ruby fluorescence measurements, and optical imaging. The beamline further features a second hutch for general purpose experiments, in which additional sample environments, such as a resistive heating, a cryostat and a Paris-Edinburgh cell are provided.[62]

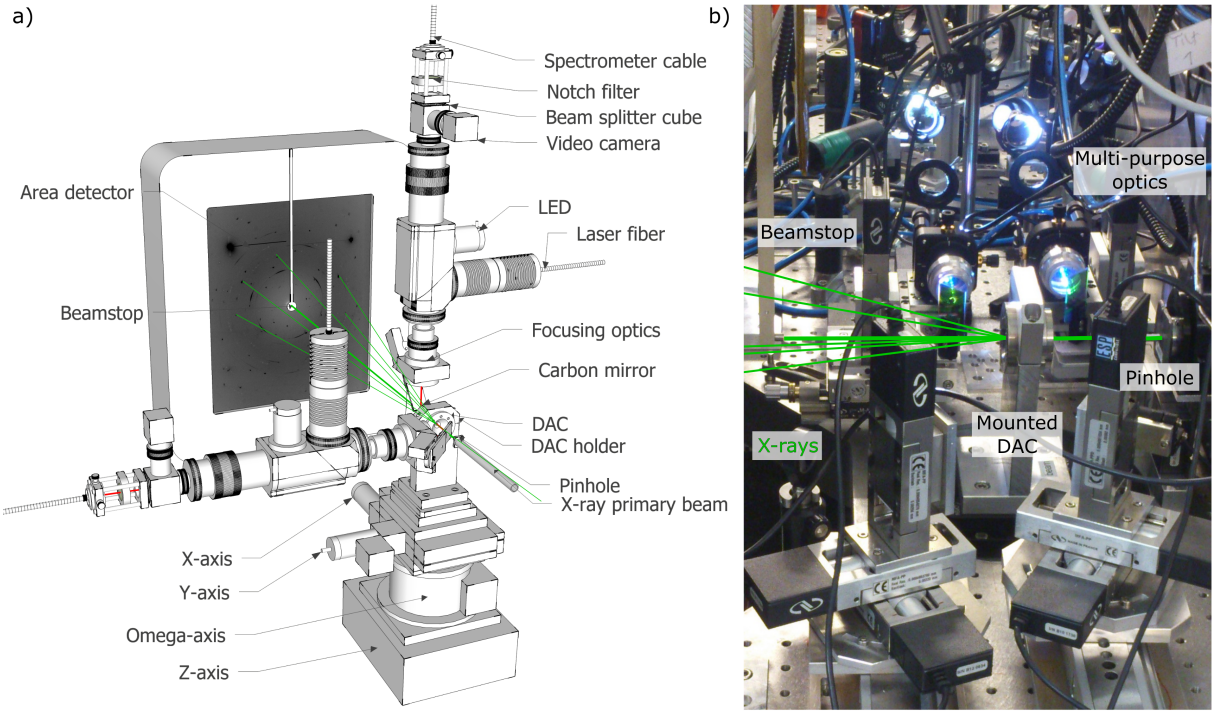

Figure 2.5.: A schematic sketch of the on-line laser heating setup at the extreme conditions beamline P02.2 (PETRA III, DESY) with laser beam paths in red and X-ray beam paths in green (a, adapted from Reference [68]), and a photograph of a slightly modified setup that has been used at P02.2 for the investigations over the course of this PhD project.

Extreme conditions beamlines, therefore, come up with customized setups for in situ high-pressure investigations in laser-heated diamond anvil cells. Due to a highly brilliant and microfocused X-ray beam, micron sized samples that consist of light-weight elements, such as P and N, can be probed by single-crystal XRD. Through advancements in data processing, even crystalline grains that contain multiple phases and domains can be analyzed, as has already been shown in literature,[69,70] and is discussed in this

thesis. The variable and short wavelength of the provided X-rays, in turn, increases the resolution of the XRD pattern, which is of particular importance considering the limited opening angle of diamond anvil cells. The on-line laser heating system, finally, enables the in situ monitoring of heat-induced sample transformations at high-pressure conditions.

Recapitulating, it is apparent that high-pressure techniques are well-developed and thus both, the synthesis and the in situ investigations of phosphorus nitrides at high-pressure conditions can be performed employing quite routine high-pressure setups, as is presented within the following chapters.

References

[1] Y. Syono, M. H. Manghnani, *"High-pressure research: Application to earth and planetary sciences"*, Terra Scientific Pub. Co, Tokyo, Japan und Washington, D.C, **2010**.

[2] H. Huppertz, *"Multianvil high-pressure / high-temperature synthesis in solid state chemistry"*, *Z. Kristallogr.* **2004**, *219*, 330.

[3] H. Huppertz, *"New synthetic discoveries via high-pressure solid-state chemistry"*, *Chem. Commun.* **2011**, *47*, 131.

[4] G. Demazeau, *"High pressure in solid-state chemistry"*, *High Pressure Res.* **2002**, *14*, 11031.

[5] R. C. Liebermann, *"Multi-anvil, high pressure apparatus: a half-century of development and progress"*, *High Pressure Res.* **2011**, *31*, 493.

[6] W. A. Bassett, *"Diamond anvil cell, 50th birthday"*, *High Pressure Res.* **2009**, *29*, 163.

[7] D. Yamazaki, E. Ito, T. Yoshino, N. Tsujino, A. Yoneda, X. Guo, F. Xu, Y. Higo, K. Funakoshi, *"Over 1 Mbar generation in the Kawai-type multianvil apparatus and its application to compression of $(Mg_{0.92}Fe_{0.08})SiO_3$ perovskite and stishovite"*, *Phys. Earth Planet. Inter.* **2014**, *228*, 262.

[8] T. Kunimoto, T. Irifune, *"Pressure generation to 125 GPa using a 6-8-2 type multianvil apparatus with nano-polycrystalline diamond anvils"*, *J. Geophys. Res.* **2010**, *215*, 12190.

[9] N. Dubrovinskaia, L. Dubrovinsky, N. A. Solopova, A. Abakumov, S. Turner, M. Hanfland, E. Bykova, M. Bykov, C. Prescher, V. B. Prakapenka, S. Petitgirard, I. Chuvashova, B. Gasharova, Y.-L. Mathis, P. Ershov, I. Snigireva, A. Snigirev, *"Terapascal static pressure generation with ultrahigh yield strength nanodiamond"*, *Sci. Adv.* **2016**, *2*, 1.

[10] D. Frost, B. Poe, R. Trønnes, C. Liebske, A. Duba, D. Rubie, *"A new large-volume multianvil system"*, *Phys. Earth Planet. Inter.* **2004**, *143-144*, 507.

[11] M. A. Manthilake, N. Walte, D. J. Frost, *"A new multi-anvil press employing six independently acting 8 MN hydraulic rams"*, *High Pressure Res.* **2012**, *42*, 1.

[12] N. Kawai, M. Togaya, A. Onodera, *"A New Device for Pressure Vessels"*, *Proc. Jpn. Acad.* **1973**, *49*, 623.

[13] D. Walker, *"Lubrication, gasketing, and precision in multianvil experiments"*, *Am. Mineral.* **1991**, *76*, 1092.

[14] K. D. Leinenweber, J. A. Tyburczy, T. G. Sharp, E. Soignard, T. Diedrich, W. B. Petuskey, Y. Wang, J. L. Mosenfelder, *"Cell assemblies for reproducible multi-anvil experiments (the COMPRES assemblies)"*, *Am. Mineral.* **2012**, *97*, 353.

[15] T. Ishii, L. Shi, R. Huang, N. Tsujino, D. Druzhbin, R. Myhill, Y. Li, L. Wang, T. Yamamoto, N. Miyajima, T. Kawazoe, N. Nishiyama, Y. Higo, Y. Tange, T. Katsura, *"Generation of pressures over 40 GPa using Kawai-type multi-anvil press with tungsten carbide anvils"*, *Rev. Sci. Instrum.* **2016**, *87*, 24501.

[16] T. Kunimoto, T. Irifune, Y. Tange, K. Wada, *"Pressure generation to 50 GPa in Kawai-type multianvil apparatus using newly developed tungsten carbide anvils"*, *High Pressure Res.* **2016**, *36*, 97.

[17] T. Ishii, Z. Liu, T. Katsura, *"A Breakthrough in Pressure Generation by a Kawai-Type Multi-Anvil Apparatus with Tungsten Carbide Anvils"*, *Engineering* **2019**, *5*, 434.

[18] H. Huppertz, *"Präparative und strukturelle Erweiterungen der Oxoboratchemie mittels Hochdruck-/Hochtemperatur-Synthesen"*, Habilitation Dissertation, Ludwig-Maximilians-Universität, Munich, **2003**.

[19] ESRF, *"ID06 Large Volume Press"*, http://www.esrf.eu/home/UsersAndScience/Experiments/MEx/id06-large-volume-press.html (last visit: 10/17/2019).

[20] T. Yu, Y. Wang, M. L. Rivers, S. R. Sutton, *"An upgraded and integrated large-volume high-pressure facility at the GeoSoilEnviroCARS bending magnet beamline of the Advanced Photon Source"*, *C. R. Geosci.* **2019**, *351*, 269.

[21] Soleil, *"PSICHÉ (Pression Structure Imagerie par Contraste à Haute Énergie)"*, https://www.synchrotron-soleil.fr/en/beamlines/psiche (last visit: 10/17/2019).

[22] DESY, *"P61B Large Volume Press – Extreme Conditions (LVP-EC)"*, https://petra3-extension.desy.de/e84814/e85529/e260846/ (last visit: 10/05/2019).

[23] D. J. Dunstan, I. L. Spain, *"Technology of diamond anvil high-pressure cells: I. Principles, design and construction"*, *J. Phys. E: Sci. Instrum.* **1989**, *22*, 913.

[24] I. L. Spain, D. J. Dunstan, *"The technology of diamond anvil high-pressure cells: II. Operation and use"*, *J. Phys. E: Sci. Instrum.* **1989**, *22*, 923.

[25] R. A. Forman, G. J. Piermarini, J. D. Barnett, S. Block, *"Pressure measurement made by the utilization of ruby sharp-line luminescence"*, *Science* **1972**, *176*, 284.

[26] I. Fujishiro, Y. Nakamura, *"Pressure Measurement by Ruby Fluorescence Method"*, *Rev. High Pressure Sci. Technol.* **1994**, *3*, 87.

[27] H.-K. Mao, J. Xu, P. M. Bell, *"Calibration of the ruby pressure gauge to 800 kbar under quasi-hydrostatic conditions"*, *J. Geophys. Res.* **1986**, *91*, 4673.

[28] Y. Fei, A. Ricolleau, M. Frank, K. Mibe, G. Shen, V. Prakapenka, *"Toward an internally consistent pressure scale"*, *Proc. Nat. Acad. Sci. U. S. A.* **2007**, *104*, 9182.

[29] E. F. O'Bannon, Z. Jenei, H. Cynn, M. J. Lipp, J. R. Jeffries, *"Contributed Review: Culet diameter and the achievable pressure of a diamond anvil cell: Implications for the upper pressure limit of a diamond anvil cell"*, *Rev. Sci. Instrum.* **2018**, *89*, 111501.

[30] B. Li, C. Ji, W. Yang, J. Wang, K. Yang, R. Xu, W. Liu, Z. Cai, J. Chen, H.-k. Mao, *"Diamond anvil cell behavior up to 4 Mbar"*, *Proc. Nat. Acad. Sci. U. S. A.* **2018**, *115*, 1713.

[31] W. C. Moss, K. A. Goettel, *"Finite element design of diamond anvils"*, *Appl. Phys. Lett.* **1987**, *50*, 25.

[32] A. Dewaele, P. Loubeyre, F. Occelli, O. Marie, M. Mezouar, *"Toroidal diamond anvil cell for detailed measurements under extreme static pressures"*, *Nat. Commun.* **2018**, *9*, 2913.

[33] Z. Jenei, E. F. O'Bannon, S. T. Weir, H. Cynn, M. J. Lipp, W. J. Evans, *"Single crystal toroidal diamond anvils for high pressure experiments beyond 5 megabar"*, *Nat. Commun.* **2018**, *9*, 3563.

[34] L. Dubrovinsky, N. Dubrovinskaia, V. B. Prakapenka, A. M. Abakumov, *"Implementation of micro-ball nanodiamond anvils for high-pressure studies above 6 Mbar"*, *Nat. Commun.* **2012**, *3*, 1163.

[35] I. Kantor, V. Prakapenka, A. Kantor, P. Dera, A. Kurnosov, S. Sinogeikin, N. Dubrovinskaia, L. Dubrovinsky, *"BX90: a new diamond anvil cell design for X-ray diffraction and optical measurements"*, *Rev. Sci. Instrum.* **2012**, *83*, 125102.

[36] D. Fan, W. Zhou, S. Wei, Y. Liu, M. Ma, H. Xie, *"A simple external resistance heating diamond anvil cell and its application for synchrotron radiation x-ray diffraction"*, *Rev. Sci. Instrum.* **2010**, *81*, 53903.

[37] T. Fedotenko, L. Dubrovinsky, G. Aprilis, E. Koemets, A. Snigirev, I. Snigireva, A. Barannikov, P. Ershov, F. Cova, M. Hanfland, N. Dubrovinskaia, *"Laser heating setup for diamond anvil cells for in situ synchrotron and in house high and ultra-high pressure studies"*, *Rev. Sci. Instrum.* **2019**, *90*, 104501.

[38] E. Bykova, G. Aprilis, M. Bykov, K. Glazyrin, M. Wendt, S. Wenz, H.-P. Liermann, J. T. Roeh, A. Ehnes, N. Dubrovinskaia, L. Dubrovinsky, *"Single-crystal diffractometer coupled with double-sided laser heating system at the Extreme Conditions Beamline P02.2 at PETRA III"*, *Rev. Sci. Instrum.* **2019**, *90*, 073907.

[39] H. Ozawa, S. Tateno, L. Xie, Y. Nakajima, N. Sakamoto, S. I. Kawaguchi, A. Yoneda, N. Hirao, *"Boron-doped diamond as a new heating element for internal-resistive heated diamond-anvil cell"*, *High Pressure Res.* **2018**, *38*, 120.

[40] A. F. Goncharov, J. C. Crowhurst, *"Pulsed laser Raman spectroscopy in the laser-heated diamond anvil cell"*, *Rev. Sci. Instrum.* **2005**, *76*, 63905.

[41] N. Holtgrewe, E. Greenberg, C. Prescher, V. B. Prakapenka, A. F. Goncharov, *"Advanced integrated optical spectroscopy system for diamond anvil cell studies at GSECARS"*, *High Pressure Res.* **2019**, *39*, 457.

[42] S. Nasu, *"High pressure Mössbauer spectroscopy using a diamond anvil cell"*, *Hyperfine Interact.* **1994**, *90*, 59.

[43] V. Potapkin, A. I. Chumakov, G. V. Smirnov, J. P. Celse, R. Rüffer, C. McCammon, L. Dubrovinsky, *"The ^{57}Fe Synchrotron Mössbauer Source at the ESRF"*, *J. Synchrotron Radiat.* **2012**, *19*, 559.

[44] Q. Wei, C. McCammon, S. A. Gilder, *"High-Pressure Phase Transition of Iron: A Combined Magnetic Remanence and Mössbauer Study"*, *Geochem. Geophys. Geosyst.* **2017**, *18*, 4646.

[45] I. Kupenko, L. Dubrovinsky, N. Dubrovinskaia, C. McCammon, K. Glazyrin, E. Bykova, T. Boffa Ballaran, R. Sinmyo, A. I. Chumakov, V. Potapkin, A. Kantor, R. Rüffer, M. Hanfland, W. Crichton, M. Merlini, *"Portable double-sided laser-heating system for Mössbauer spectroscopy and X-ray diffraction experiments at synchrotron facilities with diamond anvil cells"*, *Rev. Sci. Instrum.* **2012**, *83*, 124501.

[46] T. Meier, T. Herzig, J. Haase, *"Moissanite anvil cell design for Giga-Pascal nuclear magnetic resonance"*, *Rev. Sci. Instrum.* **2014**, *85*, 43903.

[47] T. Meier, J. Haase, *"Anvil cell gasket design for high pressure nuclear magnetic resonance experiments beyond 30 GPa"*, *Rev. Sci. Instrum.* **2015**, *86*, 123906.

[48] T. Meier, S. Khandarkhaeva, S. Petitgirard, T. Körber, A. Lauerer, E. Rössler, L. Dubrovinsky, *"NMR at pressures up to 90 GPa"*, *J. Magn. Reson.* **2018**, *292*, 44.

[49] P. V. Zinin, V. B. Prakapenka, K. Burgess, S. Odake, N. Chigarev, S. K. Sharma, *"Combined laser ultrasonics, laser heating, and Raman scattering in diamond anvil cell system"*, *Rev. Sci. Instrum.* **2016**, *87*, 123908.

[50] M. Lesik, T. Plisson, L. Toraille, J. Renaud, F. Occelli, M. Schmidt, O. Salord, A. Delobbe, T. Debuisschert, L. Rondin, P. Loubeyre, J.-F. Roch, *"Magnetic measurements on micron-size samples under high pressure using designed NV centers"*, **2018**.

[51] A. Palmer, D. M. Silevitch, Y. Feng, Y. Wang, R. Jaramillo, A. Banerjee, Y. Ren, T. F. Rosenbaum, *"Sub-Kelvin magnetic and electrical measurements in a diamond anvil cell with in situ tunability"*, *Rev. Sci. Instrum.* **2015**, *86*, 93901.

[52] A. Marizy, B. Guigue, F. Occelli, B. Leridon, P. Loubeyre, *"A symmetric miniature diamond anvil cell for magnetic measurements on dense hydrides in a SQUID magnetometer"*, *High Pressure Res.* **2017**, *37*, 465.

[53] R. Boehler, *"New diamond cell for single-crystal x-ray diffraction"*, *Rev. Sci. Instrum.* **2006**, *77*, 115103.

[54] N. Dubrovinskaia, L. Dubrovinsky, *"Crystallography taken to the extreme"*, *Phys. Scr.* **2018**, *93*, 62501.

[55] G. Shen, H. K. Mao, *"High-pressure studies with x-rays using diamond anvil cells"*, *Rep. Prog. Phys.* **2017**, *80*, 16101.

[56] E. Bykova, *"Single-crystal X-ray diffraction at extreme conditions in mineral physics and material sciences"*, Dissertation, University Bayreuth, Bayreuth, **2015**.

[57] M. Bykov, *"Structural aspects of pressure- and temperature-induced phase transitions in low-dimensional systems"*, Dissertation, University Bayreuth, Bayreuth, **2015**.

[58] L. Dubrovinsky, T. Boffa-Ballaran, K. Glazyrin, A. Kurnosov, D. Frost, M. Merlini, M. Hanfland, V. B. Prakapenka, P. Schouwink, T. Pippinger, N. Dubrovinskaia, *"Single-crystal X-ray diffraction at megabar pressures and temperatures of thousands of degrees"*, *High Pressure Res.* **2010**, *30*, 620.

[59] B. A. Zakharov, Z. Gal, D. Cruickshank, E. V. Boldyreva, *"Studying weak inter-actions in crystals at high pressures: when hardware matters"*, *Acta Crystallogr. Sect. E: Crystallogr. Commun.* **2018**, *74*, 613.

[60] H. Jin, C. H. Woodall, X. Wang, S. Parsons, K. V. Kamenev, *"A novel diamond anvil cell for x-ray diffraction at cryogenic temperatures manufactured by 3D printing"*, *Rev. Sci. Instrum.* **2017**, *88*, 35103.

[61] H. P. Liermann, Z. Konôpková, W. Morgenroth, K. Glazyrin, J. Bednarčik, E. E. McBride, S. Petitgirard, J. T. Delitz, M. Wendt, Y. Bican, A. Ehnes, I. Schwark, A. Rothkirch, M. Tischer, J. Heuer, H. Schulte-Schrepping, T. Kracht, H. Franz, *"The Extreme Conditions Beamline P02.2 and the Extreme Conditions Science Infrastructure at PETRA III"*, *J. Synchrotron Radiat.* **2015**, *22*, 908.

[62] DESY, *"P02.2 Extreme Conditions Beamline"*, http://photon-science.desy.de/facilities/petra_iii/beamlines/p022_extreme_conditions_beamline/index_eng.html (last visit: 10/17/2019).

[63] ESRF, *"ID27 - High Pressure Beamline"*, https://www.esrf.eu/UsersAndScience/Experiments/MEx/ID27 (last visit: 10/17/2019).

[64] D. L. Source, *"Beamline I15: Extreme Conditions"*, https://www.diamond.ac.uk/Instruments/Crystallography/I15-Extreme.html (last visit: 10/17/2019).

[65] C. Stan, C. Beavers, M. Kunz, N. Tamura, *"X-Ray Diffraction under Extreme Conditions at the Advanced Light Source"*, *Quantum Beam Sci.* **2018**, *2*, 4.

[66] A. L. Source, *"Beamline 12.2.2 Diffraction Under Non-Ambient Conditions"*, https://als.lbl.gov/beamlines/12-2-2/ (last visit: 10/17/2019).

[67] A. P. Source, *"Beamline 13-ID-C,D"*, https://www.aps.anl.gov/Beamlines/Directory/Details?beamline_id=21 (last visit: 10/17/2019).

[68] The schematic sketch of the on-line laser heating setup at P02.2 was kindly supplied by Dr. Elena Bykova.

[69] H. O. Sørensen, S. Schmidt, J. P. Wright, G. B. M. Vaughan, S. Techert, E. F. Garman, J. Oddershede, J. Davaasambuu, K. S. Paithankar, C. Gundlach, H. F. Poulsen, *"Multigrain crystallography"*, *Z. Kristallogr.* **2012**, *227*, 63.

[70] M. Bykov, S. Chariton, H. Fei, T. Fedotenko, G. Aprilis, A. V. Ponomareva, F. Tasnádi, I. A. Abrikosov, B. Merle, P. Feldner, S. Vogel, W. Schnick, V. B. Prakapenka, E. Greenberg, M. Hanfland, A. Pakhomova, H.-P. Liermann, T. Katsura, N. Dubrovinskaia, L. Dubrovinsky, *"High-pressure synthesis of ultraincompressible hard rhenium nitride pernitride $Re_2(N_2)(N)_2$ stable at ambient conditions"*, *Nat. Commun.* **2019**, *10*, 2994.

3. United in Nitride: The Highly Condensed Boron Phosphorus Nitride BP_3N_6

Sebastian Vogel, Amalina T. Buda, and Wolfgang Schnick

Angew. Chem. Int. Ed. **2018**, *57*, 13202;
Angew. Chem. **2018**, *130*, 13386.
DOI: 10.1002/anie.201808111

United in nitride: Unprecedented boron phosphorus nitride BP_3N_6 with entire fourfold coordination of B and P blends structural motifs of both, α-P_3N_5 and c-BN. It was prepared from reactive precursors in a one-step high-pressure high-temperature reaction, demonstrating an innovative access to mixed non-metal nitrides.

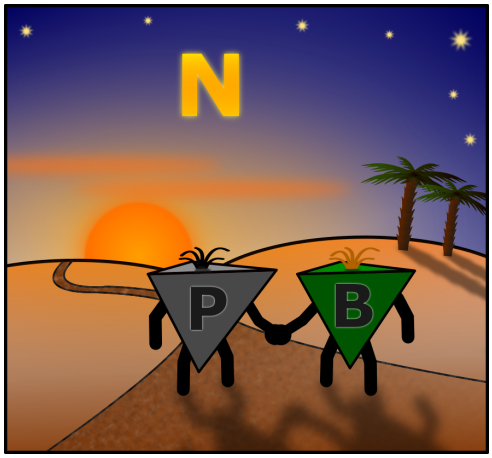

Abstract *Owing to intriguing materials properties non-metal nitrides are of special interest for both, solid-state chemistry and materials science. Mixed ternary non-metal nitrides, however, have only been sparsely investigated, as preparative chemistry lacks a systematic access, yet. Herein, we report on the highly condensed boron phosphorus nitride BP_3N_6, which was synthesized from $(PNCl_2)_3$, NH_4N_3 and h-BN in a high-pressure high-temperature reaction. By increasing partial pressure of HCl during synthesis using NH_4Cl, single-crystals of BP_3N_6 up to 80 µm in length were obtained. The unprecedented framework-type structure determined by single-crystal XRD blends structural motifs of both, α-P_3N_5 and c-BN, rendering BP_3N_6 a double nitride. The compound was further investigated by Rietveld refinement, EDX, temperature-dependent PXRD, FTIR and solid-state NMR spectroscopy. The formation of BP_3N_6 through use of reactive precursors exemplifies an innovative access to mixed non-metal nitrides.*

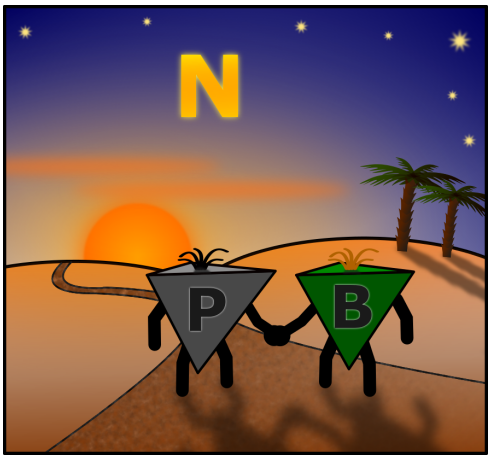

Non-metal nitrides are of fundamental interest in solid-state chemistry and materials sciences, as they show intriguing properties such as high thermal/mechanical stability, photocatalytic activity or chemical inertness.[1–5] Binary nitrides with condensed covalent structures, namely BN,[6] Si_3N_4[7,8] and P_3N_5,[9,10] as well as numerous triazine- and heptazine-based compounds summarized in the blanket term "carbon nitride" (C_3N_4)[11,12] have been investigated extensively in terms of structural and materials characteristics. In non-metal nitrides, B and C are usually found in threefold N coordination, while Si and P form tetrahedra-based structures. Coordination numbers, however, can be increased applying high pressures, as reported for c-BN,[13,14] γ-P_3N_5[15] and γ-Si_3N_4,[16] featuring BN_4, PN_5 and SiN_6 polyhedra, respectively, and an ultrahard sp^3 hybridized C_3N_4 polymorph has been discussed on the basis of ab initio calculations.[17]

In contrast to numerous binary non-metal nitride phases, mixed ternary representatives have not been accessible for quite some time. This may be due to small interdiffusion coefficients of the constituting binary refractory nitrides, which prevents a straight forward synthesis by direct solid-state reaction. Silicon

phosphorus nitride $SiPN_3$, which may be understood as the formal reaction product of Si_3N_4 and P_3N_5, has been prepared by ammonolysis of $Cl_3SiNPCl_3$ at −78 °C and subsequent condensation at 800 °C.[18] Thus, the unfavorable reaction of binary nitrides was bypassed and thermodynamic sinks have been avoided by using a preorganized molecular precursor that contains the targeted motif of N-linked and tetrahedrally coordinated Si and P atoms within itself, following a gentle reaction pathway. Predetermining the motif of N-linked B and Si atoms, $Cl_2BNHSiCl_3$ has been successfully employed as a molecular precursor for amorphous $Si_3B_3N_7$.[19,20] Within the B/C/N system, BC_2N has been proposed as a superhard ternary nitride with mechanical properties ousting c-BN as the second hardest material.[21–25] Thus, mixed non-metal nitrides have only been accessible by multi-step syntheses starting from molecular precursor compounds.

In this contribution, we report on the serendipitous discovery of the double nitride BP_3N_6, which was obtained during explorative investigation of phosphorus nitrides employing reactive P/N precursors. At high-pressure (HP) and high-temperature (HT) conditions $(PNCl_2)_3$, NH_4N_3, and NH_4Cl were reacted in a h-BN crucible. At elevated temperatures NH_4N_3 dissociates into N_2 and NH_3, generating high partial pressure of N_2, which prevents decomposition of targeted P/N compounds, following Le Chatelier's principle.[26] Molecular $(PNCl_2)_3$ and NH_4Cl, in turn, have been used as starting materials for P_3N_5 synthesis in pressure ampoules.[27] Furthermore, NH_4Cl has been employed as a mineralizer in HP/HT reactions, facilitating single-crystal growth of P/N compounds, which may be due to reversible bond cleavage and reformation of the P–N bonds catalyzed by in situ formed HCl.[28,29] Following Equation 3.1, the reaction of $(PNCl_2)_3$ and NH_4N_3 most likely generates sufficiently high partial pressure of HCl to attack the crucible material h-BN, providing intermediate reactive boron species for BP_3N_6 formation. Conceivable intermediate species could be BCl_3, $(BNCl_2)_3$ or $(BClNH)_3$, with the latter being probably formed in situ from BCl_3 and NH_4Cl.[30]

$$2\,(PNCl_2)_3 + 3\,NH_4N_3 + 2\,\text{h-BN} \longrightarrow 2\,BP_3N_6 + 12\,HCl + 4\,N_2 \tag{3.1}$$

According to Equation 3.1, powdered samples of BP_3N_6 were subsequently obtained starting from $(PNCl_2)_3$, NH_4N_3, and stoichiometric amounts of h-BN. The starting materials were finely ground, compressed to 8 GPa and heated to 1100 °C in a multianvil apparatus.[31] The as-synthesized sample was washed with de-ionized water to yield colorless crystals of BP_3N_6 with h-BN as a minor side phase

from crucible residues (< 5 wt-%). Formation of single crystals up to 80 µm in length, as illustrated in Figure 3.1, however, was achieved by adding 25–30 wt-% of NH_4Cl to the mixture of starting materials, suggesting that a high partial pressure of HCl is essential for crystal growth. More detailed information on the HP/HT synthesis of BP_3N_6 is provided in Chapter A.

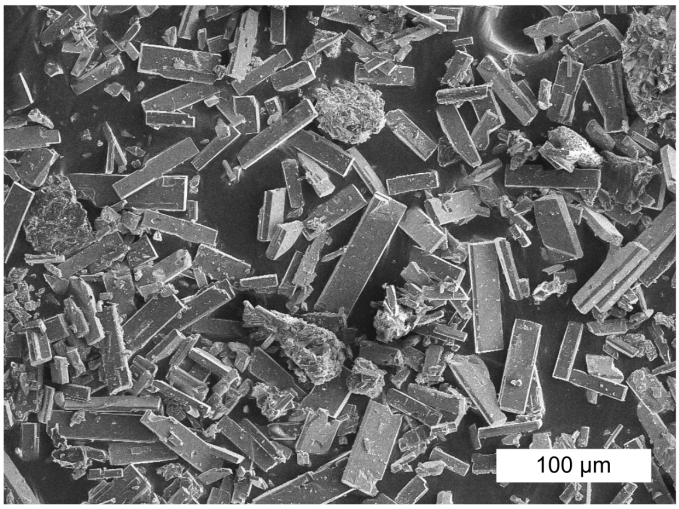

Figure 3.1.: Representative SEM image of single-crystals of BP_3N_6. See also Figure A.1.

The structure of BP_3N_6 was solved and refined from single-crystal X-ray diffraction data ($P2_1/c$ (no. 14), $a = 5.0272(11)$, $b = 4.5306(12)$, $c = 17.332(3)$ Å, $\beta = 106.387(9)°$, $Z = 4$, $R1 = 0.037$; more details in Chapter A) and elemental composition was confirmed by EDX measurements (Table A.5).[32] Furthermore, the structure model was verified by Rietveld refinement (Figure A.3, Table A.6). Figure 3.2 illustrates the highly condensed framework of BP_3N_6, blending structural motifs of both, α-P_3N_5 and c-BN.[9,13,14] Pairs of edge-sharing PN_4 tetrahedra (blue) and allside vertex-sharing BN_4 tetrahedra (green) form chain-like substructures of *vierer* rings* running along a, which are interconnected by all-side vertex-sharing PN_4 tetrahedra (gray) to form a highly condensed B/P/N network. With respect to the entire fourfold coordination of B and P, BP_3N_6 can be classified as a double nitride rather than a boron nitridophosphate. According to the Niggli formula ${}^{3}_{\infty}\left[B^{[4]}P^{[4]}{}_3N^{[2]}{}_2N^{[3]}{}_4\right]$, N is found in two- and threefold coordination in a 2 : 4 ratio. The topology of this four nodal B/P/N network is represented by the point symbol $(3^7.4^9.5^{11}.6)(3^6.4^8.5^6.6)(3^4.4^5.5^4.6^2)(3^4.4^5.5^6)$ determined by TOPOS

*The term *"vierer ring"* has been defined by Liebau and is derived from the German word *vier* (engl. four) describing a ring consisting of four tetrahedra.[33]

software.[34,35] To the best of our knowledge, this topology has not been observed for any compound so far, thus BP_3N_6 represents a new structure type. BP_3N_6 remains stable up to at least 1000 °C under Ar atmosphere, as indicated by temperature-dependent PXRD (Figure A.4). P–N (1.545(2)–1.583(2) Å for $N^{[2]}$ and 1.656(2)–1.675(2) Å for $N^{[3]}$) and B–N bond lengths (1.547(3)–1.574(3) Å) are consistent with values reported for related compounds.[9,13,14,36] Moreover, the Madelung part of the lattice energy of BP_3N_6 was determined to 90 556 kJ·mol^{-1}, which is in good agreement to the sum of the Madelung part of lattice energy of formally constituting BN and P_3N_5 (91 732 kJ·mol^{-1}, 1.3 % difference).[37] CHARDI analysis revealed effective coordination numbers of 3.80–3.99 for B and P and mean total charges of +3.07, +4.98 and −2.98 for B, P and N, respectively, in line with the refined structure model.[38] To quantify polyhedra distortions in BP_3N_6, minimum bonding ellipsoids (MBEs) of the BN_4 and PN_4 tetrahedra were fitted, using the PIEFACE software.[39] More detailed information on MAPLE, CHARDI and MBE analyses is provided in Chapter A (A.7–A.9).

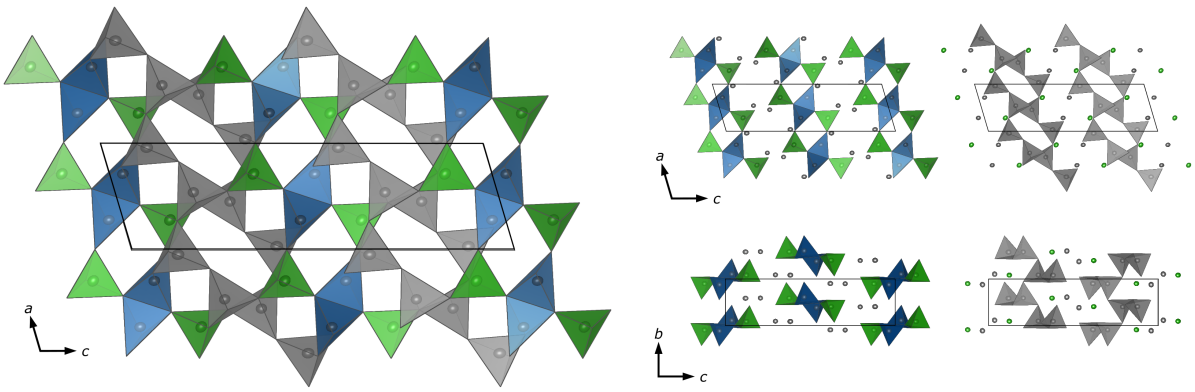

Figure 3.2.: The crystal structure of BP_3N_6 is built up from edge-sharing PN_4 tetrahedra (blue) that form chain-like substructures with all-side vertex-sharing BN_4 tetrahedra (green), which are interconnected to a highly condensed framework by all-side vertex-sharing PN_4 tetrahedra (gray). Ellipsoids of P (gray) and B (green) are displayed at 99 % probability level.

To rule out incomplete condensation of intermediate species or NH_x functionality caused by harsh acidic reaction conditions, BP_3N_6 was further investigated by FTIR and NMR spectroscopy. The FTIR spectrum of BP_3N_6 (Figure A.6) shows broad absorption bands below 1700 cm^{-1}, which have been similarly observerd for related P/N and B/N compounds as well and can be assigned to various combinations of vibrational $(B/P)N_4$ modes of the B/P/N framework.[40–43] Additional weak absorption between

2900–3400 cm^{-1} may be attributable to minor NH_x functionality in BP_3N_6 or amorphous side phases. To confirm the absence of any hydrogen in the title compound's structure and to verify the refined structure model, ^{11}B, ^{31}P, $^{31}P\{^1H\}$ and ^1H solid-state MAS NMR spectra were recorded. The ^{11}B NMR spectrum (Figure 3.3, $I(^{11}B) = 3/2$) shows one narrow major signal at 2.8 ppm, which can be assigned to the one crystallographic B site in the BP_3N_6 structure. The chemical shift (2.8 ppm) is in the typical range of tetrahedrally coordinated B and quadrupolar interaction is small but not zero, as indicated by a wide spinning sideband pattern (Figure A.7).[44,45] The minor ^{11}B signal at 18.4–26.7 ppm corresponds to the minor side phase h-BN observed in PXRD analysis as well and a broad shoulder at the major ^{11}B signal is most likely related to additional amorphous side phases.[45,46]

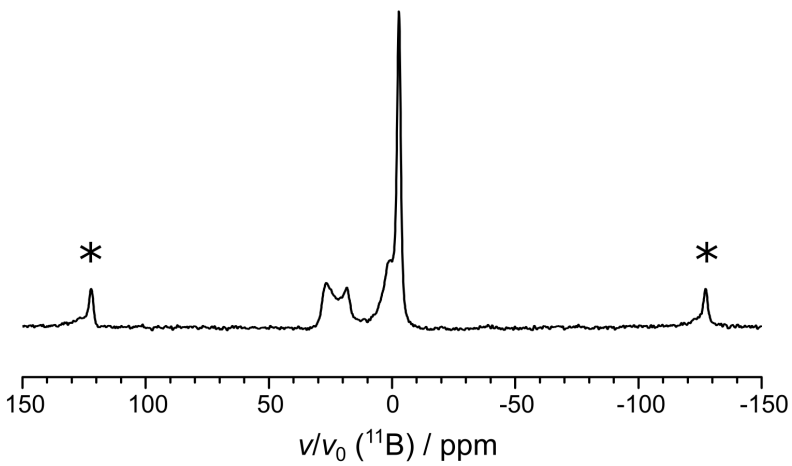

Figure 3.3.: ^{11}B NMR spectrum, showing one narrow major signal at 2.8 ppm, which corresponds to one crystallographic B site in the BP_3N_6 structure. The broad minor signal (18.4–26.7 ppm) can be assigned to the minor side phase of h-BN.[45,46] Spinning sidebands are marked with asterisks.

The ^{31}P NMR spectrum (Figure 3.4, black) shows three signals at 0.68, −3.85 and −10.8 ppm with an integral ratio of 1.1 : 0.9 : 1.0, which correspond to the three crystallographic P sites of equal multiplicity (Wyckoff sites 4*e*) in the BP_3N_6 structure model. Chemical shifts are in the same region as observed for related compounds.[27,28,47,48] As the ^{31}P signals are absent in the $^{31}P\{^1H\}$ cross polarization NMR spectrum (Figure 3.4, gray), there is no final evidence on hydrogen being present in the BP_3N_6 structure. Thus, the broad ^{31}P signal in the $^{31}P\{^1H\}$ NMR spectrum (25–50 ppm) corresponds to minor amorphous side phases containing P and H, which may have formed upon temperature quenching. Thus, minor NH_x

functionality observed in the FTIR spectrum most likely corresponds to these amorphous side phases rather than to BP_3N_6. Entire NMR spectra are provided in Chapter A (Figures A.7, A.8).

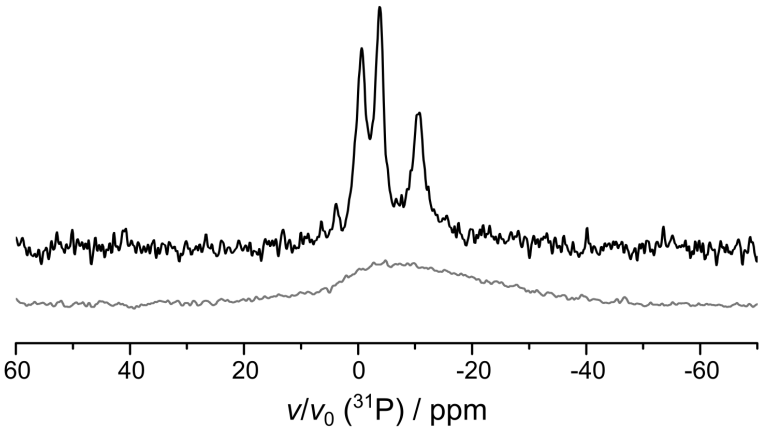

Figure 3.4.: ^{31}P spectrum (black) of BP_3N_6 showing three signals with a 1.1 : 0.9 : 1.0 integral ratio, which can be assigned to the three crystallographic P sites of equal multiplicity in the BP_3N_6 structure. As these signals are absent in the $^{31}P\{^1H\}$ NMR spectrum (gray), there is no evidence of hydrogen being present in bulk BP_3N_6.

Recently, we have reported on the first nitridoborophosphate anion in $Li_{47}B_3P_{14}N_{42}$, raising the question of a ternary boron phosphorus nitride.[46] Starting from simple reactive P/N precursors, this contribution reports on unprecedented BP_3N_6, of which single-crystals were obtained in an explorative one-step HP/HT synthesis. High partial pressure of HCl, which was formed in situ from $(PNCl_2)_3$, NH_4N_3 and NH_4Cl, is suggested to be essential for both, providing reactive intermediate boron species from h-BN and facilitating crystal growth by acid catalyzed reversible cleavage and reformation of P–N and B–N bonds. Consequently, the preparation of BP_3N_6 exemplifies an innovative access to mixed non-metal nitrides, which may even be simplified when h-BN is replaced by more reactive boron species. By analogy with P_3N_5, high-pressure polymorphs of BP_3N_6 with increased coordination numbers for P or even B may be not far to seek and considering high thermal and mechanical stability of BN, BP_3N_6 will be examined on its elastic properties in future investigations. Vickers hardness may be determined by nanoindentation measurements and isothermal bulk modulus may be revealed from pressure-dependent in situ XRD measurements in diamond anvil cells using synchrotron radiation.

Acknowledgements

Financial support by the Deutsche Forschungsgemeinschaft (DFG, SCHN 377/18-1) and the Fonds der Chemischen Industrie (FCI) for a fellowship for Sebastian Vogel is gratefully acknowledged. We thank Dr. Peter Mayer and PD Dr. Constantin Hoch for single-crystal data collection and Dr. Thomas Bräuniger, Christian Minke and Otto Zeman for NMR, REM and EDX investigations. Inspiring discussions with Dr. Simon Kloß and Dr. Philipp Bielec (all at Department of Chemistry of LMU Munich) are gratefully appreciated.

References

[1] W. Schnick, *"Solid-State Chemistry with Nonmetal Nitrides"*, *Angew. Chem. Int. Ed. Engl.* **1993**, *32*, 806; *Angew. Chem.* **1993**, *105*, 846.

[2] F. L. Riley, *"Silicon Nitride and Related Materials"*, *J. Am. Ceram. Soc.* **2000**, *83*, 245.

[3] J. Kopac, P. Krajnik, *"High-performance grinding—A review"*, *J. Mater. Process. Technol.* **2006**, *175*, 278.

[4] X. Wang, K. Maeda, A. Thomas, K. Takanabe, G. Xin, J. M. Carlsson, K. Domen, M. Antonietti, *"A metal-free polymeric photocatalyst for hydrogen production from water under visible light"*, *Nat. Mater.* **2009**, *8*, 76.

[5] J. Wen, J. Xie, X. Chen, X. Li, *"A review on γ-C_3N_4-based photocatalysts"*, *Appl. Surf. Sci.* **2017**, *391*, 72.

[6] R. S. Pease, *"Crystal Structure of Boron Nitride"*, *Nature* **1950**, *165*, 722.

[7] D. Hardie, K. H. Jack, *"Crystal Structures of Silicon Nitride"*, *Nature* **1957**, *180*, 332.

[8] R. Marchand, Y. Laurent, J. Lang, M. T. Le Bihan, *"Structure du nitrure de silicium α "*, *Acta Crystallogr. Sect. B: Struct. Sci. Cryst. Eng. Mater.* **1969**, *25*, 2157.

[9] S. Horstmann, E. Irran, W. Schnick, *"Synthesis and Crystal Structure of Phosphorus(V) Nitride α-P_3N_5"*, *Angew. Chem. Int. Ed. Engl.* **1997**, *36*, 1873; *Angew. Chem.* **1997**, *109*, 1938.

[10] S. Horstmann, E. Irran, W. Schnick, *"Phosphor(V)-nitrid α-P_3N_5: Synthese ausgehend von Tetraaminophosphoniumiodid und Kristallstrukturaufklärung mittels Synchrotron-Pulver-Röntgenbeugung"*, *Z. Anorg. Allg. Chem.* **1998**, *624*, 620.

[11] A. Schwarzer, T. Saplinova, E. Kroke, *"Tri-s-triazines (s-heptazines)—From a "mystery molecule" to industrially relevant carbon nitride materials"*, *Coord. Chem. Rev.* **2013**, *257*, 2032.

[12] F. K. Keßler, Y. Zheng, D. Schwarz, C. Merschjann, W. Schnick, X. Wang, M. J. Bojdys, *"Functional carbon nitride materials – design strategies for electrochemical devices"*, *Nat. Rev. Mater.* **2017**, *2*, 17030.

[13] R. H. Wentorf, *"Cubic Form of Boron Nitride"*, *J. Chem. Phys.* **1957**, *26*, 956.

[14] R. H. Wentorf, *"Synthesis of the Cubic Form of Boron Nitride"*, *J. Chem. Phys.* **1961**, *34*, 809.

[15] K. Landskron, H. Huppertz, J. Senker, W. Schnick, *"High-Pressure Synthesis of γ-P_3N_5 at 11 GPa and 1500 °C in a Multianvil Assembly: A Binary Phosphorus(V) Nitride with a Three-Dimensional Network Structure from PN_4 Tetrahedra and Tetragonal PN_5 Pyramids"*, *Angew. Chem. Int. Ed.* **2001**, *40*, 2643, *Angew. Chem.* **2001**, *113*, 2713.

[16] A. Zerr, R. Riedel, G. Miehe, G. Serghiou, M. Schwarz, E. Kroke, H. Fueß, P. Kroll, R. Boehler, *"Synthesis of cubic silicon nitride"*, *Nature* **1999**, *400*, 340.

[17] A. Y. Liu, M. L. Cohen, *"Prediction of new low compressibility solids"*, *Science* **1989**, *245*, 841.

[18] H.-P. Baldus, W. Schnick, J. Lücke, *"Silicon Phosphorus Nitride, the First Ternary Compound in the Silicon-Phosphorus-Nitrogen System"*, *Chem. Mater.* **1993**, *5*, 845.

[19] H.-P. Baldus, M. Jansen, *"Novel High-Performance Ceramics—Amorphous Inorganic Networks from Molecular Precursors"*, *Angew. Chem. Int. Ed. Engl.* **1997**, *36*, 328; *Angew. Chem.* **1997**, *109*, 338.

[20] M. Jansen, J. C. Schön, L. van Wüllen, *"The route to the structure determination of amorphous solids: a case study of the ceramic $Si_3B_3N_7$"*, *Angew. Chem. Int. Ed.* **2006**, *45*, 4244; *Angew. Chem.* **2006**, *118*, 4350.

[21] A. Y. Liu, R. M. Wentzcovitch, M. L. Cohen, *"Atomic arrangement and electronic structure of BC_2N"*, *Phys. Rev. B: Condens. Matter Mater. Phys.* **1989**, *39*, 1760.

[22] Y. Tateyama, T. Ogitsu, K. Kusakabe, S. Tsuneyuki, S. Itoh, *"Proposed synthesis path for heterodiamond BC_2N"*, *Phys. Rev. B: Condens. Matter Mater. Phys.* **1997**, *55*, R10161.

[23] V. L. Solozhenko, D. Andrault, G. Fiquet, M. Mezouar, D. C. Rubie, *"Synthesis of superhard cubic BC_2N"*, *Appl. Phys. Lett.* **2001**, *78*, 1385.

[24] Y. Zhang, H. Sun, C. Chen, *"Superhard cubic BC_2N compared to diamond"*, *Phys. Rev. Lett.* **2004**, *93*, 195504.

[25] K. Yuge, A. Seko, Y. Koyama, F. Oba, I. Tanaka, *"First-principles-based phase diagram of the cubic BNC ternary system"*, *Phys. Rev. B: Condens. Matter Mater. Phys.* **2008**, *77*, 334.

[26] F. Karau, W. Schnick, *"A nitridic clathrate: $P_4N_4(NH)_4(NH_3)$"*, *Angew. Chem. Int. Ed.* **2006**, *45*, 4505; *Angew. Chem.* **2006**, *118*, 4617.

[27] W. Schnick, J. Lücke, F. Krumeich, *"Phosphorus Nitride P_3N_5: Synthesis, Spectroscopic, and Electron Microscopic Investigations"*, *Chem. Mater.* **1996**, *8*, 281.

[28] A. Marchuk, F. J. Pucher, F. W. Karau, W. Schnick, *"A high-pressure polymorph of phosphorus nitride imide"*, *Angew. Chem. Int. Ed.* **2014**, *53*, 2469; *Angew. Chem.* **2014**, *126*, 2501.

[29] A. Marchuk, V. R. Celinski, J. Schmedt auf der Günne, W. Schnick, *"$MH_4P_6N_{12}$ (M = Mg, Ca): new imidonitridophosphates with an unprecedented layered network structure type"*, *Chem. – Eur. J.* **2015**, *21*, 5836.

[30] C. A. Brown, A. W. Laubengayer, *"B-Trichloroborazole1"*, *J. Am. Chem. Soc.* **1955**, *77*, 3699.

[31] H. Huppertz, *"Multianvil high-pressure / high-temperature synthesis in solid state chemistry"*, *Z. Kristallogr.* **2004**, *219*, 330.

[32] Crystal data of BP_3N_6 from single-crystal XRD refinement: $M = 187.78\,\mathrm{g{\cdot}mol^{-1}}$, monoclinic, $P2_1/c$ (no. 14), $a = 5.0272(11)$, $b = 4.5306(12)$ and $c = 17.332(3)\,\text{Å}$, $\beta = 106.387(9)°$, $V = 378.72(15)\,\text{Å}^3$, $Z = 4$, $\rho = 3.293\,\mathrm{g{\cdot}cm^{-3}}$, $\mu = 1.43\,\mathrm{cm^{-1}}$, Mo-K$\alpha$ ($\lambda = 0.71073\,\text{Å}$, Bruker D8 Venture), $T = 293\,\mathrm{K}$, 7378 observed reflections, 1662 independent reflections, 91 parameters, $R_{\mathrm{int}} = 0.0482$, $R_\sigma = 0.0454$, $R1 = 0.0369$, $wR2 = 0.0966$, $GoF = 1.111$, residual electron density 0.737, $-0.578\,e{\cdot}\text{Å}^{-3}$. Further details on the crystal structure investigation may be obtained from the Fachinformationszentrum Karlsruhe, 76344 Eggenstein-Leopoldshafen, Germany (fax: (+49) 7247-808-666; e-mail: crysdata@fiz-karlsruhe.de), on quoting the depository number CSD-434784.

[33] F. Liebau, *"Structural Chemistry of Silicates: Structure, Bonding, and Classification"*, Springer Berlin Heidelberg, Berlin, Heidelberg, **1985**.

[34] V. A. Blatov, A. P. Shevchenko, D. M. Proserpio, *"Applied Topological Analysis of Crystal Structures with the Program Package ToposPro"*, *Cryst. Growth Des.* **2014**, *14*, 3576.

[35] V. A. Blatov, A. P. Shevchenko, *"ToposPro Vers. 5.1.0.7"*, Samara, **2016**.

[36] S. Horstmann, E. Irran, W. Schnick, *"Phosphorus(V) Nitride Imide HP_4N_7: Synthesis from a Molecular Precursor and Structure Determination with Synchrotron Powder diffraction"*, *Angew. Chem. Int. Ed. Engl.* **1997**, *36*, 1992; *Angew. Chem.* **1997**, *109*, 2085.

[37] R. Hoppe, *"On the Madelung Part of Lattice Energy"*, *Z. Naturforsch. A: Phys. Sci.* **1995**, *50*, 555.

[38] R. Hoppe, S. Voigt, H. Glaum, J. Kissel, H. P. Müller, K. Bernet, *"A new route to charge distributions in ionic solids"*, *J. Less-Common Met.* **1989**, *156*, 105.

[39] J. Cumby, J. P. Attfield, *"Ellipsoidal analysis of coordination polyhedra"*, *Nat. Commun.* **2017**, *8*, 14235.

[40] W. Schnick, J. Lücke, *"Darstellung, Kristallstruktur und IR-spektroskopische Untersuchung von Phosphor(V)-nitrid-imid, HPN_2"*, *Z. Anorg. Allg. Chem.* **1992**, *610*, 121.

[41] S. Horstmann, E. Irran, W. Schnick, *"Synthese, Kristallstruktur und Eigenschaften von Phosphor(V)-nitridimid HP_4N_7"*, *Z. Anorg. Allg. Chem.* **1998**, *624*, 221.

[42] K. Landskron, H. Huppertz, J. Senker, W. Schnick, *"Multianvil-Synthese, Pulver-Röntgenstrukturanalyse, ^{31}P-MAS-NMR- und FTIR-Spektroskopie sowie Materialeigenschaften von γ-P_3N_5, einer Hochdruckphase von binärem Phosphor(V)nitrid mit verzerrt quadratischen PN_5-Pyramiden und PN_4-Tetraedern"*, *Z. Anorg. Allg. Chem.* **2002**, *628*, 1465.

[43] R. M. Chrenko, *"Ultraviolet and infrared spectra of cubic boron nitride"*, *Solid State Commun.* **1974**, *14*, 511.

[44] T. Bräuniger, M. Jansen, *"Solid-state NMR Spectroscopy of Quadrupolar Nuclei in Inorganic Chemistry"*, *Z. Anorg. Allg. Chem.* **2013**, *639*, 857.

[45] G. Jeschke, W. Hoffbauer, M. Jansen, *"A comprehensive NMR study of cubic and hexagonal boron nitride"*, *Solid State Nucl. Magn. Reson.* **1998**, *12*, 1.

[46] E.-M. Bertschler, T. Bräuniger, C. Dietrich, J. Janek, W. Schnick, *"$Li_{47}B_3P_{14}N_{42}$ – A Lithium Nitridoborophosphate with $[P_3N_9]^{12-}$, $[P_4N_{10}]^{10-}$, and the Unprecedented $[B_3P_3N_{13}]^{15-}$ Ion"*, *Angew. Chem. Int. Ed.* **2017**, *56*, 4806; *Angew. Chem.* **2017**, *129*, 4884.

[47] D. Baumann, W. Schnick, *"High-pressure polymorph of phosphorus nitride imide HP_4N_7 representing a new framework topology"*, *Inorg. Chem.* **2014**, *53*, 7977.

[48] D. Baumann, W. Schnick, *"Pentacoordinate phosphorus in a high-pressure polymorph of phosphorus nitride imide $P_4N_6(NH)$"*, *Angew. Chem. Int. Ed.* **2014**, *53*, 14490; *Angew. Chem.* **2014**, *126*, 14718.

4. Rivalry under Pressure: The Coexistence of Ambient-Pressure Motifs and Close-Packing in Silicon Phosphorus Nitride Imide SiP_2N_4NH

Sebastian Vogel, Amalina T. Buda, and Wolfgang Schnick

Angew. Chem. Int. Ed. **2019**, *58*, 3398;
Angew. Chem. **2019**, *131*, 3436.
DOI: 10.1002/anie.201813789

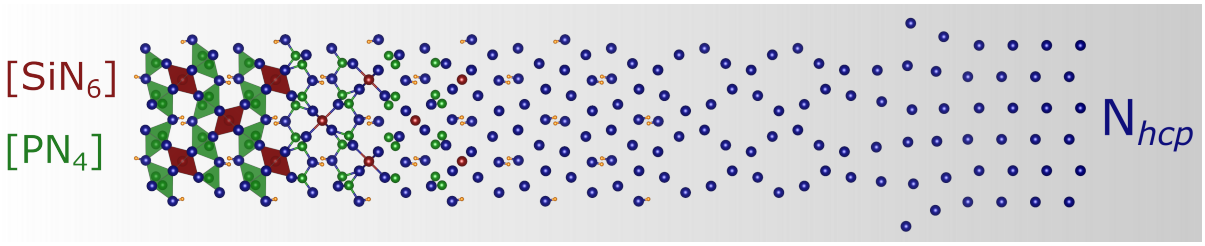

Under pressure: The silicon phosphorus nitride imide SiP_2N_4NH was synthesized in a high-pressure high-temperature reaction, using HCl as a mineralizer. Its highly condensed structure is built up from SiN_6 octahedra and PN_4 tetrahedra and can be derived from a significantly distorted hexagonal close-packing of nitride anions.

Abstract *Non-metal nitrides such as BN, Si_3N_4, and P_3N_5 meet numerous demands on high-performance materials, and their high-pressure polymorphs exhibit outstanding mechanical properties. Herein, we present the silicon phosphorus nitride imide SiP_2N_4NH featuring sixfold coordinated Si. Using the multianvil technique, SiP_2N_4NH was obtained by high-pressure high-temperature synthesis at 8 GPa and 1100 °C with in situ formed HCl acting as a mineralizer. Its structure was elucidated by a combination of single-crystal X-ray diffraction and solid-state NMR measurements. Moreover, SiP_2N_4NH was characterized by energy-dispersive X-ray spectroscopy and (temperature-dependent) powder X-ray diffraction. The highly condensed Si/P/N framework features PN_4 tetrahedra as well as the rare motif of SiN_6 octahedra, and is discussed in the context of ambient-pressure motifs competing with close-packing of nitride anions, representing a missing link in the high-pressure chemistry of non-metal nitrides.*

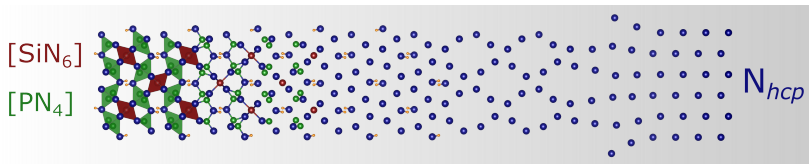

A broad range of applications makes refractory non-metal nitrides a special field of interest for materials sciences and inorganic chemistry.[1–4] Especially, high-pressure polymorphs with increased coordination numbers, for example, spinel-type γ-Si_3N_4, show outstanding mechanical hardness and high thermal stability.[5,6] Such high-pressure polymorphs of non-metal nitrides, however, are still very rare in number.

Binary nitrides such as h-BN and β-Si_3N_4 feature high thermal and mechanical stability, and thus find applications as hot-zone components, bearings, or grinding devices.[3,4,7,8] P_3N_5 is used as gate-insulator material and flame retardant, and has recently been proposed for pyrotechnical applications.[9–12] The discovery of mixed non-metal nitrides such as $SiPN_3$ and $Si_3B_3N_7$ opened systematic access towards sintering additives and highly resilient fibers and cords, respectively, attesting non-metal nitrides a broad range of applications.[2,13–15] Moreover, ternary compounds of B, C, and N have been investigated extensively as several B/C/N phases have been proposed with mechanical properties almost reaching those of diamond.[16,17] The outstanding materials properties of non-metal nitrides are even surpassed by those of their respective high-pressure polymorphs such as c-BN, γ-P_3N_5, and γ-Si_3N_4, which feature improved mechanical properties such as increased hardness and bulk moduli.[5,6,18–20] Further high-pressure poly-

morphs, such as superhard spinel-type BeP_2N_4 with P in sixfold coordination of N, have been predicted from theoretical calculations.[21,22] Thus, transitions from ambient-pressure to high-pressure polymorphs involve fundamental changes in both, the structural and materials properties and are of fundamental interest for high-pressure and materials sciences as well as inorganic chemistry.

In principle, the total energy of a solid material can be minimized either by increasing the packing density and the number of interatomic contacts (= coordination number) or through the formation of strong directed bonds. The former is the predominant effect in ionic compounds with omnidirectional electrostatic bonds such as alkali metal halides or oxides. The latter is the prevalent situation for covalent compounds such as non-metal nitrides, which results in trigonal planar coordination of B and tetrahedra-based networks for Si and P at ambient pressure.[7–9,23] High-pressure polymorphs of non-metal nitrides such as c-BN, γ-P_3N_5, and γ-Si_3N_4, in contrast, form structures that are dominated by close-packing of nitride anions and feature four-, five-, and sixfold coordinated $B^{[4]}$, $P^{[5]}$, and $Si^{[6]}$ (coordination numbers given in superscripted square brackets).[5,6,18–20] Entire sixfold N coordination of P and Si has been proposed by DFT calculations at 35.5 GPa in V_3O_5-type P_3N_5 and 160 GPa in $CaTi_2O_4$-related Si_3N_4, which can both be derived from a close-packing of nitride anions.*[24,25] Thus, the structural chemistry of non-metal nitrides may be best described by the increasing influence of a close-packing of nitride anions with pressure. Recently, we reported on the covalent double nitride BP_3N_6.[26] Its structure blends motifs of α-P_3N_5 and c-BN, but cannot be derived from any close-packing. γ-Si_3N_4 and HP-$MgSiN_2$, in contrast, are prominent examples of high-pressure phases with the rare motif of sixfold coordinated Si embedded in a close-packing of nitride anions.[5,6,27] An intermediate nitride material, illustrating the qualitative change in structural behavior of non-metal nitrides, however, has not been reported yet and is considered to be the missing link in structural research of non-metal nitrides.

Herein, we report on the highly condensed silicon phosphorus nitride imide SiP_2N_4NH ($\kappa = n(T)/n(N) = 3/5 = 0.6$, T = Si, P),† which features SiN_6 octahedra and PN_4 tetrahedra, blending ambient- and high-pressure motifs. Employing the multianvil technique, SiP_2N_4NH was obtained from a one-step high-pressure (HP) high-temperature (HT) reaction, in which in situ generated HCl acted as a mineralizer.

*The presence of a close-packing does not necessarily imply a more ionic type of covalent bonding in non-metal nitrides as the covalency and ionicity of T–N bonds (T = B, P, Si) should not (only) be discussed on the basis of the respective coordination spheres.

† The degree of condensation κ gives the ratio of central atoms (T) and connecting vertices (X) in polyhedra-based structures $\kappa = n(T)/n(X)$.

Amorphous Si_3N_4, $(PNCl_2)_3$, and NH_4N_3 were reacted at 8 GPa and 1100 °C following the nominal molar ratios given in Equation 4.1. The highest yield, however, was achieved with an excess of $(PNCl_2)_3$ (×2) and NH_4N_3 (×2.5). Single crystals of SiP_2N_4NH that were up to 25 µm in length were obtained by adding 25 wt-% of NH_4Cl to the mixture of starting materials, which increased the HCl partial pressure during synthesis, facilitating reversible T–N (T = Si, P) bond cleavage and reformation (see Chapter B, Figure B.1).[26,28,29]

$$4\,Si_3N_4 + 8\,(PNCl_2)_3 + 15\,NH_4N_3 \longrightarrow 12\,SiP_2N_4NH + 48\,HCl + 20\,N_2 \tag{4.1}$$

SiP_2N_4NH can be understood as the formal reaction product of $SiPN_3$ and PNNH in a 1 : 1 ratio. Under high-pressure conditions, however, the formation of the title compound may be favored as it appears to be 12 % denser than a mixture of $SiPN_3$ and PNNH (Table B.8).[13,28,30] Preparation of mixed non-metal nitrides has been a challenging and sophisticated issue for quite some time. $SiPN_3$, for instance, has been synthesized following a multi-step procedure by condensation of preorganized molecular precursors.[13] Thus, the synthesis of SiP_2N_4NH in a one-step HP/HT reaction starting from reactive precursors and using a high partial pressure of in situ generated HCl represents an innovative process to access tailored mixed non-metal nitrides.

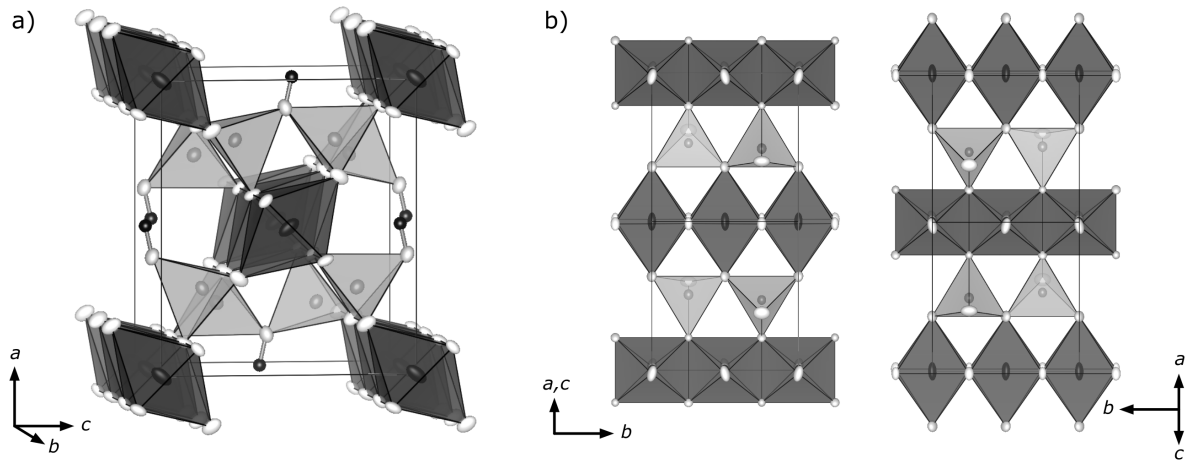

Figure 4.1.: Crystal structure of SiP_2N_4NH. Si (black) is in sixfold coordination of N (white) forming linear chains along b, which are interconnected to a highly condensed $^3_\infty\left[Si^{[6]}P^{[4]}{}_2N^{[3]}{}_4N^{[2]}H\right]$ framework by PN_4 tetrahedra (gray). H (black) is selectively bound to N1 as suggested by NMR experiments. Projections in (101) illustrate the Si/P/N network as a hierarchical variant of hypothetical $CaCl_2$-type "SiN_2" with inserted PN_4 tetrahedra. Ellipsoids are displayed at 99 % probability.

The crystal structure of SiP_2N_4NH was elucidated from single-crystal X-ray diffraction data (*Pnma* (no. 62), $a = 8.3111(18)$, $b = 5.3963(11)$, $c = 7.2392(14)$ Å, $Z = 4$, $R1 = 0.028$) and confirmed by Rietveld refinement (Figure B.4).[31] Further information on the structure determination is provided in Chapter B. The elemental composition of SiP_2N_4NH was confirmed by EDX measurements (Table B.1), and the H atom was localized by a combination of solid-state NMR measurements and difference Fourier synthesis (Figure B.3). The title compound is stable towards decomposition and phase transition up to at least 1000 °C under Ar atmosphere, as indicated by temperature-dependent PXRD (Figures B.5 and B.6). The highly condensed structure of SiP_2N_4NH is built up from edge-sharing SiN_6 octahedra forming linear chains along *b*, which are interconnected by all-side vertex-sharing PN_4 tetrahedra forming layers parallel to the *bc* plane (Figure 4.1). P1 and P2 are linked by N1, which was found to bind one equivalent of H. The remaining N sites interconnect three central vertices (P, Si), and thus the Si/P/N network is represented by the Niggli formula $^{3}_{\infty}\left[Si^{[6]}P^{[4]}{}_2N^{[3]}{}_4N^{[2]}H\right]$.[32,33] The SiP_2N_4NH structure appears related to sillimanite-type Al_2SiO_5, and its network may be interpreted as a hierarchical variant of hypothetical $CaCl_2$-type "SiN_2" with inserted PN_4 tetrahedra (Figures 4.1 and B.7).[34,35]

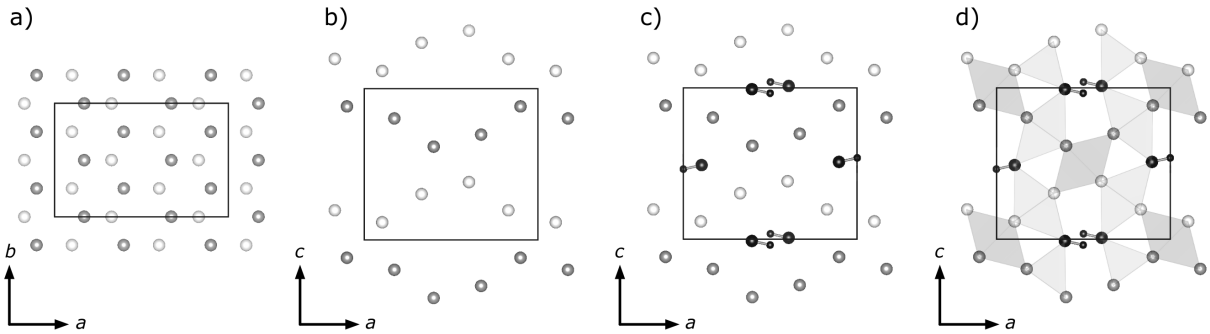

Figure 4.2.: The anionic substructure of SiP_2N_4NH can be derived from a hexagonal close-packing of nitride anions (a, b) with corrugated A (white) and B layers (gray). The substructure is completed by imide groups (black, c), providing distorted octahedral and tetrahedral voids for Si and P, respectively (d).

An anionic substructure of SiP_2N_4NH may be derived from a hexagonal close-packing (ABAB) of nitride anions (N2, N3, N4) with significantly corrugated A and B layers parallel to the *ab* plane (Figure 4.2a, b). The widened anionic substructure is completed by imide groups (N1H1, Figure 4.2c), providing distorted octahedral and tetrahedral voids for Si and P, respectively (Figure 4.2d). Thus, the SiP_2N_4NH structure may be best described by the coexistence of ambient-pressure motifs and distor-

ted close-packing, which represents an intermediate state of ambient- and high-pressure polymorphs in the structural chemistry of non-metal nitrides. Interatomic P–N distances (1.5848(14)–1.6513(11) Å) are in the typical range of tetrahedra-based P/N networks, and the elongated P1,2–N1H1 distances of 1.6805(15)/1.6844(15) Å are attributable to selective N1–H1 bonding, as observed in similar compounds as well.[28,36] The interatomic Si–N distances are 1.8031(9)/1.8037(9) Å for equatorial and 2.0146(10) Å for axial N positions, corresponding to elongated SiN_6 octahedra. The average interatomic Si–N distance of 1.874 Å, however, is in line with the value reported for γ-Si_3N_4 (1.8627(1) Å).[5,6] More detailed information on the crystal structure is provided in Chapter B.

To confirm the Si/P/N framework structure obtained from XRD analysis and to localize the H atoms in bulk SiP_2N_4NH, ^{1}H, ^{31}P, ^{31}P{^{1}H}, and ^{29}Si{^{1}H} MAS NMR measurements were performed. The ^{31}P spectrum shows two signals at $\delta = 4.4$ and 10.3 ppm, which appear slightly shifted downfield when compared to fourfold N-coordinated P, for which values of $\delta = -65$ to 0.7 ppm have been reported thus far (Figure 4.3a).[26,37] The signals, however, can be assigned to the two crystallographic P sites in SiP_2N_4NH, and the integral ratio of 1.0 : 1.1 is in good agreement with equal site multiplicity of P1 and P2 (both Wyckoff 4*c*). The presence of both signals in the ^{31}P{^{1}H} spectrum and the absence of a significant change in the integral ratio confirmed the presence of H in bulk SiP_2N_4NH and proved both P positions to be in almost equidistant spacing from H. The ^{29}Si{^{1}H} spectrum shows one major resonance at $\delta = -205$ ppm (Figure 4.3b), in line with one crystallographic Si site in SiP_2N_4NH and in good agreement with the ^{29}Si resonance reported for Si[6] in γ-Si_3N_4 ($\delta = -225$ ppm).[38] An additional minor ^{29}Si signal at $\delta = -101$ ppm may be assigned to Si/O/H species, resulting from partial surface hydrolysis during water treatment as reported in prior NMR studies on amorphous Si_3N_4.[39] In the ^{1}H NMR spectrum, one resonance at 6.6 ppm was observed, exhibiting a weak shoulder (Figure 4.3c), which most likely originates from the Si/O/H species mentioned above. Thus, one crystallographic H position is suggested for SiP_2N_4NH, as presented by selective N1–H1 bonding above. To confirm the experimental findings and conclusions from XRD and NMR investigations, SiP_2N_4NH was analyzed by the CHARDI method (see Chapter B, Figure B.12, Tables B.10 and B.11).[40] The effective coordination numbers of Si1, P1, and P2 were determined to 5.41, 3.97, and 3.92, in line with elongated octahedral and tetrahedral and coordination of Si and P. The total charges of Si1, P1, and P2 (+3.94, +5.09, +5.01) as well as the mean total charge of N (−3.04) are in very good agreement with formal oxidation states of +IV, +V, and −III.

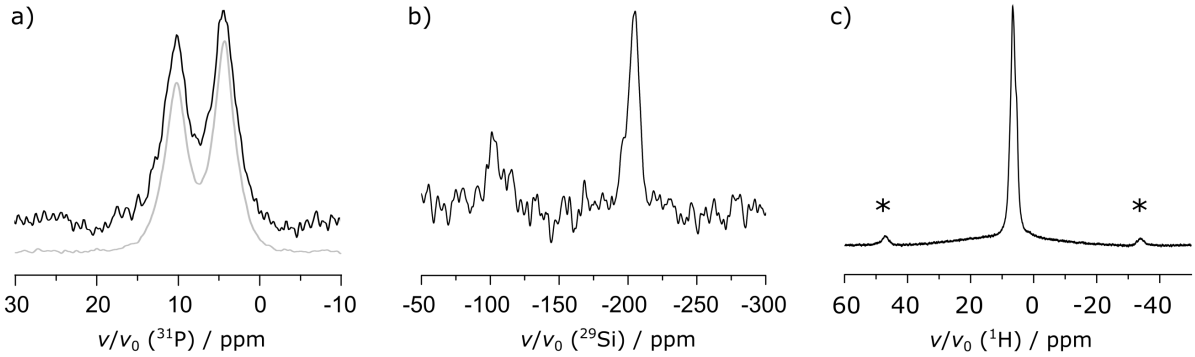

Figure 4.3.: NMR spectra of SiP_2N_4NH. Observation of two resonances in the ^{31}P (a, black) and $^{31}P\{^1H\}$ (a, gray) spectra and one major resonance in the $^{29}Si\{^1H\}$ spectrum (b) is in line with findings from XRD refinement. One ^1H signal (c) suggests one H position, represented by one imide group in SiP_2N_4NH. Spinning sidebands are marked with asterisks, and the entire NMR spectra are provided in Figure B.9.

Adapting the synthetic approach, which we have recently reported for the double nitride BP_3N_6, SiP_2N_4NH was prepared from amorphous Si_3N_4, $(PNCl_2)_3$, and NH_4N_3 in a HP/HT reaction, establishing a systematic access towards mixed non-metal nitride materials. With interconnecting PN_4 tetrahedra and SiN_6 octahedra, the title compound's structure illustrates the competition of ambient-pressure motifs and close-packing of nitride anions. Thus, the structure of SiP_2N_4NH represents an intermediate state of ambient- and high-pressure polymorphs and provides insight into the structural behavior of non-metal nitrides at high pressures. Resuming the discussion, the attempt of close-packing may increase with pressure, suggesting mixed non-metal nitrides such as BP_3N_6 and SiP_2N_4NH to adopt structures with simple close-packed anionic substructures and regular sixfold coordination of P and Si or even B. Thus, future investigations may focus on in situ high-pressure investigations of mixed non-metal nitrides to examine structural behavior under high-pressure conditions.

Acknowledgements

Financial support by the Deutsche Forschungsgemeinschaft (DFG, SCHN 377/18-1) and the Fonds der Chemischen Industrie (FCI) through a fellowship for Sebastian Vogel is gratefully acknowledged. We thank Dr. Peter Mayer and Daniel Beck for single-crystal data collection, Dr. Thomas Bräuniger, Christian Minke, and Otto Zeman for NMR measurements, and Dr. Christian Maak for SEM and EDX inves-

tigations. Inspiring discussions with PD Dr. Constantin Hoch, Sebastian Wendl, Dr. Christian Maak, and Dr. Simon Kloß (all Department of Chemistry of LMU Munich) are gratefully appreciated.

References

[1] W. Schnick, *"Solid-State Chemistry with Nonmetal Nitrides"*, *Angew. Chem. Int. Ed. Engl.* **1993**, *32*, 806; *Angew. Chem.* **1993**, *105*, 846.

[2] H.-P. Baldus, M. Jansen, *"Novel High-Performance Ceramics—Amorphous Inorganic Networks from Molecular Precursors"*, *Angew. Chem. Int. Ed. Engl.* **1997**, *36*, 328; *Angew. Chem.* **1997**, *109*, 338.

[3] F. L. Riley, *"Silicon Nitride and Related Materials"*, *J. Am. Ceram. Soc.* **2000**, *83*, 245.

[4] J. Eichler, C. Lesniak, *"Boron nitride (BN) and BN composites for high-temperature applications"*, *J. Eur. Ceram. Soc.* **2008**, *28*, 1105.

[5] A. Zerr, R. Riedel, G. Miehe, G. Serghiou, M. Schwarz, E. Kroke, H. Fueß, P. Kroll, R. Boehler, *"Synthesis of cubic silicon nitride"*, *Nature* **1999**, *400*, 340.

[6] M. Schwarz, G. Miehe, A. Zerr, E. Kroke, B. T. Poe, H. Fueß, R. Riedel, *"Spinel-Si_3N_4: Multi-Anvil Press Synthesis and Structural Refinement"*, *Adv. Mater.* **2000**, *12*, 883.

[7] D. Hardie, K. H. Jack, *"Crystal Structures of Silicon Nitride"*, *Nature* **1957**, *180*, 332.

[8] R. S. Pease, *"Crystal Structure of Boron Nitride"*, *Nature* **1950**, *165*, 722.

[9] S. Horstmann, E. Irran, W. Schnick, *"Synthesis and Crystal Structure of Phosphorus(V) Nitride α-P_3N_5"*, *Angew. Chem. Int. Ed. Engl.* **1997**, *36*, 1873; *Angew. Chem.* **1997**, *109*, 1938.

[10] T. Kobayashi, Y. Hirota, *"Inversion-mode InP MISFET employing phosphorus-nitride gate insulator"*, *Electronics Letters* **1982**, *18*, 180.

[11] M. S. Choudhary, J. K. Fink, K. Lederer, H. A. Krässig, *"Investigations of the action of flame retardants in cellulose. II: Investigation of the flame-retardant action of polyphosphonitride in cellulose"*, *J. Appl. Polym. Sci.* **1987**, *34*, 863.

[12] E.-C. Koch, S. Cudziło, *"Safer Pyrotechnic Obscurants Based on Phosphorus(V) Nitride"*, *Angew. Chem. Int. Ed.* **2016**, *55*, 15439; *Angew. Chem.* **2016**, *128*, 15665.

[13] H.-P. Baldus, W. Schnick, J. Lücke, *"Silicon Phosphorus Nitride, the First Ternary Compound in the Silicon-Phosphorus-Nitrogen System"*, *Chem. Mater.* **1993**, *5*, 845.

[14] M. Jansen, J. C. Schön, L. van Wüllen, *"The route to the structure determination of amorphous solids: a case study of the ceramic $Si_3B_3N_7$"*, *Angew. Chem. Int. Ed.* **2006**, *45*, 4244; *Angew. Chem.* **2006**, *118*, 4350.

[15] P. Baldus, M. Jansen, D. Sporn, *"Ceramic Fibers for Matrix Composites in High-Temperature Engine Applications"*, *Science* **1999**, *285*, 699.

[16] A. Y. Liu, R. M. Wentzcovitch, M. L. Cohen, *"Atomic arrangement and electronic structure of BC_2N"*, *Phys. Rev. B: Condens. Matter Mater. Phys.* **1989**, *39*, 1760.

[17] Y. Tateyama, T. Ogitsu, K. Kusakabe, S. Tsuneyuki, S. Itoh, *"Proposed synthesis path for heterodiamond BC_2N"*, *Phys. Rev. B: Condens. Matter Mater. Phys.* **1997**, *55*, R10161.

[18] R. H. Wentorf, *"Cubic Form of Boron Nitride"*, *J. Chem. Phys.* **1957**, *26*, 956.

[19] R. H. Wentorf, *"Synthesis of the Cubic Form of Boron Nitride"*, *J. Chem. Phys.* **1961**, *34*, 809.

[20] K. Landskron, H. Huppertz, J. Senker, W. Schnick, *"High-Pressure Synthesis of γ-P_3N_5 at 11 GPa and 1500 °C in a Multianvil Assembly: A Binary Phosphorus(V) Nitride with a Three-Dimensional Network Structure from PN_4 Tetrahedra and Tetragonal PN_5 Pyramids"*, *Angew. Chem. Int. Ed.* **2001**, *40*, 2643, *Angew. Chem.* **2001**, *113*, 2713.

[21] F. J. Pucher, S. R. Römer, F. W. Karau, W. Schnick, *"Phenakite-type BeP_2N_4 – a possible precursor for a new hard spinel-type material"*, *Chem. – Eur. J.* **2010**, *16*, 7208.

[22] W. Y. Ching, S. Aryal, P. Rulis, W. Schnick, *"Electronic structure and physical properties of the spinel-type phase of BeP_2N_4 from all-electron density functional calculations"*, *Phys. Rev. B* **2011**, *83*, 155109.

[23] R. Marchand, F. Tessier, A. Le Sauze, N. Diot, *"Typical features of nitrogen in nitride-type compounds"*, *Int. J. Inorg. Mater.* **2001**, *3*, 1143.

[24] J. Dong, A. A. Kinkhabwala, P. F. McMillan, *"High-pressure polymorphism in phosphorus nitrides"*, *Phys. Status Solidi B* **2004**, *241*, 2319.

[25] P. Kroll, J. von Appen, *"Post-Spinel Phases of Silicon Nitride"*, *Phys. Status Solidi B* **2001**, *226*, R6.

[26] S. Vogel, A. T. Buda, W. Schnick, *"United in Nitride: The Highly Condensed Boron Phosphorus Nitride BP_3N_6"*, *Angew. Chem. Int. Ed.* **2018**, *57*, 13202; *Angew. Chem.* **2018**, *130*, 13386.

[27] M. Andrade, D. Dzivenko, G. Miehe, R. Boehler, H. T. Hintzen, R. Riedel, *"High-pressure high-temperature synthesis and structure of β-$MgSiN_2$"*, *Phys. Status Solidi RRL* **2011**, *5*, 196.

[28] A. Marchuk, F. J. Pucher, F. W. Karau, W. Schnick, *"A high-pressure polymorph of phosphorus nitride imide"*, *Angew. Chem. Int. Ed.* **2014**, *53*, 2469; *Angew. Chem.* **2014**, *126*, 2501.

[29] A. Marchuk, V. R. Celinski, J. Schmedt auf der Günne, W. Schnick, *"$MH_4P_6N_{12}$ (M = Mg, Ca): new imidonitridophosphates with an unprecedented layered network structure type"*, *Chem. – Eur. J.* **2015**, *21*, 5836.

[30] W. Schnick, J. Lücke, *"Darstellung, Kristallstruktur und IR-spektroskopische Untersuchung von Phosphor(V)-nitrid-imid, HPN_2"*, *Z. Anorg. Allg. Chem.* **1992**, *610*, 121.

[31] Crystal data of SiP_2N_4NH from single-crystal XRD refinement: $M = 161.09\,\mathrm{g{\cdot}mol^{-1}}$, orthorhombic, *Pnma* (no. 62), $a = 8.3111(18)$, $b = 5.3963(11)$, and $c = 7.2392(14)$ Å, $V = 324.67(12)$ Å^3, $Z = 4$, $\rho = 3.296\,\mathrm{g{\cdot}cm^{-3}}$, $\mu = 1.514\,\mathrm{cm^{-1}}$, Mo-K$\alpha$ ($\lambda = 0.71073$ Å, Bruker D8 Venture), $T = 293$ K, 4513 observed reflections, 878 independent reflections, 49 parameters, $R_{\mathrm{int}} = 0.0345$, $R_\sigma = 0.0273$, $R1 = 0.0284$, $wR2 = 0.0736$, $GoF = 1.120$, residual electron density 0.662, $-0.700\,e{\cdot}$Å^{-3}. CSD-1880683 (SiP_2N_4NH) contains the supplementary crystallographic data for this paper. These data can be obtained free of charge from The Cambridge Crystallographic Data Centre.

[32] U. Müller, *"Anorganische Strukturchemie"*, Vieweg + Teubner, Wiesbaden, 6th Ed., **2008**.

[33] J. Lima-de-Faria, E. Hellner, F. Liebau, E. Makovicky, E. Parthé, *"Nomenclature of inorganic structure types. Report of the International Union of Crystallography Commission on Crystallographic Nomenclature Subcommittee on the Nomenclature of Inorganic Structure Types"*, *Acta Crystallogr. Sect. A: Found. Adv.* **1990**, *46*, 1.

[34] W. H. Taylor, *"The structure of sillimanite and mullite"*, *Z. Kristallogr. - Cryst. Mater.* **1928**, *68*, 503.

[35] A. K. van Bever, W. Nieuwenkamp, *"Die Kristallstruktur von Calciumchlorid, $CaCl_2$"*, *Z. Kristallogr. – Cryst. Mater.* **1935**, *90*, 374.

[36] S. Vogel, W. Schnick, *"SrP_3N_5NH: A Framework-Type Imidonitridophosphate Featuring Structure-Directing Hydrogen Bonds"*, *Chem. – Eur. J.* **2018**, *24*, 14275.

[37] W. Schnick, J. Lücke, F. Krumeich, *"Phosphorus Nitride P_3N_5: Synthesis, Spectroscopic, and Electron Microscopic Investigations"*, *Chem. Mater.* **1996**, *8*, 281.

[38] T. Sekine, M. Tansho, M. Kanzaki, *"^{29}Si magic-angle-spinning nuclear-magnetic-resonance study of spinel-type Si_3N_4"*, *Appl. Phys. Lett.* **2001**, *78*, 3050.

[39] E. A. Leone, S. Curran, M. E. Kotun, G. Carrasquillo, R. Weeren, S. C. Danforth, *"Solid-State ^{29}Si NMR Analysis of Amorphous Silicon Nitride Powder"*, *J. Am. Ceram. Soc.* **1996**, *79*, 513.

[40] R. Hoppe, S. Voigt, H. Glaum, J. Kissel, H. P. Müller, K. Bernet, *"A new route to charge distributions in ionic solids"*, *J. Less-Common Met.* **1989**, *156*, 105.

5. Stishovite's Relative: A Post-Coesite Form of Phosphorus Oxonitride

Sebastian Vogel, Dominik Baumann, Robin Niklaus, Elena Bykova, Maxim Bykov, Natalia Dubrovinskaia, Leonid Dubrovinsky, and Wolfgang Schnick

Angew. Chem. Int. Ed. **2018**, *57*, 6691;
Angew. Chem. **2018**, *130*, 6801.
DOI: 10.1002/anie.201803610

Phosphorus gives high five: The phase diagram of phosphorus oxonitride (PON) was extended by a post-coesite form of PON, in which P is fivefold coordinated by O and N, which has not been reported for any PON form before. Post-coesite PON adopts a stishovite-related structure and suggests an unexhausted polymorphism including sixfold coordinated P in PON structures.

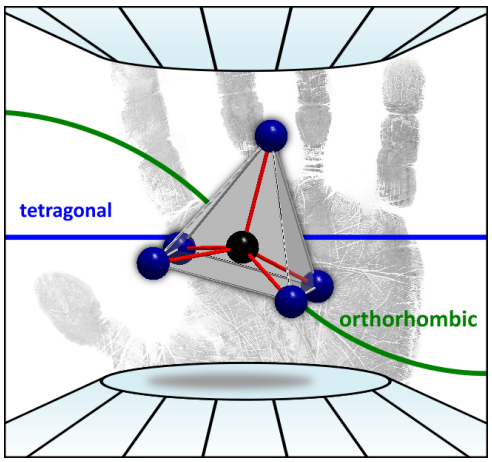

Abstract *Phosphorus oxonitride (PON) is isoelectronic with SiO_2 and may exhibit a similar broad spectrum of intriguing properties as silica. However, PON has only been sparsely investigated under high-pressure conditions and there has been no evidence on a PON polymorph with a coordination number of P greater than 4. Herein, we report a post-coesite (pc) PON polymorph exhibiting a stishovite-related structure with P in a (5+1) coordination. The pc-PON was synthesized using the multianvil technique and characterized by powder X-ray diffraction, solid-state NMR spectroscopy, TEM measurements and in situ synchrotron X-ray diffraction in diamond anvil cells. The structure model was verified by single-crystal X-ray diffraction at 1.8 GPa and the isothermal bulk modulus of pc-PON was determined to K_0 = 163(2) GPa. Moreover, an orthorhombic PON polymorph (o-PON) was observed under high-pressure conditions and corroborated as the stable modification at pressures above 17 GPa by DFT calculations.*

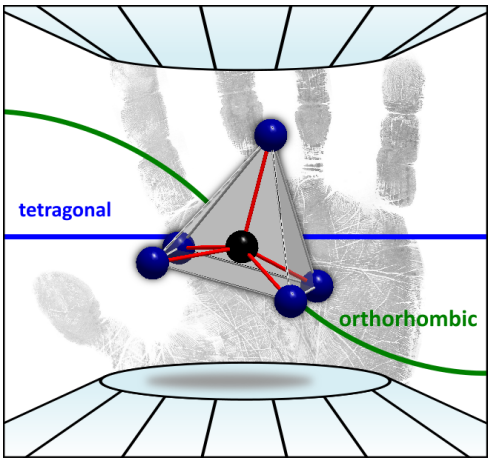

The pressure-coordination rule, stating that the coordination number increases with an increase of pressure,[1] has already been verified for fundamental inorganic nitrides and oxides, such as BN,[2] Si_3N_4,[3] P_3N_5,[4] CO_2,[5–8] and SiO_2.[9–15] Respective high-pressure polymorphs show intriguing properties, such as increased incompressibility, high density, or changes in types of chemical bonding. For instance, rutile-type SiO_2 (stishovite), with Si situated in an octahedral sixfold coordination by O, is one of the hardest oxides known.[9,16,17] Extensive in situ investigations in diamond anvil cells revealed post-stishovite SiO_2 polymorphs with $CaCl_2$-, α-PbO_2-, and high-pressure PdF_2-type structures, which all have the motif of SiO_6 octahedra in common.[10–15]

Phosphorus oxonitride PON is isoelectronic with silica and adopts cristobalite-, moganite- and quartz-type structures, which are isotypic with the eponymous SiO_2 forms.[18–20] Furthermore, an additional δ-PON modification with a unique structure related to a theoretically predicted SiO_2 polymorph has been synthesized at 12 GPa while at 15.5 GPa a coesite-type (coe) PON form has been prepared, which hitherto represents the top end of the PON phase diagram.[21,22] PON polymorphs with an increased

coordination number of P, however, seem to be feasible, considering findings from fundamental structural research on solid-state P/N and P/O compounds. Square pyramidal and trigonal bipyramidal PN_5 units have been reported in the high-pressure phases γ-P_3N_5 and γ-HP_4N_7 and sixfold coordinated P has been predicted for the high-pressure phases δ-P_3N_5 and spinel-type BeP_2N_4.[4,23–26] Recently, five- and sixfold O-coordinated P has been reported for $TiPO_4$-V and a distorted $CaCl_2$-related form of $AlPO_4$, respectively.[27,28] In contrast, high-pressure polymorphs of PON with an increased coordination number of P (CN > 4), are still unknown. Considering the kinship of PON and SiO_2, a stishovite-type PON polymorph with a sixfold coordination of P may be plausible and is considered the missing link in fundamental structural research on phosphorus (oxo)nitrides.

Herein, we report on a stishovite-related post-coesite (pc) form of PON with a (5+1) coordination of P, which was prepared from cristobalite-type (cri) PON at 20 GPa using a 1000 t hydraulic press and the multianvil technique based on a modified Walker-type setup.[29,30] Energy dispersive X-ray (EDX) spectroscopy showed no other elements than P, O, and N in the sample and any presence of N–H or O–H functionality was ruled out by FTIR spectroscopy.

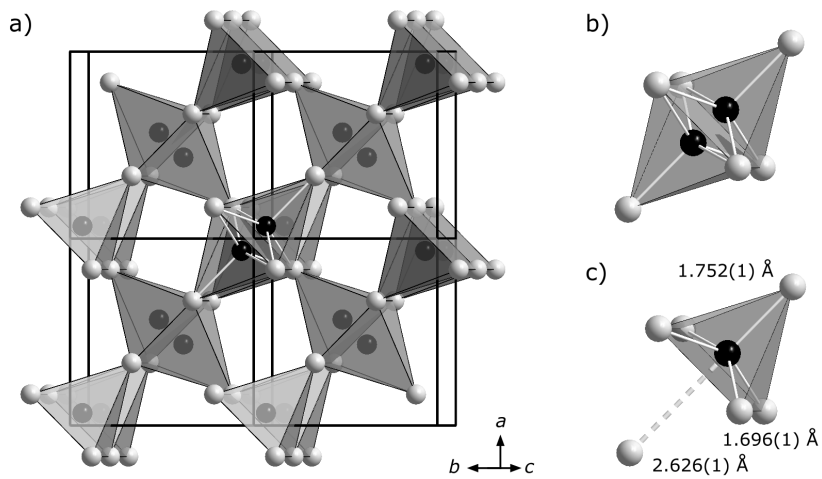

Figure 5.1.: The crystal structure of pc-PON (a) shows a split position for P located in octahedral coordination environment by O and N (b). An occupation of 0.5 of the P position leads to a (5+1) coordination with distorted square pyramidal geometry (c). P black, N/O gray.

The pc-PON structure was solved and refined from powder X-ray diffraction (PXRD) pattern ($P4_2/mnm$ (no. 136), $a = 4.62782(10)$, $c = 2.46042(4)$ Å, $Z = 2$, $R_{\mathrm{Bragg}} = 0.021$) and cell metrics were

confirmed by selected area electron diffraction (SAED) tilting series.[31] pc-PON adopts a stishovite-related structure with one P site located in an octahedral coordination sphere of O and N (Figure 5.1a). The refined coordinates of P are close to Wyckoff position $2a$ ($m.mm$), but refinement indicated a significant displacement. Thus, P was refined at Wyckoff position $4f$ ($m.2m$), which results in a split position of P (site occupation factor $s.o.f. = 0.5$) with a 0.874(1) Å distance between the two electron density maxima (Figure 5.1b). There is, however, no evidence for any superstructure caused by a systematically ordering of P in pc-PON, as there were no additional reflections observed during PXRD, TEM measurements or single-crystal XRD presented below.

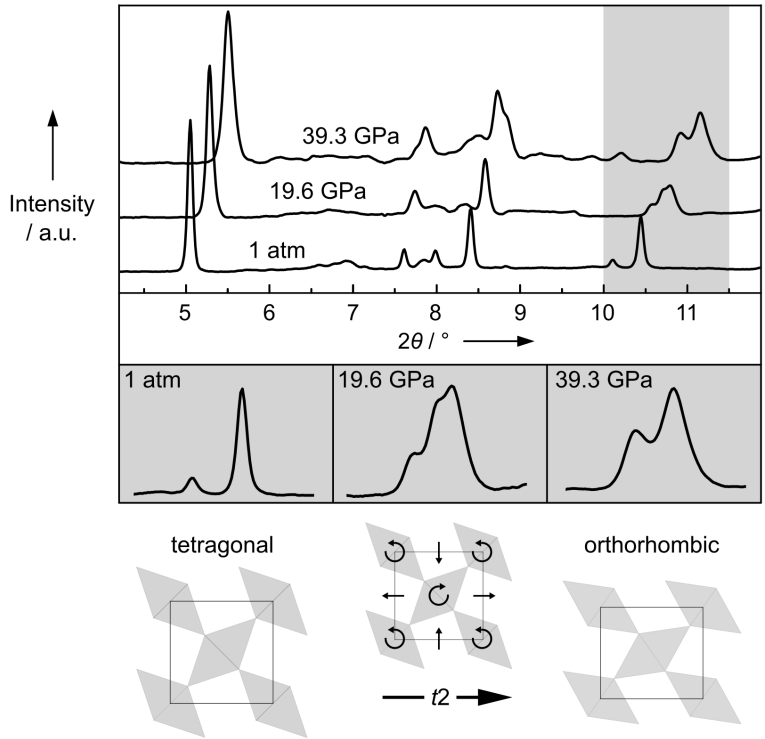

Figure 5.2.: Selected PXRD patterns from synchrotron measurements at high-pressure conditions ($\lambda = 0.288\,74$ Å) with expanded regions of interest and a schematic illustration of the tetragonal → orthorhombic phase transition assumed for PON.

Considering the split position, P is in a (5+1) coordination by O and N with distorted square pyramidal geometry for the first coordination sphere (Figure 5.1c). The $P(N,O)_5$ pyramids share common edges along c and common vertices along $\langle 110 \rangle$. The interatomic distances between P and (N,O) are 1.696(1) Å for equatorial and 1.752(1) Å for axial position, which is in good agreement with the fivefold

coordinated P positions in γ-HP_4N_7 and γ-P_3N_5.[4,23] The P–(N,O) distance of the second axial (N,O) position in pc-PON is 2.626(1) Å corresponding to minor interactions only and thus, this (N,O) position is assigned to the second coordination sphere. The ^{31}P solid-state MAS NMR spectrum of pc-PON shows one broadened signal at $\delta = -86.9$ ppm (FWHM = 20 ppm), in line with one crystallographic position of P in the pc-PON structure. Peak broadening may be caused by varying local N/O coordination of P and has been observed in other PON modifications before.[21,22] Moreover, statistic occupation of the split position of P can enhance peak broadening in this case. A simplified description of the pc-PON structure may be revealed by reducing the split position of P to its center of gravity, resulting in an octahedral coordination of P by N and O atoms. This simplified structure model would be isotypic with stishovite (rutile-type SiO_2) as the P($4f$, $m.2m$) site ($s.o.f. = 0.5$) would be transformed into a P($2a$, $m.mm$) site ($s.o.f. = 1$). Thus, pc-PON may be understood as the analog of stishovite in the phase diagram of PON and represents the first phosphorus oxonitride with exclusively fivefold coordination of P. More detailed information on the synthesis of pc-PON and its characterization by PXRD, TEM, EDX, NMR and FTIR is provided in Chapter C.

To investigate pc-PON on its elastic properties, in situ XRD measurements with synchrotron radiation in diamond anvil cells (DAC) were performed. At an initial pressure of 1.8 GPa a single-crystal data set was collected, which verifies the structure model presented above.[32] Owing to the measuring geometry of DACs the single-crystal (SC) XRD data set is incomplete (77 %). A comparison of the electron density maps and respective standard deviations, however, indicate that PXRD and SC-XRD refinements are tantamount in quality and accuracy, as presented in Chapter C. Subsequently, 16 PXRD patterns up to a maximum pressure of almost 40 GPa were collected, in which the PXRD pattern of pc-PON is preserved up to a pressure of approximately 20 GPa. At pressures exceeding 20 GPa, however, a new phase is observed, as reflections in the region $10.0° < 2\theta < 11.5°$ change significantly (Figure 5.2). The coexistence of both phases at 19.6 GPa is a strong indication for a second order phase transition, which was described by a translationengleiche symmetry reduction ($t2$) to the orthorhombic crystal system ($P4_2/mnm$ (no. 136) $\rightarrow$ $Pnnm$ (no. 58)). In order to gain further information on the nature of the tetragonal $\rightarrow$ orthorhombic phase transition, the recovered sample was re-measured at ambient conditions, showing tetragonal symmetry again. Thus, the orthorhombic (o) PON phase is solely stabilized at high pressures and may be the initial product of the multianvil synthesis at 20 GPa, while the tetragonal pc-PON phase might form

upon pressure quenching. In turn, pc-PON is unstable at ambient conditions as well, but kinetically inert towards transformation to cri-PON, as indicated by temperature-dependent PXRD.

This reversible tetragonal → orthorhombic phase transition of PON is of remarkable similarity to the stishovite ($P4_2/mnm$) → $CaCl_2$-type SiO_2 ($Pnnm$) phase transition of silica, which is characterized by an alternating tilting of the SiO_6 octahedra in the *a*-*b* plane with increasing pressure.[10,33] Considering a spontaneous strain analysis of pc- and o-PON, the phase transition in PON appears to proceed in a similar way, suggesting an alternating tilting of the P coordination polyhedra and a $CaCl_2$-related structure for o-PON (Figure 5.2).[33] More detailed information on the experimental setup and the synchrotron measurements as well as on the spontaneous strain formalism is provided in Chapter C.

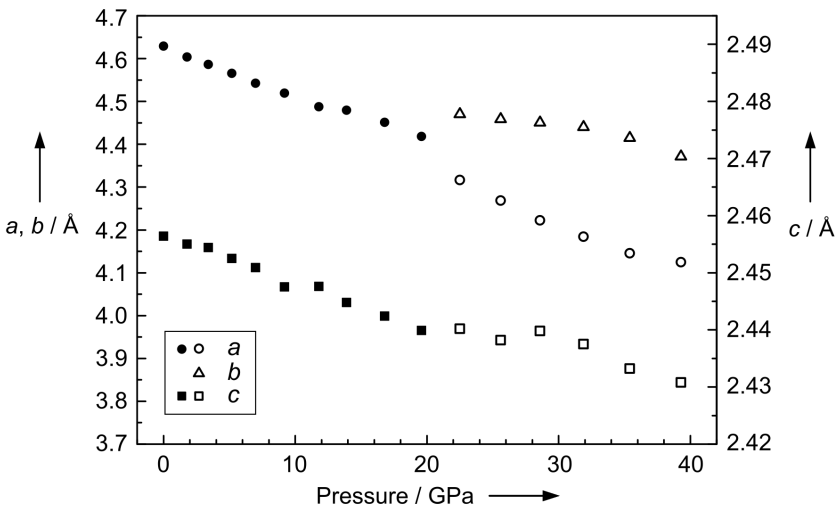

Figure 5.3.: Refined lattice parameters of pc-PON (black) and o-PON (white) as a function of pressure.

Lattice parameters of pc- and o-PON were refined from PXRD data with the method of Le Bail using tetragonal ($P4_2/mnm$, $p < 20$ GPa) and orthorhombic ($Pnnm$, $p > 20$ GPa) metrics, respectively (Figure 5.3). Subsequently, the isothermal bulk modulus K_0 of pc-PON was determined to 163(2) GPa from the equation of state and with that, pc-PON exhibits a twice as high bulk modulus than cri-PON ($K_0 = 80$ GPa).[34] However, pc-PON seems to be significantly more compressible than stishovite ($K_0 = 310$ GPa), which may be due to the (5+1) coordination polyhedra of P being less rigid than the SiO_6 octahedra.[33] Furthermore, the lattice parameter a was found to be notably more compressible than c ($K_0(a^3) = 109(2)$ GPa, $K_0(c^3) = 927(35)$ GPa), which may be an effect of the $P(N,O)_5$ pyramids

sharing common vertices along ⟨110⟩, but common edges along c. Thus, a decrease in volume upon compression in pc-PON is mostly effected by a contraction of the cell along a, which in turn corresponds to an axial compression of the $P(N,O)_{5+1}$ polyhedra and a decrease of the axial P–(O,N) interatomic distances. Consequently, a hitherto unreported regular sixfold coordination of P in phosphorus (oxo)nitrides might be plausible for PON at sufficiently high pressure and may lead to a significant increase of its incompressibility and bulk modulus. More detailed information on the elastic properties of pc-PON is provided in Chapter C.

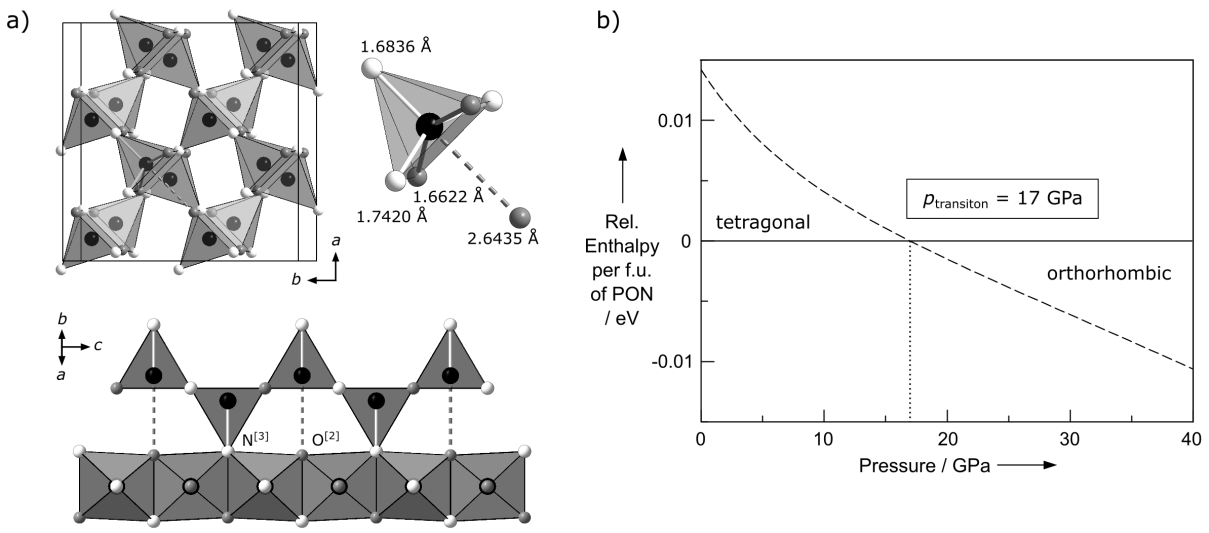

Figure 5.4.: Approximated structure model of pc-PON from structure relaxation with N/O-order used for DFT calculations (a). P black, O gray, N white. Relative enthalpy plot with transition pressure of 17 GPa derived from calculated E-V data of pc- and o-PON (b).

To confirm the experimental findings and to corroborate o-PON as the high-pressure polymorph, DFT calculations within the generalized gradient approximation (GGA) were performed. Accounting for the split position of P a $2 \times 2 \times 2$ supercell was constructed with P at the center of the N/O octahedra and different charge neutral N/O-ordering models were constructed to approximate statistical N/O-disorder. Disregarding unreasonable or computationally collapsing structures, relaxation of the supercell resulted in an alternating displacement of P atoms from the center of the $P(N/O)_6$ octahedra, in line with the experimental findings of the split position of P (Figure 5.4a). This systematic ordering of P appears as a coupled feature of the introduced N/O-ordering, as the displacement of each P site is systematically

directed towards an axial N position. As a result N and O are found exclusively in three- and twofold coordination, respectively, as expressed by the Niggli formula $^{3}_{\infty}\left[P^{[5]}O^{[2]}N^{[3]}\right]$.[35] Thus, the axial P–N interaction seems to be more favorable than the axial P–O interaction. Concerning the experimental data presented above, there are, however, no indications of a superstructure caused by a systematic ordering of P. Considering the favored axial P–N interaction this random distribution of P may be correlated with a N/O-disorder in pc-PON.

The tetragonal structure model was used for construction of an orthorhombic model and subsequent energy-volume calculations of both cells. The respective total energies of both phases corroborate o-PON the stable modification above 17 GPa. The transition pressure was determined from the relative enthalpy plot (Figure 5.4b) and is in accordance with the experimental findings, considering the approximated structure model used for the DFT calculations. More detailed information on the theoretical study of both PON polymorphs is provided in Chapter C.

Recapitulating, the phase diagram of PON is extended by two high-pressure polymorphs. pc-PON adopts a stishovite-related structure with a split position of P in a (5+1) coordination and has been considered the missing link in fundamental structural research on phosphorus (oxo)nitrides, previously. In addition, o-PON is found to be the stable polymorph at pressures over 20 GPa, which has been proven by ab initio calculations, as well. In turn, P is just on the brink of a regular sixfold coordination in PON polymorphs and its experimental evidence will be the great goal of future high-pressure investigations.

Acknowledgements

Financial support by the Deutsche Forschungsgemeinschaft (DFG, SCHN 377/18-1) and the Fonds der Chemischen Industrie (FCI) for a fellowship for Sebastian Vogel is gratefully acknowledged. N.D. and L.D. thank the German Research Foundation [Deutsche Forschungsgemeinschaft (DFG)] and the Federal Ministry of Education and Research [Bundesministerium für Bildung und Forschung (BMBF), Germany] for financial support: projects DU 954/11-1, DU 393/9-2, and DU 393/10-1 (DFG) and Grant No. 5K16WC1 (BMBF). Parts of this research were carried out at the extreme conditions beamline P02.2 at DESY, a member of the Helmholtz Association (HGF). We thank Prof. Oliver Oeckler (University of Leipzig) for his support concerning structure solution and refinement of powder X-ray diffraction patterns and Dr. Irina Chuvashova (University of Bayreuth) for support in preliminary XRD measurements. Furthermore, we thank Dr. Thomas Bräuniger and Christian Minke for solid-state MAS NMR

measurements and Dr. Lukas Neudert (all at Department of Chemistry of LMU Munich) for TEM and EDX investigations. Inspiring discussions with PD Dr. Constantin Hoch, Dr. Simon Kloß and Dr. Philipp Bielec (all at Department of Chemistry of LMU Munich) are gratefully appreciated.

References

[1] A. Neuhaus, *"Structural Behavior, and Valence State of Inorganic Matter in the Realm of Higher and Highest Pressure"*, *Chimia* **1964**, *18*, 93.

[2] R. H. Wentorf, *"Cubic Form of Boron Nitride"*, *J. Chem. Phys.* **1957**, *26*, 956.

[3] A. Zerr, R. Riedel, G. Miehe, G. Serghiou, M. Schwarz, E. Kroke, H. Fueß, P. Kroll, R. Boehler, *"Synthesis of cubic silicon nitride"*, *Nature* **1999**, *400*, 340.

[4] K. Landskron, H. Huppertz, J. Senker, W. Schnick, *"High-Pressure Synthesis of γ-P_3N_5 at 11 GPa and 1500 °C in a Multianvil Assembly: A Binary Phosphorus(V) Nitride with a Three-Dimensional Network Structure from PN_4 Tetrahedra and Tetragonal PN_5 Pyramids"*, *Angew. Chem. Int. Ed.* **2001**, *40*, 2643, *Angew. Chem.* **2001**, *113*, 2713.

[5] F. Datchi, B. Mallick, A. Salamat, S. Ninet, *"Structure of polymeric carbon dioxide CO_2-V"*, *Phys. Rev. Lett.* **2012**, *108*, 125701.

[6] V. Iota, C. S. Yoo, H. Cynn, *"Quartzlike Carbon Dioxide: An Optically Nonlinear Extended Solid at High Pressures and Temperatures"*, *Science* **1999**, *283*, 1510.

[7] A. Sengupta, C.-S. Yoo, *"Coesite-like CO_2: An analog to SiO_2"*, *Phys. Rev. B: Condens. Matter Mater. Phys.* **2010**, *82*, 12105.

[8] V. Iota, C.-S. Yoo, J.-H. Klepeis, Z. Jenei, W. Evans, H. Cynn, *"Six-fold coordinated carbon dioxide VI"*, *Nat. Mater.* **2007**, *6*, 34.

[9] S. M. Stishov, S. V. Popova, *"A new dense modification of silica"*, *Geokhimiya* **1961**, *10*, 837.

[10] Y. Tsuchida, T. Yagi, *"A new, post-stishovite highpressure polymorph of silica"*, *Nature* **1989**, *340*, 217.

[11] L. S. Dubrovinsky, S. K. Saxena, P. Lazor, R. Ahuja, O. Eriksson, J. M. Wills, B. Johansson, *"Experimental and theoretical identification of a new high-pressure phase of silica"*, *Nature* **1997**, *388*, 362.

[12] N. A. Dubrovinskaia, L. S. Dubrovinsky, S. K. Saxena, F. Tutti, S. Rekhi, T. Le Bihan, *"Direct transition from cristobalite to post-stishovite α-PbO_2-like silica phase"*, *Eur. J. Mineral.* **2001**, *13*, 479.

[13] L. S. Dubrovinsky, N. A. Dubrovinskaia, S. Saxena, F. Tutti, S. Rekhi, T. Le Bihan, G. Shen, J. Hu, *"Pressure-induced transformations of cristobalite"*, *Chem. Phys. Lett.* **2001**, *333*, 264.

[14] P. Dera, C. T. Prewitt, N. Z. Boctor, R. J. Hemley, *"Characterization of a high-pressure phase of silica from the Martian meteorite Shergotty"*, *Am. Mineral.* **2002**, *87*, 1018.

[15] Y. Kuwayama, K. Hirose, N. Sata, Y. Ohishi, *"The pyrite-type high-pressure form of silica"*, *Science* **2005**, *309*, 923.

[16] J.-M. Léger, J. Haines, M. Schmidt, J. P. Petitet, A. S. Pereira, J. A. H. da Jornada, *"Discovery of hardest known oxide"*, *Nature* **1996**, *383*, 401.

[17] L. S. Dubrovinsky, N. A. Dubrovinskaia, V. Swamy, J. Muscat, N. M. Harrison, R. Ahuja, B. Holm, B. Johansson, *"Materials science. The hardest known oxide"*, *Nature* **2001**, *410*, 653.

[18] L. Boukbir, R. Marchand, Y. Laurent, P. Bacher, G. Roult, *"Preparation and time-of-flight neutron diffraction study of the cristobalite-type PON phosphorus oxynitride"*, *Ann. Chim. Fr.* **1989**, *14*, 475.

[19] J. Haines, C. Chateau, J.-M. Léger, A. Le Sauze, N. Diot, R. Marchand, S. Hull, *"Crystal structure of moganite-type phosphorus oxynitride: Relationship to other twinned-quartz-based structures"*, *Acta Cryst.* **1999**, *55*, 677.

[20] J.-M. Léger, J. Haines, L. S. de Oliveira, C. Chateau, A. Le Sauze, R. Marchand, S. Hull, *"Crystal structure and high pressure behaviour of the quartz-type phase of phosphorus oxynitride PON"*, *J. Phys. Chem. Solids* **1999**, *60*, 145.

[21] D. Baumann, S. J. Sedlmaier, W. Schnick, *"An unprecedented AB_2 tetrahedra network structure type in a high-pressure phase of phosphorus oxonitride (PON)"*, *Angew. Chem. Int. Ed.* **2012**, *51*, 4707; *Angew. Chem.* **2012**, *124*, 4784.

[22] D. Baumann, R. Niklaus, W. Schnick, *"A high-pressure polymorph of phosphorus oxonitride with the coesite structure"*, *Angew. Chem. Int. Ed.* **2015**, *54*, 4388; *Angew. Chem.* **2015**, *127*, 4463.

[23] D. Baumann, W. Schnick, *"Pentacoordinate phosphorus in a high-pressure polymorph of phosphorus nitride imide $P_4N_6(NH)$"*, *Angew. Chem. Int. Ed.* **2014**, *53*, 14490; *Angew. Chem.* **2014**, *126*, 14718.

[24] P. Kroll, W. Schnick, *"A Density Functional Study of Phosphorus Nitride P_3N_5: Refined Geometries, Properties, and Relative Stability of α-P_3N_5 and γ-P_3N_5 and a Further Possible High-Pressure Phase δ-P_3N_5 with Kyanite-Type Structure"*, *Chem. – Eur. J.* **2002**, *8*, 3530.

[25] F. J. Pucher, S. R. Römer, F. W. Karau, W. Schnick, *"Phenakite-type BeP_2N_4 – a possible precursor for a new hard spinel-type material"*, *Chem. – Eur. J.* **2010**, *16*, 7208.

[26] W. Y. Ching, S. Aryal, P. Rulis, W. Schnick, *"Electronic structure and physical properties of the spinel-type phase of BeP_2N_4 from all-electron density functional calculations"*, *Phys. Rev. B* **2011**, *83*, 155109.

[27] M. Bykov, E. Bykova, M. Hanfland, H.-P. Liermann, R. K. Kremer, R. Glaum, L. S. Dubrovinsky, S. van Smaalen, *"High-Pressure Phase Transformations in $TiPO_4$: A Route to Pentacoordinated Phosphorus"*, *Angew. Chem. Int. Ed.* **2016**, *55*, 15053; *Angew. Chem.* **2016**, *128*, 15277.

[28] J. Pellicer-Porres, A. M. Saitta, A. Polian, J. P. Itie, M. Hanfland, *"Six-fold-coordinated phosphorus by oxygen in $AlPO_4$ quartz homeotype under high pressure"*, *Nat. Mater.* **2007**, *6*, 698.

[29] D. Walker, *"Lubrication, gasketing, and precision in multianvil experiments"*, *Am. Mineral.* **1991**, *76*, 1092.

[30] H. Huppertz, *"Multianvil high-pressure / high-temperature synthesis in solid state chemistry"*, *Z. Kristallogr.* **2004**, *219*, 330.

[31] Crystal data of pc-PON from PXRD refinement ($p = 1\,\mathrm{atm}$): $M = 60.98\,\mathrm{g{\cdot}mol^{-1}}$, tetragonal, $P4_2/mnm$ (no. 136), $a = 4.62782(10)$ and $c = 2.46042(4)\,\text{Å}$, $V = 52.694(4)\,\text{Å}^3$, $Z = 2$, $\rho = 3.843\,\mathrm{g{\cdot}cm^{-3}}$, $\mu = 17.54\,\mathrm{cm^{-1}}$, Mo-K$\alpha_1$-radiation ($\lambda = 0.71073\,\text{Å}$), $T = 293\,\mathrm{K}$, 97 measured reflections, 34 parameters, Stoe Stadi P powder diffractometer with MYTHEN 1K Si strip detector and Ge(111) monochromator, peak shape modelled by fundamental parameters approach,[36, 37] background function: shifted Chebychev (19 parameters), $R_{\mathrm{Bragg}} = 0.02108$, $R_{\mathrm{p}} = 0.03484$, $R_{\mathrm{wp}} = 0.04621$, $R_{\mathrm{exp}} = 0.03484$, $GoF = 1.327$. Further details on the crystal structure investigation may be obtained from the Fachinformationszentrum Karlsruhe, 76344 Eggenstein-Leo-

poldshafen, Germany (fax: (+49) 7247-808-666; e-mail: crysdata@fiz-karlsruhe.de), on quoting the depository number CSD-433717.

[32] Crystal data of pc-PON from XRD refinement ($p = 1.8\,\mathrm{GPa}$): $M = 60.98\,\mathrm{g{\cdot}mol^{-1}}$, tetragonal, $P4_2/mnm$ (no. 136), $a = 4.6027(3)$ and $c = 2.4560(3)\,\text{Å}$, $V = 52.030(9)\,\text{Å}^3$, $Z = 2$, $\rho = 3.892\,\mathrm{g{\cdot}cm^{-3}}$, $\mu = 1.8\,\mathrm{cm^{-1}}$, synchrotron radiation (PETRA III, DESY, Hamburg, Germany, $\lambda = 0.288\,74\,\text{Å}$), $T = 293\,\mathrm{K}$, 244 observed reflections, 113 independent reflections, 9 parameters, $R_{\mathrm{int}} = 0.0463$, $R_\sigma = 0.0513$, $R1 = 0.0513$, $wR2 = 0.1110$, $GoF = 1.343$, residual electron density 0.602, $-0.601\,e{\cdot}\text{Å}^{-3}$. Further details on the crystal structure investigation may be obtained from the Fachinformationszentrum Karlsruhe, 76344 Eggenstein- Leopoldshafen, Germany (fax: (+49) 7247-808-666; e-mail: crysdata@fiz-karlsruhe.de), on quoting the depository number CSD-434035.

[33] D. Andrault, R. J. Angel, J. L. Mosenfelder, T. Le Bihan, *"Equation of state of stishovite to lower mantle pressures"*, *Am. Mineral.* **2003**, *88*, 301.

[34] K. J. Kingma, R. E. G. Pacalo, P. F. McMillan, *"High-Pressure Stability of the Cristobalite Framework in PON and PN(NH)"*, *Eur. J. Solid State Inorg. Chem.* **1997**, *34*, 679.

[35] U. Müller, *"Anorganische Strukturchemie"*, Vieweg + Teubner, Wiesbaden, 6th Ed., **2008**.

[36] R. W. Cheary, A. Coelho, *"A fundamental parameters approach to X-ray line-profile fitting"*, *J. Appl. Crystallogr.* **1992**, *25*, 109.

[37] R. W. Cheary, A. A. Coelho, J. P. Cline, *"Fundamental Parameters Line Profile Fitting in Laboratory Diffractometers"*, *J. Res. Natl. Inst. Stand. Technol.* **2004**, *109*, 1.

6. Boron Phosphorus Nitride at Extremes: PN_6 Octahedra in the High-Pressure Polymorph β-BP_3N_6

Sebastian Vogel, Maxim Bykov, Elena Bykova, Sebastian Wendl, Simon D. Kloß, Anna Pakhomova, Stella Chariton, Egor Koemets, Natalia Dubrovinskaia, Leonid Dubrovinsky, and Wolfgang Schnick

Angew. Chem. Int. Ed. **2019**, *58*, 9060;
Angew. Chem. **2019**, *131*, 9158.
DOI: 10.1002/anie.201902845

Extreme conditions: α-BP_3N_6 was investigated in situ upon cold compression to a maximum pressure of 42 GPa, at which laser heating induced a phase transition into its high-pressure polymorph β-BP_3N_6. β-BP_3N_6 is the first nitride to contain PN_6 octahedra, representing a much sought-after structural motif in fundamental research on non-metal nitrides.

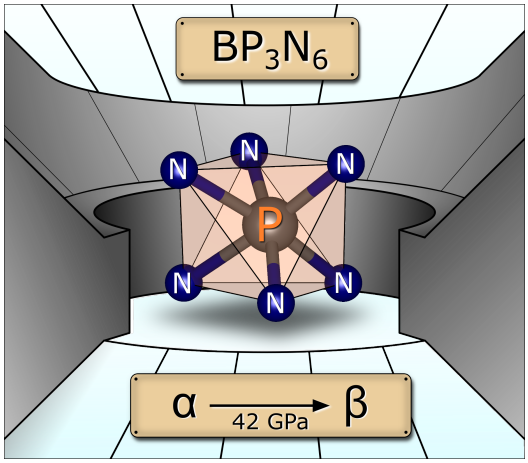

Abstract *The high-pressure behavior of non-metal nitrides is of special interest for inorganic and theoretical chemistry as well as materials science, as these compounds feature intriguing elastic properties. The double nitride α-BP_3N_6 was investigated by in situ single-crystal X-ray diffraction (XRD) upon cold compression to a maximum pressure of about 42 GPa, and its isothermal bulk modulus at ambient conditions was determined to be 146(6) GPa. At maximum pressure the sample was laser-heated, which resulted in the formation of an unprecedented high-pressure polymorph, β-BP_3N_6. Its structure was elucidated by single-crystal XRD, and can be described as a decoration of a distorted hexagonal close-packing of N with B in tetrahedral and P in octahedral voids. Hence, β-BP_3N_6 is the first nitride to contain PN_6 octahedra, representing the much sought-after proof of principle for sixfold N-coordinated P that has been predicted for numerous high-pressure phases of nitrides.*

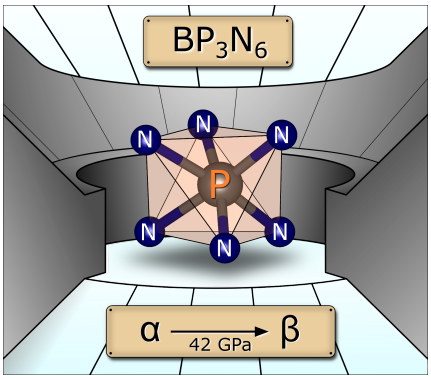

The polymorphism of non-metal oxides and nitrides is considered to be one of the most diverse field of structural chemistry. Investigations on high-pressure polymorphs of non-metal nitrides are an extensive field of research, as these phases can show outstanding mechanical properties such as low compressibility and high mechanical hardness.[1–7] Moreover, numerous intriguing high-pressure polymorphs have been proposed from theoretical investigations, but experimental evidence is still lacking.

Under ambient conditions, the structural chemistry of non-metal nitrides, namely those of boron, carbon, silicon, or phosphorus, are dominated by an sp^2/sp^3 hybridization of the non-metal atoms, leading to three- and fourfold N coordination. Coordination numbers, however, typically increase with pressure.[8] h-BN, for instance, consists of graphene-like layers, featuring B in threefold coordination of N (= $B^{[3]}$, coordination numbers given in superscripted square brackets).[9–11] Its high-pressure polymorph c-BN (sphalerite structure type) is built up from all-side vertex-sharing BN_4 tetrahedra and is classified as a superhard material.[1,2,5] Moreover, DFT calculations have predicted that a rock-salt-type BN polymorph featuring $B^{[6]}$ is supposed to be stable under very high loads of 850–1200 GPa.[12–14] Numerous triazine- and heptazine-based sp^2-C/N compounds, summarized in the blanket term carbon nitrides, have been

investigated intensively as they show intriguing photocatalytic properties.[15–18] In contrast, there have only been few experimental hints on sp^3-C/N compounds, which, however, have been suspected to be superhard materials from theoretical studies.[19–22] The tetrahedra-based Si/N network of phenakite-type β-Si_3N_4 exhibits outstanding thermal and mechanical properties, which makes it an indispensable refractive material for high-performance applications.[23–25] At pressures exceeding 13 GPa, spinel-type γ-Si_3N_4 has been reported as the stable polymorph, featuring both, SiN_4 tetrahedra and SiN_6 octahedra.[3,4] Entire sixfold N coordination of Si, however, has thus far only been assumed in pyrite-type SiN_2 and suggested from DFT calculations at $p > 160$ GPa for Si_3N_4 in a predicted $CaTi_2O_4$-type polymorph.[21,26,27]

By analogy with Si_3N_4, phosphorus nitride P_3N_5 forms a tetrahedra-based structure at ambient conditions.[28] At 11 GPa, α-P_3N_5 is transformed into the high-pressure polymorph γ-P_3N_5, which features the unique motif of PN_5 square pyramids.[29] Hitherto, PN_6 octahedra have only been reported for molecular hexaazidophosphates,[30,31] but have been predicted from theoretical studies for hypothetical kyanite-type and V_3O_5-type P_3N_5 as well as for spinel-type BeP_2N_4 and hR4-$LiPN_2$.[32–38] In contrast, five- and sixfold O-coordinated P has been reported in $TiPO_4$-V and $CaCl_2$-related $AlPO_4$, respectively, and a (5+1) mixed O/N coordination of P was observed in a stishovite-related modification of the silica analogue PON.[39–41] However, neither mixed non-metal nitrides, such as $SiPN_3$, $Si_3B_3N_7$, BP_3N_6, or SiP_2N_4NH, nor the binary nitride P_3N_5 itself have been investigated at pressures > 11 GPa, and there has been no experimental evidence for any PN_6 units in nitride materials as yet.[42–45]

Herein, we report on the high-pressure polymorph β-BP_3N_6, which features octahedrally coordinated P in a distorted hexagonal close-packing of nitride anions. Targeting sixfold N-coordinated P, α-BP_3N_6 appeared as a promising candidate (α-BP_3N_6 denotes the phase previously reported by our group).[42] The monoclinic, tetrahedra-based double nitride crystallizes as block-like single-crystals (see Chapter D, Figure D.1), suitable for in situ single-crystal X-ray diffraction (XRD) at high pressures using diamond anvil cells (DACs) and synchrotron radiation. Moreover, a pressure-induced increase in the coordination number of P appeared more likely than a higher coordination number of B, considering the high-pressure behavior of the binary nitrides BN and P_3N_5 discussed above.[1,2,29]

For in situ experiments, a DAC was loaded with two single-crystals of α-BP_3N_6, and Ne was used as the pressure-transmitting medium (details provided in Chapter D). The elastic properties of α-BP_3N_6 were investigated by stepwise cold compression to a maximum pressure of 42.4(1) GPa (Figure 6.1a). At each step, a single-crystal data set was collected, providing information on the evolution of the lattice

parameters and structure with pressure. The unit cell of α-BP_3N_6 contracts isotropically (Figure D.2), and its isothermal bulk modulus K_0 is 146(6) GPa, as determined by fitting pressure–volume data using the second-order Birch-Murnaghan equation of state (Figure 6.1a).[46,47] The results of the pressure-dependent single-crystal XRD refinements of α-BP_3N_6 are summarized in Table D.2.[48] A detailed discussion of the α-BP_3N_6 structure is provided in literature.[42] The pressure-induced distortions of α-BP_3N_6 are predominated by an alignment of the nitride anions, which is achieved through tilting and regular contraction of the TN_4 tetrahedra (T = B, P; Figure 6.1b), as pointed out by a pressure-dependent geometrical analysis following the minimal bonding ellipsoid (MBE) formalism (Figure D.3 and Table D.4).[49] Surprisingly, the mean interatomic B–N distances appeared to be significantly more compressible ($\Delta d = 0.081$ Å, >5 %) than the interatomic P–N distances ($\Delta d = 0.044$ Å, <3 %; Table D.3 and Figure D.2).

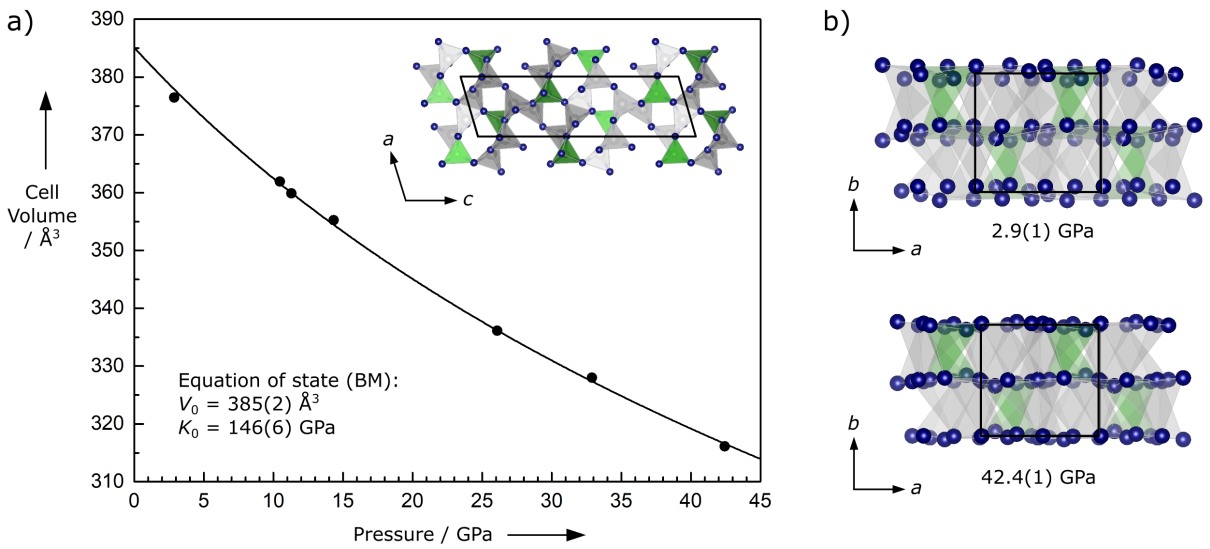

Figure 6.1.: a) The structure of α-BP_3N_6 contracts uniformly upon pressure load, and its isothermal bulk modulus is 146(6) GPa, as determined from equation of state. b) The structural distortions are predominated by an alignment of the nitride anions. B: green, N: blue, P: gray.

Upon cold compression of α-BP_3N_6, no evidence for any phase transition was observed, and the single-crystals remained intact. To facilitate a pressure-induced phase transition, a single-crystal was laser-heated on-line from one side at about 42 GPa ($\lambda = 1070$ nm; details provided in Chapter D). After a 3 s flash, a significant change of the XRD pattern was observed (Figure D.5). Subsequent XRD inves-

tigations of the temperature-quenched sample suggested the formation of crystalline multi-phase grains (Figure D.6). A data set of a previously unknown orthorhombic phase ($a = 8.667(1)$, $b = 7.411(4)$, $c = 4.0115(4)$ Å; $V = 257.7(2)$ Å^3 at 42.4(1) GPa) was integrated, from which the β-BP_3N_6 structure was solved and refined in space group $Pna2_1$ (No. 33).[50] More detailed information on the data analysis of the multi-phase grains and the refinement of the single-crystal XRD data is provided in Chapter D.

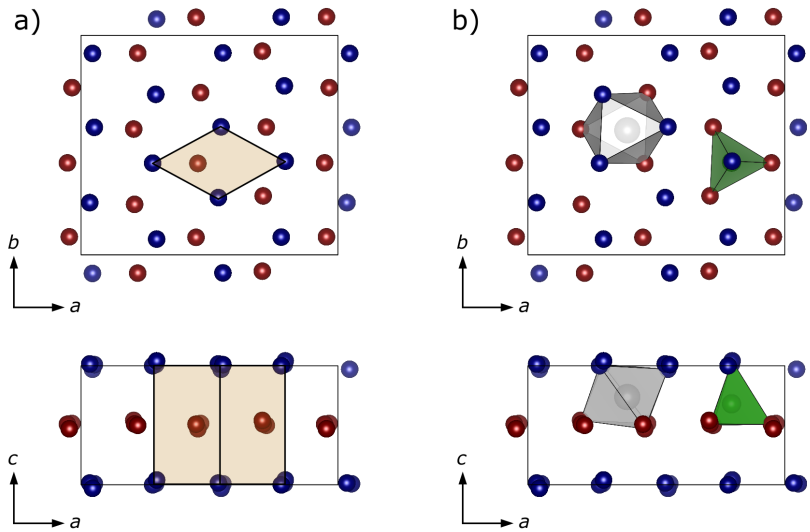

Figure 6.2.: a) The structure of β-BP_3N_6 can be described as a decoration of a distorted hexagonal close-packing (hcp) of N. The A and B layers are displayed in blue and red, and a theoretical primitive hcp unit cell is illustrated in orange. b) B and P occupy tetrahedral (green) and octahedral voids (gray), respectively.

The β-BP_3N_6 structure can be described as a decoration of a distorted hexagonal close-packing of N, in which B and P occupy $^1/_{12}$ of the tetrahedral and $^1/_2$ of the octahedral voids, respectively (Figure 6.2). Thus the B/P/N network is built up from BN_4 tetrahedra and PN_6 octahedra as expressed by the Niggli formula $^3_\infty\left[B^{[4]}P^{[6]}{}_3N^{[4]}{}_4N^{[3]}{}_2\right]$ (Figure D.8).[10,11] Herein, both, $P^{[6]}$ and $N^{[4]}$ are unprecedented structural motifs within the compound class of phosphorus nitrides. The β-BP_3N_6 structure can be broken down into $\left[BP_3N_{8/2}N_{6/3}\right]$ building units consisting of three edge-sharing PN_6 octahedra and one BN_4 tetrahedron. Interconnected building units form chain-like substructures along a (Figure 6.3a), which are connected along c to form the highly condensed framework (Figure 6.3b). As a consequence, all BN_4 tetrahedra are oriented in the same direction, resulting in a polar network (space group $Pna2_1$). To the

best of our knowledge, there is no experimental evidence for such a network in the literature, and thus the β-BP_3N_6 structure can be considered as a new network type.

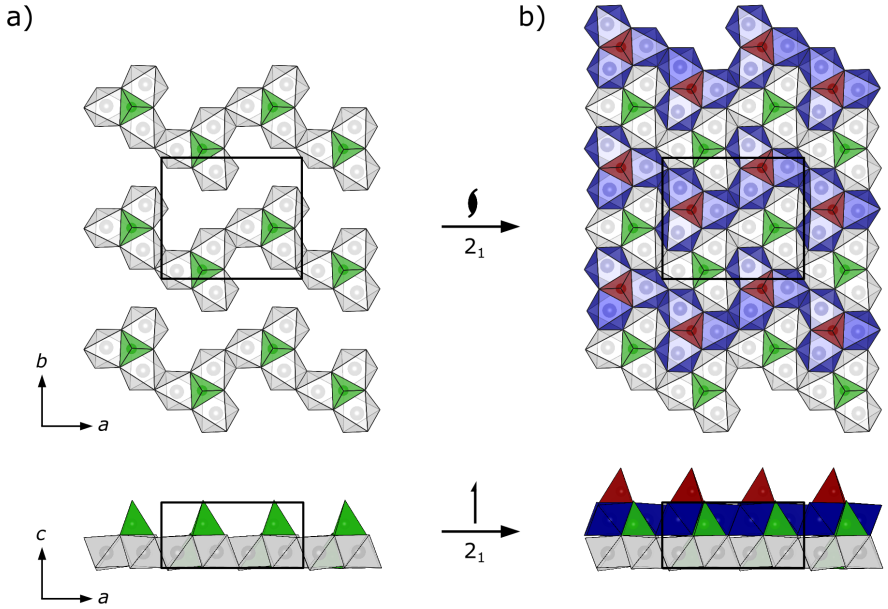

Figure 6.3.: a) Interconnected $\left[BP_3N_{8/2}N_{6/3}\right]$ building units consisting of three edge-sharing PN_6 octahedra and one BN_4 tetrahedron form chain-like substructures along *a*. b) The highly condensed polar B/P/N network is created by the 2_1 screw axes running along *c*. B: green/red, P: gray/blue.

The α-BP_3N_6⟶ β-BP_3N_6 phase transition is characterized by a significant change in volume and density (23 %; Figure D.7), and thus can be described as a reconstructive phase transition. This finding is in line with the observed fragmentation of a single-crystal of α-BP_3N_6 into multi-domain grains upon laser heating (Figures D.4–D.6). After in situ characterization at 42 GPa, a pressure-quenched sample of β-BP_3N_6 was re-investigated at ambient conditions. The corresponding single-crystal data refinement shows no transformation of the β-BP_3N_6 structure, suggesting β-BP_3N_6 to be metastable at ambient conditions (Tables D.5–D.7). The lattice parameters *a*, *b*, and *c* expanded by 3.7, 3.7, and 4.2 %, which corresponds to a total increase of 12 % in the unit cell volume (Figure D.7).

At 42.4(1) GPa, the mean interatomic P–N (1.74(1) Å) and B–N distances (1.50(1) Å) in β-BP_3N_6 are in good agreement with the values suggested for PN_6 octahedra in hypothetical kyanite-type P_3N_5 (1.69 Å at 43 GPa) and reported for c-BN (1.51 Å at 42.7 GPa).[32,51] At ambient pressure, the atomic positions (Table D.7) could only be refined with high uncertainties owing to the lack of high-quality XRD data

(see Chapter D). Hence, we desist from a detailed quantitative discussion of the interatomic distances at ambient pressure within this manuscript (Table D.8). The averaged interatomic P–N and B–N distances, however, increased significantly upon pressure quenching to 1.81(4) and 1.59(6) Å, respectively.

At about 42 GPa, the PN_6 and BN_4 coordination polyhedra appeared to be significantly distorted, as indicated by the interatomic T–N distances and N–T–N angles (T = B, P; Tables D.8 and D.9). To quantify the distortions of the coordination polyhedra at 42.4(1) GPa, they were described by MBEs (Figure D.10 and Table D.11).[49] The PN_6 octahedra as well as the BN_4 tetrahedra show medium distortions, as indicated by moderate shape parameters and center displacements. An overlay of the normalized coordination polyhedra at 42.4(1) GPa and ambient pressure is provided in Chapter D (Figure D.9) and suggests no fundamental changes in the structure upon pressure quenching.

To evaluate the β-BP_3N_6 structure from an electrostatic point of view, CHARDI and MAPLE calculations were performed.[52,53] CHARDI analysis of the β-BP_3N_6 structure at 42.4(1) GPa revealed mean total charges of +3.07, +4.98, and −3.00 for B, P, and N, which is in very good agreement with the respective formal oxidation states (+III, +V, −III). The effective coordination numbers of B and P are 3.94 and 5.68, in line with four- and sixfold coordination. The Madelung part of the lattice energy (MAPLE) of β-BP_3N_6 is 92 631 kJ·mol^{-1} at 42.4(1) GPa, which is in fair agreement with the values of α-BP_3N_6 (90 556 kJ·mol^{-1})[42] and the sum of the binary nitrides (90049–91 877 kJ·mol^{-1}).[1,2,9,28,29] More detailed information on the CHARDI and MAPLE analyses is provided in Chapter D (Tables D.12 and D.13).

In conclusion, α-BP_3N_6 was investigated by pressure-dependent single-crystal XRD measurements to a maximum pressure of about 42 GPa, at which laser heating induced a phase transition into its high-pressure polymorph β-BP_3N_6. Upon pressure load the structure of α-BP_3N_6 contracted isotropically, and its isothermal bulk modulus is 146(6) GPa, as determined from pressure–volume data. The structure of β-BP_3N_6 was elucidated from single-crystal XRD at about 42 GPa and ambient pressure, and can be described as an unprecedented decoration of a hexagonal close-packing. The highly condensed structure is assigned a new polar network type that is built up from BN_4 tetrahedra and PN_6 octahedra. The latter motif has been proposed for various phosphorus nitrides in multiple theoretical studies, but had previously not been confirmed experimentally. Thus, β-BP_3N_6 provides fundamental new insights into the high-pressure behavior of non-metal nitrides and paths the way for the future exploration of numerous predicted high-pressure polymorphs of, for example, P_3N_5, BeP_2N_4, or $LiPN_2$.

Acknowledgements

Financial support by the Deutsche Forschungsgemeinschaft (DFG, project SCHN 377/18-1) and the Fonds der Chemischen Industrie (FCI, PhD fellowship to Sebastian Vogel) is gratefully acknowledged. Parts of this research were carried out at the extreme conditions beamline P02.2 at DESY, a member of the Helmholtz Association (HGF). We thank Dr. Alexander Kurnosov (Bayerisches Geoinstitut, Bayreuth) and Timofey Fedotenko (University of Bayreuth) for assistance during pressure loading.

References

[1] R. H. Wentorf, *"Cubic Form of Boron Nitride"*, *J. Chem. Phys.* **1957**, *26*, 956.

[2] R. H. Wentorf, *"Synthesis of the Cubic Form of Boron Nitride"*, *J. Chem. Phys.* **1961**, *34*, 809.

[3] A. Zerr, R. Riedel, G. Miehe, G. Serghiou, M. Schwarz, E. Kroke, H. Fueß, P. Kroll, R. Boehler, *"Synthesis of cubic silicon nitride"*, *Nature* **1999**, *400*, 340.

[4] M. Schwarz, G. Miehe, A. Zerr, E. Kroke, B. T. Poe, H. Fueß, R. Riedel, *"Spinel-Si_3N_4: Multi-Anvil Press Synthesis and Structural Refinement"*, *Adv. Mater.* **2000**, *12*, 883.

[5] J. Haines, J. M. Léger, G. Bocquillon, *"Synthesis and Design of Superhard Materials"*, *Annu. Rev. Mater. Res.* **2001**, *31*, 1.

[6] J. Z. Jiang, F. Kragh, D. J. Frost, K. Ståhl, H. Lindelov, *"Hardness and thermal stability of cubic silicon nitride"*, *J. Phys.: Condens. Matter* **2001**, *13*, L515.

[7] L. Vel, G. Demazeau, J. Etourneau, *"Cubic boron nitride - Synthesis, physicochemical properties and applications"*, *Mater. Sci. Eng. B* **1991**, *10*, 149.

[8] A. Neuhaus, *"Structural Behavior, and Valence State of Inorganic Matter in the Realm of Higher and Highest Pressure"*, *Chimia* **1964**, *18*, 93.

[9] R. S. Pease, *"Crystal Structure of Boron Nitride"*, *Nature* **1950**, *165*, 722.

[10] U. Müller, *"Anorganische Strukturchemie"*, Vieweg + Teubner, Wiesbaden, 6th Ed., **2008**.

[11] J. Lima-de-Faria, E. Hellner, F. Liebau, E. Makovicky, E. Parthé, *"Nomenclature of inorganic structure types. Report of the International Union of Crystallography Commission on Crystallographic Nomenclature Subcommittee on the Nomenclature of Inorganic Structure Types"*, *Acta Crystallogr. Sect. A: Found. Adv.* **1990**, *46*, 1.

[12] R. M. Wentzcovitch, M. L. Cohen, P. K. Lam, *"Theoretical study of BN, BP, and BAs at high pressures"*, *Phys. Rev. B* **1987**, *36*, 6058.

[13] N. E. Christensen, I. Gorczyca, *"Optical and structural properties of III-V nitrides under pressure"*, *Phys. Rev. B: Condens. Matter Mater. Phys.* **1994**, *50*, 4397.

[14] L. Hromadová, R. Martoňák, *"Pressure-induced structural transitions in BN from ab initio metadynamics"*, *Phys. Rev. B: Condens. Matter Mater. Phys.* **2011**, *84*, 241252.

[15] A. Schwarzer, T. Saplinova, E. Kroke, *"Tri-s-triazines (s-heptazines)—From a "mystery molecule" to industrially relevant carbon nitride materials"*, *Coord. Chem. Rev.* **2013**, *257*, 2032.

[16] F. K. Keßler, Y. Zheng, D. Schwarz, C. Merschjann, W. Schnick, X. Wang, M. J. Bojdys, *"Functional carbon nitride materials – design strategies for electrochemical devices"*, *Nat. Rev. Mater.* **2017**, *2*, 17030.

[17] X. Wang, K. Maeda, A. Thomas, K. Takanabe, G. Xin, J. M. Carlsson, K. Domen, M. Antonietti, *"A metal-free polymeric photocatalyst for hydrogen production from water under visible light"*, *Nat. Mater.* **2009**, *8*, 76.

[18] J. Wen, J. Xie, X. Chen, X. Li, *"A review on γ-C_3N_4-based photocatalysts"*, *Appl. Surf. Sci.* **2017**, *391*, 72.

[19] E. Horvath-Bordon, R. Riedel, P. F. McMillan, P. Kroll, G. Miehe, P. A. van Aken, A. Zerr, P. Hoppe, O. Shebanova, I. McLaren, S. Lauterbach, E. Kroke, R. Boehler, *"High-pressure synthesis of crystalline carbon nitride imide, $C_2N_2(NH)$"*, *Angew. Chem. Int. Ed.* **2007**, *46*, 1476; *Angew. Chem.* **2007**, *119*, 1498.

[20] A. Y. Liu, M. L. Cohen, *"Prediction of new low compressibility solids"*, *Science* **1989**, *245*, 841.

[21] E. Kroke, *"Novel group 14 nitrides"*, *Coord. Chem. Rev.* **2004**, *248*, 493.

[22] H. Dong, A. R. Oganov, Q. Zhu, G.-R. Qian, *"The phase diagram and hardness of carbon nitrides"*, *Sci. Rep.* **2015**, *5*, 1.

[23] D. Hardie, K. H. Jack, *"Crystal Structures of Silicon Nitride"*, *Nature* **1957**, *180*, 332.

[24] H. Lange, G. Wötting, G. Winter, *"Silicon Nitride—From Powder Synthesis to Ceramic Materials"*, *Angew. Chem. Int. Ed. Engl.* **1991**, *30*, 1579; *Angew. Chem.* **1991**, *103*, 1606.

[25] F. L. Riley, *"Silicon Nitride and Related Materials"*, *J. Am. Ceram. Soc.* **2000**, *83*, 245.

[26] K. Niwa, H. Ogasawara, M. Hasegawa, *"Pyrite form of group-14 element pernitrides synthesized at high pressure and high temperature"*, *Dalton Trans.* **2017**, *46*, 9750.

[27] P. Kroll, J. von Appen, *"Post-Spinel Phases of Silicon Nitride"*, *Phys. Status Solidi B* **2001**, *226*, R6.

[28] S. Horstmann, E. Irran, W. Schnick, *"Synthesis and Crystal Structure of Phosphorus(V) Nitride α-P_3N_5"*, *Angew. Chem. Int. Ed. Engl.* **1997**, *36*, 1873; *Angew. Chem.* **1997**, *109*, 1938.

[29] K. Landskron, H. Huppertz, J. Senker, W. Schnick, *"High-Pressure Synthesis of γ-P_3N_5 at 11 GPa and 1500 °C in a Multianvil Assembly: A Binary Phosphorus(V) Nitride with a Three-Dimensional Network Structure from PN_4 Tetrahedra and Tetragonal PN_5 Pyramids"*, *Angew. Chem. Int. Ed.* **2001**, *40*, 2643, *Angew. Chem.* **2001**, *113*, 2713.

[30] H. W. Roesky, *"Preparation of Hexaazidophosphates"*, *Angew. Chem. Int. Ed. Engl.* **1967**, *6*, 637; *Angew. Chem.* **1967**, *79*, 651.

[31] P. Portius, P. W. Fowler, H. Adams, T. Z. Todorova, *"Experimental and theoretical characterization of the hexaazidophosphate(V) ion"*, *Inorg. Chem.* **2008**, *47*, 12004.

[32] P. Kroll, W. Schnick, *"A Density Functional Study of Phosphorus Nitride P_3N_5: Refined Geometries, Properties, and Relative Stability of α-P_3N_5 and γ-P_3N_5 and a Further Possible High-Pressure Phase δ-P_3N_5 with Kyanite-Type Structure"*, *Chem. – Eur. J.* **2002**, *8*, 3530.

[33] J. Dong, A. A. Kinkhabwala, P. F. McMillan, *"High-pressure polymorphism in phosphorus nitrides"*, *Phys. Status Solidi B* **2004**, *241*, 2319.

[34] Z. Raza, I. Errea, A. R. Oganov, A. M. Saitta, *"Novel superconducting skutterudite-type phosphorus nitride at high pressure from first-principles calculations"*, *Sci. Rep.* **2014**, *4*, 5889.

[35] F. J. Pucher, S. R. Römer, F. W. Karau, W. Schnick, *"Phenakite-type BeP_2N_4 – a possible precursor for a new hard spinel-type material"*, *Chem. – Eur. J.* **2010**, *16*, 7208.

[36] W. Y. Ching, S. Aryal, P. Rulis, W. Schnick, *"Electronic structure and physical properties of the spinel-type phase of BeP_2N_4 from all-electron density functional calculations"*, *Phys. Rev. B* **2011**, *83*, 155109.

[37] T. Dennenwaldt, J. Ciston, U. Dahmen, W.-Y. Ching, F. J. Pucher, W. Schnick, C. Scheu, *"High-resolution spectroscopy of bonding in a novel BeP_2N_4 compound"*, *Microsc. Microanal.* **2014**, *20*, 664.

[38] J. Lv, X. Yang, D. Xu, Y.-X. Huang, H.-B. Wang, H. Wang, *"High-pressure polymorphs of $LiPN_2$: A first-principles study"*, *Front. Phys.* **2018**, *13*, 9592.

[39] M. Bykov, E. Bykova, M. Hanfland, H.-P. Liermann, R. K. Kremer, R. Glaum, L. S. Dubrovinsky, S. van Smaalen, *"High-Pressure Phase Transformations in $TiPO_4$: A Route to Pentacoordinated Phosphorus"*, *Angew. Chem. Int. Ed.* **2016**, *55*, 15053; *Angew. Chem.* **2016**, *128*, 15277.

[40] J. Pellicer-Porres, A. M. Saitta, A. Polian, J. P. Itie, M. Hanfland, *"Six-fold-coordinated phosphorus by oxygen in $AlPO_4$ quartz homeotype under high pressure"*, *Nat. Mater.* **2007**, *6*, 698.

[41] S. Vogel, D. Baumann, R. Niklaus, E. Bykova, M. Bykov, N. Dubrovinskaia, L. Dubrovinsky, W. Schnick, *"Stishovite's Relative: A Post-Coesite Form of Phosphorus Oxonitride"*, *Angew. Chem. Int. Ed.* **2018**, *57*, 6691; *Angew. Chem.* **2018**, *130*, 6801.

[42] S. Vogel, A. T. Buda, W. Schnick, *"United in Nitride: The Highly Condensed Boron Phosphorus Nitride BP_3N_6"*, *Angew. Chem. Int. Ed.* **2018**, *57*, 13202; *Angew. Chem.* **2018**, *130*, 13386.

[43] H.-P. Baldus, W. Schnick, J. Lücke, *"Silicon Phosphorus Nitride, the First Ternary Compound in the Silicon-Phosphorus-Nitrogen System"*, *Chem. Mater.* **1993**, *5*, 845.

[44] H.-P. Baldus, M. Jansen, *"Novel High-Performance Ceramics—Amorphous Inorganic Networks from Molecular Precursors"*, *Angew. Chem. Int. Ed. Engl.* **1997**, *36*, 328; *Angew. Chem.* **1997**, *109*, 338.

[45] S. Vogel, A. T. Buda, W. Schnick, *"Rivalry under Pressure: The Coexistence of Ambient-Pressure Motifs and Close-Packing in Silicon Phosphorus Nitride Imide SiP_2N_4NH"*, *Angew. Chem. Int. Ed.* **2019**, *58*, 3398; *Angew. Chem.* **2019**, *131*, 3436.

[46] F. D. Murnaghan, *"The compressibility of media under extreme pressures"*, *Proc. Natl. Acad. Sci. U.S.A.* **1944**, *30*, 244.

[47] F. Birch, *"Finite Elastic Strain of Cubic Crystals"*, *Phys. Rev.* **1947**, *71*, 809.

[48] Detailed information on the crystal data of α-BP_3N_6 from pressure-dependent single-crystal XRD refinement is provided in the Chapter D. CSD-1898716, 1898717, 1898718, 1898720, 1898721, 1898722, 1898723, and 1898724 contain the supplementary crystallographic data for this paper. These data can be obtained free of charge from The Cambridge Crystallographic Data Centre.

[49] J. Cumby, J. P. Attfield, *"Ellipsoidal analysis of coordination polyhedra"*, *Nat. Commun.* **2017**, *8*, 14235.

[50] Crystal data of β-BP_3N_6 from single-crystal XRD refinement at 42.4(1) GPa: $M = 187.78\,\mathrm{g{\cdot}mol^{-1}}$, orthorhombic, $Pna2_1$ (no. 33), $a = 8.6666(10)$, $b = 7.411(4)$, and $c = 4.0115(4)$ Å, $V = 257.65(14)$ Å^3, $Z = 4$, $\rho = 4.841\,\mathrm{g{\cdot}cm^{-3}}$, $\mu = 0.217\,\mathrm{cm^{-1}}$, synchrotron radiation ($\lambda = 0.28940$ Å, DESY, PETRA III, P02.2), $T = 293$ K, 1265 observed reflections, 771 independent reflections, 41 parameters, $R_{\mathrm{int}} = 0.0653$, $R_\sigma = 0.0617$, $R1 = 0.0794$, $wR2 = 0.2114$, $GoF = 1.121$, residual electron density 1.614, −2.431 $e{\cdot}$Å^{-3}. CSD-1898722 and 1898719 (β-BP_3N_6 at 42.4(1) GPa, β-BP_3N_6 at ambient pressure) contain the supplementary crystallographic data for this paper. These data can be obtained free of charge from The Cambridge Crystallographic Data Centre.

[51] F. Datchi, A. Dewaele, Y. Le Godec, P. Loubeyre, *"Equation of state of cubic boron nitride at high pressures and temperatures"*, *Phys. Rev. B: Condens. Matter Mater. Phys.* **2007**, *75*, 127.

[52] R. Hoppe, S. Voigt, H. Glaum, J. Kissel, H. P. Müller, K. Bernet, *"A new route to charge distributions in ionic solids"*, *J. Less-Common Met.* **1989**, *156*, 105.

[53] R. Hoppe, *"On the Madelung Part of Lattice Energy"*, *Z. Naturforsch. A: Phys. Sci.* **1995**, *50*, 555.

7. Nitride Spinel: An Ultraincompressible High-Pressure Form of BeP_2N_4

Sebastian Vogel, Maxim Bykov, Elena Bykova, Sebastian Wendl, Simon D. Kloß, Anna Pakhomova, Natalia Dubrovinskaia, Leonid Dubrovinsky, and Wolfgang Schnick

Angew. Chem. Int. Ed. **2019** (accepted);

Angew. Chem. **2019** (accepted).

DOI: 10.1002/anie.201910998

Nitride spinel: At 47 GPa and 1800 K phenakite-type BeP_2N_4 was transformed into the spinel-type form of BeP_2N_4 using a laser-heated diamond anvil cell. Its crystal structure was investigated using pressure-dependent in situ synchrotron XRD measurements and its isothermal bulk modulus was determined to > 300 GPa, which renders spinel-type BeP_2N_4 an ultraincompressible material.

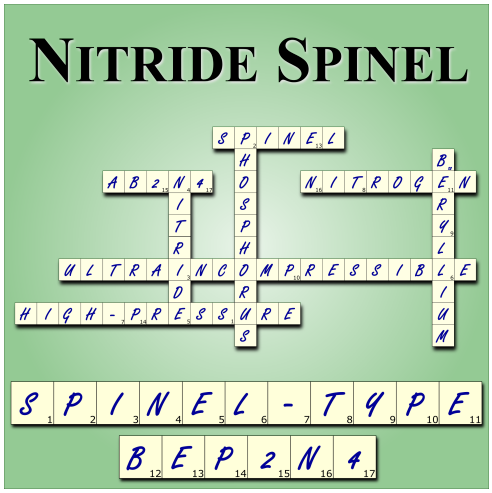

Abstract *Owing to its outstanding elastic properties, the nitride spinel γ-Si_3N_4 is of considered interest for materials scientists and chemists. DFT calculations suggest that Si_3N_4-analog beryllium phosphorus nitride BeP_2N_4 adopts the spinel structure at elevated pressures as well and shows outstanding elastic properties. Herein, we investigate phenakite-type BeP_2N_4 by single-crystal synchrotron X-ray diffraction and report the phase transition into the spinel-type phase at 47 GPa and 1800 K in a laser-heated diamond anvil cell. The structure of spinel-type BeP_2N_4 was refined from pressure-dependent in situ synchrotron powder X-ray diffraction measurements down to ambient pressure, which proves spinel-type BeP_2N_4 a quenchable and metastable phase at ambient conditions. Its isothermal bulk modulus was determined to 325(8) GPa from equation of state, which indicates that spinel-type BeP_2N_4 is an ultraincompressible material.*

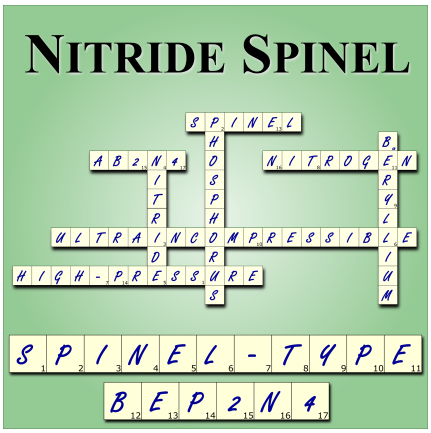

Due to a broad range of materials properties and applications, oxide spinels with the general formula AB_2O_4 (A, B = metal ions) are an extensively investigated field of research and numerous compounds have been reported.[1] In contrast, only few representatives of nitride spinels (AB_2N_4) have been prepared, as yet.[2] However, they have already been proven to compete with oxide materials for outstanding materials properties, especially with regard to mechanical resilience.[3]

The synthesis of the group 14 nitrides γ-Si_3N_4,[3,4] γ-Ge_3N_4,[5,6] and Sn_3N_4[7] heralded a new era of nitride chemistry, as these compounds represent the first nitride spinels.[2] γ-Si_3N_4 has been prepared in diamond anvil cells (DAC),[3] multianvil presses,[4] as well as in shockwave experiments,[8] and recently even the preparation of macroscopic transparent polycrystalline γ-Si_3N_4 windows has been achieved.[9] The isothermal bulk modulus K_0 and the Vickers hardness H_V of γ-Si_3N_4 have been determined to K_0 = 290–317 GPa[3,9–11] and H_V = 30–43 GPa,[9,10,12,13] which makes it one of the most incompressible and hardest low-density materials.

Due to the topological rigidity of spinels, they are considered to intrinsically feature outstanding elastic properties, which might be further enhanced by strong covalent A–N and B–N bonds in the case

of nitride spinels.[14–17] The elemental diversity of nitride spinels, however, is comparatively small, as experimental and theoretical research on nitride spinels has most widely been limited to the binary and ternary nitrides of C, Si, Ge, Sn, Pb, Ti, and Zr,[17–20] and only nitride spinels of tetravalent cations (A^{IV}, B^{IV} = Si, Ge, Sn)[3,5–7,21] have been prepared, as yet. Besides tetravalent cations, a nitride spinel with the general formula AB_2N_4 may also be composed of A^{VI} and B^{III} ($A^{VI}B_2^{III}N_4$) or A^{II} and B^{V} cations ($A^{II}B_2^{V}N_4$), when electrostatic neutrality is stipulated. The II-V combination has been reported for several phosphorus(V) nitride materials with the general formula $M^{II}P_2N_4$ (M^{II} = Be, Ca, Sr, Ba, Mn, Cd), which form PN_4 tetrahedra based networks.[22–26] To the best of our knowledge, a spinel-type phase, however, has not been reported for any $A^{VI}B_2^{III}N_4$ or $A^{II}B_2^{V}N_4$, as yet.

Theoretical investigations have predicted spinel-type (sp) BeP_2N_4 as a stable polymorph at elevated pressures, which makes it a promising candidate for the first $A^{II}B_2^{V}N_4$-type nitride spinel.[22,27–29] Hitherto, only phenakite-type (phe) BeP_2N_4 has been reported, which is isoelectronic and homeotypic with β-Si_3N_4 and features BeN_4 and PN_4 tetrahedra.[22,30,31] By analogy with the Si_3N_4 polymorphism, phe-BeP_2N_4 is considered to undergo a phase transition into the regular spinel structure with Be and P occupying tetrahedral and octahedral voids of the cubic close-packing of N, respectively.[22] BeN_4 tetrahedra are a common motif in crystal chemistry of beryllium nitrides,[32,33] whereas PN_6 octahedra have only been reported in the high-pressure polymorph β-BP_3N_6, recently.[34]

The phenakite- to spinel-type transition pressure of BeP_2N_4 has been predicted to 14–24 GPa from DFT calculations and due to its covalent character, sp-BeP_2N_4* is suggested to be quenchable to ambient pressure as a metastable phase.[22,27,28] Its isothermal bulk modulus has been calculated to be in the range of 263–291 GPa, which emphasizes the kinship with γ-Si_3N_4.[22,27–29] Moreover, the Vickers hardness H_V of sp-BeP_2N_4 has been estimated to approximately $H_V = 45$ GPa using (semi)empirical approaches, which would make it a promising candidate for a superhard low-density material.[28,35,36]

Herein, we report on the phe-BeP_2N_4 $\longrightarrow$ sp-BeP_2N_4 phase transition at 47 GPa, which was investigated in a laser-heated DAC employing in situ synchrotron X-ray diffraction (XRD) measurements. The structure of sp-BeP_2N_4 was refined using the Rietveld method and its elastic properties have been investigated upon cold decompression to ambient pressure.

*Within this contribution the spinel-type phase of BeP_2N_4 is denoted as sp-BeP_2N_4 rather than γ-BeP_2N_4, which has been used in some previous references to emphasize the structural relation to γ-Si_3N_4. A β-BeP_2N_4, however, has not been reported, as yet.

phe-BeP_2N_4 was initially synthesized from Be_3N_2 and P_3N_5 in a large volume press at 7 GPa and 1500 °C, employing the multianvil technique (Equation 7.1, more details are provided in Chapter E).[22]

$$Be_3N_2 + 2\,P_3N_5 \longrightarrow 3\,\text{phe-}BeP_2N_4 \tag{7.1}$$

To select a suitable particle for in situ high-pressure investigations and to verify the phenakite-type structure of BeP_2N_4, several polycrystalline grains were screened by synchrotron XRD measurements at ambient conditions (Figure E.2). Integration of the most intense domain of a multi-domain crystalline grain yielded a suitable single-crystal data set (Figure E.3), from which the structure of phe-BeP_2N_4 was elucidated ($R\bar{3}$ (no. 148), $a = 12.6979(15)$, $c = 8.3595(10)$ Å, $V = 1167.3(5)$ Å^3, $Z = 18$). All atoms were refined with anisotropic displacement parameters and the mean interatomic Be–N and P–N distances are 1.734(15) and 1.636(8) Å, respectively, which is in line with values that have been reported for the binary nitrides.[32,33,37] The here obtained structural model verifies the model previously reported by Pucher et al. that has been solved and refined from powder XRD data (Table E.1, E.4).[22,38] Figure 7.1 illustrates the single-crystal structure of phe-BeP_2N_4 as well as the constituting BeN_4 and PN_4 tetrahedra. More detailed information on the synchrotron XRD measurement and the structure refinement of phe-BeP_2N_4 is provided in Chapter E (Table E.1–E.4).

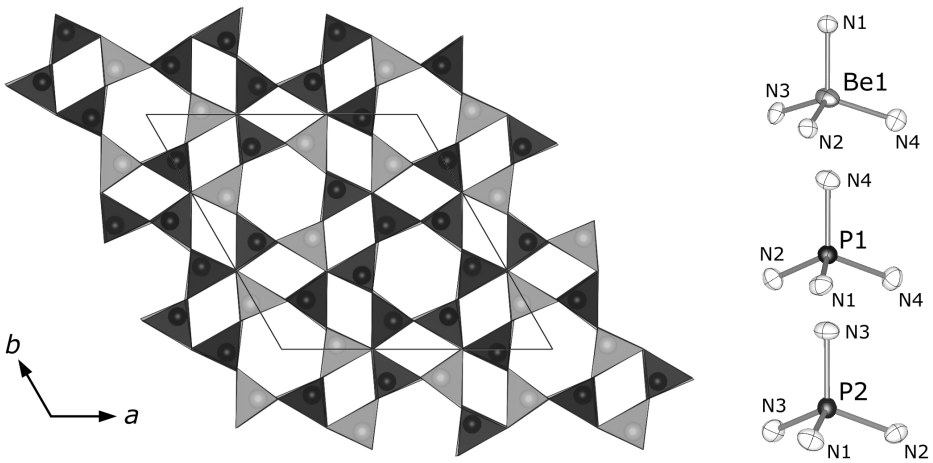

Figure 7.1.: Crystal structure of phe-BeP_2N_4 as obtained from single-crystal synchrotron XRD. Be (gray) and P (black) are in fourfold N coordination and ellipsoids are displayed at 99 % probability level.

To investigate the predicted phe-BeP_2N_4 $\longrightarrow$ sp-BeP_2N_4 phase transition, the pre-selected particle of phe-BeP_2N_4 was loaded in a DAC with Ne serving as a pressure transmitting medium and ruby as an internal pressure standard. The sample was cold-compressed in two steps to a maximum pressure of 47.3(9) GPa. At both steps a XRD step scan was collected that could be indexed with the metrics of phe-BeP_2N_4 (Figure E.4, Table E.5). Owing to very low intensities, a refinement of the integrated data, however, was not feasible at those pressures. At 47.3(9) GPa the unit cell of phe-BeP_2N_4 has contracted by approximately 16 vol-% in comparison to the ambient pressure model (Figure E.6).

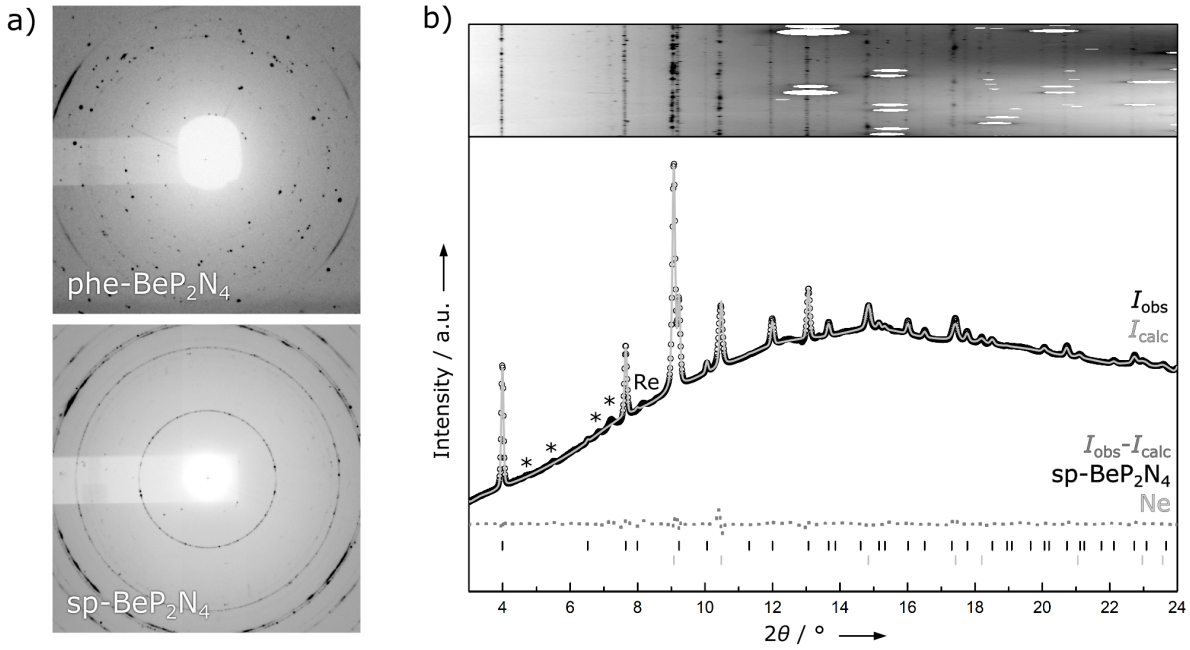

Figure 7.2.: (a) XRD scans of the BeP_2N_4 sample before (top) and after laser heating at 47.3(9) GPa (bottom), corresponding to phe- and sp-BeP_2N_4, respectively. (b) Rietveld refinement of sp-BeP_2N_4 and Ne at 47.3(9) GPa from in situ X-ray measurements using synchrotron radiation ($\lambda = 0.2894$ Å). Observed and calculated XRD intensities: black circles, gray line; difference plot: dotted gray line; positions of Bragg reflections of sp-BeP_2N_4 and Ne: black and gray vertical bars. Reflections of minor residues of phe-BeP_2N_4 are marked by asterisks and weak scattering of the Re gasket is labelled.[22]

To induce the phase transition into the spinel-type structure, the phe-BeP_2N_4 particle was laser-heated from both sides to an average temperature of 1800(200) K at 47.3(9) GPa (NIR fiber laser, $\lambda = 1070$ nm). This pressure was deemed sufficient for the formation of PN_6 octahedra, as this motif was recently proven at 42 GPa in β-BP_3N_6.[34] The sample was monitored with in situ synchrotron XRD scans for the

course of the heating period. After a few seconds, unidentified Bragg reflections appeared and heating for another minute led to an almost full conversion of phe-BeP_2N_4 (Figure 7.2 and E.5). Subsequently, the sample was allowed to cool down to ambient temperature after which a XRD wide scan was collected. The powder XRD pattern of the new phase matched the Bragg reflections of the predicted spinel-type phase (Figure 7.2 and E.5).[25] Therefore, the experimental pressure of about 47 GPa is proven sufficiently high for the phe-BeP_2N_4 $\longrightarrow$ sp-BeP_2N_4 phase transition, but the minimum transition pressure may be most likely significantly lower, considering theoretical investigations on sp-BeP_2N_4 (p_{trans} = 14–24 GPa)[22,28] and experimental examinations of isoelectronic γ-Si_3N_4 ($p_{\text{trans}} \approx 13$ GPa).[3,4,11]

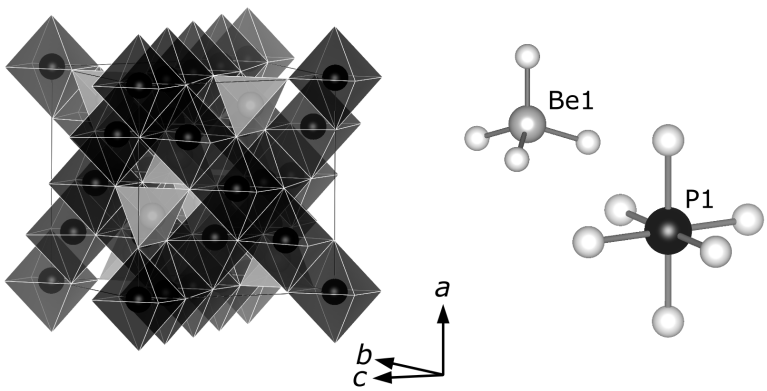

Figure 7.3.: The crystal structure of sp-BeP_2N_4 as refined from PXRD data collected at 47.3(9) GPa. Be (gray) occupies tetrahedral and P (black) octahedral voids in a cubic close-packing of N (white), corresponding to the regular spinel structure.

Single-crystal XRD measurements of sp-BeP_2N_4, however, were not feasible, as the title compound did not form any adequate domains (Figure 7.2a). Thus, the sp-BeP_2N_4 structure was refined on PXRD data obtained at 47.3(9) GPa employing the Rietveld method (Table E.6).[39] The DFT-based model was used as a starting point for the refinement and was subsequently corroborated by the experimental data.[25] sp-BeP_2N_4 crystallizes in the regular spinel structure ($Fd\bar{3}m$, no. 227, $a = 7.1948(2)$ Å, $V = 372.44(3)$ Å^3, $Z = 8$) with site symmetries Be($8b$, $\bar{4}3m$), P($16c$, $.\bar{3}m$), and N($32e$, $.3m$).[25,40] More detailed information on the structure refinement is provided in Chapter E (Tables E.6–E.9, Figure E.7). No experimental evidence for Be/P disorder or an inverse spinel structure was observed. This is in agreement with the calculations presented by Pucher et al. that characterized the inverse spinel-type BeP_2N_4 to be unfavored towards phe- and sp-BeP_2N_4.[22] The refined crystal structure of sp-BeP_2N_4 and the respective coordi-

nation polyhedra of Be and P are illustrated in Figure 7.3. The interatomic Be–N and P–N distances at 47.3(9) GPa are 1.635(2) and 1.755(2) Å, respectively, corresponding to fourfold coordinated Be and sixfold coordinated P.

To verify the sp-BeP_2N_4 structure in terms of electrostatics, the Madelung part of lattice energy (MAPLE) was analyzed.[41] The calculated MAPLE value of sp-BeP_2N_4 is 58 140 kJ·mol^{-1}, which is in very good agreement with the values calculated for phe-BeP_2N_4 (58 542 kJ·mol^{-1}, $\Delta E = 0.7\,\%$) and the weighted sum of the binary nitrides P_3N_5 and Be_3N_2 (58 992 kJ·mol^{-1}, $\Delta E = 1.4\,\%$). More detailed information on MAPLE calculations are provided in Table E.10.

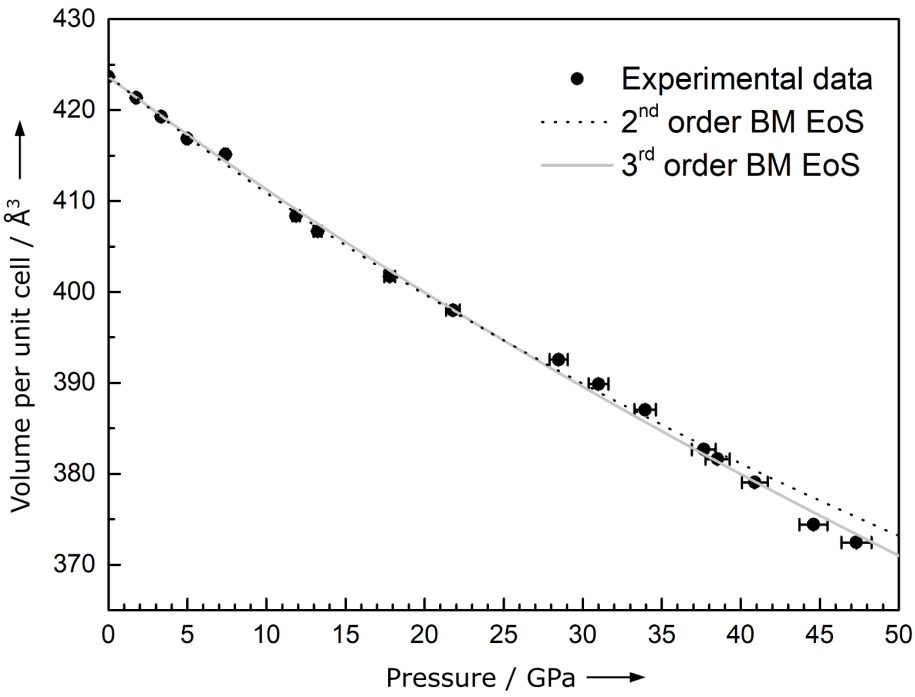

Figure 7.4.: The pressure-volume data from pressure-dependent Rietveld refinements were fitted with a 2nd and 3rd order Birch-Murnaghan equation of state (BM EoS,), with fitting parameters provided in the main text. The isothermal bulk modulus of > 300 GPa renders sp-BeP_2N_4 an ultraincompressible material.[14]

Incremental cold decompression of sp-BeP_2N_4 to ambient pressure was monitored by in situ PXRD measurements at 17 pressure points (Figure E.6, Table E.9). The pressure-dependent Rietveld refinements show that sp-BeP_2N_4 is quenchable to ambient conditions. The expansion of the unit cell upon decompression from 47.3(9) GPa to ambient pressure was 14 vol-%, while the interatomic Be–N and

P–N distances at ambient pressure expanded to 1.752(2) and 1.808(2) Å, respectively (Table E.9, Figure E.8). These values are in good agreement with values from the DFT model and with those reported for BeN_4 and PN_6 polyhedra in Be_3N_2 and β-BP_3N_6.[22,32,33]

According to DFT calculations, sp-BeP_2N_4 is considered to show a very low compressibility ($263 < K_0 < 291$ GPa).[22,27–29] Thus, the pressure-volume data from pressure-dependent Rietveld refinements were fitted with both, a 2nd and a 3rd order Birch-Murnaghan (BM) equation of state (EoS), yielding the fitting parameters $V_0 = 423.76(7)$ Å^3, $K_0 = 305(5)$ GPa, $K_0' = 4$ (fixed) and $V_0 = 423.68(6)$ Å^3, $K_0 = 325(8)$ GPa, $K_0' = 2.4(5)$, respectively (Figure 7.4 and E.9).[42,43] These findings render sp-BeP_2N_4 an ultraincompressible material,[14]† exceeding the bulk modulus of γ-Si_3N_4 as well as the predicted values from DFT calculations. Its hardness and thermal stability, however, have not been investigated experimentally, as yet. As the title compound is quenchable to ambient conditions and may form at significantly lower pressures, its synthesis may be reproduced in large volume presses, providing sample amounts suitable for future investigations in terms of its elastic, physical and optical properties. More detailed information on the BM EoS fits and the elastic properties of sp-BeP_2N_4 is provided in Chapter E.

Recapitulating, phe-BeP_2N_4 was synthesized in a high-pressure high-temperature reaction and the literature-known structure model was confirmed by single-crystal synchrotron XRD measurements. As predicted from theoretical studies, phe-BeP_2N_4 was transformed into the spinel-type phase at 47 GPa and 1800 K using a laser-heated DAC. sp-BeP_2N_4 was proven to be quenchable to ambient pressure and it is rendered an ultraincompressible material from equation of states. Therefore, the title compound is the first $A^{II}B_2^{V}N_4$-type nitride spinel and a pioneer compound that extends the still narrow field of nitride spinels by introducing ions with oxidation states +II and +V. This should encourage further experimental investigations on mixed nitride spinels, as they appear as promising compounds for next-generation materials. Thus, future investigations may deal with the incorporation of divalent (e.g. Mg, Zn, Cu, Ni) and pentavalent cations (e.g. V, Nb or Ta) into II-V nitride spinels, which might introduce intriguing optical and magnetic properties to this emerging field of research.

†The ultraincompressible character, however, does not imply an intrinsic superhard behavior of sp-BeP_2N_4, as the hardness of a certain material correlates with its shear modulus rather than with its compressibility (bulk modulus).[14,16,17,29]

Acknowledgements

Financial support by the Deutsche Forschungsgemeinschaft (DFG) project SCHN 377/18-1 and the Fonds der Chemischen Industrie (FCI) for a PhD fellowship for Sebastian Vogel are gratefully acknowledged. Parts of this research were carried out at the extreme conditions beamline P02.2 at DESY, a member of the Helmholtz Association (HGF). Scientific support provided by Tobias Giftthaler is gratefully appreciated.

References

[1] Q. Zhao, Z. Yan, C. Chen, J. Chen, *"Spinels: Controlled Preparation, Oxygen Reduction / Evolution Reaction Application, and Beyond"*, *Chem. Rev.* **2017**, *117*, 10121, and references therein.

[2] W. Schnick, *"The First Nitride Spinels—New Synthetic Approaches to Binary Group 14 Nitrides"*, *Angew. Chem. Int. Ed.* **1999**, *38*, 3309; *Angew. Chem.* **1999**, *111*, 3511.

[3] A. Zerr, R. Riedel, G. Miehe, G. Serghiou, M. Schwarz, E. Kroke, H. Fueß, P. Kroll, R. Boehler, *"Synthesis of cubic silicon nitride"*, *Nature* **1999**, *400*, 340.

[4] M. Schwarz, G. Miehe, A. Zerr, E. Kroke, B. T. Poe, H. Fueß, R. Riedel, *"Spinel-Si_3N_4: Multi-Anvil Press Synthesis and Structural Refinement"*, *Adv. Mater.* **2000**, *12*, 883.

[5] G. Serghiou, G. Miehe, O. Tschauner, A. Zerr, R. Boehler, *"Synthesis of a cubic Ge_3N_4 phase at high pressures and temperatures"*, *J. Chem. Phys.* **1999**, *111*, 4659.

[6] K. Leinenweber, M. O'Keeffe, M. Somayazulu, H. Hubert, P. F. McMillan, G. H. Wolf, *"Synthesis and Structure Refinement of the Spinel, γ-Ge_3N_4"*, *Chem. – Eur. J.* **1999**, *5*, 3076.

[7] N. Scotti, W. Kockelmann, J. Senker, St. Traßel, H. Jacobs, *"Sn_3N_4, ein Zinn(IV)-nitrid – Synthese und erste Strukturbestimmung einer binären Zinn-Stickstoff-Verbindung"*, *Z. Anorg. Allg. Chem.* **1999**, *625*, 1435.

[8] T. Sekine, H. He, T. Kobayashi, M. Zhang, F. Xu, *"Shock-induced transformation of β-Si_3N_4 to a high-pressure cubic-spinel phase"*, *Appl. Phys. Lett.* **2000**, *76*, 3706.

[9] N. Nishiyama, R. Ishikawa, H. Ohfuji, H. Marquardt, A. Kurnosov, T. Taniguchi, B.-N. Kim, H. Yoshida, A. Masuno, J. Bednarcik, E. Kulik, Y. Ikuhara, F. Wakai, T. Irifune, *"Transparent polycrystalline cubic silicon nitride"*, *Sci. Rep.* **2017**, *7*, 44755.

[10] A. Zerr, M. Kempf, M. Schwarz, E. Kroke, M. Göken, R. Riedel, *"Elastic Moduli and Hardness of Cubic Silicon Nitride"*, *J. Am. Ceram. Soc.* **2002**, *85*, 86.

[11] N. Nishiyama, J. Langer, T. Sakai, Y. Kojima, A. Holzheid, N. A. Gaida, E. Kulik, N. Hirao, S. I. Kawaguchi, T. Irifune, Y. Ohishi, *"Phase relations in silicon and germanium nitrides up to 98 GPa and 2400 °C"*, *J. Am. Ceram. Soc.* **2019**, *102*, 2195.

[12] J. Z. Jiang, F. Kragh, D. J. Frost, K. Ståhl, H. Lindelov, *"Hardness and thermal stability of cubic silicon nitride"*, *J. Phys.: Condens. Matter* **2001**, *13*, L515.

[13] I. Tanakaa, F. Oba, T. Sekine, E. Ito, A. Kubo, K. Tatsumi, H. Adachi, T. Yamamoto, *"Hardness of cubic silicon nitride"*, *J. Mater. Res.* **2002**, *17*, 731.

[14] M. T. Yeung, R. Mohammadi, R. B. Kaner, *"Ultraincompressible, Superhard Materials"*, *Annu. Rev. Mater. Res.* **2016**, *46*, 465.

[15] R. Marchand, F. Tessier, A. Le Sauze, N. Diot, *"Typical features of nitrogen in nitride-type compounds"*, *Int. J. Inorg. Mater.* **2001**, *3*, 1143.

[16] J. Haines, J. M. Léger, G. Bocquillon, *"Synthesis and Design of Superhard Materials"*, *Annu. Rev. Mater. Res.* **2001**, *31*, 1.

[17] T. D. Boyko, A. Moewes, *"The hardness of group 14 spinel nitrides revisited"*, *J. Ceram. Soc. Japan* **2016**, *124*, 1063.

[18] J. Dong, J. Deslippe, O. F. Sankey, E. Soignard, P. F. McMillan, *"Theoretical study of the ternary spinel nitride system Si_3N_4–Ge_3N_4"*, *Phys. Rev. B: Condens. Matter Mater. Phys.* **2003**, *67*, 340.

[19] W. Y. Ching, S.-D. Mo, I. Tanaka, M. Yoshiya, *"Prediction of spinel structure and properties of single and double nitrides"*, *Phys. Rev. B: Condens. Matter Mater. Phys.* **2001**, *63*, 64102.

[20] W. Y. Ching, S.-D. Mo, L. Ouyang, I. Tanaka, M. Yoshiya, *"Prediction of the new spinel phase of Ti_3N_4 and $SiTi_2N_4$ and the metal-insulator transition"*, *Phys. Rev. B: Condens. Matter Mater. Phys.* **2000**, *61*, 10609.

[21] E. Soignard, P. F. McMillan, K. Leinenweber, *"Solid Solutions and Ternary Compound Formation among Ge_3N_4–Si_3N_4 Nitride Spinels Synthesized at High Pressure and High Temperature"*, *Chem. Mater.* **2004**, *16*, 5344.

[22] F. J. Pucher, S. R. Römer, F. W. Karau, W. Schnick, *"Phenakite-type BeP_2N_4 – a possible precursor for a new hard spinel-type material"*, *Chem. – Eur. J.* **2010**, *16*, 7208.

[23] F. W. Karau, L. Seyfarth, O. Oeckler, J. Senker, K. Landskron, W. Schnick, *"The stuffed framework structure of SrP_2N_4: challenges to synthesis and crystal structure determination"*, *Chem. – Eur. J.* **2007**, *13*, 6841.

[24] F. W. Karau, W. Schnick, *"High-pressure synthesis and X-ray powder structure determination of the nitridophosphate BaP_2N_4"*, *J. Solid State Chem.* **2005**, *178*, 135.

[25] F. J. Pucher, A. Marchuk, P. J. Schmidt, D. Wiechert, W. Schnick, *"Luminescent nitridophosphates CaP_2N_4:Eu^{2+} , SrP_2N_4:Eu^{2+}, BaP_2N_4:Eu^{2+}, and $BaSr_2P_6N_{12}$:Eu^{2+}"*, *Chem. – Eur. J.* **2015**, *21*, 6443.

[26] F. J. Pucher, F. W. Karau, J. Schmedt auf der Günne, W. Schnick, *"CdP_2N_4 and MnP_2N_4 - Ternary Transition-Metal Nitridophosphates"*, *Eur. J. Inorg. Chem.* **2016**, *2016*, 1497.

[27] W. Y. Ching, S. Aryal, P. Rulis, W. Schnick, *"Electronic structure and physical properties of the spinel-type phase of BeP_2N_4 from all-electron density functional calculations"*, *Phys. Rev. B* **2011**, *83*, 155109.

[28] Y.-C. Ding, B. Xiao, *"Electronic Structure, Mechanical Properties and Intrinsic Hardness of a New Superhard Material BeP_2N_4"*, *Acta Phys.-Chim. Sin.* **2011**, *27*, 1621.

[29] M. Zhang, H. Yan, Y. Zhao, Q. Wei, *"Mechanical properties and atomistic deformation mechanism of spinel-type BeP_2N_4"*, *Comput. Mater. Sci.* **2014**, *83*, 457.

[30] W. L. Bragg, *"The Structure of Phenacite, Be_2SiO_4"*, *Proc. R. Soc. London Ser. A* **1927**, *113*, 642.

[31] D. Hardie, K. H. Jack, *"Crystal Structures of Silicon Nitride"*, *Nature* **1957**, *180*, 332.

[32] M. v. Stackelberg, R. Paulus, *"Untersuchungen über die Kristallstruktur der Nitride und Phosphide zweiwertiger Metalle"*, *Z. Phys. Chem.* **1933**, *22B*, 305.

[33] P. Eckerlin, A. Rabenau, *"Die Struktur einer neuen Modifikation von Be_3N_2"*, *Z. Anorg. Allg. Chem.* **1960**, *304*, 218.

[34] S. Vogel, M. Bykov, E. Bykova, S. Wendl, S. D. Kloß, A. Pakhomova, S. Chariton, E. Koemets, N. Dubrovinskaia, L. Dubrovinsky, W. Schnick, *"Boron Phosphorus Nitride at Extremes: PN_6 Octahedra in the High-Pressure Polymorph β-BP_3N_6"*, *Angew. Chem. Int. Ed.* **2019**, *58*, 9060; *Angew. Chem.* **2019**, *131*, 9158.

[35] C.-M. Sung, M. Sung, *"Carbon nitride and other speculative superhard materials"*, *Mater. Chem. Phys.* **1996**, *43*, 1.

[36] F. Gao, *"Theoretical model of intrinsic hardness"*, *Phys. Rev. B: Condens. Matter Mater. Phys.* **2006**, *73*, 22.

[37] S. Horstmann, E. Irran, W. Schnick, *"Synthesis and Crystal Structure of Phosphorus(V) Nitride α-P_3N_5"*, *Angew. Chem. Int. Ed. Engl.* **1997**, *36*, 1873; *Angew. Chem.* **1997**, *109*, 1938.

[38] Crystal data of phe-BeP_2N_4 from single-crystal XRD refinement at ambient pressure: $M = 126.99\,\mathrm{g{\cdot}mol^{-1}}$, hexagonal, $R\bar{3}$ (no. 148), $a = 12.6979(15)$, $c = 8.3595(10)$ Å, $V = 1167.3(5)$ Å^3, $Z = 18$, $\rho = 3.252\,\mathrm{g{\cdot}cm^{-3}}$, $\mu = 0.144\,\mathrm{cm^{-1}}$, synchrotron radiation ($\lambda = 0.289\,40$ Å, DESY, PETRA III, P02.2), $T = 293$ K, 2852 observed reflections, 1241 independent reflections, 64 parameters, $R_{\mathrm{int}} = 0.0656$, $R_\sigma = 0.0763$, $R1 = 0.0668$, $wR2 = 0.0.1403$, $GoF = 1.015$, residual electron density 1.145, −1.078 $e{\cdot}$Å^{-3}. CSD-1946333 contains the supplementary crystallographic data for this paper. These data can be obtained free of charge from The Cambridge Crystallographic Data Centre.

[39] H. M. Rietveld, *"A profile refinement method for nuclear and magnetic structures"*, *J. Appl. Crystallogr.* **1969**, *2*, 65.

[40] Detailed information on the crystallographic data of sp-BeP_2N_4 from pressure-dependent Rietveld refinements is provided in Chapter E. CSD-1946347 (47.3 GPa), 1946344 (44.6 GPa), 1946343 (40.9 GPa), 1946342 (38.5 GPa), 1946340 (37.7 GPa), 1946339 (34.0 GPa), 1946338 (31.0 GPa), 1946337 (28.5 GPa), 1946336 (21.8 GPa), 1946335 (17.8 GPa), 1946334 (12.6 GPa), 1946346 (11.9 GPa), 1946349 (7.4 GPa), 1946341 (5.0 GPa), 1946348 (3.3 GPa), 1946332 (1.8 GPa), and 1946345 (1 atm) contain the supplementary crystallographic data for this compound. These data can be obtained free of charge from The Cambridge Crystallographic Data Centre.

[41] R. Hoppe, S. Voigt, H. Glaum, J. Kissel, H. P. Müller, K. Bernet, *"A new route to charge distributions in ionic solids"*, *J. Less-Common Met.* **1989**, *156*, 105.

[42] F. D. Murnaghan, *"The compressibility of media under extreme pressures"*, *Proc. Natl. Acad. Sci. U.S.A.* **1944**, *30*, 244.

[43] F. Birch, *"Finite Elastic Strain of Cubic Crystals"*, *Phys. Rev.* **1947**, *71*, 809.

8. Summary

The research objective of this thesis was a fundamental investigation of phosphorus nitrides in terms of their preparation and high-pressure behavior. Therefore, the presented publications cover both, the development of an unprecedented synthetic approach for phosphorus nitrides, and their structural investigation at ambient- and high-pressure conditions. This thesis may thus formally be divided into two major parts.

Within the first part that is covered by Chapter 3 and 4, an innovative preparative strategy for mixed phosphorus nitrides is developed. Herein, high-pressure high-temperature conditions are used to prevent the thermal decompositon of the targeted compounds, following Le Chatelier's principle. The reaction of $(PNCl_2)_3$ and NH_4N_3 grants the in situ formation of HCl, which appears essential for mobilization of the refractory nitrides BN and Si_3N_4 that are used as starting materials. This synthetic approach facilitates the initial syntheses of boron phosphorus nitride BP_3N_6 and silicon phosphorus nitride imide SiP_2N_4NH, as presented in Chapter 3 and 4, respectively. Their unprecedented structures, as elucidated from single-crystal XRD analyses and solid-state NMR measurements, moreover, provide intriguing insights into the structural chemistry of phosphorus nitrides.

The second part of this thesis covers the structural investigation of phosphorus nitrides at high pressures. Prior to this thesis, phosphorus nitrides were sparsely investigated at pressures > 16 GPa and their structural investigations were mostly restricted to ex situ XRD measurements using in-house diffractometers. Within the Chapters 5, 6, and 7, therefore, various polymorphs of PON, BP_3N_6, and BeP_2N_4 were investigated in situ at maximum pressures of about 50 GPa, employing laser-heated diamond anvil cells and 3rd generation synchrotron radiation.

The stishovite-related post-coesite polymorph of PON is presented in Chapter 5, in which experimental results from in situ and ex situ examinations, as well as supporting DFT calculations are reported. Chapter 6, in turn, concerns the pressure-dependent structural investigations of BP_3N_6. Herein, the elastic

properties of α-BP_3N_6 are examined and the formation of its high-pressure polymorph β-BP_3N_6 is reported. The structure elucidation of β-BP_3N_6 provides the first experimental proof of sixfold N-coordinated P in a nitride material, which was predicted for numerous high-pressure phases of phosphorus nitrides, previously. Likewise, the preparation and examination of a spinel-type form of Si_3N_4-analog BeP_2N_4 is presented in Chapter 7. Spinel-type BeP_2N_4 features remarkable elastic properties and is therefore discussed in the context of superhard and ultraincompressible nitride materials. More detailed information on the certain publications of this thesis is provided below in individual summaries of the Chapters

3: United in Nitride: The Highly Condensed Boron Phosphorus Nitride BP_3N_6,

4: Rivalry under Pressure: The Coexistence of Ambient-Pressure Motifs and Close-Packing in Silicon Phosphorus Nitride Imide SiP_2N_4NH,

5: Stishovite's Relative: A Post-Coesite Form of Phosphorus Oxonitride,

6: Boron Phosphorus Nitride at Extremes: PN_6 Octahedra in the High-Pressure Polymorph **β**-BP_3N_6, and

7: Nitride Spinel: An Ultraincompressible High-Pressure Form of BeP_2N_4.

8.1. United in Nitride: The Highly Condensed Boron Phosphorus Nitride BP_3N_6

Published in: S. Vogel et al., *Angew. Chem. Int. Ed.* **2018**, *57*, 13202;
Angew. Chem. **2018**, *130*, 13386.
Access via: DOI: 10.1002/anie.201808111
Reprinted at: Chapter 3, Supporting Information in Chapter A

The first boron phosphorus nitride, BP_3N_6, was prepared in a high-pressure high-temperature reaction at 8 GPa and 1100 °C, using the multianvil technique. $(PNCl_2)_3$, NH_4N_3, and h-BN were used as starting materials following Equation 8.1. The in situ formed HCl is considered to act as a mineralizing agent during the synthesis, providing reactive intermediate boron species and facilitating phase formation.

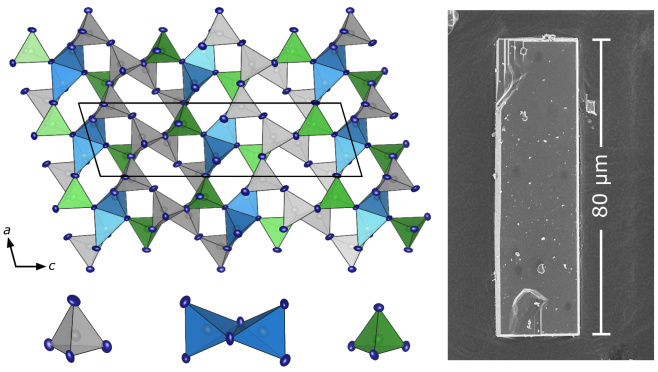

Figure 8.1.: A single-crystal of BP_3N_6 and its atomic structure featuring PN_4 (blue, gray) and BN_4 tetrahedra (green).

Single-crystals of BP_3N_6 up to 80 µm in length were obtained by adding up to 25 wt-% NH_4Cl to the mixture of starting materials. The structure of BP_3N_6 was elucidated from single-crystal XRD ($P2_1/c$ (no. 14), $a = 5.027(1)$, $b = 4.531(1)$, $c = 7.332(3)$ Å, $\beta = 106.387(9)°$, $Z = 4$) and verified by Rietveld refinement. BP_3N_6 is built up from edge-sharing PN_4 tetrahedra and all-side vertex-sharing PN_4 and BN_4 tetrahedra, formally blending structural motifs of the binary nitrides α-P_3N_5 and c-BN, which renders BP_3N_6 a double nitride.

$$2\,(PNCl_2)_3 + 3\,NH_4N_3 + 2\,\text{h-BN} \xrightarrow[1100\,°C]{8\,GPa} 2\,BP_3N_6 + 12\,HCl + 4\,N_2 \tag{8.1}$$

The elemental composition of the title compound was confirmed by EDX spectroscopy, and ^{11}B, ^{31}P, $^{31}P\{^1H\}$, and ^1H solid-state MAS NMR measurements verified the as-refined structure model from XRD. The topology of the highly condensed B/P/N network ($\kappa = 4/6 \approx 0.67$) was determined by TOPOS and its electrostatic plausibility was examined by supplemental MAPLE and CHARDI calculations.

8.2. Rivalry under Pressure: The Coexistence of Ambient-Pressure Motifs and Close-Packing in Silicon Phosphorus Nitride Imide SiP_2N_4NH

Published in: S. Vogel et al., *Angew. Chem. Int. Ed.* **2019**, *58*, 3398;
Angew. Chem. **2019**, *131*, 3436.
Access via: DOI: 10.1002/anie.201813789
Reprinted at: Chapter 4, Supporting Information in Chapter B

The preparation and structure elucidation of silicon phosphorus nitride imide SiP_2N_4NH is presented. Employing the multianvil technique, the title compound was synthesized in a high-pressure high-temperature reaction (8 GPa, 1100 °C) starting from amorphous Si_3N_4, $(PNCl_2)_3$, and NH_4N_3 (Equation 8.2). It is assumed that the in situ formed HCl facilitates the reversible cleavage and (re)formation of the T–N bonds (T = Si, P). The structure of SiP_2N_4NH was elucidated by a synergy of single-crystal XRD (*Pnma* (no. 62), $a = 8.311(2)$, $b = 5.396(1)$, $c = 7.239(2)$ Å, $Z = 4$) and solid-state MAS NMR measurements ($^{29}Si\{^1H\}$, ^{31}P, $^{31}P\{^1H\}$, ^1H). The highly condensed structure of SiP_2N_4NH ($\kappa = 3/5 = 0.6$) features PN_4 tetrahedra, as well as the rare motif of SiN_6 octahedra and can be derived from a distorted hexagonal close-packing of N. The title compound is therefore discussed as an intermediate phase that blends ambient- and high-pressure motifs.

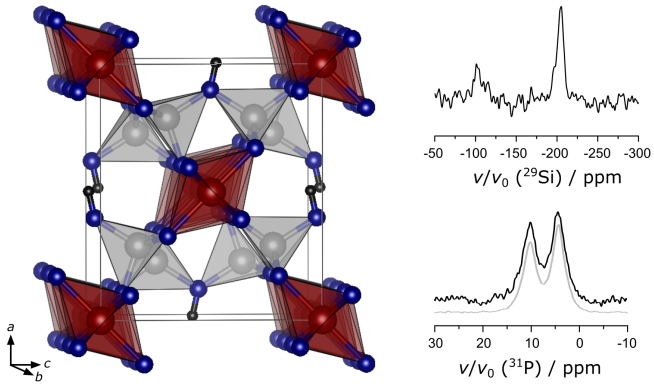

Figure 8.2.: Crystal structure of SiP_2N_4NH and corresponding solid-state NMR spectra. Si: red, P: gray.

$$4\,Si_3N_4 + 8\,(PNCl_2)_3 + 15\,NH_4N_3 \xrightarrow[1100\,^\circ C]{8\,GPa} 12\,SiP_2N_4NH + 48\,HCl + 20\,N_2 \tag{8.2}$$

An additional Rietveld refinement verifies the presented structure model, and its electrostatic plausibility was examined by CHARDI analysis. The elemental composition of SiP_2N_4NH was confirmed by EDX spectroscopy, and its thermal stability was investigated by temperature-dependent PXRD measurements.

8.3. Stishovite's Relative: A Post-Coesite Form of Phosphorus Oxonitride

Published in: S. Vogel et al., *Angew. Chem. Int. Ed.* **2018**, *57*, 6691;
Angew. Chem. **2018**, *130*, 6801.
Access via: DOI: 10.1002/anie.201803610
Reprinted at: Chapter 5, Supporting Information in Chapter C

A stishovite-related post-coesite (pc) polymorph of phosphorus oxonitride PON is reported, which was prepared at 20 GPa in a multianvil apparatus. Its structure was elucidated from powder X-ray diffraction data using the charge-flipping algorithm and the Rietveld method ($P4_2/mnm$ (no. 136), $a = 4.6278(1)$, $c = 2.46042(4)$ Å, $Z = 2$), and the cell metrics were further confirmed by selected area electron diffraction (SAED) tilting series. The title compound adopts a stishovite-related structure, but features a (5+1) coordination of P rather than a regular sixfold coordination that is observed in rutile-type SiO_2 (stishovite). This is owed to a split position of P that is located in the octahedral coordination sphere of O and N. pc-PON was investigated by ^{31}P solid-state MAS NMR, TEM-EDX, as well as FTIR spectroscopy, and temperature-dependent PXRD measurements proved pc-PON as a metastable polymorph at ambient pressure. The title compound's structure was further verified by a single-crystal XRD measurement at 1.8 GPa using a diamond anvil cell and synchrotron radiation, and its isothermal bulk modulus was calculated with $K_0 = 163(2)$ GPa from pressure-dependent PXRD investigations. Moreover, an additional phase transition into an orthorhombic PON form is reported at 20 GPa, for which a $CaCl_2$-related structure is suggested. The presented experimental results are supplemented and confirmed by GGA-based DFT calculations.

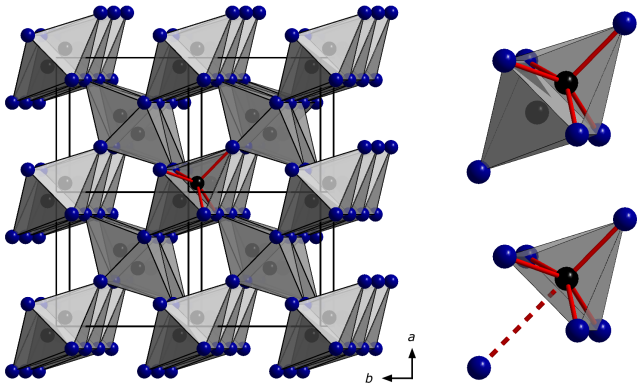

Figure 8.3.: Crystal structure of pc-PON featuring a split position of P (black, $s.o.f. = 0.5$) within a (5+1) coordination of O and N (blue).

8.4. Boron Phosphorus Nitride at Extremes: PN_6 Octahedra in the High-Pressure Polymorph β-BP_3N_6

Published in: S. Vogel et al., *Angew. Chem. Int. Ed.* **2019**, *58*, 9060;
Angew. Chem. **2019**, *131*, 9158.
Access via: DOI: 10.1002/anie.201902845
Reprinted at: Chapter 6, Supporting Information in Chapter D

The double nitride BP_3N_6 was investigated in a laser-heated diamond anvil cell by pressure-dependent synchrotron X-ray diffraction. α-BP_3N_6 contracts uniformly upon cold compression, showing only slight structural distortions and its isothermal bulk modulus was calculated with $K_0 = 146(6)$ GPa from pressure-volume data. At 42 GPa laser heating of α-BP_3N_6 induced a phase transition into its high-pressure polymorph β-BP_3N_6. The unique structure of β-BP_3N_6 was elucidated from single-crystal synchrotron X-ray diffraction at 42 GPa ($Pna2_1$ (no. 33), $a = 8.667(1)$, $b = 7.411(4)$, $c = 4.0115(4)$ Å, $Z = 4$) and is described as an unprecedented decoration of a hexagonal close-packing of N with B occupying $1/12$ of the tetrahedral and P occupying $1/2$ of the octahedral voids. This structural model was further verified by MAPLE and CHARDI calculations. β-BP_3N_6 is quenchable to ambient conditions and its structure shows only marginal structural distortions upon pressure quenching. The title compound is discussed in the context of fundamental structural chemistry of non-metal nitrides, as sixfold N-coordinated P had been an unprecedented, but much sought-after structural motif, previously.

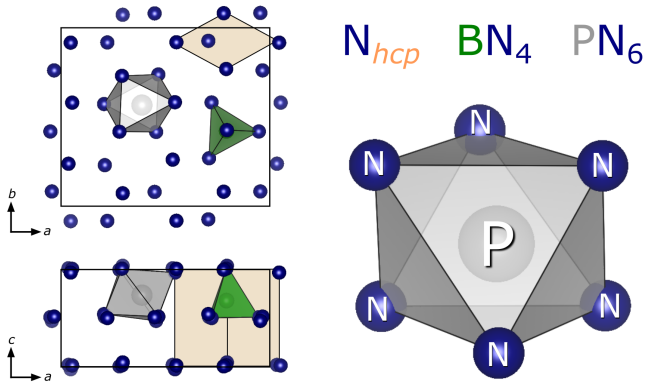

Figure 8.4.: B and P occupy tetrahedral and octahedral voids of a hexagonal close-packing of N atoms leading to BN_4 tetrahedra (green) and PN_6 octahedra (gray).

8.5. Nitride Spinel: An Ultraincompressible High-Pressure Form of BeP_2N_4

Published in: S. Vogel et al., *Angew. Chem. Int. Ed.* **2019** (accepted);
Angew. Chem. **2019** (accepted).
Access via: DOI: 10.1002/anie.201910998
Reprinted at: Chapter 7, Supporting Information in Chapter E

Phenakite-type BeP_2N_4 was synthesized in a high-pressure high-temperature reaction at 7 GPa and 1500 °C, starting from Be_3N_2 and P_3N_5. Its structure was verified by single-crystal synchrotron X-ray diffraction at ambient pressure ($R\bar{3}$ (no. 148), $a = 12.698(2)$, $c = 8.360(1)$ Å, $Z = 18$) before a suitable particle of phe-BeP_2N_4 was cold compressed in a diamond anvil cell. At a maximum pressure of about 47 GPa laser-heating the sample to 1800 K induced the phase transition into the spinel-type phase (sp) that had been predicted from DFT calculations, before. The sp-BeP_2N_4 structure was refined from powder synchrotron X-ray diffraction measurements using the Rietveld method ($p = 47.3(9)$ GPa, $Fd\bar{3}m$ (no. 227), $a = 7.1948(2)$ Å, $Z = 8$). Corresponding to the regular spinel structure, Be and P occupy $1/8$ of the tetrahedral and $1/2$ of the octahedral voids in a cubic close-packing of N, respectively. Additional MAPLE calculations were performed that confirm the as-refined structure. Furthermore, sp-BeP_2N_4 was investigated upon cold decompression to ambient pressure, of which pressure-dependent structural data were obtained. The title compound is quenchable to ambient conditions and its isothermal bulk modulus was calculated with $K_0 = 325(8)$ GPa from equation of states, which renders sp-BeP_2N_4 an ultraincompressible material. The presented results are discussed in the context of previous DFT calculations as well as other incompressible nitride spinels (e. g. γ-Si_3N_4) and prospects for future investigations are outlined.

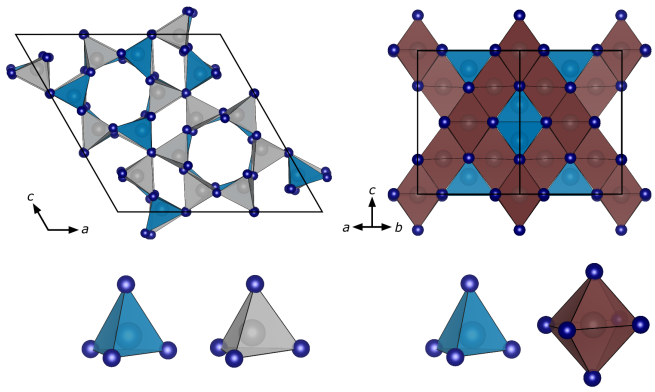

Figure 8.5.: Crystal structure of phenakite-type (left) and spinel-type BeP_2N_4 (right) with respective coordination polyhedra of Be (blue) and P (gray, red).

9. Discussion and Outlook

This thesis presents new fundamental investigations on the preparation and high-pressure behavior of phosphorus nitrides. Within the first part, the high-pressure high-temperature synthesis of mixed phosphorus nitrides is advanced through the development of an innovative preparative approach. As presented in Chapter 3 and 4, this enabled the synthesis of boron phosphorus nitride α-BP_3N_6 and silicon phosphorus nitride imide SiP_2N_4NH, enhancing both, the elemental and the structural diversity of phosphorus nitrides. Employing diamond anvil cells and microfocused synchrotron X-ray diffraction, the work presented in Chapter 5, 6, and 7 further greatly expands the pressure range, in which phosphorus nitrides are experimentally investigated. These studies provide unprecedented examinations of the elastic properties of phosphorus nitrides and gave rise to the first nitride phases, β-BP_3N_6 and spinel-type BeP_2N_4, that feature sixfold N-coordinated P, which can be regarded as a milestone in the structural research of phosphorus nitrides.

In the following sections, key results are discussed in the context of previous investigations and established scientific concepts, in order to deduce the most important achievements made in this thesis. Moreover, prospects for additional investigations are outlined to gain future progress within the field of P/N compounds and nitride materials in general.

9.1. Progress in Nitride Synthesis

Prior to this thesis, phosphorus nitrides have mainly been synthesized using three major preparative approaches, namely the mineralizer-assisted (e. g. α-P_3N_5),[1,2] the molecular precursor (e. g. $SiPN_3$),[3] and the high-pressure high-temperature (HP/HT) approach (e. g. BeP_2N_4),[4] as briefly outlined in Chapter 1.3. The preparative method that is devised in this thesis and denoted as the *acid-assisted HP/HT technique* below, in contrast, can be described as the formal combination of these three established ap-

proaches, granting access to previously inaccessible compounds. Herein, molecular $(PNCl_2)_3$ and NH_4N_3 are reacted with a refractory binary nitride (e. g. h-BN) at high pressures and high temperatures to form a crystalline mixed phosphorus nitride, as exemplarily shown for α-BP_3N_6 in Equation 9.1.

$$2\,(PNCl_2)_3 + 3\,NH_4N_3 + 2\,\text{h-BN} \xrightarrow[1100\,^\circ\text{C}]{8\,\text{GPa}} 2\,\alpha\text{-}BP_3N_6 + 12\,HCl + 4\,N_2 \tag{9.1}$$

Although the mechanism of the acid-assisted HP/HT technique was not investigated in situ over the course of this PhD project, a reasonable scientific theory that describes its mode of action in simplified terms may be deduced from ex situ observations and preexisting simple scientific concepts that originate from molecular and nano chemistry. For this purpose, the single-crystal formation of α-BP_3N_6 and SiP_2N_4NH, as presented in Chapter 3 and 4, is divided into three major regimes, namely (*i*) the *decomposition* of the solid-state precursors, (*ii*) the *nucleation*, and (*iii*) the *crystal growth*. The over-all reaction may thus be described as a non-topotactic rearrangement of T and N atoms or small T–N species (T = B, Si, P), as is discussed below and schematically illustrated in Figure 9.1.

In an initial step the heat-induced *decomposition* of $(PNCl_2)_3$ and NH_4N_3 likely results in the formation of molecular $[P_aN_bCl_cH_d]^m$ species as well as N_2 and HCl (Equation 9.2). Herein, the stated $[P_aN_bCl_cH_d]^m$ species may correspond to mono- or oligomers of derivates of phosphorus amides, imides, or chlorides,[5,6] with a, b, c, and d serving as variables for non-negative integers and m accounting for possible charges. One therefore may think about PCl_5, $P(NH_2)_4^+$, $Cl_2P(NH_2)^+$, or $Cl_3PNPCl_3^+$ as intermediate species, for instance.

$$(PNCl_2)_3 + NH_4N_3 \xrightarrow{\text{HP/HT}} [P_aN_bCl_cH_d]^m + HCl + N_2 \tag{9.2}$$

At the applied HT/HP conditions, the in situ formed HCl most likely exists in the supercritical state, considering its critical point at p_{crit} = 82.56 bar and T_{crit} = 51.53 °C.[7] It was shown that even refractory BN and Si_3N_4 can be used as starting materials, which suggests that strong acids (e. g. HCl) facilitate their mobilization by the cleavage of B–N and Si–N bonds, as has previously been assumed for P–N bonds,[8–10] and discussed for the Si_3N_4/HF system as well.[11] Thus, intermediate $[T_aN_bCl_cH_d]^m$ species (T = B, Si) are likely also provided in situ by the HCl-assisted dissolution of refractory BN and Si_3N_4 (Equation 9.3). Here, monomeric Cl_2BNH_2, Cl_3SiNH_2, or $Cl_2Si(NH_2)_2$, dimeric $Cl_3SiNHBCl_2$,

or $Cl_3SiNHB(NH)_2$, as well as ionic $ClBNH_2^+$, $B(NH_2)_4^-$, or $Cl_2SiNH_2^+$ may be considered as plausible intermediate species, for instance.

$$T_xN_{y,bulk} + HCl \xrightarrow{HP/HT} (T_xN_{y,bulk}) + [T_aN_bCl_cH_d]^m \tag{9.3}$$

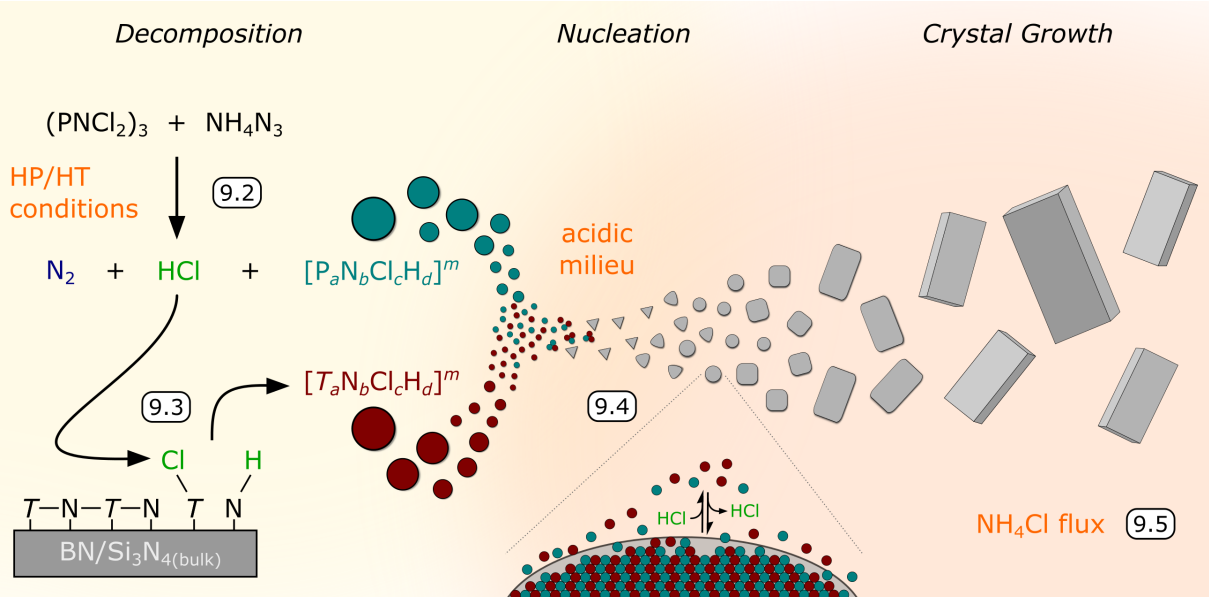

Figure 9.1.: The acid-assisted HP/HT technique may be formally divided into three major steps. The initial *decomposition* of the solid-state precursors is facilitated by HP/HT conditions as well as in situ formed HCl, and likely results in the formation of $[T_aN_bCl_cH_d]^m$ species (T = B, Si, P; Equations 9.2 and 9.3). These intermediate species may randomly condense during the reversible process of *nucleation* to form crystallites of the thermodynamically stable phase (Equation 9.4). The formation of single-crystals (*crystal growth*), finally, is greatly enhanced by NH_4Cl, which is considered to act as a mineralizer that grants the migration of all involved intermediate species (Equation 9.5).

In a subsequent stochastic process all intermediate species may migrate, intermix, and condense randomly into macromolecular nuclei by the reversible formation of T–N bonds (T = B, Si, P; Equation 9.4), entering the regime of *nucleation*. The surfaces of the as-formed nuclei are likely saturated with Cl and H, providing reactive sites for further polycondensation or re-dissolution, depending on the stability of the nuclei. Since this equilibrium equation is highly reversible, the formation of defects is prevented, yielding highly ordered crystallites that subsequently can grow within the regime of *crystal growth*.

$$[T_1N_bCl_cH_d]^m + [T_2N_{b'}Cl_{c'}H_{d'}]^{m'} \rightleftharpoons [H_{d-1}Cl_cN_bT_1 - N - T_2N_{b'-1}Cl_{c'-1}H_{d'}]^n + HCl \tag{9.4}$$

It was shown that α-BP_3N_6 and SiP_2N_4NH are obtained as crystalline powders, when no mineralizer is used. Their single-crystal growth, however, is greatly enhanced by adding about 25 wt-% of NH_4Cl to the mixture of starting materials, which suggests NH_4Cl to act as a mineralizer for phosphorus nitrides. This is in line with findings from previous studies, in which single-crystals of β-PNNH and various (imide)nitridophosphates were obtained by adding minor amounts of NH_4Cl to the respective mixture of starting materials.[12–14] Whereas NH_4Cl completely dissociates into gaseous NH_3 and HCl at ambient pressure and 350 °C,[15] it is considered to form a liquid phase at elevated pressures and temperatures that can be described as a chemical equilibrium of an ionic and a molecular melt (Equation 9.5).[16,17]

$$NH_4Cl_{(s)} \xrightarrow{\Delta T, \Delta p} (NH_4^+ + Cl^-)_{(l)} \rightleftharpoons (NH_3 + HCl)_{(l)} \tag{9.5}$$

Therefore, it appears plausible that NH_4Cl acts as a flux medium during the whole equilibrium reaction, which facilitates the migration of all intermediate species. This greatly enhances the growth of single-crystals, which finally proceeds until all intermediate species are converted into bulk material and the system enters its global thermodynamic minimum, corresponding to α-BP_3N_6 and SiP_2N_4NH, respectively. Moreover, it is plausible that an Ostwald ripening mechanism further assists the formation of large single-crystals.[18]

One should finally emphasize that the above conclusions are solely drawn from ex situ observations and thus, should be considered a scientific hypothesis with any experimental evidences being subject of future investigations. In situ experiments in diamond anvil cells, however, appear doubtful, as both, the diamond anvils and the gasket materials may likely suffer from the harsh synthetic conditions. Future examinations may thus focus on large volume press setups that are designed for in situ studies, such as ID6 (ESRF),[19] GSECARS (APS),[20] PSICHÉ (Soleil),[21] or soon P61B (DESY),[22] as presented in Chapter 2. Nevertheless, the presented theory appears plausible, when compared to previous suggestions on the modes of action of related preparative techniques that employ mineralizers or flux media for nitride synthesis.

The high-pressure metathesis, for instance, was developed for the preparation of rare-earth and transition metal nitridophosphates and facilitates the growth of single-crystals through in situ formed LiF acting as a flux during the process of crystallization at HP/HT conditions, as lithium halides were shown to serve as a solvent for nitride anions.[23–25] The ammonothermal method, in turn, uses supercritical NH_3

as a solvent for the synthesis and crystallization of nitrides.[26,27] Herein, either ammonoacid, ammono-neutral, or ammonobasic conditions are adjusted by adding catalytic amounts of a respective mineralizer (e. g. NH_4Cl, $NaNH_2$). Thus, one may imagine a *base-assisted HP/HT method* as well, in which amides or imides could be used to facilitate the synthesis and crystallization of unprecedented nitride materials. Finally, the employment of NH_4Cl as a nitrogen source in the HP/HT syntheses of BN[17] and the transition metal nitrides *M*N (*M* = Ti, V, Cr, Mo, W)[28–30] raises the question whether the acid-assisted HP/HT technique is limited to nitrides of B, Si, and P or may be expanded to the preparation of nitrides in a more global context.

The straightforward syntheses of α-BP_3N_6 and SiP_2N_4NH render the acid-assisted HP/HT technique a powerful tool for the synthesis of nitrides that are dominated by covalent bonds. With an increasing ionicity of the targeted nitrides, however, the formation of chlorides may be likely preferred to nitride synthesis, especially for metals with low electronegativities (e. g. alkali/earth alkaline metals). To fathom the possibilities and limits of the acid-assisted HP/HT technique, therefore, future investigations will be necessary, covering both, systematic investigations and explorative screenings. The variation of thermodynamic parameters, namely the temperature, the pressure, and the mole fraction of the starting materials, may be used to alter the elemental composition within a compound class, varying their structures and materials properties. One could, for example, increase the boron content in B/P/N networks to increase their degree of condensation κ, which may enhance their mechanical properties, as is discussed later in this chapter.

Within the scope of explorative investigations, the acid-assisted HP/HT technique may further be transferred to other systems for which very few, if any, representatives have been reported as yet. Herein, the substitution of either $(PNCl_2)_3$ or the binary nitride BN/Si_3N_4 may initially be considered, as briefly outlined below and illustrated in Figure 9.2. Hence, substituting $(PNCl_2)_3$ with $(BNHCl)_3$ may likely yield crystalline compounds within the Si/B/N system, in which only amorphous $Si_3B_3N_7$ was reported thus far.[31,32] Double nitrides of B and Si, however, are of special interest for materials scientists, considering numerous high-performance applications of BN and Si_3N_4, as well as $SiBN_3C$.[31–35] $(PNCl_2)_3$ may be further replaced by $(CNCl)_3$ (cyanuric chloride) to formally introduce C into covalent nitride materials. This preparative strategy could provide access to compounds within the B/C/N system, for instance, that has repeatedly been discussed in the context of superhard materials.[36–38]

The acid-assisted HP/HT technique may further be used for the preparation and crystallization of binary nitrides, such as BN, P_3N_5, or even C_3N_4. In a preliminary test, microcrystalline c-BN was prepared starting from $(BNHCl)_3$ and NH_4N_3. The preparation of single-crystalline P_3N_5, hence, appears plausible by the reaction of $(PNCl_2)_3$ and NH_4N_3 in the absence of BN and Si_3N_4. This, however, requires a suitable substitute for the well-established h-BN crucibles. Initial attempts, in which the mixture of starting materials was surrounded by a capsule consisting of noble metals such as Cu or Ag did not succeed, but metal halides and $CuPN_2$, as well as additional unknown phases were formed.[39] Targeting the long sought-after binary nitride C_3N_4, in turn, $(CNCl)_3$ may be reacted with NH_4N_3 in a NH_4Cl flux at HP/HT conditions. The crystallization of carbon nitrides is likely facilitated by NH_4Cl, as single-crystalline melamium halides have been prepared in the presence of ammonium halides, recently.[40] Accounting for the low thermal stability of carbon nitrides, however, the reaction temperature should be significantly decreased, which may require the substitution of NH_4Cl with NH_4F that features a significant lower melting curve at high-pressure conditions.[16,41] However, if all experimental challenges are met, one may be amply rewarded with the preparation of crystalline C_3N_4 phases, which are considered one of today's major goals of nitride chemistry.

An even larger field of unprecedented compounds may become accessible by the substitution of the binary nitrides BN and Si_3N_4. The employment of oxide compounds such as B_2O_3, SiO_2, P_2O_5, or BPO_4, for instance, formally opens the compound class of oxide nitrides, which would greatly expand the structural diversity by varying the degree of condensation of the resulting networks, as outlined in Chapter 1.2. Moreover, such oxide nitride materials, commonly denoted as oxynitrides, often feature intriguing semiconducting properties and are therefore frequently discussed in the context of photocatalysis.[42,43] Considering further the literature-known double nitrides $BeSiN_2$, Mg_2PN_3, Zn_2PN_3, $CuPN_2$, $ZnSiN_2$, and Mg_3GaN_3,[39,44–48] as well as solid solutions within the γ-$(Ge_xSi_{1-x})_3N_4$ and AlGaN system,[49,50] precursors such as Be_3N_2, Mg_3N_2, Zn_3N_2, Cu_3N, AlN, GaN, or Ge_3N_4 may be employed to access unprecedented ternary nitrides such as Be_3BN_3, AlP_3N_6, $GePN_3$, or $Ga_3Si_3N_7$, for instance. These materials likely feature intriguing optical and electronic properties, considering recent examinations of Grimm-Sommerfeld analogous semiconducting II-IV-N_2, II_2-V-N_3, and I-IV_2-N_3 nitrides.[51–56] If finally any form of cross substitution as well as the combination of multiple substitutes are considered, future explorative investigations may likely open dozens of multinary T/T'/(N/NH/O) systems, each of them counting numerous plausible $T_xT'_y$(N/NH/O)$_z$ compounds with altered $T : T'$ ratios, as illustrated in Fi-

gure 9.2. To further amplify the prospects of success the stability of any conceivable multinary compound towards its binary and elemental constituents may be previously evaluated by theoretical investigations employing data mining algorithms, as was recently exemplified by the prediction of over 200 new ternary nitrides.[57,58]

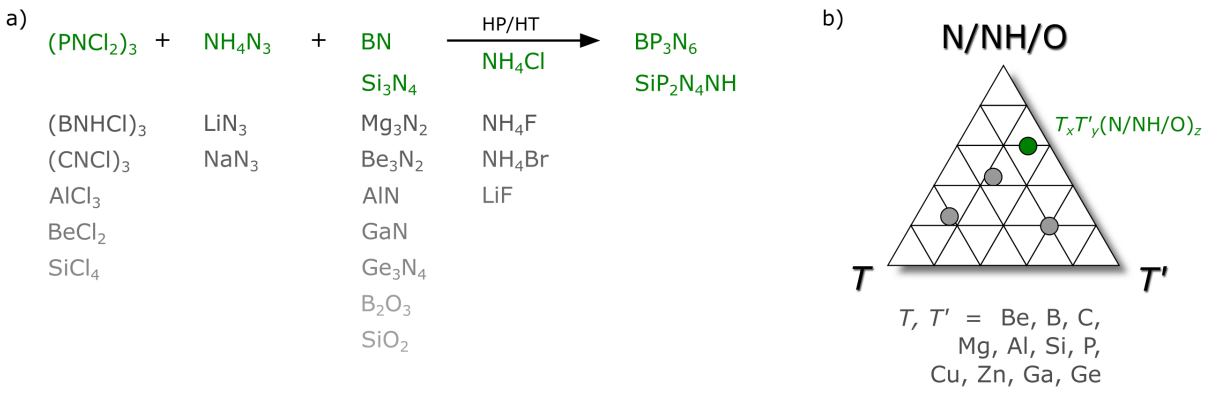

Figure 9.2.: By substituting $(PNCl_2)_3$ and/or the binary nitrides BN/Si_3N_4 with suitable compounds (a), the acid-assisted HP/HT technique may be modified to grant access to numerous novel multinary (oxide/imide) nitrides within dozens of possible T/T'/(N/NH/O) systems (b). Possible substitutes are listed under the chemical equation. Replacing NH_4N_3 and/or NH_4Cl may alter the in situ conditions and further expand the field of application.

The employment of the acid-assisted HP/HT technique, however, depends on the availability of suitable reactive precursors (e. g. $(PNCl_2)_3$, $(BNHCl)_3$, $(CNCl)_3$) as yet, which likely limits the elemental diversity of accessible compounds in the long term. It would be, therefore, highly desirable to modify this technique in a way that enables the direct reaction of two binary nitrides or oxides. Considering the above discussed HCl-assisted mobilization of the refractory nitrides BN and Si_3N_4, one can fortunately assumed that numerous nitrides or oxides can be used as starting materials, if the in situ supply of a strong acid (e. g. HCl) is granted. For this purpose, catalytic amounts of hydrogen halides, as provided by the partial dissociation of ammonium halides at HP/HT conditions (Equation 9.5) may be sufficient, which thus would make the employment of reactive precursors obsolete. Respective tests and developments, however conjecture yet, may therefore also form a part of future explorative investigations on nitride synthesis.

Recapitulating, a possible mode of action of the acid-assisted HP/HT technique was proposed from ex situ observations, and various modifications were discussed to prospectively expand its field of applicati-

on. Within the scope of future explorative investigations the acid-assisted HP/HT technique may, hence, evolve into a powerful tool, not only for the synthesis of phosphorus nitrides, but for the preparation of a broad collective of multinary nitride materials.

9.2. Phosphorus Nitrides at High Pressures

Prior to this thesis, the structural behavior of phosphorus nitrides was rarely investigated at pressures exceeding 16 GPa and examinations on their elastic properties were mostly limited to theoretical studies. Therefore, three compounds characteristic for this class, namely PON, BP_3N_6, and BeP_2N_4 were systematically investigated up to maximum pressures of about 50 GPa. Employing in situ synchrotron X-ray diffraction and diamond anvil cells, their elastic properties were probed and unprecedented high-pressure polymorphs were discovered, as is discussed for the respective compounds below.

Initially aiming for a stishovite-type PON polymorph, cristobalite-type (cri) PON was transformed into a post-coesite (pc) PON form at HP/HT conditions using a large volume press. The pressure-quenched pc-PON is structurally related to stishovite, but features a (5+1) coordination of P rather than a regular sixfold coordination, which originates from a split position of P. Its compressibility was investigated by in situ cold-compression experiments, yielding an isothermal bulk modulus of K_0(pc-PON) = 163(2) GPa. According to this, pc-PON is approximately twice as incompressible as cri-PON (K_0(cri-PON) = 80(5) GPa), in line with its significantly denser P/O/N framework (ρ(cri-PON) = 2.720 g·cm^{-3}, ρ(pc-PON) = 3.843 g·cm^{-3}, +41 %).[59] Stishovite, however, is even less compressible (K_0(sti-SiO_2) $\approx$ 310 GPa),[60] which is most likely an effect of the different elemental composition. It is, however, reasonable to assume that the $P(O/N)_{5+1}$ polyhedron is intrinsically less rigid than the SiO_6 octahedron, as it features an additional degree of freedom, accounting for the split position of P.

Additional in situ investigations up to a maximum pressure of about 40 GPa showed that pc-PON undergoes a reversible phase transition into a metastable orthorhombic PON phase at about 20 GPa. It was deduced that this orthorhombic PON phase most probably adopts a $CaCl_2$-related structure, which stishovite forms at $p > 55$ GPa, as well.[61,62] Thus, this plausible $CaCl_2$-type PON may also feature regular $P(N/O)_6$ octahedra and can be considered the initial product from the large volume press synthesis at 20 GPa. Upon pressure-quenching, however, it may transform into the as-presented pc-PON, which is kinetically stabilized even at ambient pressure. These results greatly emphasize the close structural

relation of PON and SiO_2, and suggest that PON features a diverse and yet undiscovered high-pressure polymorphism at pressures exceeding 20 GPa, as has already been shown for SiO_2.[62] Accordingly, further silica-analog high-pressure PON polymorphs with α-PbO_2-,[63–65] pyrite- (FeS_2, HP-PdF_2),[66] or Fe_2N-related structures are fathomable at sufficiently high pressures.[67] Thus, a regular sixfold coordination of P becomes even more probable, which may also enhance the incompressibility of the certain phases.

The structure of unprecedented α-BP_3N_6 blends structural motifs of α-P_3N_5 and c-BN, the latter representing the world's most incompressible nitride (K_0(c-BN) = 396(2) GPa).[68,69] Therefore, the elastic properties of α-BP_3N_6 were investigated by pressure-dependent single-crystal XRD up to a maximum pressure of 42 GPa. It was shown that the tetrahedra-based B/P/N network of α-BP_3N_6 contracts uniformly upon cold compression, showing only slight structural distortions. Its calculated isothermal bulk modulus is 146(6) GPa, which is significantly larger than bulk moduli that have been discussed for related tetrahedra-based P/N structures, such as cri-PON (K_0 = 80(5) GPa), α-PNNH (K_0 = 102(2) GPa), α-P_3N_5 (K_0 = 87–99 GPa), or β-P_4N_6NH (K_0 = 66 GPa).[59,70–72] This is likely owed to the interconnection of PN_4 and BN_4 tetrahedra, the latter being a very rigid motif within the structure of ultraincompressible c-BN. It is further conspicuous that the bulk modulus of α-BP_3N_6 can be interpreted as the approximate arithmetical mean of the bulk moduli of c-BN and α-P_3N_5 considering a 1 : 3 ratio of B : P in the α-BP_3N_6 structure (Equation 9.6).

$$146\,\mathrm{GPa} = K_0(\alpha\text{-}BP_3N_6) \approx {}^1\!/_4 \cdot K_0(\text{c-BN}) + {}^3\!/_4 \cdot K_0(\alpha\text{-}P_3N_5) \approx 170\,\mathrm{GPa} \tag{9.6}$$

Thus, the formal blending of the α-P_3N_5 and the c-BN structure causes a combination of their elastic properties, which is in line with empirical models that have previously been deduced from the bonding situations and elastic properties of numerous pnictides, chalcogenides, and halides.[73,74] Within the scope of future investigations, the elastic properties of B/P/N compounds may thus be tuned by varying the B : P ratio, providing access to unprecedented incompressible nitride materials.

To investigate its high-pressure polymorphism, α-BP_3N_6 was laser-heated at 42 GPa, which induced a phase transition into β-BP_3N_6 that was characterized by single-crystal synchrotron XRD. β-BP_3N_6 is quenchable to ambient conditions and features a 31 % higher ambient pressure density than α-BP_3N_6 (ρ(α-BP_3N_6) = 3.293 g·cm^{-3}, ρ(β-BP_3N_6) = 4.319 g·cm^{-3}), which likely renders β-BP_3N_6 significantly

less compressible than α-BP_3N_6. The unique structure of β-BP_3N_6 can be derived from a hexagonal close-packing of N, in which B occupies 1/12 of the tetrahedra voids and P occupies 1/2 of the octahedra voids (Figure 9.3b). Therefore, β-BP_3N_6 is the first phosphorus nitride that contains the long sought-after structural motif of PN_6 octahedra, providing fundamental new insights into the structural chemistry of phosphorus nitrides, which now can be discussed in the context of the high-pressure polymorphism of covalent nitrides in general:

At ambient and moderate pressures, the covalent binary nitrides of Be, B, Si, and P tend to form tetrahedra-based networks as illustrated by α-/β-Be_3N_2,[75,76] c-BN,[77] α-/β-Si_3N_4,[78] and α-P_3N_5,[1] with an exception for B, which enters a threefold N coordination in h-BN at ambient pressure.[79] The double nitrides $Si_3B_3N_7$,[31,32] phe-BeP_2N_4,[4] $SiPN_3$,[3] and $BeSiN_2$[44] may thus be understood as the formal structural combination of the constituting binary nitrides, which further applies to α-BP_3N_6, as presentend in Chapter 3. At elevated pressures, however, the coordination number of P can increase to five, as is observed in γ-P_3N_5 and γ-P_4N_6NH at 11 and 14 GPa, respectively.[80,81] The coordination number of Si, however, likely increases to six as reported for γ-Si_3N_4 at about 13 GPa.[82–84] Considering the SiP_2N_4NH structure that features SiN_6 but PN_4 polyhedra, it was further shown that Si can readily enter the sixfold N coordination at pressures < 10 GPa, which appears favored to an increase of the coordination number of P. The preparation of β-BP_3N_6 now revealed that P can likewise enter a sixfold N coordination at pressures > 40 GPa, which was also confirmed by the synthesis of spinel-type BeP_2N_6 at 47 GPa, as discussed below. Thus, the formation of PN_6 octahedra, in turn, is more favorable than increasing the coordination number of B and Be, respectively. This seems reasonable, considering that the BeN_6 motif was proposed to occur in the high-pressure forms of Be_3N_2,[85–87] and $BeSiN_2$[85] at pressures in the order of 75–140 GPa, while sixfold N-coordinated B may only be observed upon very high loads of 850–1250 GPa, as was predicted for a rocksalt-type BN.[88–90]

Based on the lessons learned from the preparation of β-BP_3N_6, phenakite-type (phe) BeP_2N_4 was investigated at high-pressure conditions as well, yielding a spinel-type (sp) BeP_2N_4 polymorph, homeotypic with γ-Si_3N_4. The preparation of sp-BeP_2N_4 was performed at about 47 GPa to subsequently investigate its elastic properties upon decompression in a sufficient pressure range. Theoretical investigations have predicted sp-BeP_2N_4 with remarkable elastic properties (K_0 = 263–291 GPa, H_V = 45 GPa), prior to this thesis.[4,91–93] The experimental isothermal bulk modulus was now even determined with K_0 = 325(8) GPa, which renders sp-BeP_2N_4 an ultraincompressible material that competes with γ-Si_3N_4

for outstanding elastic properties. The elastic properties of γ-Si_3N_4 have extensively been investigated all along, yielding an isothermal bulk modulus of K_0 = 290–317 GPa and a Vickers hardness of H_V = 30–43 GPa.[82,84,94–97] Whereas the incompressibility of a certain compound can be correlated with its valence electron density (VEC), its hardness is related to the shear modulus and thus to the strength of the interatomic bonds.[69] sp-BeP_2N_4 and γ-Si_3N_4 are isoelectronic, both featuring 32 valence electrons. The unit cell volume of sp-BeP_2N_4 at ambient pressure, however, is about 10 % smaller than the unit cell volume of γ-Si_3N_4.[82,83,94] Thus sp-BeP_2N_4 features a higher VEC than γ-Si_3N_4, which is in line with a slightly higher bulk modulus of sp-BeP_2N_4. Accounting further for the highly covalent character of the Be–N and P–N bonds,[91,98] sp-BeP_2N_4 may feature a remarkable Vickers hardness as well, which strongly encourages comprehensive future investigations on its elastic properties. For this purpose, pressure-quenched sp-BeP_2N_4 particles as obtained from laser-heated diamond anvil cells, however, may hardly serve as sufficient samples, which raises the question of an upscaled preparative access. It can be assumed that the phe-BeP_2N_4 $\longrightarrow$ sp-BeP_2N_4 transition pressure, however not screened experimentally yet, may be likely lower than the applied 47 GPa, as pointed out by previous theoretical investigations (p_{trans} = 14–24 GPa).[4,92] Therefore, sample amounts of sp-BeP_2N_4, large enough for the most desired measurements, may prospectively be obtained employing suitable large volume presses setups that are briefly described in Chapter 2.

Recapitulating, the presented in situ investigations, as summarized in Figure 9.3a, shine a light on the high-pressure behavior of phosphorus nitrides and provide the first experimental instances of sixfold N-coordinated P in nitride materials. Moreover, highly condensed phosphorus nitrides were shown to compete with established incompressible and hard materials for their remarkable elastic properties. These pioneering investigations, therefore, may encourage prospective explorations of P/N compounds, as has already been initiated by additional experiments that were performed over the course of this PhD project. Therein, P_3N_5 and $LiPN_2$ were examined in laser-heated diamond anvil cells up to a maximum pressure of about 55 GPa (Figure 9.3a). Preliminary results indicate the formation of several unprecedented P_3N_5 and $LiPN_2$ polymorphs, but final structure elucidations have been hampered by low-symmetry and insufficient data completeness. These projects, however, appear very promising when complemented with theoretical studies and advanced XRD techniques. Theoretical examinations may therefore deal with the screening of stable high-pressure phases by ab initio evolutionary simulations, as was recently reported for lithium and magnesium nitrides, for instance.[99,100] Sufficient data completeness may be

obtained by merging multiple XRD datasets of randomly oriented domains, referring to advanced data processing techniques.[101–103] To experimentally increase the data completeness, moreover, advanced synchrotron setups may be used, in which the diamond anvil cell is mounted on a flexible goniometer, as supplied by the beamlines BM01 (SNBL, ESRF) and P24 (PETRA III, DESY), for instance.[104,105]

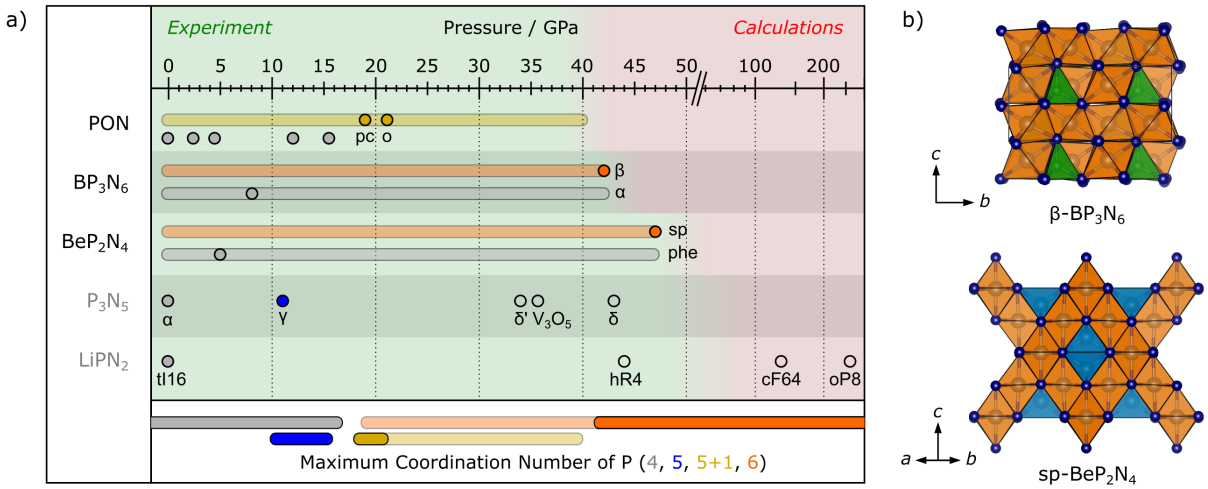

Figure 9.3.: Within this thesis, the elastic properties and high-pressure polymorphism of PON, BP_3N_6, BeP_2N_4, P_3N_5, and $LiPN_2$ were investigated at pressures of up to 50 GPa using laser-heated diamond anvil cells and synchrotron radiation (a). Colored circles mark the synthesis pressure of a certain compound and colored bars illustrate the pressure ranges, in which this compound was investigated. These studies provide intriguing insights into the high-pressure behavior of phosphorus nitrides and gave rise to the first nitrides, β-BP_3N_6 and sp-BeP_2N_4, that contain sixfold N-coordinated P (b, PN_6 octahedra: orange, BN_4 tetrahedra: green, BeN_4 tetrahedra: blue). There has been, however, no experimental evidence for any of the predicted high-pressure polymorphs of P_3N_5 and $LiPN_2$ (hollow circles) as yet.[71,106,107]

Within a broader context, laser-heated diamond anvil cells may further be used to advance the preparative P/N chemistry by granting access to P^{III}/P^{V} (nitride) pernitrides, as has been proposed from theoretical studies, previously.[106,108] Therefore, a skutterudite-like PN_3, a rutile-related PN_2, or a corundum-structured P_2N_3 may be prepared at elevated pressures and investigated on their materials properties, as some of them are suspected to feature metallicity or superconductivity.[106,108] Considering recent advancements in the high-pressure synthesis of related compounds, such as $CaCl_2$-type SN_2,[109] or the group 14 pernitrides SiN_2, GeN_2, and SnN_2,[110] unprecedented P/N compounds may be obtained from elemental $P_{red/black}$ and N_2 upon laser heating at high-pressure conditions. Moreover, NH_3, NH_4Cl, and NH_4N_3 appear as possible nitrogen sources that may likely react with elemental P at elevated temperatures. One

may further consider a top-down approach, in which a gentle thermal annealing of P_3N_5 at elevated pressures induces its partial thermal decomposition, which may result in the formation of unprecedented phosphorus(III) nitrides.

9.3. Concluding Synopsis

An innovative high-pressure high-temperature synthesis strategy was developed that granted access to unprecedented mixed phosphorus nitrides, and fundamental new insight on their structural chemistry was gained by in situ high-pressure investigations. Hence, the results presented within this thesis show that pressure is a versatile thermodynamic parameter for both, the preparation and the structural investigation of phosphorus nitrides, which thus may be generalized in a global prospect for predominantly covalent nitride materials.

There is no doubt that covalent nitrides feature an immense structural diversity as well as intriguing materials properties. Despite of extensive experimental and theoretical studies, this basic field of research is still unexhausted, as revealed in this thesis. The fundamental examinations herein may thus serve as an expedient model that paths the way for future explorations of nitride materials. Various unprecedented (oxide/imide) nitrides may be obtained by the formal combination of binary nitrides (and oxides), employing a modified acid-assisted HP/HT approach. Besides Be, B, Si, and P, additional elements such as Mg, Zn, Cu, Al, Ga, or Ge may be incorporated into predominantly covalent nitride networks, opening dozens of multinary T/T'/(N/NH/O) systems. In turn, each of these systems, most of them totally unexplored yet, counts numerous plausible $T_xT'_y$(N/NH/O)$_z$ compounds. As nitrides were shown to feature a divers polymorphism, the phase diagrams of novel compounds may be further screened for high-pressure and/or high-temperature polymorphs, using in situ techniques, such as diamond anvil cells or temperature-dependent X-ray diffraction. Finally, one could end up with an immense pool of unprecedented phases that feature intriguing structural, elastic, optical, and/or electronic properties, which would greatly expand the fundamental knowledge of nitride materials.

Thus, the global prospect of this thesis strives to deepen the understanding of nitride materials as a long-term goal, promoting fundamental research as the indispensable foundation for future technological progress and development.

9.4. References

[1] S. Horstmann, E. Irran, W. Schnick, *"Synthesis and Crystal Structure of Phosphorus(V) Nitride α-P_3N_5"*, *Angew. Chem. Int. Ed. Engl.* **1997**, *36*, 1873; *Angew. Chem.* **1997**, *109*, 1938.

[2] W. Schnick, J. Lücke, F. Krumeich, *"Phosphorus Nitride P_3N_5: Synthesis, Spectroscopic, and Electron Microscopic Investigations"*, *Chem. Mater.* **1996**, *8*, 281.

[3] H.-P. Baldus, W. Schnick, J. Lücke, *"Silicon Phosphorus Nitride, the First Ternary Compound in the Silicon-Phosphorus-Nitrogen System"*, *Chem. Mater.* **1993**, *5*, 845.

[4] F. J. Pucher, S. R. Römer, F. W. Karau, W. Schnick, *"Phenakite-type BeP_2N_4 – a possible precursor for a new hard spinel-type material"*, *Chem. – Eur. J.* **2010**, *16*, 7208.

[5] T. N. Miller, A. V. Vitola, *"Neorganicheskie soedineniia fosfora s azotom (Inorganic Compounds of Phosphorus with Nitrogen)"*, Zinatne, **1986**.

[6] D. Corbridge, *"Phosphorus - An Outline of its Chemistry, Biochemistry and Technology"*, Elsevier, Amsterdam, Oxford, New York, Tokyo, 3rd Ed., **1990**.

[7] C. Henderson, D. Lewis, P. Prichard, L. Staveley, I. Fonseca, L. Lobo, *"Some thermodynamic properties of hydrogen chloride and deuterium chloride"*, *J. Chem. Thermodyn.* **1986**, *18*, 1077.

[8] A. W. Garrison, C. E. Boozer, *"The acid-catalyzed hydrolysis of a series of phosphoramidates"*, *J. Am. Chem. Soc.* **1968**, *90*, 3486.

[9] T. A. Modro, D. H. Graham, *"Phosphoric Amides. 3.1 Acidic Cleavage of the Phosphorus-Nitrogen Bond in Acyclic and Cyclic Phosphoramidates"*, *J. Org. Chem.* **1981**, *46*, 1923.

[10] R. Greenhalgh, J. R. Blanchfield, *"The Cleavage of Phosphorus to Nitrogen Bonds with Hydogen Fluoride"*, *Can. J. Chem.* **1965**, *44*, 501.

[11] D. Martin Knotter, T. J. J. Denteneer, *"Etching Mechanism of Silicon Nitride in HF-Based Solutions"*, *Appl. Phys. Lett.* **2001**, *148*, F43.

[12] A. Marchuk, F. J. Pucher, F. W. Karau, W. Schnick, *"A high-pressure polymorph of phosphorus nitride imide"*, *Angew. Chem. Int. Ed.* **2014**, *53*, 2469; *Angew. Chem.* **2014**, *126*, 2501.

[13] A. Marchuk, *"Mineralizer-Assisted High-Pressure High-Temperature Synthesis and Characterization of Novel Phosphorus Nitride Imides and Luminescent Alkaline Earth Metal (Oxo)Nitridophosphates"*, Dissertation, Ludwig-Maximilians-Universität, Munich, **2016**.

[14] S. Vogel, W. Schnick, *"SrP_3N_5NH: A Framework-Type Imidonitridophosphate Featuring Structure-Directing Hydrogen Bonds"*, *Chem. – Eur. J.* **2018**, *24*, 14275.

[15] N. Wiberg, E. Wiberg, A. F. Holleman, *"Lehrbuch der anorganischen Chemie"*, Gruyter, Berlin, 101th Ed., **1995**.

[16] C. W. F. T. Pistorius, *"Melting Curves and Phase Transitions of the Ammonium Halides to 40 kbar"*, *J. Chem. Phys.* **1969**, *50*, 1436.

[17] J.-Q. Hu, Q.-Y. Lu, K.-B. Tang, S.-H. Yu, Y.-T. Qian, G.-E. Zhou, X.-M. Liu, J.-X. Wu, *"Synthesis and Characterization of Nanocrystalline Boron Nitride"*, *J. Solid State Chem.* **1999**, *148*, 325.

[18] P. W. Voorhees, *"The theory of Ostwald ripening"*, *J. Stat. Phys.* **1985**, *38*, 231.

[19] ESRF, *"ID06 Large Volume Press"*, http://www.esrf.eu/home/UsersAndScience/Experiments/MEx/id06-large-volume-press.html (last visit: 10/17/2019).

[20] T. Yu, Y. Wang, M. L. Rivers, S. R. Sutton, *"An upgraded and integrated large-volume high-pressure facility at the GeoSoilEnviroCARS bending magnet beamline of the Advanced Photon Source"*, *C. R. Geosci.* **2019**, *351*, 269.

[21] Soleil, *"PSICHÉ (Pression Structure Imagerie par Contraste à Haute Énergie)"*, https://www.synchrotron-soleil.fr/en/beamlines/psiche (last visit: 10/17/2019).

[22] DESY, *"P61B Large Volume Press – Extreme Conditions (LVP-EC)"*, https://petra3-extension.desy.de/e84814/e85529/e260846/ (last visit: 10/05/2019).

[23] S. D. Kloß, W. Schnick, *"Rare-earth-metal nitridophosphates through high-pressure metathesis"*, *Angew. Chem. Int. Ed.* **2015**, *54*, 11250; *Angew. Chem.* **2015**, *127*, 11402.

[24] S. D. Kloß, *"The High-Pressure Metathesis Route for the Preparation of Rare-Earth and Transition Metal Nitridophosphates"*, Dissertation, Ludwig-Maximilians-Universität, Munich, **2018**.

[25] O. Glemser, K. Beltz, P. Naumann, *"Zur Kenntnis des Systems Silicium-Stickstoff"*, *Z. Anorg. Allg. Chem.* **1957**, *291*, 51.

[26] T. Richter, R. Niewa, *"Chemistry of Ammonothermal Synthesis"*, *Inorganics* **2014**, *2*, 29.

[27] J. Häusler, W. Schnick, *"Ammonothermal Synthesis of Nitrides: Recent Developments and Future Perspectives"*, *Chem. – Eur. J.* **2018**, *24*, 11864.

[28] X. Yang, C. Li, B. Yang, W. Wang, Y. Qian, *"Thermal nitridation synthesis of MN (M = Ti, V and Cr) nanocrystals from metals and NH_4Cl"*, *Mater. Res. Bull.* **2004**, *39*, 957.

[29] X. Zhao, K.-J. Range, *"High pressure synthesis of molybdenum nitride MoN"*, *J. Alloys Compd.* **2000**, *296*, 72.

[30] T. Sasaki, T. Ikoma, K. Sago, Z. Liu, K. Niwa, T. Ohsuna, M. Hasegawa, *"High-Pressure Synthesis and Crystal Structure of MoC-Type Tungsten Nitride by Nitridation with Ammonium Chloride"*, *Inorg. Chem.* **2019**, *58*, 16379.

[31] H.-P. Baldus, M. Jansen, *"Novel High-Performance Ceramics—Amorphous Inorganic Networks from Molecular Precursors"*, *Angew. Chem. Int. Ed. Engl.* **1997**, *36*, 328; *Angew. Chem.* **1997**, *109*, 338.

[32] M. Jansen, J. C. Schön, L. van Wüllen, *"The route to the structure determination of amorphous solids: a case study of the ceramic $Si_3B_3N_7$"*, *Angew. Chem. Int. Ed.* **2006**, *45*, 4244; *Angew. Chem.* **2006**, *118*, 4350.

[33] J. Eichler, C. Lesniak, *"Boron nitride (BN) and BN composites for high-temperature applications"*, *J. Eur. Ceram. Soc.* **2008**, *28*, 1105.

[34] J. Kopac, P. Krajnik, *"High-performance grinding—A review"*, *J. Mater. Process. Technol.* **2006**, *175*, 278.

[35] F. L. Riley, *"Silicon Nitride and Related Materials"*, *J. Am. Ceram. Soc.* **2000**, *83*, 245.

[36] V. L. Solozhenko, D. Andrault, G. Fiquet, M. Mezouar, D. C. Rubie, *"Synthesis of superhard cubic BC_2N"*, *Appl. Phys. Lett.* **2001**, *78*, 1385.

[37] Y. Zhang, H. Sun, C. Chen, *"Superhard cubic BC_2N compared to diamond"*, *Phys. Rev. Lett.* **2004**, *93*, 195504.

[38] K. Yuge, A. Seko, Y. Koyama, F. Oba, I. Tanaka, *"First-principles-based phase diagram of the cubic BNC ternary system"*, *Phys. Rev. B: Condens. Matter Mater. Phys.* **2008**, *77*, 334.

[39] F. J. Pucher, F. Hummel, W. Schnick, *"$CuPN_2$: Synthesis, Crystal Structure, and Electronic Properties"*, *Eur. J. Inorg. Chem.* **2015**, *2015*, 1886.

[40] F. K. Keßler, T. J. Koller, W. Schnick, *"Synthesis and Structure of Melamium Bromide $C_6N_{11}H_{10}Br$ and Melamium Iodide $C_6N_{11}H_{10}I$"*, *Z. Anorg. Allg. Chem.* **2018**, *644*, 186.

[41] A. K. Kuriakose, E. Whalley, *"Phase Diagram of Ammonium Fluoride to 20 kbar"*, *J. Chem. Phys.* **1968**, *48*, 2025.

[42] M. Ahmed, G. Xinxin, *"A review of metal oxynitrides for photocatalysis"*, *Inorg. Chem. Front.* **2016**, *3*, 578.

[43] W. Wang, M. O. Tadé, Z. Shao, *"Nitrogen-doped simple and complex oxides for photocatalysis: A review"*, *Prog. Mater. Sci.* **2018**, *92*, 33.

[44] P. Eckerlin, *"Die Kristallstruktur von $BeSiN_2$"*, *Z. Anorg. Allg. Chem.* **1967**, *353*, 225.

[45] V. Schultz-Coulon, W. Schnick, *"Mg_2PN_3 und Ca_2PN_3 – Phosphor(V)-nitride mit eindimensional unendlichen Ketten eckenverknpfter PN_4-Tetraeder"*, *Z. Anorg. Allg. Chem.* **1997**, *623*, 69.

[46] S. J. Sedlmaier, M. Eberspächer, W. Schnick, *"High-Pressure Synthesis, Crystal Structure, and Characterization of Zn_2PN_3 – A New catena-Polynitridophosphate"*, *Z. Anorg. Allg. Chem.* **2011**, *637*, 362.

[47] T. Endo, Y. Sato, H. Takizawa, M. Shimada, *"High-pressure synthesis of new compounds, $ZnSiN_2$ and $ZnGeN_2$ with distorted wurtzite structure"*, *J. Mater. Sci. Lett.* **1992**, *11*, 424.

[48] F. Hintze, N. W. Johnson, M. Seibald, D. Muir, A. Moewes, W. Schnick, *"Magnesium Double Nitride Mg_3GaN_3 as New Host Lattice for Eu^{2+} Doping: Synthesis, Structural Studies, Luminescence, and Band-Gap Determination"*, *Chem. Mater.* **2013**, *25*, 4044.

[49] E. Soignard, P. F. McMillan, K. Leinenweber, *"Solid Solutions and Ternary Compound Formation among Ge_3N_4–Si_3N_4 Nitride Spinels Synthesized at High Pressure and High Temperature"*, *Chem. Mater.* **2004**, *16*, 5344.

[50] V. G. Deibuk, A. V. Voznyi, *"Thermodynamic stability and redistribution of charges in ternary AlGaN, InGaN, and InAlN alloys"*, *Semiconductors* **2005**, *39*, 623.

[51] J. Häusler, R. Niklaus, J. Minár, W. Schnick, *"Ammonothermal Synthesis and Optical Properties of Ternary Nitride Semiconductors Mg-IV-N_2 , Mn-IV-N_2 and Li-IV_2-N_3 (IV = Si, Ge)"*, *Chem. – Eur. J.* **2018**, *24*, 1686.

[52] M. Mallmann, C. Maak, R. Niklaus, W. Schnick, *"Ammonothermal Synthesis, Optical Properties, and DFT Calculations of Mg_2PN_3 and Zn_2PN_3"*, *Chem. – Eur. J.* **2018**, *24*, 13963.

[53] M. Mallmann, R. Niklaus, T. Rackl, M. Benz, T. G. Chau, D. Johrendt, J. Minár, W. Schnick, *"Solid Solutions of Grimm-Sommerfeld Analogous Nitride Semiconductors II-IV-N_2 with II = Mg, Mn, Zn; IV = Si, Ge – Ammonothermal Synthesis and DFT Calculations"*, *Chem. – Eur. J.* **2019**, *25*, 15887.

[54] J. Muth, A. Cai, A. Osinsky, H. Everitt, B. Cook, I. Avrutsky, *"Optical Properties of II-IV-N_2 Semiconductors"*, *MRS Online Proc. Libr.* **2004**, *831*, 4.

[55] A. Punya, T. R. Paudel, W. R. L. Lambrecht, *"Electronic and lattice dynamical properties of II-IV-N_2 semiconductors"*, *Phys. Status Solidi C* **2011**, *8*, 2492.

[56] V. L. Shaposhnikov, A. V. Krivosheeva, F. Arnaud D'Avitaya, J.-L. Lazzari, V. E. Borisenko, *"Structural, electronic and optical properties of II-IV-N_2 compounds (II = Be, Zn; IV = Si, Ge)"*, *Phys. Status Solidi B* **2008**, *245*, 142.

[57] G. Hautier, C. Fischer, V. Ehrlacher, A. Jain, G. Ceder, *"Data mined ionic substitutions for the discovery of new compounds"*, *Inorg. Chem* **2011**, *50*, 656.

[58] W. Sun, C. J. Bartel, E. Arca, S. R. Bauers, B. Matthews, B. Orvañanos, B.-R. Chen, M. F. Toney, L. T. Schelhas, W. Tumas, J. Tate, A. Zakutayev, S. Lany, A. M. Holder, G. Ceder, *"A map of the inorganic ternary metal nitrides"*, *Nat. Mater.* **2019**, *18*, 732.

[59] K. J. Kingma, R. E. G. Pacalo, P. F. McMillan, *"High-Pressure Stability of the Cristobalite Framework in PON and PN(NH)"*, *Eur. J. Solid State Inorg. Chem.* **1997**, *34*, 679.

[60] D. Andrault, R. J. Angel, J. L. Mosenfelder, T. Le Bihan, *"Equation of state of stishovite to lower mantle pressures"*, *Am. Mineral.* **2003**, *88*, 301.

[61] Y. Tsuchida, T. Yagi, *"A new, post-stishovite highpressure polymorph of silica"*, *Nature* **1989**, *340*, 217.

[62] V. Prakapenka, G. Shen, L. Dubrovinsky, M. Rivers, S. Sutton, *"High pressure induced phase transformation of SiO_2 and GeO_2: Difference and similarity"*, *J. Phys. Chem. Solids* **2004**, *65*, 1537.

[63] L. S. Dubrovinsky, N. A. Dubrovinskaia, S. Saxena, F. Tutti, S. Rekhi, T. Le Bihan, G. Shen, J. Hu, *"Pressure-induced transformations of cristobalite"*, *Chem. Phys. Lett.* **2001**, *333*, 264.

[64] M. Murakami, K. Hirose, S. Ono, Y. Ohishi, *"Stability of $CaCl_2$ -type and α-PbO_2-type SiO_2 at high pressure and temperature determined by in-situ X-ray measurements"*, *Geophys. Res. Lett.* **2003**, *30*, 11.

[65] P. Dera, C. T. Prewitt, N. Z. Boctor, R. J. Hemley, *"Characterization of a high-pressure phase of silica from the Martian meteorite Shergotty"*, *Am. Mineral.* **2002**, *87*, 1018.

[66] Y. Kuwayama, K. Hirose, N. Sata, Y. Ohishi, *"The pyrite-type high-pressure form of silica"*, *Science* **2005**, *309*, 923.

[67] T. Sekine, M. Akaishi, N. Setaka, *"Fe_2N-type SiO_2 from shocked quartz"*, *Geochim. Cosmochim. Acta* **1987**, *51*, 379.

[68] F. Datchi, A. Dewaele, Y. Le Godec, P. Loubeyre, *"Equation of state of cubic boron nitride at high pressures and temperatures"*, *Phys. Rev. B: Condens. Matter Mater. Phys.* **2007**, *75*, 127.

[69] M. T. Yeung, R. Mohammadi, R. B. Kaner, *"Ultraincompressible, Superhard Materials"*, *Annu. Rev. Mater. Res.* **2016**, *46*, 465.

[70] K. J. Kingma, R. E. Gerald Pacalo, P. F. McMillan in *Properties of the earth and planetary materials at high pressure and temperature*, Geophysical monograph, American Geophysical Union, Washington, **1998**.

[71] P. Kroll, W. Schnick, *"A Density Functional Study of Phosphorus Nitride P_3N_5: Refined Geometries, Properties, and Relative Stability of α-P_3N_5 and γ-P_3N_5 and a Further Possible High-Pressure Phase δ-P_3N_5 with Kyanite-Type Structure"*, *Chem. – Eur. J.* **2002**, *8*, 3530.

[72] A. Morales-García, E. del Corro, *"Revealing the local properties of β-HP_4N_7, a promising candidate for high pressure synthesis of new materials"*, *Mater. Res. Express* **2015**, *2*, 45904.

[73] S. Zhang, H. Li, H. Li, S. Zhou, X. Cao, *"Calculation of the bulk modulus of simple and complex crystals with the chemical bond method"*, *J. Phys. Chem. B* **2007**, *111*, 1304.

[74] X. Liu, H. Wang, W. Wang, Z. Fu, *"A simple bulk modulus model for crystal materials based on the bond valence model"*, *Phys. Chem. Chem. Phys.* **2017**, *19*, 22177.

[75] M. v. Stackelberg, R. Paulus, *"Untersuchungen über die Kristallstruktur der Nitride und Phosphide zweiwertiger Metalle"*, *Z. Phys. Chem.* **1933**, *22B*, 305.

[76] D. Hall, G. E. Gurr, G. A. Jeffrey, *"Zur Kenntnis des Systems Be_3N–Si_3N_4. V. A Refinement of the Crystal Structure of* β*-Beryllium Nitride"*, *Z. Anorg. Allg. Chem.* **1969**, *369*, 108.

[77] R. H. Wentorf, *"Cubic Form of Boron Nitride"*, *J. Chem. Phys.* **1957**, *26*, 956.

[78] D. Hardie, K. H. Jack, *"Crystal Structures of Silicon Nitride"*, *Nature* **1957**, *180*, 332.

[79] R. S. Pease, *"Crystal Structure of Boron Nitride"*, *Nature* **1950**, *165*, 722.

[80] K. Landskron, H. Huppertz, J. Senker, W. Schnick, *"High-Pressure Synthesis of* γ*-P_3N_5 at 11 GPa and 1500 °C in a Multianvil Assembly: A Binary Phosphorus(V) Nitride with a Three-Dimensional Network Structure from PN_4 Tetrahedra and Tetragonal PN_5 Pyramids"*, *Angew. Chem. Int. Ed.* **2001**, *40*, 2643, *Angew. Chem.* **2001**, *113*, 2713.

[81] D. Baumann, W. Schnick, *"Pentacoordinate phosphorus in a high-pressure polymorph of phosphorus nitride imide P_4N_6(NH)"*, *Angew. Chem. Int. Ed.* **2014**, *53*, 14490; *Angew. Chem.* **2014**, *126*, 14718.

[82] A. Zerr, R. Riedel, G. Miehe, G. Serghiou, M. Schwarz, E. Kroke, H. Fueß, P. Kroll, R. Boehler, *"Synthesis of cubic silicon nitride"*, *Nature* **1999**, *400*, 340.

[83] M. Schwarz, G. Miehe, A. Zerr, E. Kroke, B. T. Poe, H. Fueß, R. Riedel, *"Spinel-Si_3N_4: Multi-Anvil Press Synthesis and Structural Refinement"*, *Adv. Mater.* **2000**, *12*, 883.

[84] N. Nishiyama, J. Langer, T. Sakai, Y. Kojima, A. Holzheid, N. A. Gaida, E. Kulik, N. Hirao, S. I. Kawaguchi, T. Irifune, Y. Ohishi, *"Phase relations in silicon and germanium nitrides up to 98 GPa and 2400 °C"*, *J. Am. Ceram. Soc.* **2019**, *102*, 2195.

[85] S. R. Römer, P. Kroll, W. Schnick, *"A density functional study of the high-pressure chemistry of $MSiN_2$ (M = Be, Mg, Ca): prediction of high-pressure phases and examination of pressure-induced decomposition"*, *J. Phys.: Condens. Matter* **2009**, *21*, 275407.

[86] Y. Xia, Q. Li, Y. Ma, *"Novel superhard polymorphs of Be_3N_2 predicted by first-principles"*, *Comput. Mater. Sci.* **2010**, *49*, S76.

[87] U. Paliwal, K. B. Joshi, *"A theoretical study of pressure-induced phase transitions and electronic band structure of anti-A-sesquioxide type γ-Be_3N_2"*, *J. Phys. D: Appl. Phys.* **2011**, *44*, 255501.

[88] R. M. Wentzcovitch, M. L. Cohen, P. K. Lam, *"Theoretical study of BN, BP, and BAs at high pressures"*, *Phys. Rev. B* **1987**, *36*, 6058.

[89] N. E. Christensen, I. Gorczyca, *"Optical and structural properties of III-V nitrides under pressure"*, *Phys. Rev. B: Condens. Matter Mater. Phys.* **1994**, *50*, 4397.

[90] L. Hromadová, R. Martoňák, *"Pressure-induced structural transitions in BN from ab initio metadynamics"*, *Phys. Rev. B: Condens. Matter Mater. Phys.* **2011**, *84*, 241252.

[91] W. Y. Ching, S. Aryal, P. Rulis, W. Schnick, *"Electronic structure and physical properties of the spinel-type phase of BeP_2N_4 from all-electron density functional calculations"*, *Phys. Rev. B* **2011**, *83*, 155109.

[92] Y.-C. Ding, B. Xiao, *"Electronic Structure, Mechanical Properties and Intrinsic Hardness of a New Superhard Material BeP_2N_4"*, *Acta Phys.-Chim. Sin.* **2011**, *27*, 1621.

[93] M. Zhang, H. Yan, Y. Zhao, Q. Wei, *"Mechanical properties and atomistic deformation mechanism of spinel-type BeP_2N_4"*, *Comput. Mater. Sci.* **2014**, *83*, 457.

[94] J. Z. Jiang, F. Kragh, D. J. Frost, K. Ståhl, H. Lindelov, *"Hardness and thermal stability of cubic silicon nitride"*, *J. Phys.: Condens. Matter* **2001**, *13*, L515.

[95] I. Tanakaa, F. Oba, T. Sekine, E. Ito, A. Kubo, K. Tatsumi, H. Adachi, T. Yamamoto, *"Hardness of cubic silicon nitride"*, *J. Mater. Res.* **2002**, *17*, 731.

[96] A. Zerr, M. Kempf, M. Schwarz, E. Kroke, M. Göken, R. Riedel, *"Elastic Moduli and Hardness of Cubic Silicon Nitride"*, *J. Am. Ceram. Soc.* **2002**, *85*, 86.

[97] N. Nishiyama, R. Ishikawa, H. Ohfuji, H. Marquardt, A. Kurnosov, T. Taniguchi, B.-N. Kim, H. Yoshida, A. Masuno, J. Bednarcik, E. Kulik, Y. Ikuhara, F. Wakai, T. Irifune, *"Transparent polycrystalline cubic silicon nitride"*, *Sci. Rep.* **2017**, *7*, 44755.

[98] J. B. Mann, T. L. Meek, L. C. Allen, *"Configuration Energies of the Main Group Elements"*, *J. Am. Chem. Soc.* **2000**, *122*, 2780.

[99] Y. Shen, A. R. Oganov, G. Qian, J. Zhang, H. Dong, Q. Zhu, Z. Zhou, *"Novel lithium-nitrogen compounds at ambient and high pressures"*, *Sci. Rep.* **2015**, *5*, 14204.

[100] S. Yu, B. Huang, Q. Zeng, A. R. Oganov, L. Zhang, G. Frapper, *"Emergence of Novel Polynitrogen Molecule-like Species, Covalent Chains, and Layers in Magnesium–Nitrogen Mg_xN_y Phases under High Pressure"*, *J. Phys. Chem. C* **2017**, *121*, 11037.

[101] K. S. Paithankar, H. O. Sørensen, J. P. Wright, S. Schmidt, H. F. Poulsen, E. F. Garman, *"Simultaneous X-ray diffraction from multiple single crystals of macromolecules"*, *Acta Crystallogr. Sect. D: Biol. Crystallogr.* **2011**, *67*, 608.

[102] U. Zander, G. Bourenkov, A. N. Popov, D. de Sanctis, O. Svensson, A. A. McCarthy, E. Round, V. Gordeliy, C. Mueller-Dieckmann, G. A. Leonard, *"MeshAndCollect: an automated multicrystal data-collection workflow for synchrotron macromolecular crystallography beamlines"*, *Acta Crystallogr. Sect. D: Biol. Crystallogr.* **2015**, *71*, 2328.

[103] D. Tchoń, A. Makal, *"Structure and piezochromism of pyrene-1-carbaldehyde at high pressure"*, *Acta Crystallogr. Sect. B: Struct. Sci. Cryst. Eng. Mater.* **2019**, *75*, 343.

[104] V. Dyadkin, P. Pattison, V. Dmitriev, D. Chernyshov, *"A new multipurpose diffractometer PILATUS@SNBL"*, *J. Synchrotron Radiat.* **2016**, *23*, 825.

[105] DESY, *"P24 Chemical Crystallography"*, http://photon-science.desy.de/facilities/petra_iii/beamlines/p24_chemical_crystallography/index_eng.html (last visit: 10/05/2019).

[106] J. Dong, A. A. Kinkhabwala, P. F. McMillan, *"High-pressure polymorphism in phosphorus nitrides"*, *Phys. Status Solidi B* **2004**, *241*, 2319.

[107] J. Lv, X. Yang, D. Xu, Y.-X. Huang, H.-B. Wang, H. Wang, *"High-pressure polymorphs of $LiPN_2$: A first-principles study"*, *Front. Phys.* **2018**, *13*, 9592.

[108] Z. Raza, I. Errea, A. R. Oganov, A. M. Saitta, *"Novel superconducting skutterudite-type phosphorus nitride at high pressure from first-principles calculations"*, *Sci. Rep.* **2014**, *4*, 5889.

[109] D. Laniel, M. Bykov, T. Fedotenko, A. V. Ponomareva, I. A. Abrikosov, K. Glazyrin, V. Svitlyk, L. Dubrovinsky, N. Dubrovinskaia, *"High Pressure Investigation of the S–N_2 System up to the Megabar Range: Synthesis and Characterization of the SN_2 Solid"*, *Inorg. Chem.* **2019**, *58*, 9195.

[110] K. Niwa, H. Ogasawara, M. Hasegawa, *"Pyrite form of group-14 element pernitrides synthesized at high pressure and high temperature"*, *Dalton Trans.* **2017**, *46*, 9750.

A. Supporting Information for Chapter 3

United in Nitride: The Highly Condensed Boron Phosphorus Nitride BP_3N_6

Sebastian Vogel, Amalina T. Buda, and Wolfgang Schnick

Angew. Chem. Int. Ed. **2018**, *57*, 13202;

Angew. Chem. **2018**, *130*, 13386.

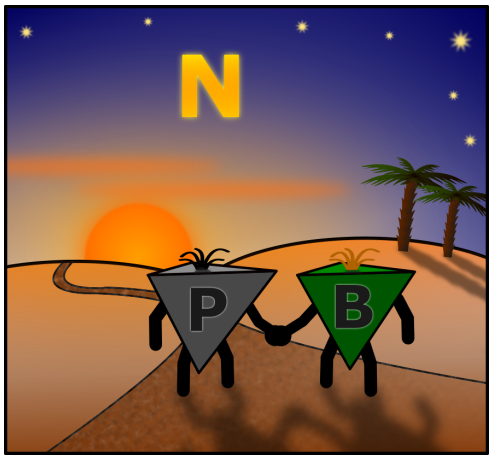

Abstract Owing to intriguing materials properties non-metal nitrides are of special interest for both, solid-state chemistry and materials science. Mixed ternary non-metal nitrides, however, have only been sparsely investigated, as preparative chemistry lacks a systematic access, yet. Herein, we report on the highly condensed boron phosphorus nitride BP_3N_6, which was synthesized from $(PNCl_2)_3$, NH_4N_3 and h-BN in a high-pressure high-temperature reaction. By increasing partial pressure of HCl during synthesis using NH_4Cl, single-crystals of BP_3N_6 up to 80 µm in length were obtained. The unprecedented framework-type structure determined by single-crystal XRD blends structural motifs of both, α-P_3N_5 and c-BN, rendering BP_3N_6 a double nitride. The compound was further investigated by Rietveld refinement, EDX, temperature-dependent PXRD, FTIR and solid-state NMR spectroscopy. The formation of BP_3N_6 through use of reactive precursors exemplifies an innovative access to mixed non-metal nitrides.

A.1. Experimental Procedures

Preparation of starting materials

NH_4N_3 was prepared according to Frierson by sublimation.[1] Stoichiometric amounts of dry NH_4NO_3 (Grüssing, 99 %) and NaN_3 (Acros Organics, 99 %) were ground and filled into a Schlenk tube. The lower end of the Schlenk tube was placed in a furnace and its valve was opened before heating the reaction mixture for 12 h at 200 °C. Colorless crystals of NH_4N_3 were obtained in the top of the Schlenk tube. Phase purity was confirmed by PXRD and FTIR measurements.

Commercial $(PNCl_2)_3$ (abcr GmbH, 98.5 %) was purified by sublimation in static vacuum at 120 °C in a dry Schlenk tube using a water-cooled cooling finger.

h-BN (abcr GmbH, 99 %) was used without any further purification.

High-pressure high-temperature synthesis

BP_3N_6 was synthesized in a high-pressure high-temperature procedure in a hydraulic 1000 t press by the multianvil technique utilizing a modified Walker module.[2,3] Under argon atmosphere (glovebox, MBraun, < 1 ppm O_2, H_2O) stoichiometric amounts of $(PNCl_2)_3$, NH_4N_3 and h-BN (abcr GmbH, 99 %) were ground in an agate mortar and packed tightly in a crucible of h-BN (Henze, Kempten). Sealed with a cap of h-BN the crucible was placed in the center of two graphite furnaces and underpinned with two MgO spacers. The furnaces were thermally isolated to the outside by a ZrO_2 sleeve and contacted by two Mo plates. The as-prepared assembly was placed in the center of a pierced octahedron (5 % Cr_2O_3 doped MgO, 18 mm edge length, Ceramic Substrates & Components Ltd, Isle of Wight). The octahedron was surrounded by eight Co-doped WC cubes with truncated edges (7 % Co, 11 mm edge length, Hawedia, Marklkofen), which were separated by pyrophyllite gaskets. More detailed information on the octahedron-within-cubes payload can be found in literature.[2] The assembly was compressed to 8 GPa within 220 min before the sample was isobarically heated to 1100 °C within 60 min. The temperature was maintained for 300 min before the sample was allowed to cool down to ambient temperature within 60 min. The assembly was decompressed within 570 min and the sample was recovered from the crucible. Residual chlorides were removed by washing with de-ionized water, yielding a colorless air- and

moisture-stable crystalline solid. In order to grow single-crystals up to 80 µm in length 25–30 wt-% of NH_4Cl were added to the mixture of starting materials.

Single-crystal X-ray diffraction (XRD)

Single-crystal X-ray diffraction data of BP_3N_6 were collected on a Bruker D8 Venture TXS diffractometer (rotating anode, Mo-Kα_1 radiation, $\lambda = 0.71073$ Å, multilayer monochromator) by combined φ- and ω-scans. Indexing, integration, semi-empiric absorption correction (multi-scan) as well as determination of the space group was performed by the APEX3 software package.[4–6] Employing SHELX-97 and the WinGX software package, the structure was solved by Direct Methods and refined against F^2 by the full-matrix least-square method.[7–9] For structure visualization the VESTA software was used.[10]

Powder X-ray diffraction (PXRD)

Powder X-ray diffraction data were collected on a STOE Stadi P diffractometer (STOE & Cie GmbH, Darmstadt, Cu-Kα_1 radiation, $\lambda = 1.5406$ Å, Ge(111) monochromator) equipped with a MYTHEN 1K Si strip detector in modified Debye-Scherrer geometry. For measurements the sample was ground and sealed in glass capillaries with an outer diameter of 0.3 mm (Hilgenberg, Malsfeld). Rietveld refinement was performed utilizing the TOPAS Academic software.[11,12] The background was described by a shifted Chebyshev polynomial and the peak profiles were modeled according to the fundamental parameters approach.[13,14] Any possible preferred orientation of crystals was accounted for with a spherical harmonics function of fourth order. Temperature-dependent PXRD measurements were performed on a STOE Stadi P diffractometer (STOE & Cie GmbH, Darmstadt, Mo-Kα_1 radiation, $\lambda = 0.71073$ Å, Ge(111) monochromator) equipped with a STOE resistance graphite furnace and an IP-PSD detector. The sample was loaded in a fused silica capillary (Hilgenberg, Malsfeld) with an outer diameter of 0.5 mm and heated from 25 to 1000 °C in steps of 25 °C with a rate of 10 °C·min^{-1} under Ar atmosphere. At each temperature step data collection was performed within 20 min, while the temperature was held constant.

Solid-state MAS NMR spectroscopy

Solid-state NMR measurements were performed on an Avance III 500 spectrometer (Bruker, Karlsruhe) equipped with a 11.7 T magnet operating at 500.25 MHz ^{1}H frequency and a commercial double-

resonance MAS probe. For measurements the sample was ground and loaded in a ZrO_2 rotor with an outer diameter of 2.5 mm. NMR spectra were collected at 20 kHz spinning frequency.

Scanning electron microscopy (SEM) and energy-dispersive X-ray (EDX) spectroscopy

For SEM imaging and EDX measurements a Dualbeam Helios Nanolab G3 UC (FEI, Hillsboro) equipped with a X-Max 80 SDD detector (Oxford Instruments, Abingdon) was used and data processing was performed with the Aztec software.[15] Before measuring, the sample was coated with carbon using an electron beam evaporator (BAL-TEC MED 020, Bal Tec AG) to ensure electrical conductivity. Accelerating voltage for both, SEM imaging and EDX spectroscopy was 5.0 kV.

Fourier transform infrared spectroscopy (FTIR)

The FTIR spectrum was collected on a Spectrum BX II spectrometer with DuraSampler ATR-device (Perkin Elmer) at ambient conditions.

A.2. Results and Discussion

SEM imaging

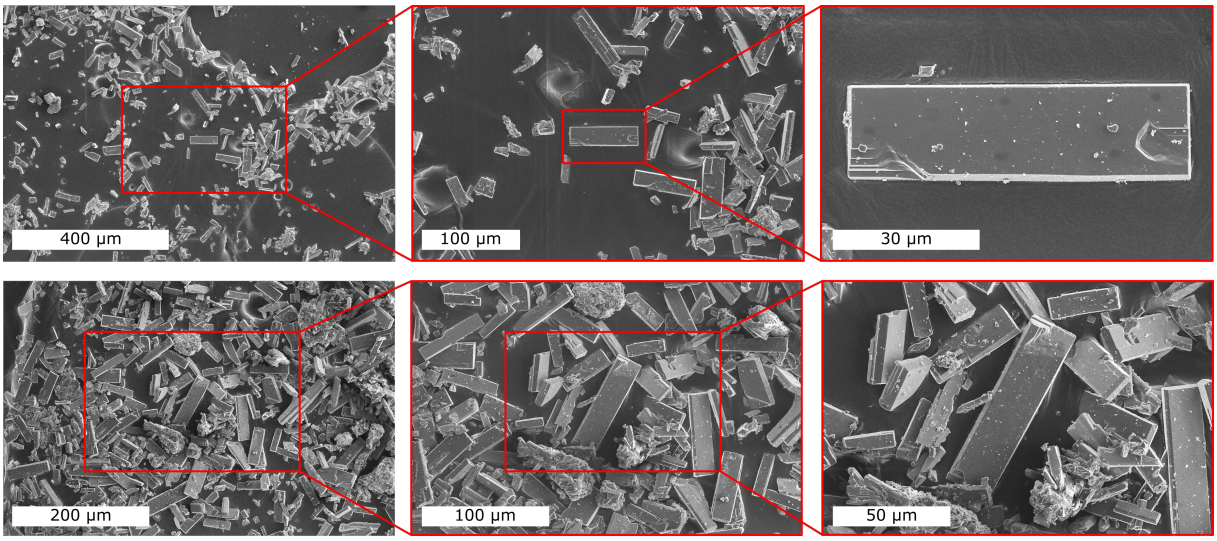

Figure A.1.: Selected SEM images of single-crystals of BP_3N_6, yielded by NH_4Cl-assisted high-pressure high-temperature synthesis.

Structure determination

Table A.1.: Crystallographic data of the single-crystal structure refinement of BP_3N_6. Standard deviations are given in brackets.

Formula	**BP_3N_6**
Crystal system	monoclinic
Space group	$P2_1/c$ (no. 14)
Molecular weight / g·mol^{-1}	187.78
Lattice parameters / Å	$a = 5.0272(11)$
	$b = 4.5306(12)$
	$c = 17.332(3)$
Angle / °	$\beta = 106.387(9)$
Cell volume / Å^3	378.72(15)
Formula units per cell	4
Calculated X-ray density / g·cm^{-3}	3.293
Linear absorption coefficient / cm^{-1}	1.43
$T_{\mathrm{min}}/T_{\mathrm{max}}$	0.879
Radiation	Mo-Kα ($\lambda = 0.71073$ Å)
Diffractometer	Bruker D8 Venture
θ-range / °	$4.22 < \theta < 35.00$
Temperature / K	293(2)
$F(000)$	368
Observed reflections	7378
Independent reflections ($> 2\sigma$)	1662 (1377)
Number of parameters	91
R_{int}; R_σ	0.0482; 0.0454
Final R indices [$I > 2\sigma(I)$]	$R1 = 0.0369$; $wR2 = 0.0966$
Final R indices (all data)	$R1 = 0.0483$; $wR2 = 0.1001$
Goodness of fit	1.111
Residual electron density / e·Å^{-3}	0.737; -0.578

Table A.2.: Refined atom coordinates and equivalent atomic displacement parameters from single-crystal structure refinement. All atoms occupy the general position with Wyckoff no. 4*e*. Standard deviations are given in brackets.

Atom	*x*	*y*	*z*	U_{eq} / Å^2
P1	0.45670(11)	0.09524(12)	0.29430(3)	0.0051(1)
P2	0.03961(11)	0.09021(12)	0.38197(3)	0.0059(1)
P3	0.71517(11)	0.11385(12)	0.03603(3)	0.0056(1)
B1	0.2850(5)	0.0921(5)	0.12344(14)	0.0057(5)
N1	0.2747(4)	0.4340(4)	0.14165(11)	0.0050(4)
N2	0.0098(4)	0.4444(4)	0.40530(11)	0.0052(4)
N3	0.5540(4)	0.4465(4)	0.29442(11)	0.0052(4)
N4	0.4252(3)	0.0145(4)	0.05722(11)	0.0049(4)
N5	0.7866(4)	0.4458(4)	0.03735(11)	0.0062(4)
N6	0.1692(4)	0.0482(4)	0.30938(12)	0.0074(4)

Table A.3.: Refined anisotropic atomic displacement parameters (Å^2) from single-crystal structure refinement. Standard deviations are given in brackets.

Atom	U_{11}	U_{22}	U_{33}	U_{23}	U_{13}	U_{12}
P1	0.0047(2)	0.0050(2)	0.0057(2)	0.0001(2)	0.0015(2)	−0.0002(2)
P2	0.0049(2)	0.0055(2)	0.0072(2)	0.0000(2)	0.0016(2)	0.0001(2)
P3	0.0044(2)	0.0064(2)	0.0061(2)	−0.0002(2)	0.0016(2)	0.0002(2)
B1	0.0058(9)	0.0054(8)	0.0065(9)	−0.0001(7)	0.0025(7)	0.0005(7)
N1	0.0044(7)	0.0030(6)	0.0073(7)	−0.0005(6)	0.0012(5)	0.0006(5)
N2	0.0031(6)	0.0042(7)	0.0075(7)	−0.0007(6)	0.0001(5)	0.0003(5)
N3	0.0062(7)	0.0051(7)	0.0043(7)	−0.0001(5)	0.0013(6)	−0.0010(5)
N4	0.0033(7)	0.0071(7)	0.0047(7)	−0.0012(6)	0.0018(5)	−0.0017(5)
N5	0.0062(7)	0.0046(7)	0.0071(8)	0.0000(6)	0.0008(6)	−0.0015(5)
N6	0.0047(7)	0.0096(7)	0.0090(8)	−0.0008(6)	0.0037(6)	−0.0016(6)

Table A.4.: Interatomic distances (Å) of BP_3N_6. Standard deviations are given in brackets.

P1–N6	1.5543(23)	P3–N5	1.5449(19)	P1–P1	2.8384(9)
P1–N1	1.6564(18)	P3–N2	1.6558(18)	P1–P2	2.8956(9)
P1–N3	1.6647(20)	P3–N4	1.6627(19)	P2–P3	2.6849(9)
P1–N3	1.6658(20)	P3–N4	1.6747(18)	P2–P3	2.8599(9)
P2–N5	1.5676(18)	B1–N4	1.5473(34)	P2–P1	2.8956(9)
P2–N6	1.5830(24)	B1–N3	1.5706(28)	P3–P3	2.4041(8)
P2–N2	1.6719(20)	B1–N2	1.5735(30)	P3–P2	2.6849(9)
P2–N1	1.6734(20)	B1–N1	1.5846(29)		

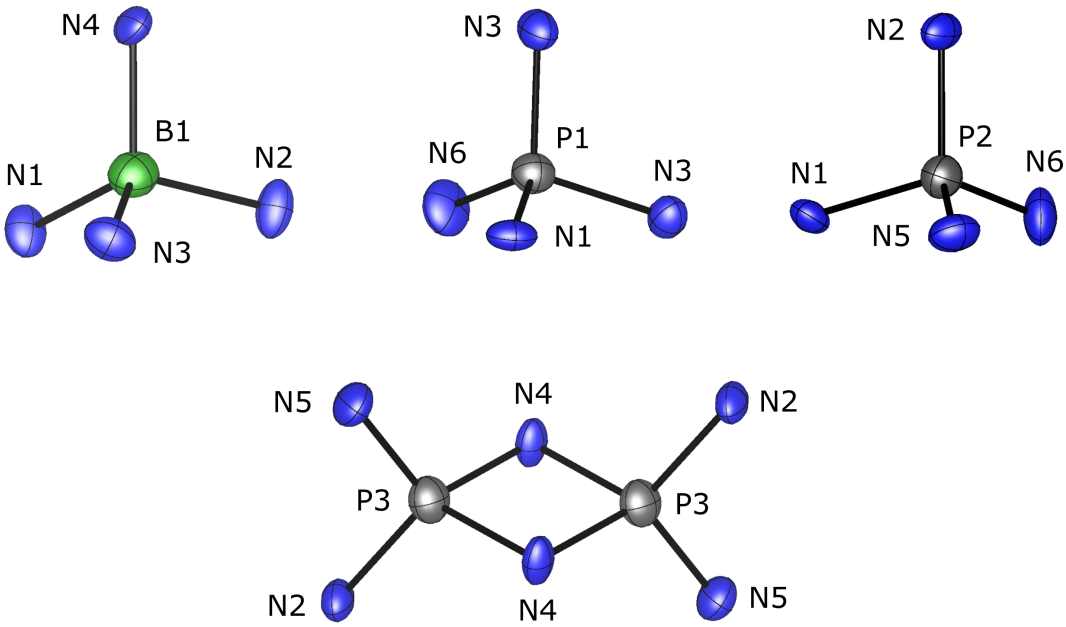

Figure A.2.: Coordination polyhedra of the BP_3N_6 structure from XRD analysis. Ellipsoids are displayed at 99 % probability level.

EDX measurements

EDX measurements (5.0 kV) of selected single-crystals detected no other elements than B, P, N and O. The normalized atomic ratio B : P : N = 1.1 : 3.0 : 5.5 is in good agreement with the nominal ratio in BP_3N_6 within the standard deviations and the precision of the method for light elements. Minor amounts of O may be attributable to surface hydrolysis of the sample, caused by water treatment.

Table A.5.: Listed EDX measurements (5.0 kV) of BP_3N_6 (atom-%). Standard deviations are given in brackets.

	1	2	3	4	5	Average	Normalized
B	11	11	12	11	11	11(1)	1.1(1)
P	31	30	30	31	32	31(1)	3.0(1)
N	57	57	56	56	57	57(1)	5.5(1)
O	1	2	2	2	1	2(1)	0.1(1)

Rietveld refinement

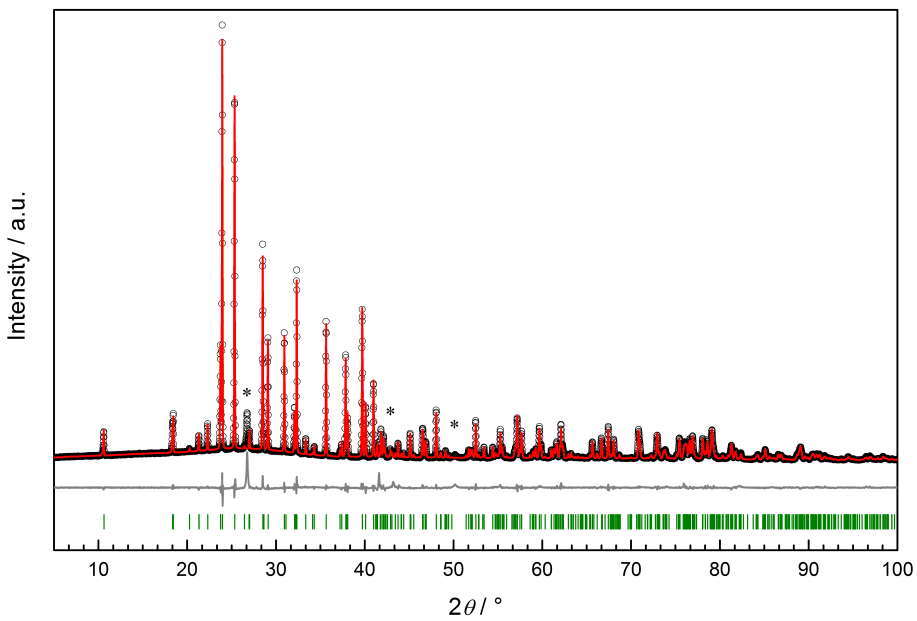

Figure A.3.: Observed (black circles) and calculated (red line) PXRD pattern (Cu-Kα_1 radiation, $\lambda = 1.5406$ Å) and difference profile (gray) from Rietveld refinement of BP_3N_6. Bragg reflections are marked by vertical green lines. Tagged reflections (*) can be assigned to h-BN as a minor side phase.[16]

Table A.6.: Crystallographic data of the Rietveld refinement of BP_3N_6.

Formula	**BP_3N_6**
Crystal system	monoclinic
Space group	$P2_1/c$ (no. 14)
Molecular weight / g·mol^{-1}	187.78
Lattice parameters / Å	$a = 5.03238(6)$
	$b = 4.53466(6)$
	$c = 17.3535(2)$
Angle / °	$\beta = 106.3652(6)$
Cell volume / Å^3	379.965(9)
Formula units per cell	4
Calculated X-ray density / g·cm^{-3}	3.28247(7)
Linear absorption coefficient / cm^{-1}	134.4
Radiation	Cu-Kα_1 ($\lambda = 1.540596$ Å)
Monochromator	Ge(111)
Diffractometer	STOE Stadi P
Detector	MYTHEN 1K
2θ-range	$5° < 2\theta < 100°$
Temperature / K	293
Data points	6334
Number of observed reflections	388
Number of parameters (thereof background)	76 (23)
Profile function	fundamental parameter approach[14]
Background function	Shifted Chebyshev
R indices	$R_{\mathrm{Bragg}} = 0.0198$
	$R_{\mathrm{p}} = 0.04162$
	$R_{\mathrm{wp}} = 0.07738$
	$R_{\mathrm{exp}} = 0.02100$
Goodness of fit	3.685

Temperature-dependent PXRD measurements

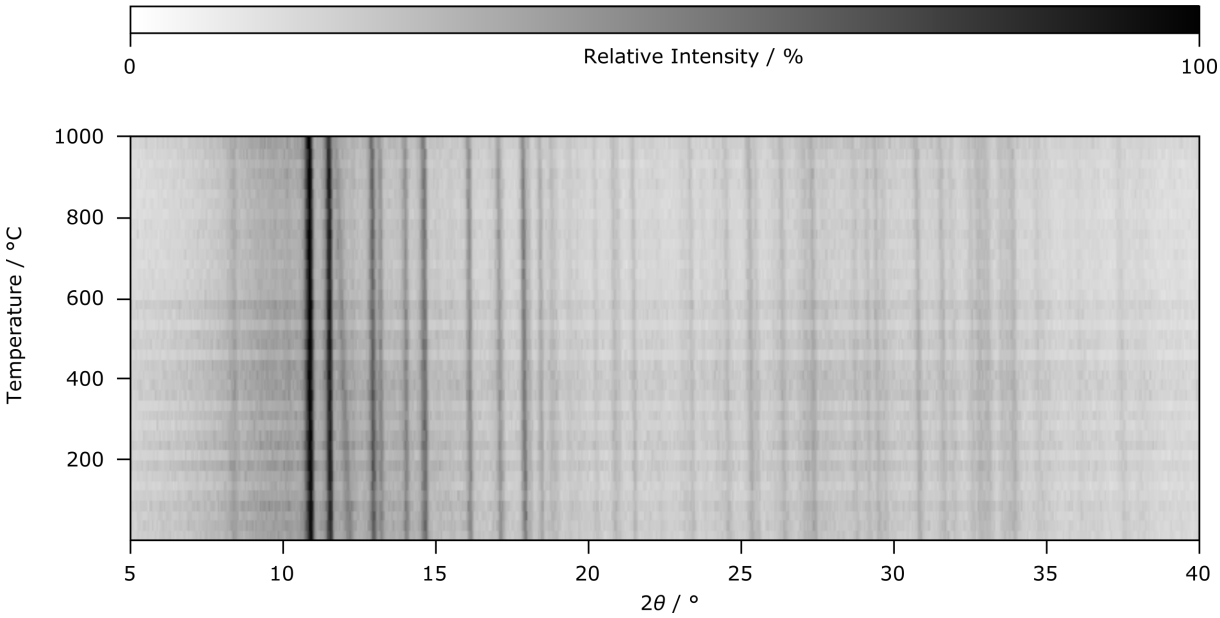

Figure A.4.: Temperature-dependent powder X-ray diffraction patterns (Mo-Kα_1 radiation, $\lambda = 0.71073$ Å) measured under Ar atmosphere showing a slight expansion of lattice parameters with increasing temperature, but neither decomposition nor any phase transition of BP_3N_6 up to 1000 °C.

MAPLE, CHARDI and MBE analysis

Table A.7.: MAPLE analysis shows a 1.3 % difference in the Madelung part of lattice energy of BP_3N_6 and the sum of the respective binary nitrides P_3N_5 and BN.[17]

	P_3N_5 + BN $\longrightarrow$	BP_3N_6	
α-P_3N_5:	78 531 kJ·mol^{-1}	BP_3N_6:	90 556 kJ·mol^{-1}
c-BN:	13 201 kJ·mol^{-1}		
	91 732 kJ·mol^{-1}		1.3 % difference

Table A.8.: CHARDI analysis revealed effective coordination numbers of 3.80–3.99 for B and P and mean total charges of 3.07, 4.98 and −2.98 for B, P and N, respectively.[18]

Polyhedron	**P1N1N3N3N6**	**P2N5N2N6N1**	**P3N4N4N2N5**	**B1N2N1N3N4**
Average bond length / Å	1.6348	1.6242	1.6353	1.5685
Polyhedral volume / $Å^3$	2.2223	2.1882	2.1313	1.9678
Distortion index	0.0249	0.0295	0.0275	0.0063
Quadratic elongation	1.0069	1.0042	1.0361	1.0044
Bond angle variance / $°^2$	28.3741	12.8966	131.3675	17.0184
Eff. coordination number	3.8410	3.8563	3.7966	3.9906
Total charge:				
P/B	5.0430	4.9420	4.9420	3.0720
N	−2.8730	−3.2100	−2.9780	−2.9060
N	−2.9550	−2.9060	−2.9780	−2.8730
N	−2.9550	−3.0780	−2.9060	−2.9550
N	−3.0780	−2.8730	−3.2100	−2.9780

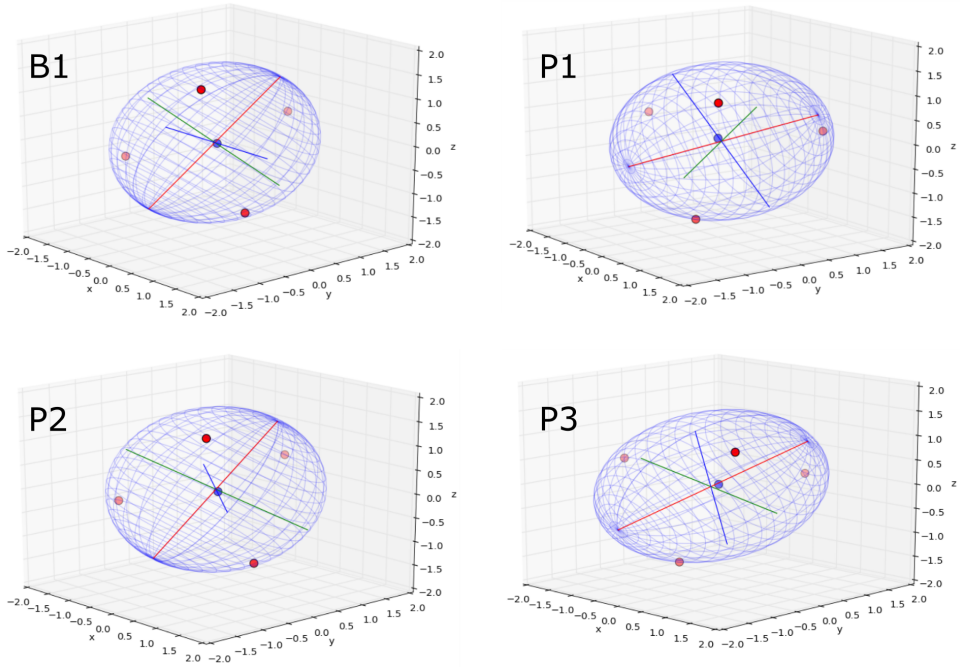

Figure A.5.: Minimum bonding ellipsoids (MBE) of BN_4 and PN_4 tetrahedra fitted by PIEFACE software.[19] B/P: blue, N: red.

Table A.9.: Ellipsoidal parameters of MBEs of BN_4 and PN_4 tetrahedra in the BP_3N_6 structure.[19] B1, P1 and P2 polyhedra show only slight distortion as indicated by small $\sigma(R)$. A significant distortion of the P3 polyhedra, in contrast, may be attributable to electrostatic repulsion of the edge-sharing $P3N_4$ tetrahedra.

	***R*1**	***R*2**	***R*3**	$\langle R \rangle$	**σ(R)**	***S***	**Center Disp.**	**CN**
B1	1.661466	1.530681	1.508961	1.567036	0.0674	0.0645	0.0414	4
P1	1.705157	1.629561	1.559843	1.631520	0.0593	0.0016	0.1046	4
P2	1.688115	1.627140	1.551409	1.622221	0.0559	−0.0104	0.0701	4
P3	0.187131	1.593247	1.390783	1.618446	0.1970	0.0215	0.1273	4

FTIR and solid-state NMR measurements

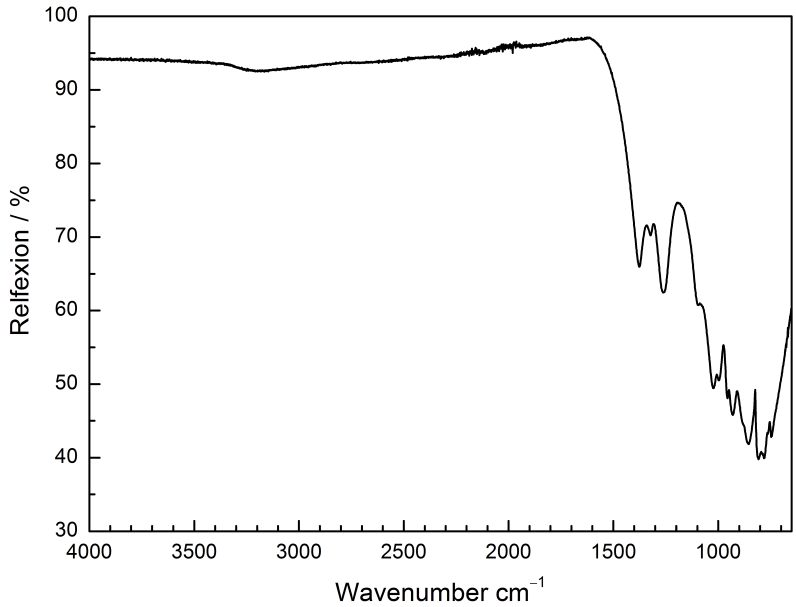

Figure A.6.: FTIR (ATR) spectrum of a representative BP_3N_6 sample showing broad absorption bands below 1700 cm^{-1}, which can be assigned to vibrational $(B/P)N_4$ modes of the B/P/N framework and have been observerd for related P/N and B/N compounds, as well.[20–23] Weak absorption in the region of 2900–3400 cm^{-1} may be attributable to NH_x functionality in minor amounts of amorphous side phases.

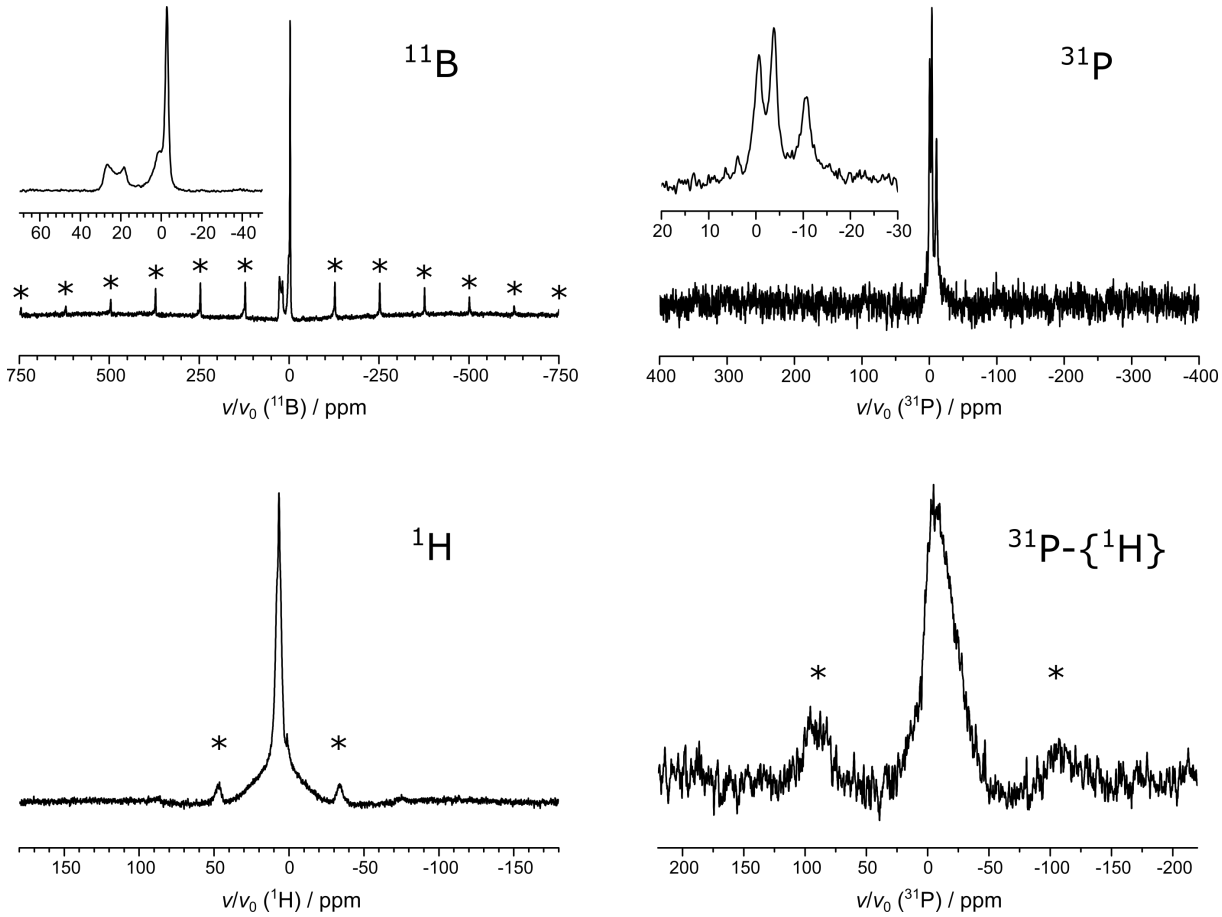

Figure A.7.: ^{11}B, ^{31}P, ^{1}H and $^{31}P\{^{1}H\}$ NMR spectra of a representative BP_3N_6 sample. The broad ^{1}H signal (FWHM= 5 ppm) as well as the broad ^{31}P signal in the $^{31}P\{^{1}H\}$ NMR spectrum can be assinged to minor amounts of amorphous side phases. Spinning sidebands are marked with asterisks.

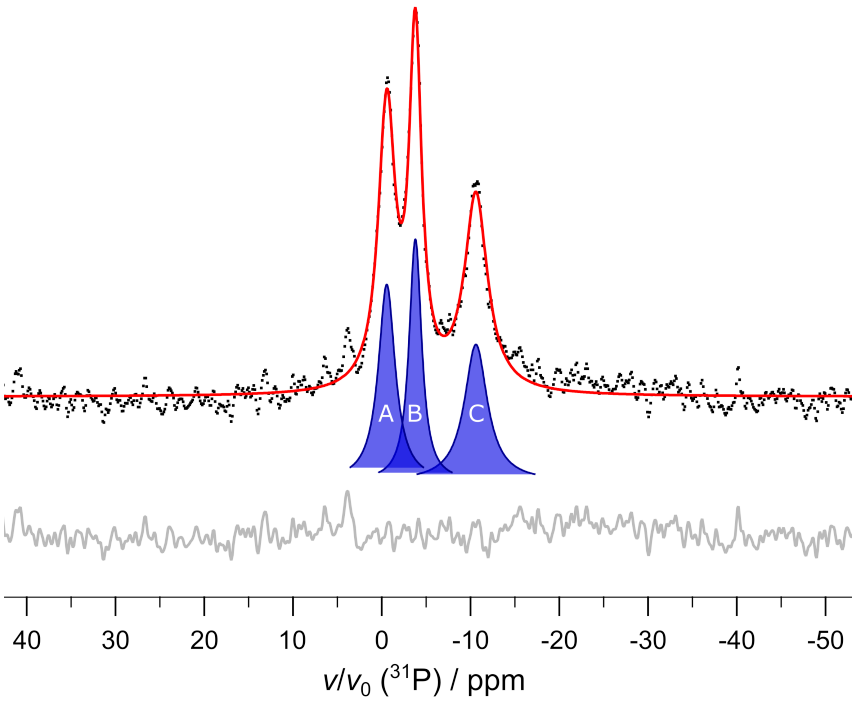

Figure A.8.: Observed (black) and calculated (red) ^{31}P NMR spectrum of BP_3N_6 and difference profile (gray) with the three ^{31}P signals deconvoled by three Voigt functions (blue). The ratio of the integrals of the three devolved signals is A : B : C = 1.1 : 0.9 : 1.0, which is in good agreement of three P sites of equal multiplicity in the BP_3N_6 structure model, within the precision of quantitative solid-state NMR spectroscopy. Deconvolution was performed by Igor Pro software.[24]

A.3. Author Contributions

S.V. Data curation: Lead; Formal analysis: Lead; Investigation: Lead; Validation: Equal; Visualization: Lead; Writing original draft: Lead; Writing review & editing: Equal

A.B. Formal analysis: Supporting; Investigation: Supporting; Writing original draft: Supporting; Writing review & editing: Supporting

W.S. Conceptualization: Lead; Funding acquisition: Lead; Project administration: Lead; Resources: Lead; Supervision: Lead; Validation: Equal; Writing original draft: Supporting; Writing review & editing: Equal

A.4. References

[1] W. J. Frierson, *"Ammonium Azide"*, *Inorg. Synth.* **1946**, *8*, 136.

[2] H. Huppertz, *"Multianvil high-pressure / high-temperature synthesis in solid state chemistry"*, *Z. Kristallogr.* **2004**, *219*, 330.

[3] D. Walker, *"Lubrication, gasketing, and precision in multianvil experiments"*, *Am. Mineral.* **1991**, *76*, 1092.

[4] *"SAINT, Data Integration Software"*, Wisconsin, USA, **1997**.

[5] Bruker AXS, *"APEX3 v2016.5-0"*, **2016**.

[6] Bruker-AXS, *"XPREP Reciprocal Space Exploration Vers. 2008/2"*, Karlsruhe, **2008**.

[7] G. M. Sheldrick, *"SHELX-97, Program for crystal structure solution and refinement"*, Universität Göttingen, **1997**.

[8] G. M. Sheldrick, *"A short history of SHELX"*, *Acta Crystallogr. Sect. A: Found. Adv.* **2008**, *64*, 112.

[9] L. J. Farrugia, *"WinGX suite for small-molecule single-crystal crystallography"*, *J. Appl. Crystallogr.* **1999**, *32*, 837.

[10] K. Momma, F. Izumi, *"VESTA 3 for three-dimensional visualization of crystal, volumetric and morphology data"*, *J. Appl. Crystallogr.* **2011**, *44*, 1272.

[11] H. M. Rietveld, *"A profile refinement method for nuclear and magnetic structures"*, *J. Appl. Crystallogr.* **1969**, *2*, 65.

[12] A. A. Coelho, *"TOPAS-Academic Vers. 4.1"*, Brisbane, **2007**.

[13] R. W. Cheary, A. Coelho, *"A fundamental parameters approach to X-ray line-profile fitting"*, *J. Appl. Crystallogr.* **1992**, *25*, 109.

[14] R. W. Cheary, A. A. Coelho, J. P. Cline, *"Fundamental Parameters Line Profile Fitting in Laboratory Diffractometers"*, *J. Res. Natl. Inst. Stand. Technol.* **2004**, *109*, 1.

[15] Oxford Instruments, *"AZtecEnergy Vers. 3.1"*, Abington, **2016**.

[16] R. S. Pease, *"Crystal Structure of Boron Nitride"*, *Nature* **1950**, *165*, 722.

[17] R. Hoppe, *"On the Madelung Part of Lattice Energy"*, *Z. Naturforsch. A: Phys. Sci.* **1995**, *50*, 555.

[18] R. Hoppe, S. Voigt, H. Glaum, J. Kissel, H. P. Müller, K. Bernet, *"A new route to charge distributions in ionic solids"*, *J. Less-Common Met.* **1989**, *156*, 105.

[19] J. Cumby, J. P. Attfield, *"Ellipsoidal analysis of coordination polyhedra"*, *Nat. Commun.* **2017**, *8*, 14235.

[20] W. Schnick, J. Lücke, *"Darstellung, Kristallstruktur und IR-spektroskopische Untersuchung von Phosphor(V)-nitrid-imid, HPN_2"*, *Z. Anorg. Allg. Chem.* **1992**, *610*, 121.

[21] S. Horstmann, E. Irran, W. Schnick, *"Synthese, Kristallstruktur und Eigenschaften von Phosphor(V)-nitridimid HP_4N_7"*, *Z. Anorg. Allg. Chem.* **1998**, *624*, 221.

[22] K. Landskron, H. Huppertz, J. Senker, W. Schnick, *"Multianvil-Synthese, Pulver-Röntgenstrukturanalyse, ^{31}P-MAS-NMR- und FTIR-Spektroskopie sowie Materialeigenschaften von γ-P_3N_5, einer Hochdruckphase von binärem Phosphor(V)nitrid mit verzerrt quadratischen PN_5-Pyramiden und PN_4-Tetraedern"*, *Z. Anorg. Allg. Chem.* **2002**, *628*, 1465.

[23] R. M. Chrenko, *"Ultraviolet and infrared spectra of cubic boron nitride"*, *Solid State Commun.* **1974**, *14*, 511.

[24] WaveMetrics, *"Igor Pro 7"*, Lake Oswego, Oregon, **2017**.

B. Supporting Information for Chapter 4

Rivalry under Pressure: The Coexistence of Ambient-Pressure Motifs and Close-Packing in Silicon Phosphorus Nitride Imide SiP_2N_4NH

Sebastian Vogel, Amalina T. Buda, and Wolfgang Schnick

Angew. Chem. Int. Ed. **2019**, *58*, 3398;

Angew. Chem. **2019**, *131*, 3436.

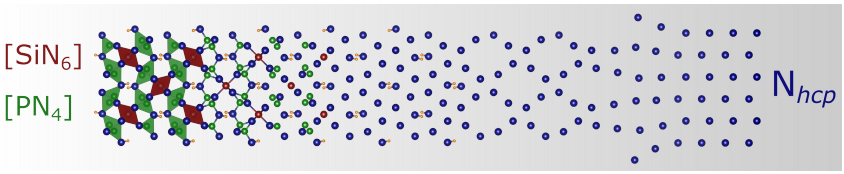

Abstract Non-metal nitrides such as BN, Si_3N_4, and P_3N_5 meet numerous demands on high-performance materials, and their high-pressure polymorphs exhibit outstanding mechanical properties. Herein, we present the silicon phosphorus nitride imide SiP_2N_4NH featuring sixfold coordinated Si. Using the multianvil technique, SiP_2N_4NH was obtained by highpressure high-temperature synthesis at 8 GPa and 1100 °C with in situ formed HCl acting as a mineralizer. Its structure was elucidated by a combination of single-crystal X-ray diffraction and solid-state NMR measurements. Moreover, SiP_2N_4NH was characterized by energy-dispersive X-ray spectroscopy and (temperature-dependent) powder X-ray diffraction. The highly condensed Si/P/N framework features PN_4 tetrahedra as well as the rare motif of SiN_6 octahedra, and is discussed in the context of ambient-pressure motifs competing with close-packing of nitride anions, representing a missing link in the high-pressure chemistry of non-metal nitrides.

B.1. Experimental Procedures

Preparation of starting materials

NH_4N_3 was prepared from stoichiometric amounts of dry NH_4NO_3 (Grüssing, 99 %) and NaN_3 (Acros Organics, 99 %) by sublimation according to Frierson.[1] The starting materials were ground and filled into a dry Schlenk tube with its lower end placed in a furnace. The mixture was heated for 12 h at 200 °C with open valve. NH_4N_3 was yield as colorless crystals at the upper end of the Schlenk tube. Phase purity was confirmed by PXRD and FTIR measurements.

Commercial $(PNCl_2)_3$ (abcr GmbH, 98.5 %) was purified by sublimation in static vacuum at 120 °C in a dry Schlenk tube using a water-cooled cooling finger.

Amorphous Si_3N_4 (UBE, SNA-00) was used without any further purification.

High-pressure high-temperature synthesis

High-pressure high-temperature reactions were performed in a hydraulic 1000 t press utilizing the multianvil technique and a modified Walker module.[2,3] In a typical batch, $(PNCl_2)_3$, NH_4N_3, and amorphous Si_3N_4 (UBE, SNA-00) were ground in a glovebox (MBraun, $<$ 1 ppm O_2, H_2O) to ensure absence of water and oxygen during synthesis. The mixture of starting materials was tightly packed into a crucible and sealed with a cap, both made of h-BN (Henze, Kempten). The sample was placed in the center of two graphite furnaces by a lower and an upper MgO spacer and subsequently set into a sleeve of ZrO_2 and sealed with Mo plates on both sides to ensure electrical contact with graphite furnaces. The as-described assembly was pasted into the center of a pierced octahedron (5 % Cr_2O_3 doped MgO, 18 mm edge length, Ceramic Substrates & Components Ltd, Isle of Wight). The octahedron was compressed in a steady manner between eight Co-doped WC cubes with truncated edges (7 % Co, 11 mm edge length, Hawedia, Marklkofen), separated by pyrophyllite gaskets. More detailed information on the octahedron-within-cubes payload can be found in literature.[2] The sample was compressed to 8 GPa before it was heated to 1100 °C within 1 h. Pressure and temperature were kept for 8 h before the sample was allowed to cool down within another hour. The sample pellet was obtained after slow decompression and washed with de-ionized water to remove residual chlorides such as $NH_4Mg(H_2O)_6Cl_2$, which is formed during

synthesis in supercritical HCl from stating materials and MgO spacers.[4] In order to grow single-crystals up to 25 µm in length 25 wt-% of NH_4Cl were added to the mixture of starting materials.

Single-crystal X-ray diffraction (XRD)

Single-crystal XRD data sets were conducted on a Bruker D8 Venture TXS diffractometer (rotating anode, Mo-Kα radiation, $\lambda = 0.71073$ Å, multilayer monochromator) by combined φ- and ω-scans. Indexing, integration, semi-empiric absorption correction (multi-scan) and determination of the space group was performed by the APEX3 software package.[5–7] The structure was solved using the SHELXT algorithm and refined against F^2 by the full-matrix least-square method, employing SHELX-97 and the WinGX software package.[8–11] For structure visualization the VESTA software was used.[12]

Powder X-ray diffraction (PXRD)

Powder X-ray diffraction patterns were recorded on a STOE Stadi P diffractometer (STOE & Cie GmbH, Darmstadt, Cu-Kα_1 radiation, $\lambda = 1.5406$ Å, Ge(111) monochromator) by a MYTHEN 1K Si strip detector in modified Debye-Scherrer geometry. The sample was tightly filled into glass capillaries with an outer diameter of 0.3 mm (Hilgenberg, Malsfeld) and rotated during measurement. Rietveld refinement was performed employing the TOPAS Academic software.[13,14] Peak profiles were modeled using the fundamental parameters approach and the background was described by shifted Chebyshev polynomial.[15,16] Any preferred orientation of crystals was considered by spherical harmonics function of fourth order.

Temperature-dependent PXRD measurements were performed on a STOE Stadi P diffractometer (STOE & Cie GmbH, Darmstadt, Mo-Kα_1 radiation, $\lambda = 0.71073$ Å, Ge(111) monochromator), equipped with a STOE resistance graphite furnace and an IP-PSD detector. The sample was tightly filled into a fused silica capillary (Hilgenberg, Malsfeld) with an outer diameter of 0.5 mm and heated under Ar atmosphere from 25 to 1000 °C in steps of 25 °C with a rate of 10 °C·min^{-1}. At each temperature step data collection was performed within 20 min, while the temperature was held constant.

Solid-state MAS NMR spectroscopy

^{1}H, ^{31}P, ^{31}P{^{1}H} and ^{29}Si{^{1}H} MAS NMR spectra were conducted on a Avance III 500 spectrometer (Bruker, Karlsruhe) using an 11.7 T magnet operating at 500.25 MHz ^{1}H frequency, equipped with a

commercial double-resonance MAS probe. The sample was ground and packed into a ZrO_2 rotor with an outer diameter of 2.5 mm and NMR spectra were collected at 20 kHz spinning frequency.

Fourier-Transform infrared (FTIR) spectroscopy

FTIR spectra were collected at ambient conditions using a Spectrum BX II spectrometer with DuraSampler ATR-device (Perkin Elmer).

Scanning electron microscopy (SEM) and energy-dispersive X-ray (EDX) spectroscopy

A Dualbeam Helios Nanolab G3 UC (FEI, Hillsboro) equipped with a X-Max 80 SDD detector (Oxford Instruments, Abingdon) was used for scanning electron microscopy and energy-dispersive X-ray spectroscopy. The sample was coated with carbon using an electron beam evaporator (BAL-TEC MED 020, Bal Tec AG) and data were analyzed using the Aztec software.[17]

B.2. Results and Discussion

Scanning electron microscopy (SEM) and energy-dispersive X-ray (EDX) spectroscopy

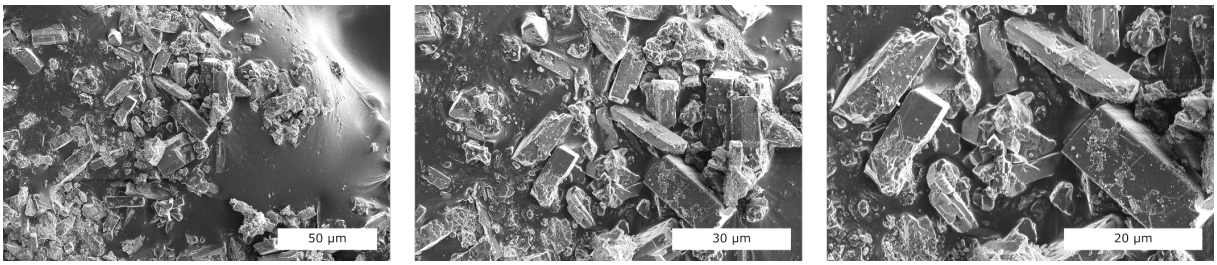

Figure B.1.: SEM images of generic sample of SiP_2N_4NH with single-crystals up to 25 µm in length.

Table B.1.: EDX measurements (atom-%) of six generic crystals (C1–C6) of SiP_2N_4NH. Minor amounts of oxygen may be attributable to partial surface hydrolysis and some trace amounts of chlorine may be due to residuals from side phases, which have been removed by washing with de-ionized water.

	C1	C2	C3	C4	C5	C6	measured	ratio	ideal
Si	14.6	10.5	10.1	10.9	11.9	13.1	12(2)	1.0	1
P	31.6	24.6	21.8	22.6	25.5	27.5	26(4)	2.2	2
N	50.5	60.3	67.0	62.6	58.8	53.3	59(6)	5.0	5
O	2.6	4.3	0.0	3.5	3.5	5.5	3(2)	0.3	0
Cl	0.8	0.3	1.1	0.4	0.3	0.5	1(1)	0.0	0

Structure determination

Table B.2.: Crystallographic data on SiP_2N_4NH from single-crystal refinement.

Formula	**SiP_2N_4NH**
Crystal system	orthorhombic
Molecular weight / g·mol^{-1}	161.09
Space group	*Pnma* (no. 62)
Lattice parameters / Å	$a = 8.3111(18)$
	$b = 5.3963(11)$
	$c = 7.2392(14)$
Cell volume / Å^3	324.67(12)
Formula units per cell	4
Calculated X-ray density / g·cm^{-3}	3.296
Linear absorption coefficient / cm^{-1}	1.514
$T_{\min}/T_{\max}$	0.9313
Radiation	Mo-Kα ($\lambda = 0.71073$ Å)
Diffractometer	Bruker D8 Venture
θ-range / °	$3.73 < \theta < 37.03$
Temperature / K	293(2)
$F(000)$	316
Observed reflections	4513
Independent reflections ($> 2\sigma$)	878 (752)
Number of parameters	49
Restraints	1
R_{int}; R_σ	0.0345; 0.0273
Final R indices [$I > 2\sigma(I)$]	$R1 = 0.0284$; $wR2 = 0.0736$
Final R indices (all data)	$R1 = 0.0349$; $wR2 = 0.0762$
Goodness of fit	1.120
Residual electron density / e·Å^{-3}	0.662; -0.700

Table B.3.: Wyckoff position, fractional coordinates and thermal displacement parameters of SiP_2N_4NH from single-crystal refinement.

Atom	Wyck.	x	y	z	U_{eq}/U_{iso} / Å^2
P1	4c	0.21395(5)	1/4	0.68550(6)	0.0031(1)
P2	4c	0.21466(5)	1/4	0.29344(6)	0.0035(1)
Si1	4a	0	0	0	0.0051(1)
N1	4c	0.10557(18)	1/4	0.48953(19)	0.0058(3)
N2	4c	0.10186(16)	1/4	0.11694(19)	0.0030(3)
N3	4c	0.39864(16)	1/4	0.61733(19)	0.0034(3)
N4	8d	0.32844(12)	0.5005(2)	0.30340(14)	0.0048(2)
H1	4c	0.001(4)	1/4	0.463(16)	0.37(11)

Table B.4.: Anisotropic displacement parameters (Å^2) of SiP_2N_4NH from single-crystal refinement.

Atom	U_{11}	U_{22}	U_{33}	U_{23}	U_{13}	U_{12}
P1	0.0038(2)	0.0024(2)	0.0032(2)	0	0.0006(1)	0
P2	0.0039(2)	0.0028(2)	0.0038(2)	0	−0.0005(1)	0
Si1	0.0060(2)	0.0021(2)	0.0073(2)	0.0001(1)	−0.0033(1)	0.0004(1)
N1	0.0052(5)	0.0085(6)	0.0036(5)	0	−0.0007(4)	0
N2	0.0035(5)	0.0019(5)	0.0036(5)	0	−0.0015(4)	0
N3	0.0027(5)	0.0026(5)	0.0049(5)	0	0.0014(4)	0
N4	0.0050(4)	0.0030(3)	0.0065(4)	0.0008(3)	−0.0019(3)	−0.0011(3)

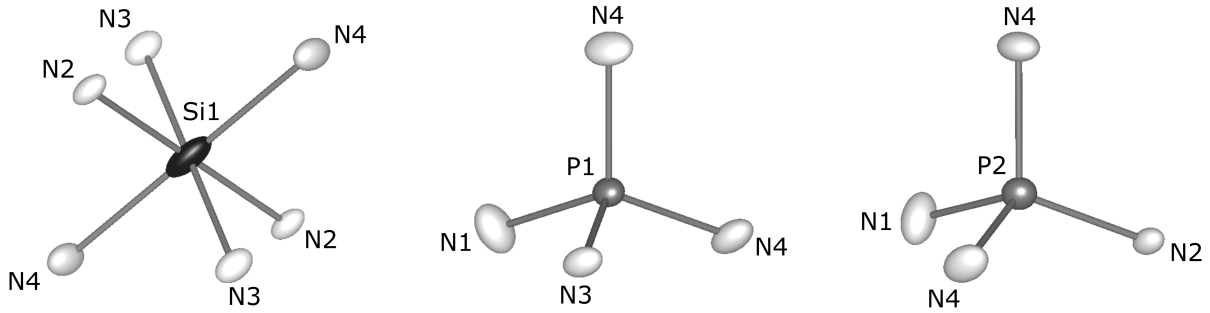

Figure B.2.: Coordination polyhedra of Si1, P1 and P2 with ellipsoids displayed at 99 % probability level.

Table B.5.: Interatomic distances (Å) of SiP_2N_4NH from single-crystal refinement.

Si1–N3	1.8031(9)	P1–N3	1.6124(14)	P2–N2	1.5848(14)
Si1–N3	1.8031(9)	P1–N4	1.6326(11)	P2–N4	1.6513(11)
Si1–N2	1.8037(9)	P1–N4	1.6326(11)	P2–N4	1.6513(11)
Si1–N2	1.8037(9)	P1–N1	1.6805(15)	P2–N1	1.6844(15)
Si1–N4	2.0146(10)				
Si1–N4	2.0146(10)				

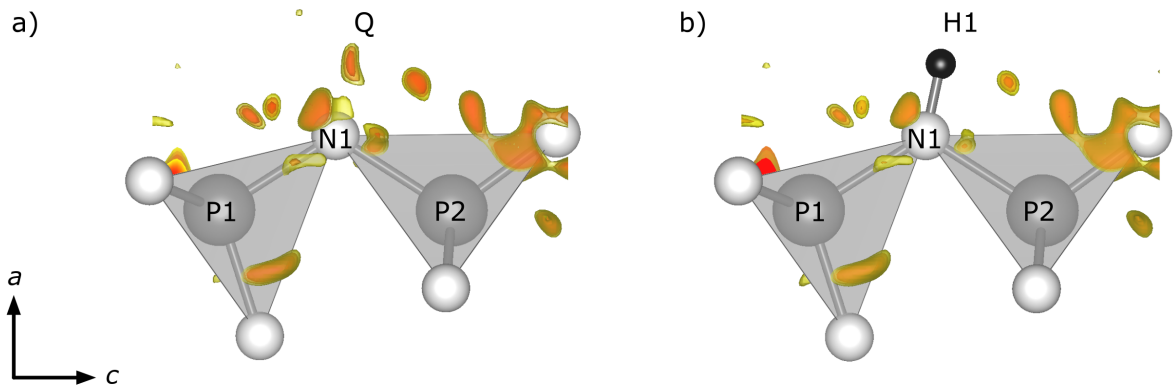

Figure B.3.: Difference Fourier map ($F_{obs} - F_{calc}$) from single-crystal refinement of 'SiP_2N_5' (a) and SiP_2N_4NH (b). Isosurface levels are 0.7, 0.74 and 0.78 electron·a_0^{-3}, respectively (a_0 = Bohr radius).

Table B.6.: Interatomic angles (°) of SiP_2N_4NH from single-crystal refinement.

N3–P1–N4	111.445(36)	N3–Si1–N3	180
N3–P1–N4	111.445(36)	N3–Si1–N2	83.151(4)
N3–P1–N1	104.591(75)	N3–Si1–N2	96.849(3)
N4–P1–N4	111.107(53)	N3–Si1–N4	89.829(53)
N4–P1–N1	109.000(36)	N3–Si1–N4	90.171(53)
N4–P1–N1	109.000(36)	N3–Si1–N2	96.849(3)
N2–P2–N4	111.964(36)	N3–Si1–N2	83.151(4)
N2–P2–N4	111.964(36)	N3–Si1–N4	90.171(53)
N2–P2–N1	111.138(73)	N3–Si1–N4	89.829(53)
N4–P2–N4	109.890(53)	N2–Si1–N2	180
N4–P2–N1	105.764(36)	N2–Si1–N4	89.912(52)
N4–P2–N1	105.764(36)	N2–Si1–N4	90.088(52)
		N2–Si1–N4	90.088(52)
		N2–Si1–N4	89.912(52)
		N4–Si1–N4	180.000(41)

Rietveld refinement

Table B.7.: Crystallographic data of SiP_2N_4NH from Rietveld refinement.

Formula	**SiP_2N_4NH**
Crystal system	orthorhombic
Space group	*Pnma* (no. 62)
Molecular weight / g·mol^{-1}	187.78
Lattice parameters / Å	$a = 8.33606(14)$
	$b = 5.38714(7)$
	$c = 7.23899(11)$
Cell volume / Å^3	325.085(8)
Formula units per cell	4
Calculated X-ray density / g·cm^{-3}	3.27049(8)
Linear absorption coefficient / cm^{-1}	143.2
Radiation	Cu-Kα_1 ($\lambda = 1.540596$ Å)
Monochromator	Ge(111)
Diffractometer	STOE Stadi P
Detector	MYTHEN 1K
2θ-range	$10° < 2\theta < 100°$
Temperature / K	293
Data points	6000
Number of observed reflections	190
Number of parameters (thereof background)	51 (18)
Profile function	fundamental parameter approach[16]
Background function	Shifted Chebyshev
R indices	$R_{\mathrm{Bragg}} = 0.0253$
	$R_{\mathrm{p}} = 0.0569$
	$R_{\mathrm{wp}} = 0.0803$
	$R_{\mathrm{exp}} = 0.0500$
Goodness of fit	1.605

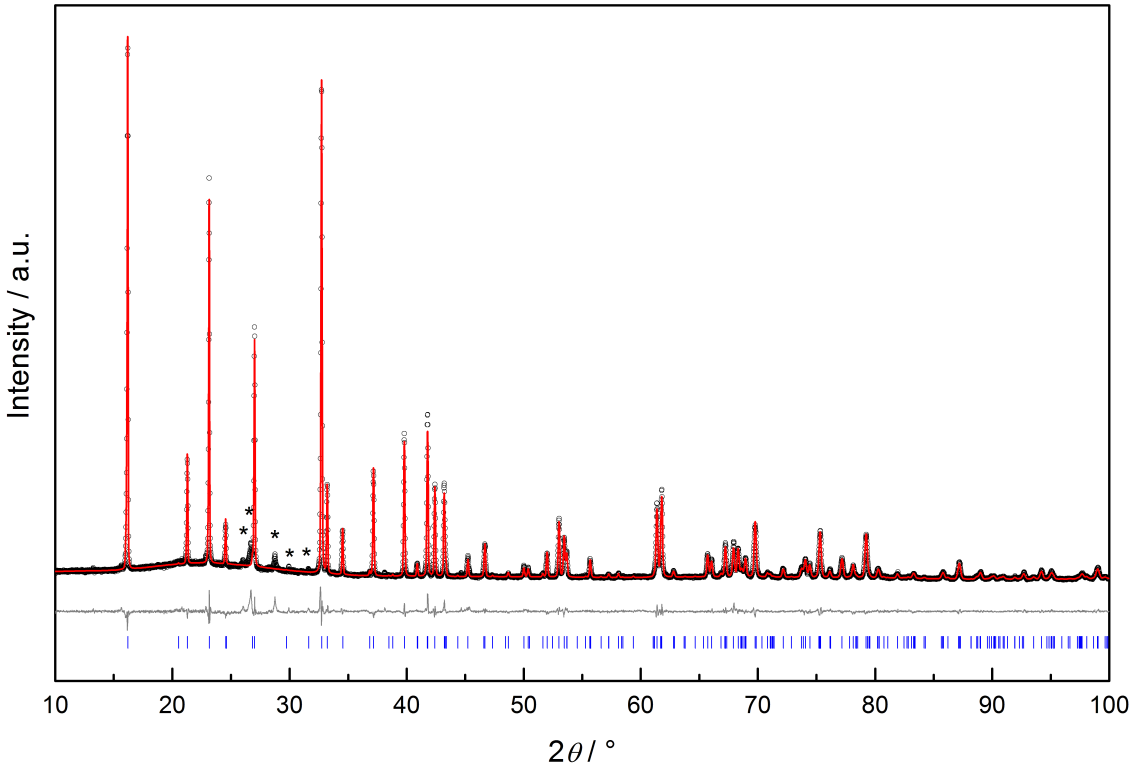

Figure B.4.: Observed (black) and calculated (red) powder X-ray diffraction pattern with difference plot (gray). Positions of Bragg reflections of SiP_2N_4NH are displayed by vertical blue lines. Minor amounts of unknown side phases are marked with asterisks.

Temperature-dependent PXRD

Temperature-dependent PXRD proves SiP_2N_4NH to be stable up to 1000 °C at ambient pressure under Ar atmosphere (Figure B.5). Within this temperature range, high-pressure phases tend to transform into ambient-pressure polymorphs. Herein, no phase transition is observed, suggesting SiP_2N_4NH to be stable at ambient pressure. The structural motif of SiN_6 octahedra, however, suggests SiP_2N_4NH to be a high-pressure phase, as Si favors fourfold coordination in highly condensed compounds at ambient conditions. A conceivable phase transition of SiP_2N_4NH, however, may be kinetically unfavored and even higher temperatures may be needed to induce the formation of a possible ambient-pressure polymorph.

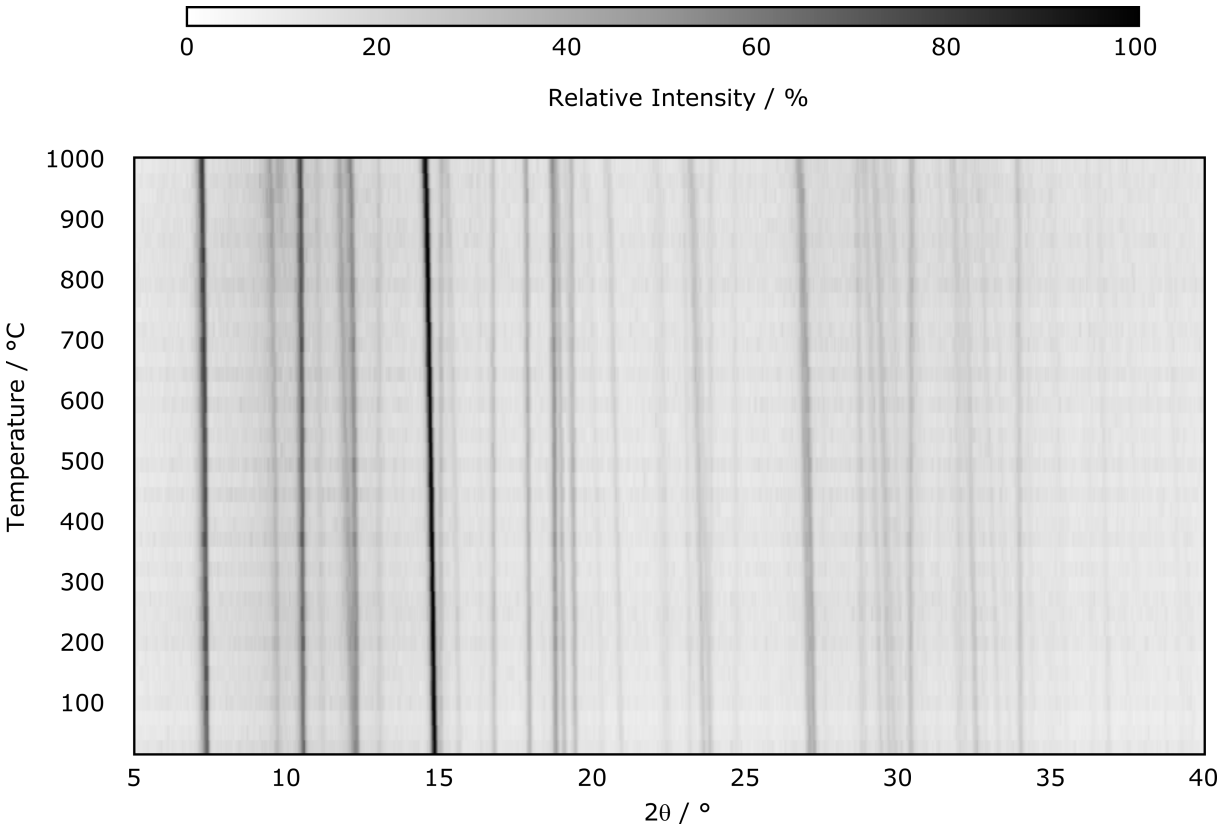

Figure B.5.: Temperature-dependent powder X-ray diffraction patterns (Mo-Kα_1 radiation, $\lambda = 0.71073$ Å) measured under Ar atmosphere. A slight shift to lower angles with increasing temperature correspond to thermal expansion of the cell (4.3 % in volume). Neither phase transition nor decomposition is observed.

Moreover, Rietveld refinements of temperature-dependent PXRD patterns were performed and evolution of lattice parameters are illustrated in Figure B.6.[13] At 1000 °C the thermal expansion of the unit cell is 4.3 % in volume with respect to ambient temperature (25 °C). This increase is predominated by expansion of lattice parameters *a* and *c* (2.8 %, 1.6 %). The lattice parameter *b*, in contrast, shows only marginal changes with temperature (–0.1 %), which may be due to the SiN_6 octahedra sharing common edges along [010] and thus, the SiP_2N_4NH structure being more rigid along *b*.

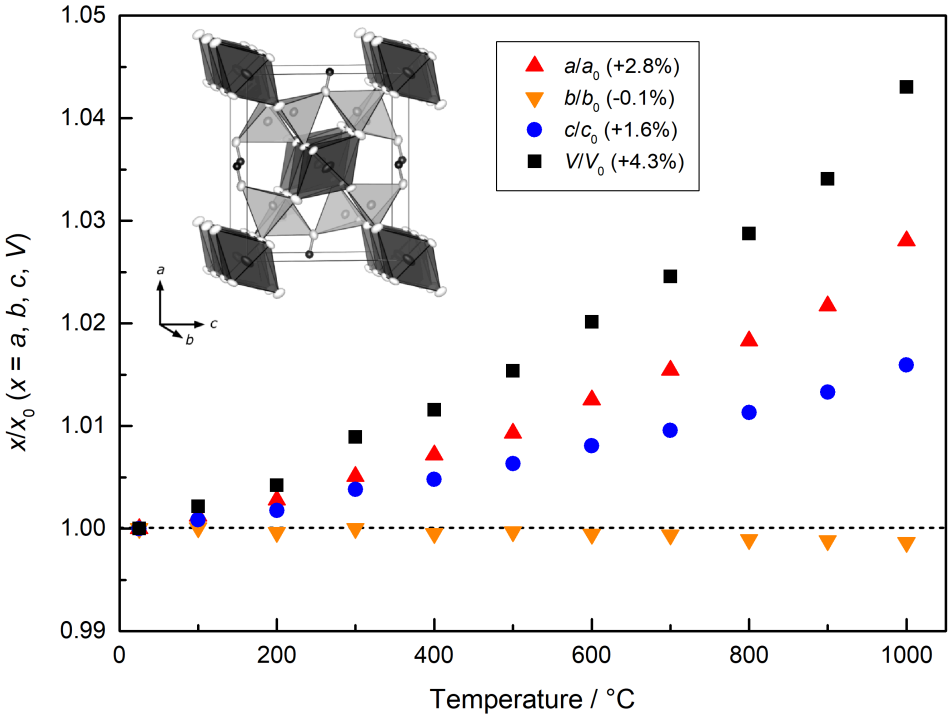

Figure B.6.: Temperature-dependent evolution of lattice parameters of SiP_2N_4NH from Rietveld refinements. The expansion of the unit cell with increasing temperature is attributable to expansion of lattice parameters *a* and *c* (2.8 %, 1.6 %).

Structure description and analysis

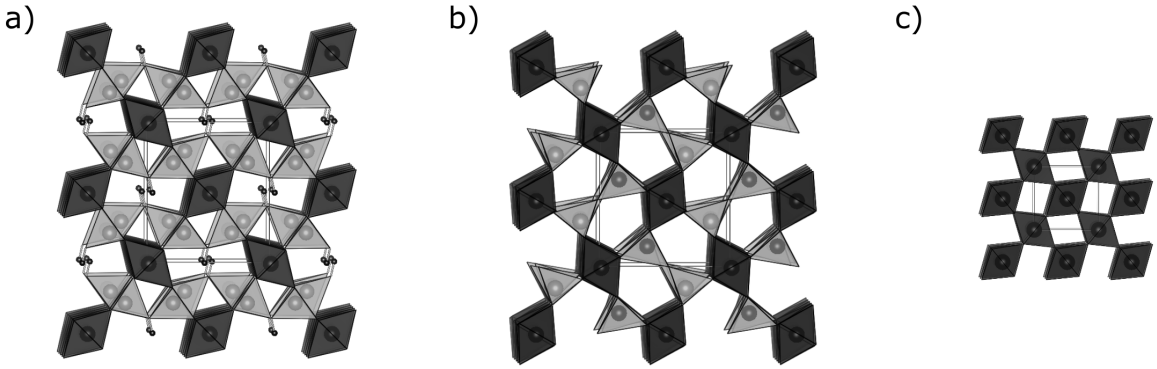

Figure B.7.: The structure of SiP_2N_4NH (a) appears related to sillimanite (Al_2SiO_5, b) with slightly different topology as illustrated by the respective point symbols $(3^1 4.4^2 2.5^9)(3^8.4^8.5^5)^2$ and $(3^1 2.4^2 0.5^1 3)(3^6.4^8.5^7)^2$ determined by TOPOS software.[18–21] Both structures may be derived as a hierarchical variant from the $CaCl_2$ structure (c) by replacing the anion sites with TX_4 tetrahedra (T = P/Al, Si; X = N/O).

Table B.8.: SiP_2N_4NH may be understood as the formal combination of $SiPN_3$ and PNNH in a 1 : 1 ratio. Due to the densification effect, the formation of SiP_2N_4NH appears to be favored at high-pressure conditions.

	V / Å^3	Z	V per f.u. / Å^3	Density / g·cm^{-3}	Ref.
α-PNNH	149.7	4	37.4	2.662	[22]
β-PNNH	294.6	8	36.8	2.705	[23]
$SiPN_3$	223.6	4	55.9	3.003	[24]
$SiPN_3$ + β-PNNH	741.8	8	92.7	2.885	
SiP_2N_4NH	324.7	4	81.2	3.296	this work

Minimal bonding ellipsoids (MBE) analysis

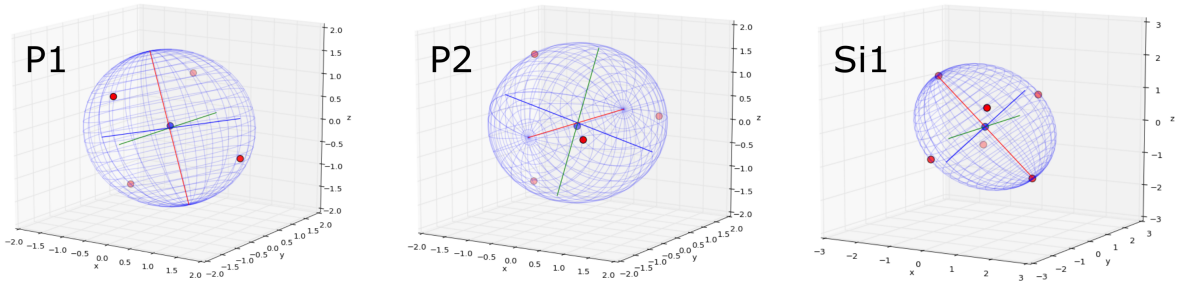

Figure B.8.: Minimal bonding ellipsoids (MBE) of $P1N_4$, $P2N_4$ and $Si1N_6$ polyhedra in SiP_2N_4NH determined by PIEFACE software.[25] P, Si: blue, N: red.

Table B.9.: Parameters of MBEs in SiP_2N_4NH indicating almost regular tetrahedral coordination of P1 and P2 and a distortion of SiN_6 polyhedra, due to slight axial elongation.[25]

	$R1$	$R2$	$R3$	$\langle R \rangle$	σ(R)	S	Center Disp.	CN
P1	1.6716	1.6490	1.5949	1.6385	0.0322	−0.0193	0.0542	4
P2	1.6556	1.6544	1.6148	1.6416	0.0189	−0.0233	0.0725	4
Si1	2.0147	1.9078	1.6925	1.8716	0.1340	−0.0598	0	6

Solid-state NMR and FTIR spectroscopy

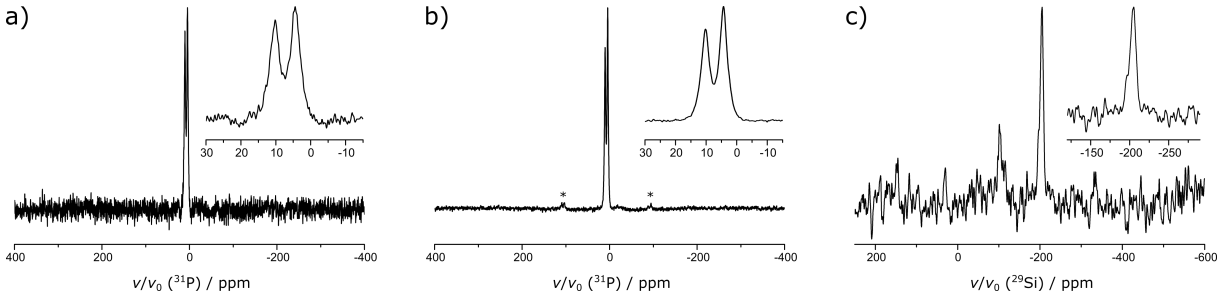

Figure B.9.: ^{31}P (a), ^{31}P{^{1}H} (b) and ^{29}Si{^{1}H} (c) NMR spectra of SiP_2N_4NH. The ^{29}Si{^{1}H} spectrum shows one additional signal at −101 ppm, which most likely corresponds to Si/O/H species.[26] Spinning sidebands are marked with asterisks.

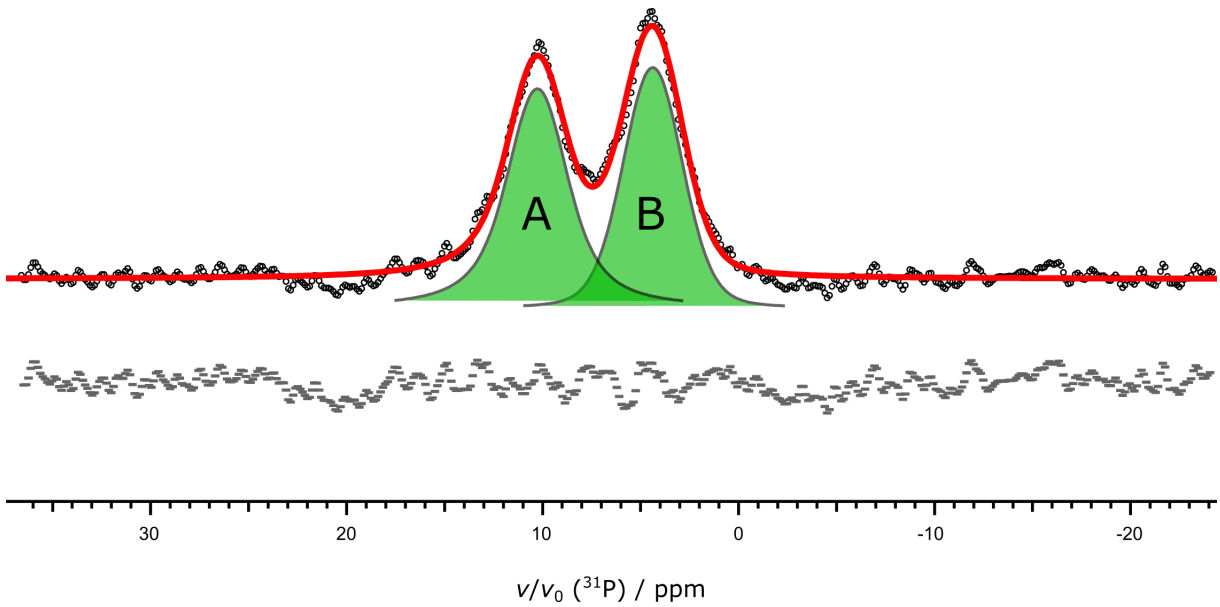

Figure B.10.: The conducted ^{31}P NMR spectrum (black circles) was deconvolved by two Voigt functions (green) with an integral ration of A : B = 1.13(3) : 1.00(3), which is in line with two crystallographic P sites with equal multiplicity in SiP_2N_4NH. Difference plot is given in gray. Deconvolution was performed by Igor Pro software.[27]

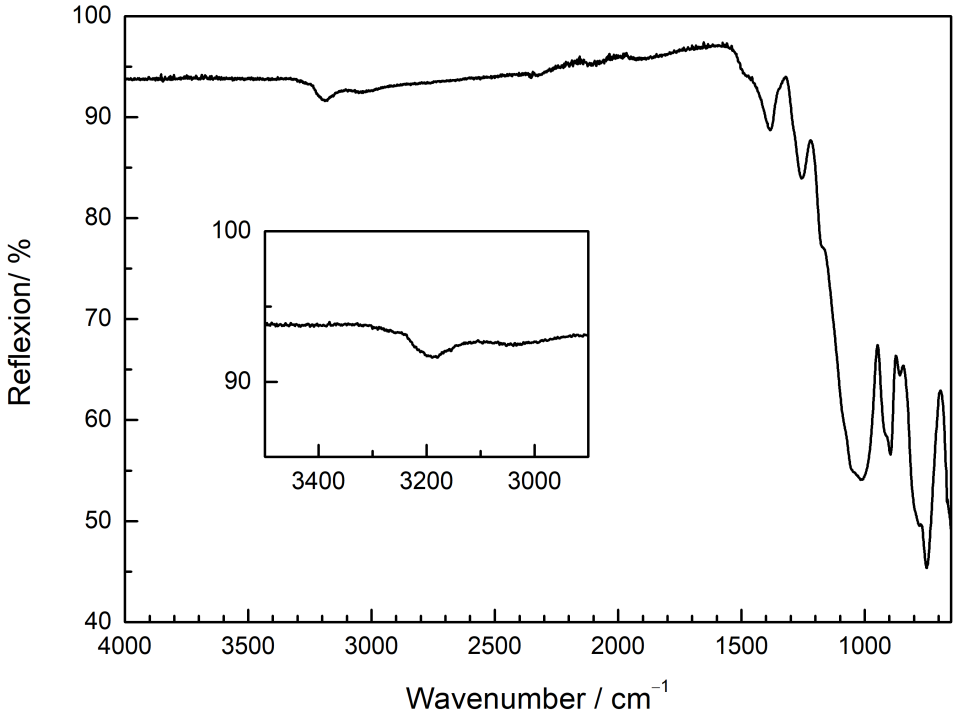

Figure B.11.: The FTIR spectrum (ATR) of a generic SiP_2N_4NH sample shows broad absorption bands at 2900–3300 cm^{-1}, which can be assigned to vibrational NH modes. Strong absorption bands at $< 1600\,cm^{-1}$ correspond to various combinations of vibrational Si/P/N modes of the condensed network and have been observed in related compounds as well.[22,28]

CHARDI analysis

CHARDI analyses of as-presented SiP_2N_4NH and hypothetical 'SiP_2N_5' have been performed, with the latter featuring an unsaturated N1 site (Table B.10, B.11).[29] In both structures effective coordination numbers of P1, P2 and Si1 are 3.97, 3.92 and 5.41, in line with tetrahedral and elongated octahedral coordination spheres of P and Si. In hypothetical 'SiP_2N_5' total charges of Si1, N2, N3 and N4 (+3.94, −3.17, −3.02, −2.85) are in good agreement with the respective formal oxidation states +IV/−III. In contrast total charges of P1, P2 and N1 (+5.57, +5.49, −2.12) appear too high considering formal oxidation states +V/−III. Much more reasonable values for these sites (+5.09, +5.01, −3.13), however, are obtained using the as-presented SiP_2N_4NH structure model, while values of Si1, N2, N3 and N4 do not change significantly (Figure B.12). Thus, CHARDI analyses confirm findings from XRD and NMR investigations as well as a selective N1–H1 bonding.

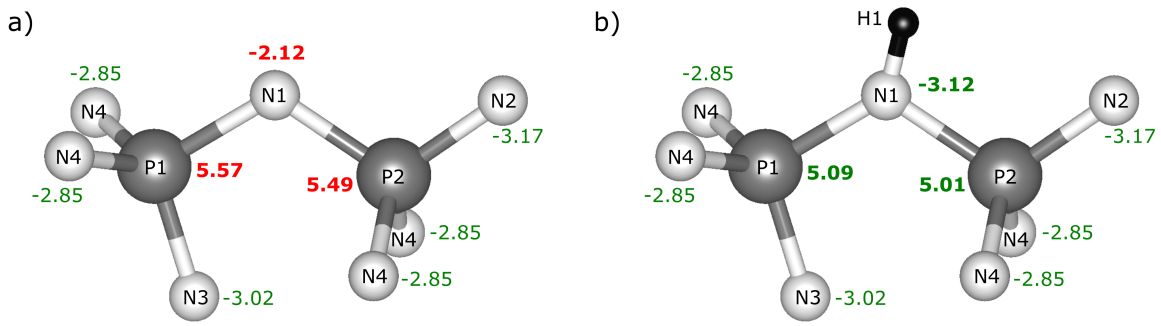

Figure B.12.: Total charges of P and N sites determined by CHARDI analysis in hypothetical 'SiP_2N_5' with unsaturated N1 site (a) and SiP_2N_4NH with one equivalent H binding to N1 site (b).[29]

Table B.10.: Results from CHARDI analysis of 'SiP_2N_5'.[29] Total charges of P1, P2 and N1 differ significantly from formal oxidation states (+V/–III), which is attributable to the lack of charge neutrality.

Polyhedron	**P1N1N3N4N4**	**P2N1N2N4N4**	**Si1N2N2N3N3N4N4**
Average bond length / Å	1.6397	1.6429	1.8738
Polyhedral volume / $Å^3$	2.2567	2.2699	8.6731
Distortion index	0.01265	0.0177	0.05009
Quadratic elongation	1.0019	1.0022	1.0104
Bond angle variance / $°^2$	6.9447	8.5725	17.0733
Eff. coordination number	3.9658	3.9182	5.4112
Total charges:			
P/Si	**5.569**	**5.492**	3.939
N1	**−2.120**	**−2.120**	
N2		−3.167	−3.167
N3	−3.024		−3.024
N4	−2.845	−2.845	−2.845

Table B.11.: Results from CHARDI analysis of SiP_2N_4NH.[29] Introduction of H with selective N1–H1 bonding obtained reasonable total charges of all atoms, confirming experimental findings from XRD and NMR investigations.

Polyhedron	**P1 N1N3N4N4**	**P2 N1N2N4N4**	**Si1 N2N2N3N3N4N4**
Average bond length / Å	1.6395	1.6429	1.8738
Polyhedral volume / $Å^3$	2.2561	2.2699	8.6735
Distortion index	0.0125	0.0177	0.0501
Quadratic elongation	1.0019	1.0022	1.0104
Bond angle variance / $°^2$	6.9349	8.6259	17.0694
Eff. coordination number	3.9666	3.9181	5.411
Total charges:			
P/Si	**5.088**	**5.011**	3.940
N1	**−3.122**	**−3.122**	
N2		−3.167	−3.167
N3	−3.022		−3.022
N4	−2.845	−2.845	−2.845

B.3. Author Contributions

S.V. Conceptualization: Equal; Formal analysis: Lead; Investigation: Lead; Validation: Equal; Visualization: Lead; Writing original draft: Lead; Writing review & editing: Equal

A.B. Formal analysis: Supporting; Investigation: Supporting; Validation: Supporting; Writing review & editing: Supporting

W.S. Conceptualization: Equal; Funding acquisition: Lead; Project administration: Lead; Resources: Lead; Supervision: Lead; Validation: Equal; Writing original draft: Supporting; Writing review & editing: Equal

B.4. References

[1] W. J. Frierson, *"Ammonium Azide"*, *Inorg. Synth.* **1946**, *8*, 136.

[2] H. Huppertz, *"Multianvil high-pressure / high-temperature synthesis in solid state chemistry"*, *Z. Kristallogr.* **2004**, *219*, 330.

[3] D. Walker, *"Lubrication, gasketing, and precision in multianvil experiments"*, *Am. Mineral.* **1991**, *76*, 1092.

[4] R. E. Marsh, *"Structure of magnesium chlorite hexahydrate. Corrigendum"*, *Acta Crystallogr. Sect. C: Cryst. Struct. Commun.* **1991**, *47*, 1775.

[5] *"SAINT, Data Integration Software"*, Wisconsin, USA, **1997**.

[6] Bruker AXS, *"APEX3 v2016.5-0"*, **2016**.

[7] Bruker-AXS, *"XPREP Reciprocal Space Exploration Vers. 2008/2"*, Karlsruhe, **2008**.

[8] G. M. Sheldrick, *"SHELX-97, Program for crystal structure solution and refinement"*, Universität Göttingen, **1997**.

[9] G. M. Sheldrick, *"A short history of SHELX"*, *Acta Crystallogr. Sect. A: Found. Adv.* **2008**, *64*, 112.

[10] G. M. Sheldrick, *"SHELXT - integrated space-group and crystal-structure determination"*, *Acta Crystallogr. Sect. A: Found. Adv.* **2015**, *71*, 3.

[11] L. J. Farrugia, *"WinGX suite for small-molecule single-crystal crystallography"*, *J. Appl. Crystallogr.* **1999**, *32*, 837.

[12] K. Momma, F. Izumi, *"VESTA 3 for three-dimensional visualization of crystal, volumetric and morphology data"*, *J. Appl. Crystallogr.* **2011**, *44*, 1272.

[13] H. M. Rietveld, *"A profile refinement method for nuclear and magnetic structures"*, *J. Appl. Crystallogr.* **1969**, *2*, 65.

[14] A. A. Coelho, *"TOPAS-Academic Vers. 4.1"*, Brisbane, **2007**.

[15] R. W. Cheary, A. Coelho, *"A fundamental parameters approach to X-ray line-profile fitting"*, *J. Appl. Crystallogr.* **1992**, *25*, 109.

[16] R. W. Cheary, A. A. Coelho, J. P. Cline, *"Fundamental Parameters Line Profile Fitting in Laboratory Diffractometers"*, *J. Res. Natl. Inst. Stand. Technol.* **2004**, *109*, 1.

[17] Oxford Instruments, *"AZtecEnergy Vers. 3.1"*, Abington, **2016**.

[18] V. A. Blatov, A. P. Shevchenko, D. M. Proserpio, *"Applied Topological Analysis of Crystal Structures with the Program Package ToposPro"*, *Cryst. Growth Des.* **2014**, *14*, 3576.

[19] V. A. Blatov, A. P. Shevchenko, *"ToposPro Vers. 5.1.0.7"*, Samara, **2016**.

[20] W. H. Taylor, *"The structure of sillimanite and mullite"*, *Z. Kristallogr. - Cryst. Mater.* **1928**, *68*, 503.

[21] A. K. van Bever, W. Nieuwenkamp, *"Die Kristallstruktur von Calciumchlorid, $CaCl_2$"*, *Z. Kristallogr. – Cryst. Mater.* **1935**, *90*, 374.

[22] W. Schnick, J. Lücke, *"Darstellung, Kristallstruktur und IR-spektroskopische Untersuchung von Phosphor(V)-nitrid-imid, HPN_2"*, *Z. Anorg. Allg. Chem.* **1992**, *610*, 121.

[23] A. Marchuk, F. J. Pucher, F. W. Karau, W. Schnick, *"A high-pressure polymorph of phosphorus nitride imide"*, *Angew. Chem. Int. Ed.* **2014**, *53*, 2469; *Angew. Chem.* **2014**, *126*, 2501.

[24] H.-P. Baldus, W. Schnick, J. Lücke, *"Silicon Phosphorus Nitride, the First Ternary Compound in the Silicon-Phosphorus-Nitrogen System"*, *Chem. Mater.* **1993**, *5*, 845.

[25] J. Cumby, J. P. Attfield, *"Ellipsoidal analysis of coordination polyhedra"*, *Nat. Commun.* **2017**, *8*, 14235.

[26] E. A. Leone, S. Curran, M. E. Kotun, G. Carrasquillo, R. Weeren, S. C. Danforth, *"Solid-State ^{29}Si NMR Analysis of Amorphous Silicon Nitride Powder"*, *J. Am. Ceram. Soc.* **1996**, *79*, 513.

[27] WaveMetrics, *"Igor Pro 7"*, Lake Oswego, Oregon, **2017**.

[28] M. Schwarz, G. Miehe, A. Zerr, E. Kroke, B. T. Poe, H. Fueß, R. Riedel, *"Spinel-Si_3N_4: Multi-Anvil Press Synthesis and Structural Refinement"*, *Adv. Mater.* **2000**, *12*, 883.

[29] R. Hoppe, S. Voigt, H. Glaum, J. Kissel, H. P. Müller, K. Bernet, *"A new route to charge distributions in ionic solids"*, *J. Less-Common Met.* **1989**, *156*, 105.

C. Supporting Information for Chapter 5

Stishovite's Relative: A Post-Coesite Form of Phosphorus Oxonitride

Sebastian Vogel, Dominik Baumann, Robin Niklaus, Elena Bykova, Maxim Bykov, Natalia Dubrovinskaia, Leonid Dubrovinsky, and Wolfgang Schnick

Angew. Chem. Int. Ed. **2018**, *57*, 6691;

Angew. Chem. **2018**, *130*, 6801.

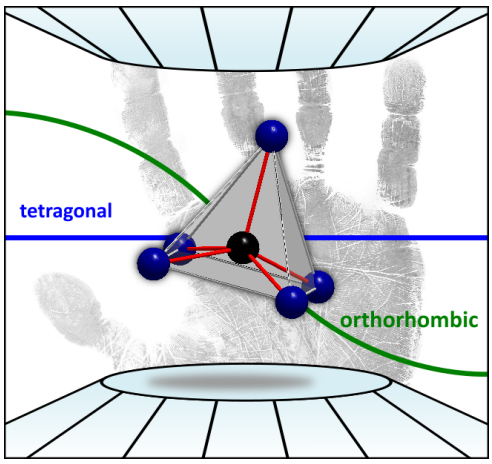

Abstract Phosphorus oxonitride (PON) is isoelectronic with SiO_2 and may exhibit a similar broad spectrum of intriguing properties as silica. However, PON has only been sparsely investigated under high-pressure conditions and there has been no evidence on a PON polymorph with a coordination number of P greater than 4. Herein, we report a post-coesite (pc) PON polymorph exhibiting a stishovite-related structure with P in a (5+1) coordination. The pc-PON was synthesized using the multianvil technique and characterized by powder X-ray diffraction, solid-state NMR spectroscopy, TEM measurements and in situ synchrotron X-ray diffraction in diamond anvil cells. The structure model was verified by single-crystal X-ray diffraction at 1.8 GPa and the isothermal bulk modulus of pc-PON was determined to $K_0 = 163(2)$ GPa. Moreover, an orthorhombic PON polymorph (o-PON) was observed under high-pressure conditions and corroborated as the stable modification at pressures above 17 GPa by DFT calculations.

C.1. Experimental Procedures

Preparation of starting materials

P_3N_5 was prepared according to Stock and Hoffmann from P_4S_{10} (Acros Organics, > 98 %) in a continuous flow of dry ammonia (5.0, Air Liquide).[1] P_4S_{10} was loaded in a fused silica boat and saturated by a continuous flow of dry ammonia at 298 K for 4 h before it was heated at 1123 K for another 4 h. The product was washed with concentrated HCl, de-ionized water, and ethanol then dried in vacuum to yield an orange powder. Phase purity was confirmed by PXRD and FTIR spectroscopy.

cri-PON was prepared according to a modified literature protocol by heating stoichiometric amounts of P_3N_5 and P_4O_{10} in a corundum crucible for 48 h at 1053 K in a sealed silica ampoule filled with argon.[2] Phase purity was confirmed by PXRD and FTIR spectroscopy.

High-pressure high-temperature synthesis

pc-PON was prepared in a high-pressure high-temperature procedure using a 1000 t hydraulic press (Voggenreiter, Mainleus, Germany) and the multianvil technique based on a modified Walker-type setup.[3,4] As a starting material cri-PON was ground, packed in a capsule and sealed with a cap both consisting of hexagonal boron nitride (Henze, Kempten, Germany). The capsule was placed in the center of two graphite tubes using two MgO spacers (Cesima Caramics, Wust-Fischbach, Germany). The assembly was put in the center of an Cr_2O_3 doped MgO octahedron (5 % Cr_2O_3, edge length 10 mm, Ceramic Substrates & Components Ltd, Isle of Wight, United Kingdom) equipped with a sleeve of ZrO_2 (Cesima Ceramics, Wust-Fischbach, Germany) acting as a thermal insulator. To enable electric contact between the surrounding anvils and the graphite tubes two molybdenum plates were used. The as-prepared octahedron was compressed between eight truncated cubes of cobalt doped tungsten carbide (6 % Co, truncated edge length 5 mm, Hawedia, Marklkofen, Germany) and the sample was heated by an electric resistance heating with a maximal power of 3000 W.

The assembly was compressed to 20 GPa within 11 h and than heated up to 1500 K within 10 min. The temperature was kept for another 15 min before the heating was turned off and the sample was slowly decompressed within 33 h. pc-PON was isolated as an air- and moisture-stable gray crystalline powder.

Powder X-ray diffraction (PXRD)

Powder X-ray diffraction measurements were performed on a STOE Stadi P powder diffractometer (STOE & Cie GmbH, Darmstadt, Germany; Mo-Kα_1 radiation, $\lambda = 0.71073$ Å) equipped with a Ge(111) monochromator and MYTHEN 1K Si-strip detector (Dectrics, Baden-Daettwil, Switzerland) in modified Debye-Scherrer geometry. For measurements the sample was loaded into tube capillaries (Hilgenberg, Malsfeld, Germany) with an outer diameter of 0.2 mm. Indexing, structure solution and refinement from the PXRD pattern was performed using the TOPAS-Academic V4.1 software.[5] Indexing was achieved with the SVD-algorithm and intensities were extracted with the Pawley-method.[6,7] The charge-flipping algorithm was used for structure solution and the pc-PON structure model was subsequently refined with the Rietveld method.[8–11] Peak profiles were modeled using the fundamental parameters approach and a possible preferred orientation of crystals was accounted for with a spherical harmonics function of fourth order.[12] The background was described using a shifted Chebyshev polynomial. Absorption was treated with a capillary absorption correction. Temperature-dependent PXRD data were collected on a STOE Stadi P powder diffractometer (STOE & Cie GmbH, Darmstadt, Germany; Mo-Kα_1 radiation, $\lambda = 0.71073$ Å)) equipped with a Ge(111) monochromator, a STOE resistance graphite furnace and an IPPSD detector. The sample was loaded in a fused silica capillary (Hilgenberg, Malsfeld, Germany) with an outer diameter of 0.5 mm and heated from 298 to 1073 K in steps of 20 K with a rate of 5 K·min^{-1} under Ar atmosphere. The temperature was held constant for data collection.

Transmission electron microscopy (TEM)

TEM experiments were performed on a Titan 80–300 (FEI, USA) with a field emission gun operated at 300 kV. EDX spectra were recorded on a TOPS 30 EDX spectrometer (EDAX, Germany). Bright field images as well as selected area electron diffraction (SAED) patterns were recorded using an UltraScan 1000 camera (Gatan, USA, resolution: 2k×2k). Corresponding data were processed and evaluated with the software ES Vision and Digital Micrograph.[13,14] The PON crystals were ground in absolute ethanol and drop-casted on copper TEM grids coated with a holey carbon film (S160, Plano GmbH, Germany) and further fixed on a doubletilt holder.

Computational details

Density functional theory (DFT) calculations were conducted for both, the pc- and the o-PON phase. The structural relaxation of pc- PON was performed with the Vienna ab initio simulation package (VASP).[15–17] Total energies of the unit cells were converged to 10^{-6} eV/atom with residual atomic forces below 10^{-4} eV. The exchange correlation was treated within the generalized gradient approximation (GGA) of Perdew, Burke, and Ernzerhof (PBE) and the projector-augmented-wave (PAW) method.[18–21] For all calculations a plane-wave cut-off of 535 eV was used. The Brillouin zone was sampled on a Λ-centered k-mesh produced from the method of Monkhorst and Pack of $6 \times 6 \times 12$.[22] E-V data were obtained from structural relaxations at a range of constant volumes (86 to 107 %) corresponding to compression and expansion of the unit cells. A variation in lattice parameters a and b was introduced manually in order to converge tetragonal to orthorhombic PON at constant volume owing to its marginal difference in total energy. Due to the close similarity of the E-V curves, the step size in volume compression was 0.25 % below 15 GPa and subsequently increased to 1 % with increasing pressure. The enthalpy difference ΔH was derived from $H = E + pV$ in the volume region between 32 and 54 Å^3, with the pressure p obtained from the numerical differentiation of $p = \partial E / \partial V$.

Solid-state MAS NMR spectroscopy

A ^{31}P solid-state MAS NMR spectrum was collected using a DSX Advance III 500 spectrometer (Bruker, Karlsruhe, Germany) with a magnetic field of 11.7 T, corresponding to a Larmor frequency of $\nu(^{31}\mathrm{P}) =$ 202.5 MHz. The sample was placed in a ZrO_2 rotor of 1.3 mm in outer diameter, which was mounted in a commercial pneumatic MAS probe (Bruker, Karlsruhe, Germany) and spun at rotation frequency of $\nu_{\mathrm{rot}} = 50$ kHz. Experimental data were analyzed with device-specific software.

Fourier transform infrared spectroscopy (FTIR)

The FTIR spectrum was collected on a Spectrum BX II spectrometer with DuraSampler ATR-device (Perkin Elmer) at ambient conditions.

Diamond anvil cell (DAC)

For in situ high-pressure investigations up to a maximum pressure of almost 40 GPa a BX90 diamond anvil cell (DAC) was used.[23] The DAC was equipped with Boehler-Almax type diamond anvils with 350 µm diameter culets and a rhenium gasket, which was preindented to a thickness of 35 µm and drilled to an inner diameter of 160 µm. Neon was used as pressure-transmitting medium and ruby spheres served as a pressure standard. The DAC was loaded with a polycrystalline particle of pc-PON and compressed to an initial pressure of 1.8 GPa after neon pressure-loading.

Synchrotron measurements

In situ XRD experiments were performed at the extreme-conditions beamline P02.2 of PETRA III (DESY, Hamburg, Germany).[24] The X-ray beam with a wavelength of 0.288 74 Å was focused by a Kirkpatrick-Baez mirror system to a size of $1.8 \times 1.9\,\mu m^2$ ($V \times H$) and diffraction intensities were collected on a PerkinElmer XRD 1621 flat-panel detector. At 1.8 GPa a single-crystal data set was collected by an ω scan ($\omega_{max} = \pm 38°$; $\Delta\omega = 0.5°$; $t_{exposure} = 10\,s$). Indexing and integration of the reflection intensities were performed using CrysAlisPro software.[25] A single crystal of an orthoenstatite ($(Mg_{1.93},Fe_{0.06})(Si_{1.93},Al_{0.06})O_6$, *Pbca*, $a = 8.8117(2)$, $b = 5.18320(10)$, $c = 18.2391(3)$ Å), was used to calibrate instrument model of CrysAlisPro software (sample-to-detector distance, the detector's origin, offsets of the goniometer angles and rotation of the X-ray beam and the detector around the instrument axis). The structure was solved with SHELXT and refined in anisotropic approximation against F^2 on all data by full-matrix least squares with SHELXL.[26,27] In order to examine the behavior of pc-PON under high-pressure conditions a series of 16 wide scans ($\omega_{max} = \pm 20°$; $t_{exposure} = 40\,s$) up to a maximum pressure of almost 40 GPa were collected. Respective pressure values were determined by the ruby fluorescence method.[28,29] Powder X-ray diffraction patterns were revealed by masking single-crystal reflections from diamond and neon followed by subsequent integration using the Dioptas software.[30] Lattice parameters were determined by Le Bail refinements with Jana2006 using a pseudo-Voigt function and a manually adjusted background for profile fitting.[31]

Equation of state

For a quantitative evaluation of the elastic properties of pc-PON the p-V data were fitted by the second order Birch-Murnaghan equation (Equation C.1) using the EoSFit7 software.[32–34] Herein, V is the volume of the unit cell at the pressure p, V_0 corresponds to the cell volume at a theoretical pressure of zero, and K_0 is the isothermal bulk modulus.

$$p(V) = \frac{3}{2}K_0\left[\left(\frac{V}{V_0}\right)^{-\frac{7}{3}} - \left(\frac{V}{V_0}\right)^{-\frac{5}{3}}\right] \tag{C.1}$$

C.2. Results and Discussion

Crystal structure of pc-PON from PXRD at 1 atm

Indexing of the PXRD pattern suggested tetragonal symmetry with lattice parameters $a = 4.6184(2)$ and $c = 2.455\,36(9)$ Å. Analysis of systematically absent reflections indicated space group $P4_2/mnm$ (no. 136) in which charge flipping led to identification of all atom positions, refined by a subsequent Rietveld refinement (Figure C.1). A minor amount of γ-HP_4N_7 was not refined.[35] The increased background in the region $5° < 2\theta < 20°$ can be assigned to non-crystalline material, formed by amorphization at high-pressure conditions during synthesis. All atoms are situated on $4f$ sites with $m.2m$ site symmetry and thus, respective x and y coordinates were constrained to one common parameter. The refined coordinates of P are close to Wyckoff position $2a$ but refinement indicated a significant displacement, which results in a split position of P with a 0.874(1) Å distance between the two electron density maxima. Thus, the site occupation factor of P was set to 0.5. Accounting for the mixed anion position of N and O the isotropic atomic displacement parameters were constrained to one common parameter and the respective site occupation factors were set to 0.5 (Table C.2). A crystallographic ordering of P at its split position as suggested from DFT calculations presented below was simulated using the modified DFT structure model (Figure C.2). The simulated PXRD pattern shows additional reflections and thus does not match the experimental one. Moreover, no superstructure reflections were observed during single-crystal XRD and TEM measurements. Thus, there is no evidence for any superstructure caused by a systematically ordering of P in pc-PON. Owing to a marginal X-ray scattering contrast of O and N no indications for any crystallographic N/O-ordering in pc-PON are obtained from PXRD measurements. Previous investigations by neutron diffraction have indicated similarly a random N/O-disorder in cri-PON, which was used as a starting material for pc-PON.[36] Due to small sample quantities (< 15 mg per batch) additional investigations by neutron diffraction are, however, not feasible for pc-PON.

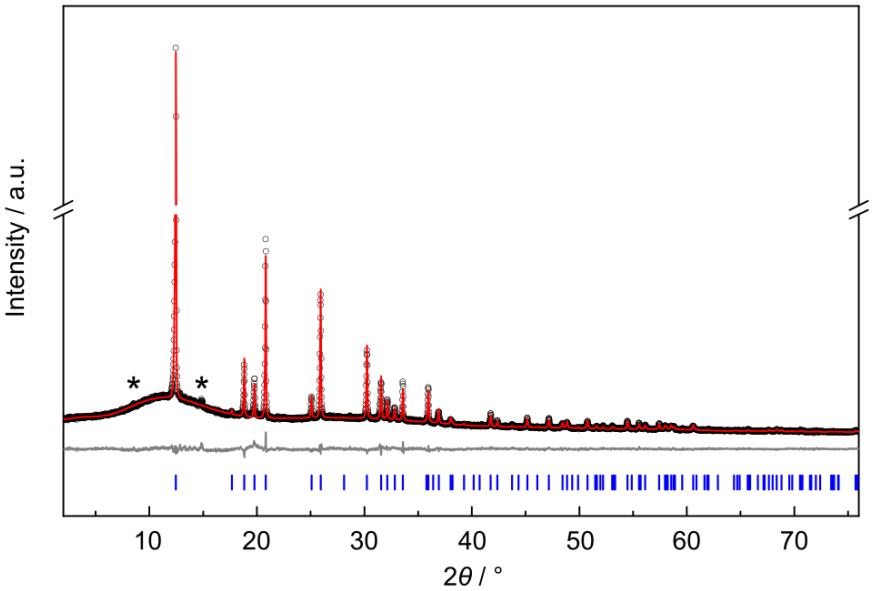

Figure C.1.: Observed (black circles) and calculated (red line) PXRD pattern (Mo-Kα_1 radiation, $\lambda = 0.71073$ Å) and difference profile (gray) from Rietveld refinement of pc-PON. Peak positions are marked by vertical blue lines. Tagged reflections (*) can be assigned to γ-HP_4N_7 as minor side phase.[35]

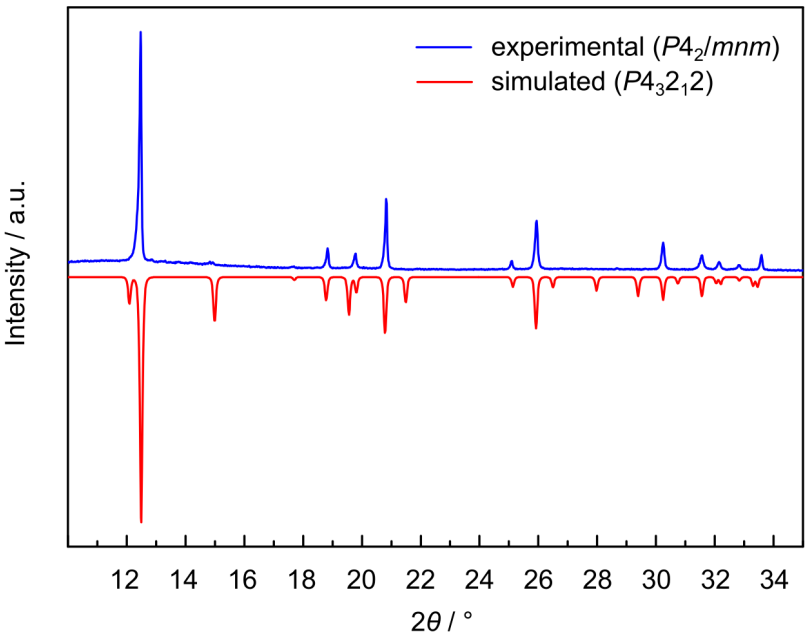

Figure C.2.: Experimental PXRD of pc-PON (blue) and a simulated PXRD using the modified DFT structure model presented below with a crystallographic ordering of P (red). As the simulated PXRD pattern does not match the experimental one, there is no indication for any long-range ordering of P in pc-PON.

Table C.1.: Crystallographic data on pc-PON based on Rietveld refinement ($p = 1$ atm).

Formula	**PON**
Crystal system	tetragonal
Space group (no.)	$P4_2/mnm$ (136)
Lattice parameters / Å	$a = 4.62782(10)$
	$c = 2.46042(4)$
Cell volume / Å^3	$V = 52.694(4)$
Formula units per cell	2
Calculated X-ray density / g·cm^{-3}	3.843
Linear absorption coefficient / cm^{-1}	17.54
Radiation	Mo-Kα_1 ($\lambda = 0.71073$ Å)
θ-range / °	1.000–38.177
Temperature / K	293
Data points	4958
Number of observed reflections	97
Number of parameters (thereof background)	34 (19)
R indices	$R_{\mathrm{Bragg}} = 0.02108$
	$R_{\mathrm{p}} = 0.03535$
	$R_{\mathrm{wp}} = 0.04621$
	$R_{\mathrm{exp}} = 0.03484$
Goodness of fit	1.327

Table C.2.: Crystallographic data on pc-PON based on Rietveld refinement ($p = 1$ atm).[a]

	x	y	z	U_{iso} / Å^2	*s.o.f.*
P1 ($4f$)	0.0668(2)	0.0668(2)	0	0.0070(3)	0.5
O1 ($4f$)	0.3345(2)	0.3345(2)	0	0.0045(4)	0.5
N1 ($4f$)	0.3345(2)	0.3345(2)	0	0.0045(4)	0.5

[a] The site occupation factors ($s.o.f.$) for all atoms were set to 0.5 accounting for the split position of P and the mixed anion position of N and O, respectively.

Table C.3.: Interatomic distances (Å) and angles (°) of pc-PON based on Rietveld refinement ($p = 1$ atm).

P1–(N/O)1	1.6964(8)	(N/O)1–P1–(N/O)1	79.36(5)
P1–(N/O)1	1.7521(12)	(N/O)1–P1–(N/O)1	104.93(5)
P1–(N/O)1	2.6263(12)	(N/O)1–P1–(N/O)1	180

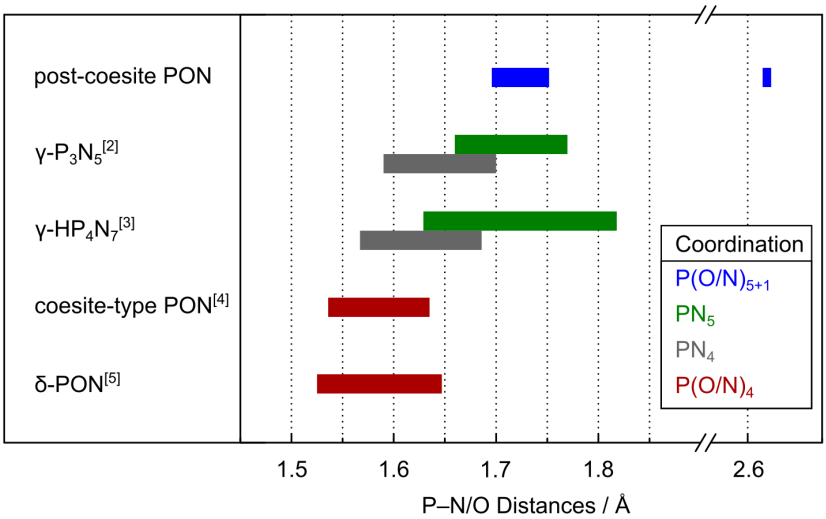

Figure C.3.: Bar chart of interatomic distances between P and N/O in pc-PON and related compounds.[35–39]

Table C.4.: Calculated X-ray densities of selected SiO_2 and PON phases. The calculated X-ray density of pc-PON was determined to 3.843 g·cm^{-3} corresponding to an increase of 20.1 % relative to coe-PON and 42.2 % to cri-PON, thus, pc-PON represents the densest PON phase so far.[36,38] However, the increase in density upon transition is less than reported for the respective SiO_2 phases (48.2 and 85.1 %), which may be attributable to the sixfold coordination of Si in stishovite, resulting in a significant higher density.[40–42]

	Cristobalite	**Coesite**	**Stishovite**	**cri-PON**	**coe-PON**	**pc-PON**
Density / g·cm^{-3}	2.318	2.896	4.291	2.702	3.200	3.843
Ref.	[40]	[41]	[42]	[36]	[38]	this work

TEM and EDX measurements

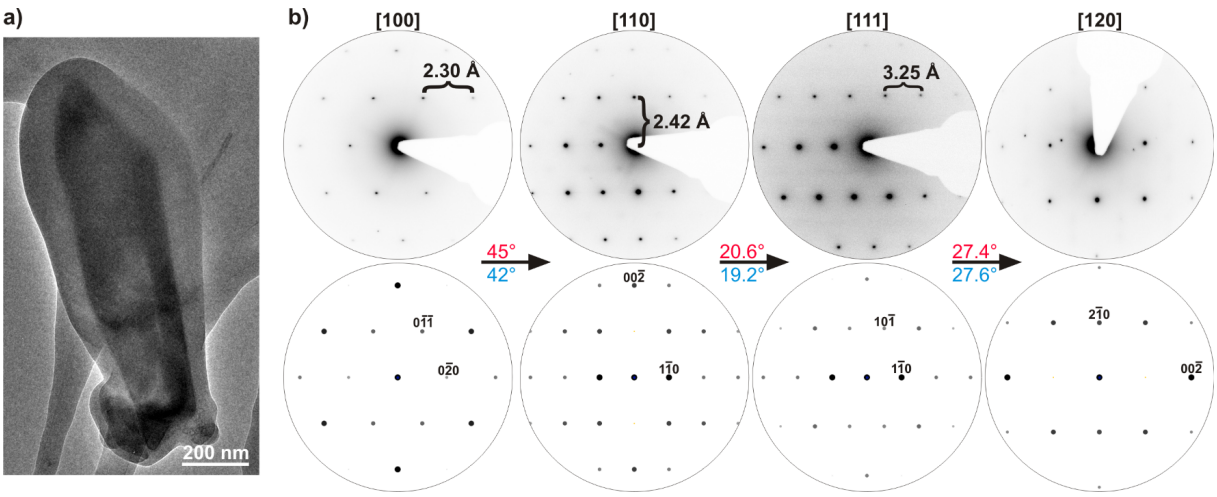

Figure C.4.: Bright-field image of pc-PON crystallite (a). SAED-tilting series (b, top) with corresponding simulations (b, bottom) with tilting angles (experimental blue, simulated red) and exemplarily indexed reflections. Simulations based on structural data, obtained from PXRD refinement (structure model in space group $P4_2/mnm$ with $a = 4.627\,82(10)$ Å and $c = 2.460\,42(4)$ Å). D-values directly measured from SAED patterns: $d_{020} = 2.30$ Å, $d_{001} = 2.42$ Å and $d_{110} = 3.25$ Å.

Table C.5.: TEM-EDX measurements (300 kV) of pc-PON in atom-%, showing no other elements than P, O and N in the sample. The measured atomic ratio, within the standard deviations and the precision of the methods for light elements, is close to P : O : N= 1 : 1 : 1.

	1	2	3	4	5	6	7	mean value	ideal value
P	43.1	41.0	41.6	42.7	35.5	40.2	42.2	40.9(26)	33.0
O	30.8	31.7	31.0	32.2	29.8	31.7	31.2	31.0(9)	33.0
N	26.1	27.3	27.4	25.1	34.7	28.1	27.6	28.0(31)	33.0

^{31}P solid-state NMR and FTIR measurements of pc-PON

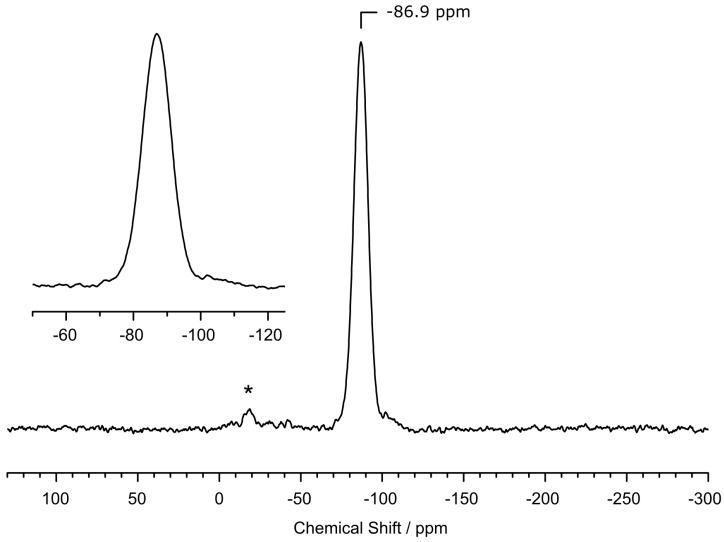

Figure C.5.: ^{31}P solid-state MAS NMR spectrum of pc-PON ($B_0 = 11.7\,\mathrm{T}$, $\nu(^{31}\mathrm{P}) = 202.5\,\mathrm{MHz}$, $\nu_{\mathrm{rot}} = 50\,\mathrm{kHz}$) showing one broadened signal at $\delta = -86.9\,\mathrm{ppm}$ ($\Delta\nu_{\mathrm{FWHM}} = 20\,\mathrm{ppm}$), which can be assigned to the one crystallographic position of P in the pc-PON structure. Peak broadening can be caused by varying local N/O coordination of P and has been observed in other PON modifications as well.[38,39] A statistic occupation of the split position of P may enhance peak broadening in this case. The marked signal at $\delta = -17\,\mathrm{ppm}$ (*) can be assigned to a minor contamination of γ-HP_4N_7.[35]

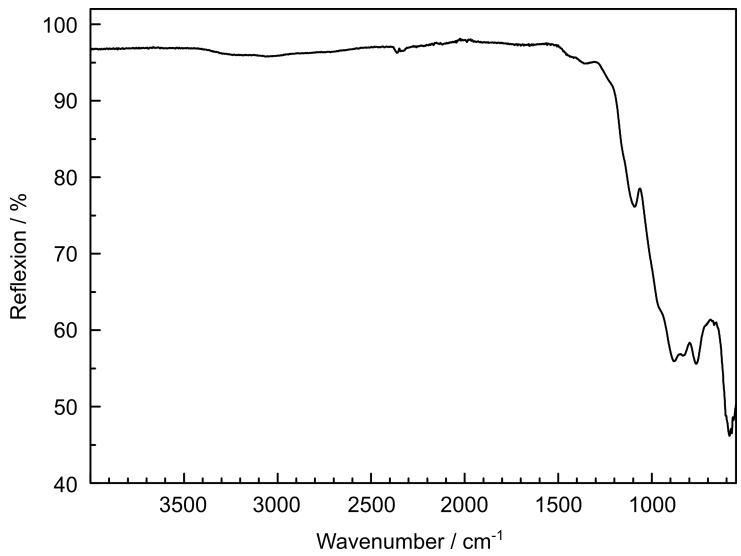

Figure C.6.: FTIR spectra of pc-PON (ATR). In contrast to H–P–N compounds (e.g. HPN_2, HP_4N_7) pc-PON does not show any significant signals in the region 2300–3300 cm^{-1}, which indicates the absence of N–H and O–H bonds in the PON sample.[35,41,43–46]

Crystal structure of pc-PON from single-crystal XRD at 1.8 GPa

Table C.6.: Crystallographic data on pc-PON based on single-crystal refinement ($p = 1.8$ GPa).

Formula	**PON**
Crystal system	tetragonal
Space group (no.)	$P4_2/mnm$ (136)
Lattice parameters / Å	$a = 4.6027(3)$
	$c = 2.4560(3)$
Cell volume / Å^3	$V = 52.030(9)$
Formula units per cell	2
Calculated X-ray density / g·cm^{-3}	3.892
Linear absorption coefficient / cm^{-1}	1.8
Device	PETRA III, DESY
Radiation	Synchrotron ($\lambda = 0.288\,74$ Å)
θ-range / °	2.542–17.163
Temperature / K	293
Number of observed reflections	244
Independent reflections ($> 2\sigma$)	113 (100)
Number of parameters	9
$F(000)$	60
Residual electron density / e·Å^{-3}	0.602; −0.601
R indices	$R_{\text{int}} = 0.0463$;
	$R_\sigma = 0.0513$;
	$R1 = 0.0513(> 2\sigma)$;
	$wR2 = 0.1110(> 2\sigma)$;
	$R1 = 0.0577$ (all data);
	$wR2 = 0.1169$ (all data);
Goodness of fit	1.343

Table C.7.: Refined atomic coordinates, isotropic displacement parameters and site occupation factors ($s.o.f.$) in pc-PON based on single-crystal refinement ($p = 1.8$ GPa).

	x	y	z	U_{eq} / Å^2	*s.o.f.*
P1 ($4f$)	0.0661(2)	0.0661(2)	0	0.0094(3)	0.5
O1 ($4f$)	0.3325(3)	0.3325(3)	0	0.0139(4)	0.5
N1 ($4f$)	0.3325(3)	0.3325(3)	0	0.0139(4)	0.5

Table C.8.: Anisotropic displacement parameters (Å^2) of pc-PON based on single-crystal refinement ($p = 1.8$ GPa).

	U_{11}	U_{22}	U_{33}	U_{23}	U_{13}	U_{12}
P1 ($4f$)	0.0105(4)	0.0105(4)	0.0072(5)	0	0	−0.0008(3)
O1 ($4f$)	0.0164(6)	0.0164(6)	0.0089(7)	0	0	−0.0027(6)
N1 ($4f$)	0.0164(6)	0.0164(6)	0.0089(7)	0	0	−0.0027(6)

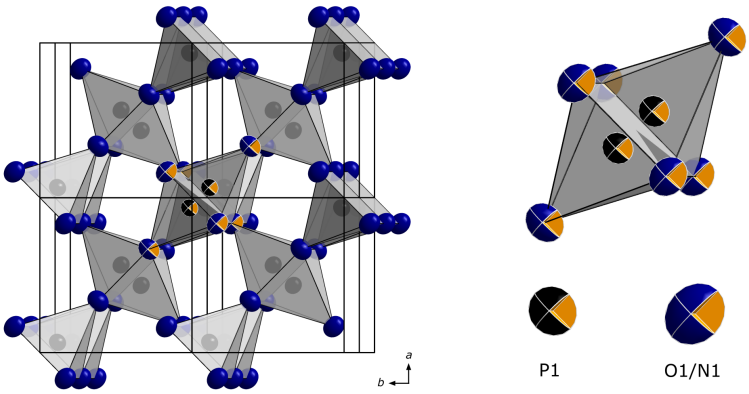

Figure C.7.: Crystal structure of pc-PON from single-crystal structure refinement. Ellipsoids are displayed at 90 % probability level. P: black, N,O: blue.

Table C.9.: Interatomic distances (Å) and angles (°) of pc-PON based on single-crystal refinement ($p = 1.8$ GPa).

P1–(N/O)1	1.6976(14)	(N/O)1–P1–(N/O)1	79.92(8)
P1–(N/O)1	1.7341(21)	(N/O)1–P1–(N/O)1	104.68(8)
P1–(N/O)1	2.5946(21)	(N/O)1–P1–(N/O)1	180

Table C.10.: Comparison of crystallographic data of pc-PON from powder and single-crystal X-ray refinements.

Formula	**PON**	
Crystal system	tetragonal	
Space group (no.)	$P4_2/mnm$ (136)	
Lattice parameters / Å	$a = 4.62782(10)$	$a = 4.6027(3)$
	$c = 2.46042(4)$	$c = 2.4560(3)$
Cell volume / Å^3	$V = 52.694(4)$	$V = 52.030(9)$
Z	2	
Sample	Powder	Single-crystal
Radiation source	Mo-Kα_1	Synchrotron
Wavelength / Å	0.71073	0.28874
Obs. indep. reflections	97	113
θ-range / °	1.000–38.177	2.542–17.163
Resolution / Å	0.57	0.49
Temperature / K	293	
Pressure / GPa	10^{-4}	1.8
Goodness of fit	1.327	1.343
CSD deposition number	433717	434035

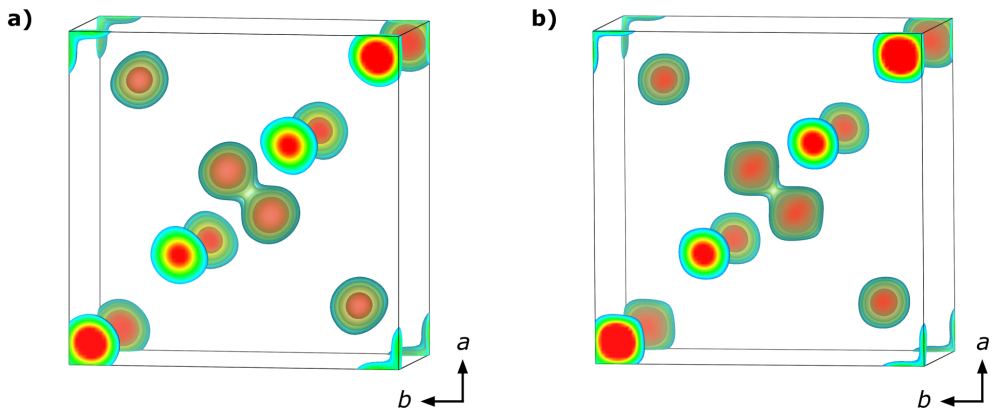

Figure C.8.: Isosurfaces of the electron density for pc-PON based on PXRD (a) and single-crystal XRD refinement (b), indicating that both refinements are tantamount in quality and accuracy. Isosurface levels are 20, 13, 9, and 6 electron·a_0^{-3}, respectively (a_0 = Bohr radius).

High-pressure PXRD patterns of pc- and o-PON from synchrotron measurements

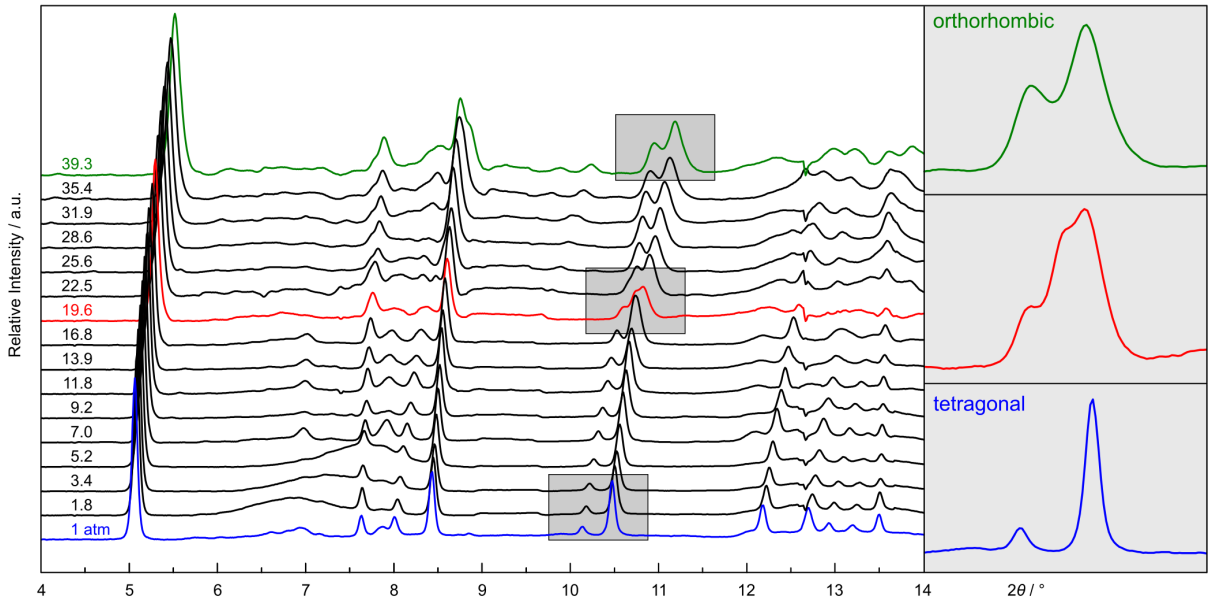

Figure C.9.: Pressure-dependent powder X-ray diffraction patterns from synchrotron measurements (λ = 0.288 74 Å) showing two different types of pattern. Corresponding pressures (GPa) are given on the left side. The pc-PON structure (blue pattern) seems to be preserved up to ca. 20 GPa. At higher pressures, however, a new phase is observed (green pattern), as the reflections in the region $10.0° < 2\theta < 11.5°$ change significantly. At 19.6 GPa the phases coexist, as both types of pattern superpose (red pattern). The regions of interest are highlighted and enlarged on the right side. The broad signals in the range $6° < 2\theta < 9°$ up to 5.2 GPa can be assigned to a liquid neon phase in the DAC.

Temperature-dependent PXRD of pc-PON

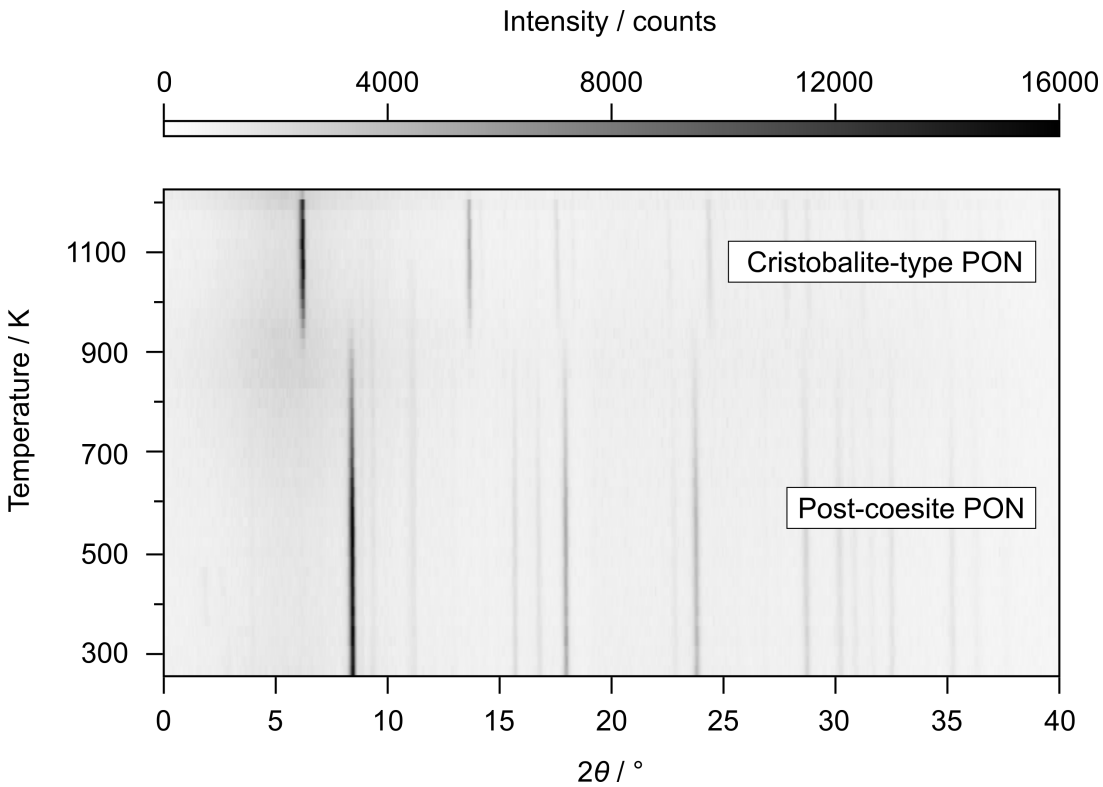

Figure C.10.: Temperature-dependent X-ray diffraction patterns from pc-PON (Mo-Kα_1, $\lambda = 0.71073$ Å) collected in steps of 20 K. At ca. 900 K phase transition to cri-PON is observed, proving pc-PON to be metastable at ambient conditions.

Tetragonal to orthorhombic phase transition in PON, spontaneous strain formalism

To compare the nature of the phase transition from tetragonal to orthorhombic symmetry in PON to SiO_2, it is described in terms of spontaneous strains as reported in former works for SiO_2.[47] Therefore, the lattice parameters of the pc-PON ($P4_2/mnm$, high-symmetry phase) are extrapolated into the pressure regime of o-PON (*Pnnm*, low-symmetry phase). Hereby, symmetry-breaking (*sb*) and non-symmetry-breaking (*nsb*) elements of the spontaneous strain are distinguished.[48,49] The respective non-zero components ε_{11sb}, ε_{22sb}, ε_{11nsb}, ε_{22nsb}, ε_{33nsb} and V_S are calculated according to equations C.2–C.5 where a_0, c_0 and V_0 corresponds to the extrapolated parameters of the tetragonal phase and a, b, c and V to those of the orthorhombic one.

$$\varepsilon_{11sb} = -\varepsilon_{22sb} = (a-b)/2a_0 \tag{C.2}$$

$$\varepsilon_{11nsb} = \varepsilon_{22nsb} = (a+b)/2a_0 - 1 \tag{C.3}$$

$$\varepsilon_{33nsb} = c/c_0 - 1 \tag{C.4}$$

$$V_S = V/V_0 - 1 \tag{C.5}$$

Figure C.11 illustrates the calculated spontaneous strain components and the volume strain V_S. An evaluation of the observed phase transition in terms of spontaneous strain is justified as the relation $V_S = \varepsilon_{11nsb} + \varepsilon_{33nsb}$ is almost preserved in the whole pressure range. The non-symmetry-breaking elements of the spontaneous strain ε_{11nsb}, ε_{22nsb}, ε_{33nsb} as well as the volume strain V_S remain small in the whole pressure range. The symmetry-breaking components ε_{11sb} and ε_{22sb}, however, show the largest magnitude by far. Almost identical results were obtained for rutile-type ($P4_2/mnm$) $\rightarrow$ $CaCl_2$-type (*Pnnm*) phase transition in SiO_2 corroborating the kinship of both compounds. Although, we were not able to extract any structural information on o-PON, the mechanism of phase transition seems to be similar to the one observed in SiO_2. Thus, one would expect a tilting of the P coordination polyhedra in the *a*-*b* plane with increasing pressure and a $CaCl_2$-related structure for o-PON.

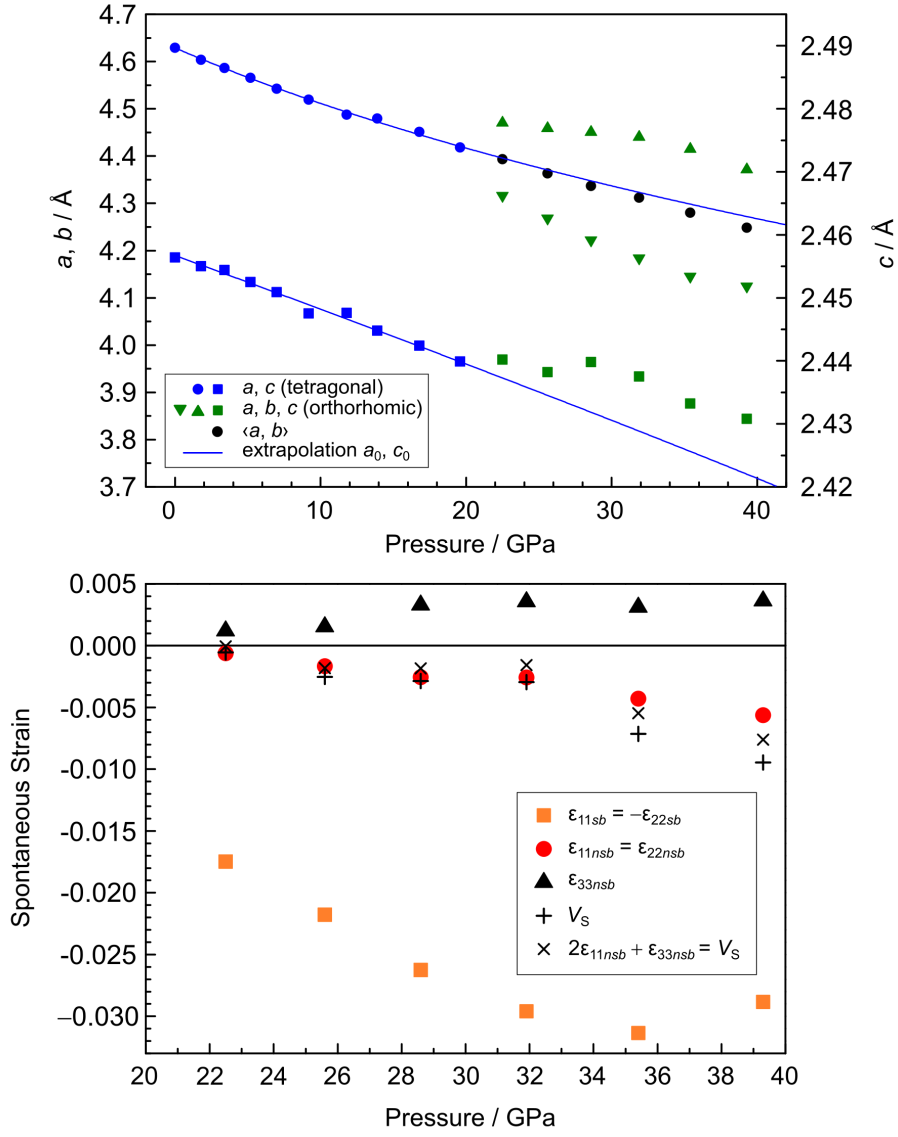

Figure C.11.: Evolution of the lattice parameters with pressure (top) and calculated symmetry-breaking (*sb*) and non-symmetry-breaking (*nsb*) components of spontaneous strain as a function of pressure with ε_{11sb} (orange) appearing the largest component (bottom).

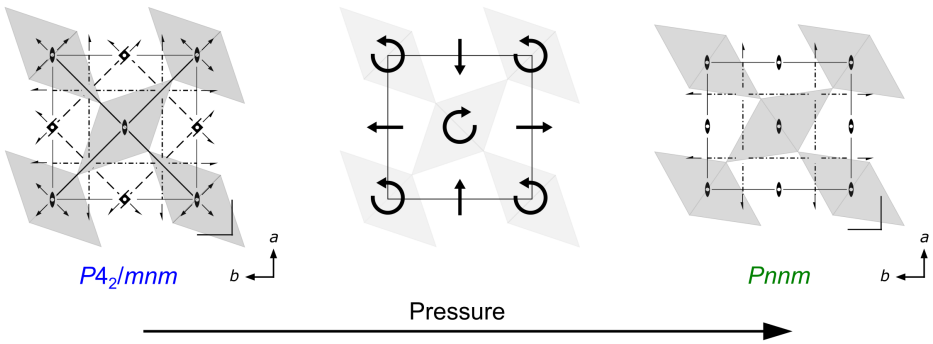

Figure C.12.: Schematic illustration of the stishovite → $CaCl_2$-type SiO_2 phase transition, which is characterized by an alternating tilting of the SiO_6 octahedra in the *a*-*b* plane. A similar mechanism is assumed for the tetragonal → orthorhombic phase transition in PON, considering reduction of symmetry and findings from spontaneous strain formalism.

Equation of states and elastic properties of pc-PON

In order to classify pc-PON on its elastic properties, equations of state were fitted using a second order Birch-Murnaghan equation with V_0 = 52.64(2) Å^3 and $K_0 = 163(2)$ GPa. Corresponding parameters refined from the calculated *p*-*V* data obtained from DFT calculations were determined to be $V_0 = 53.8(2)$ Å and $K_0 = 164(9)$ GPa. Keeping in mind that GGA based calculations typically show a systematic overestimation of the cell volume, the calculated data are in very good agreement with the experimental ones. A corresponding refinement of o-PON was not possible. Due to softening effects up to 30 GPa there are not enough reliable pressure points. Therefore, the as-refined equations of state of pc-PON are extrapolated to the pressure regime of o-PON (blue lines, Figure C.13). By analogy with stishovite and $CaCl_2$-type SiO_2 the orthorhombic phase (o-PON) appears slightly more compressible than the tetragonal one (pc-PON).[47] However, as only small deviations from the extrapolated equations of state are observed, one would expect a minor change of the bulk modulus upon transition.

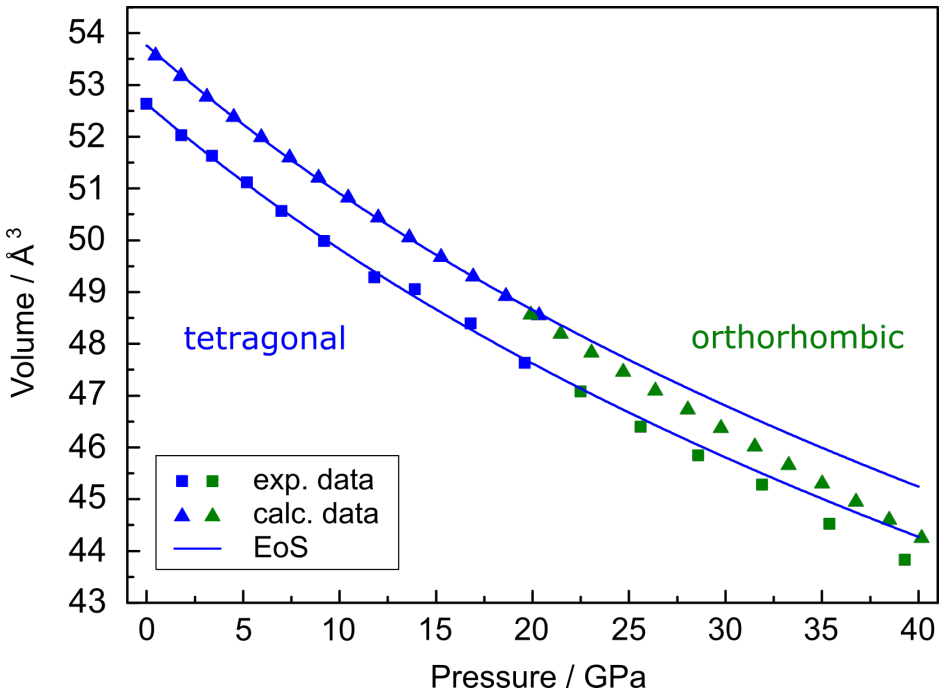

Figure C.13.: Experimental and calculated pressure points of tetragonal (blue) and o-PON (green) and extrapolated equations of state of pc-PON (blue lines).

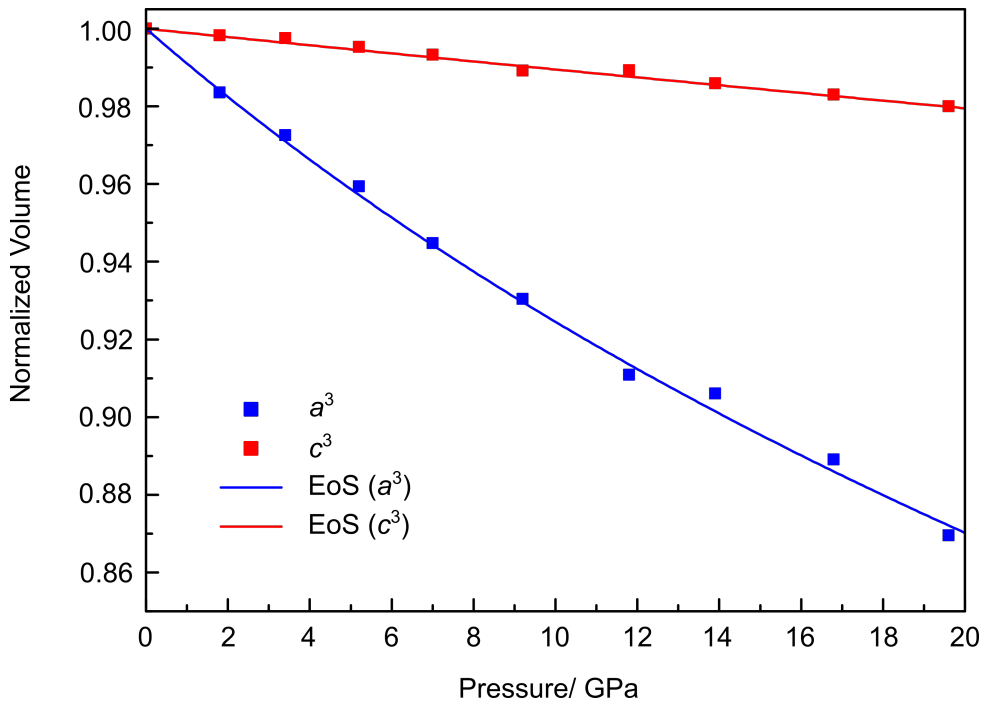

Figure C.14.: Pressure evolution of a^3 and c^3 in pc-PON and refined equations of state (second order Birch-Murnaghan) with $K_0(a^3) = 109(2)$ GPa and $K_0(c^3) = 927(35)$ GPa, respectively.

DFT calculations

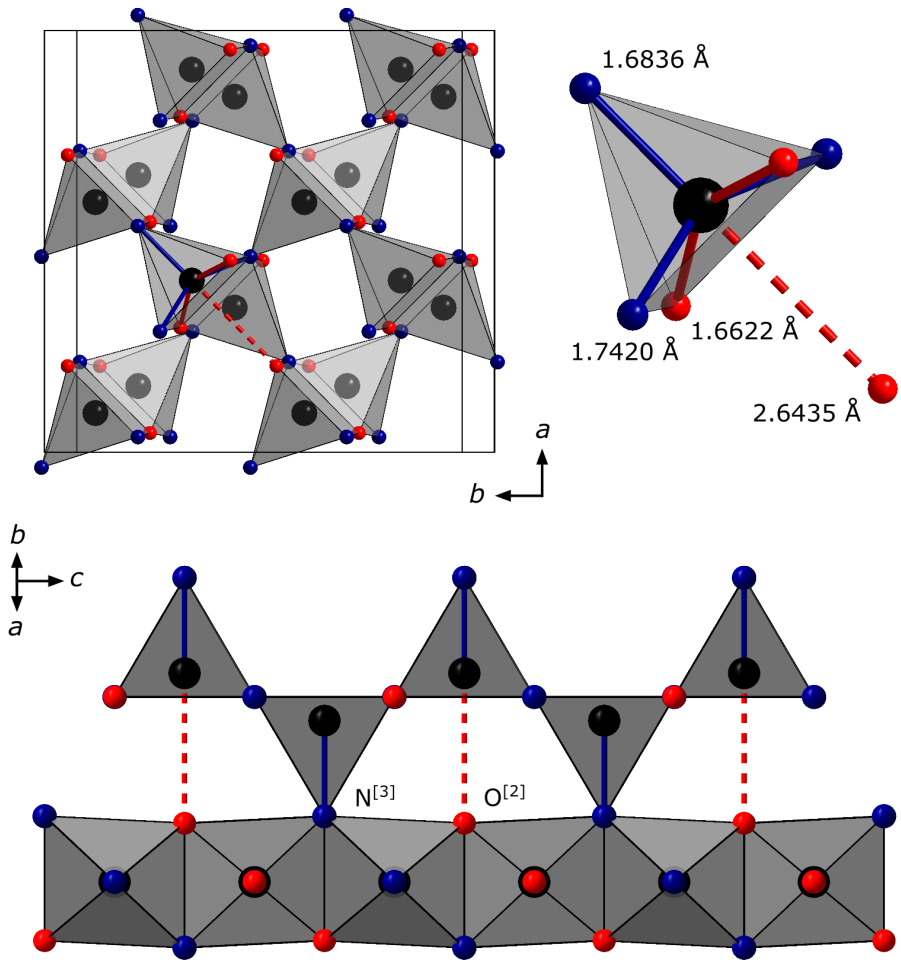

Figure C.15.: Structure model of pc-PON from structure relaxation with N/O-order used for DFT calculations (top). The alternating displacement of the P atoms appears as a coupled feature of the introduced N/O-ordering model resulting in $N^{[3]}$ and $O^{[2]}$, which are bound to three and two P atoms, respectively (bottom). P: black, O: red, N: blue.

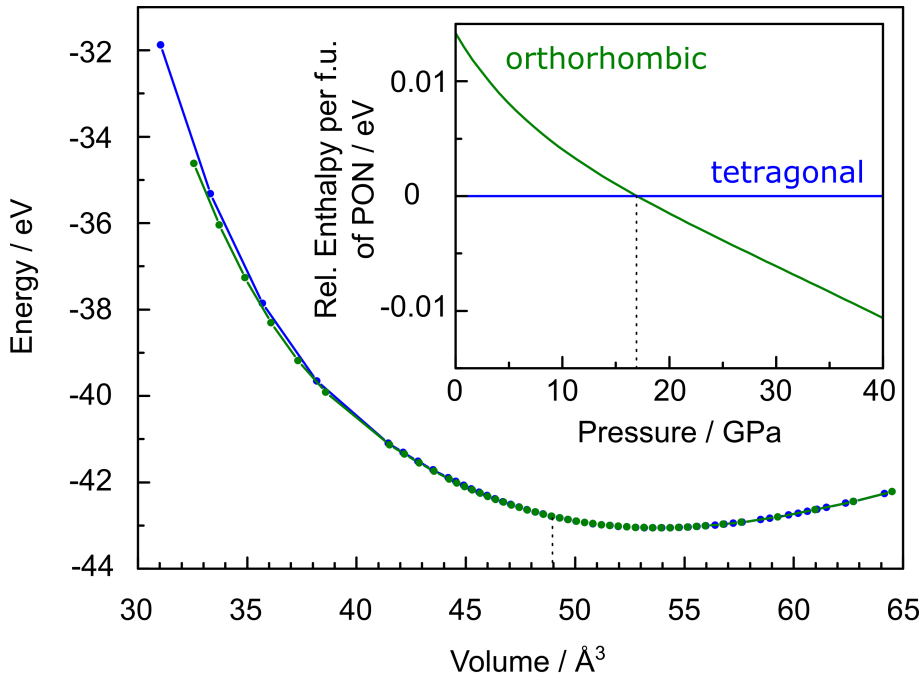

Figure C.16.: *E-V* curves of pc- (blue) and o-PON (green) from DFT calculations for two formulas of PON and relative enthalpy per formula unit of PON as a function of pressure with transition pressure of 17 GPa (inlay).

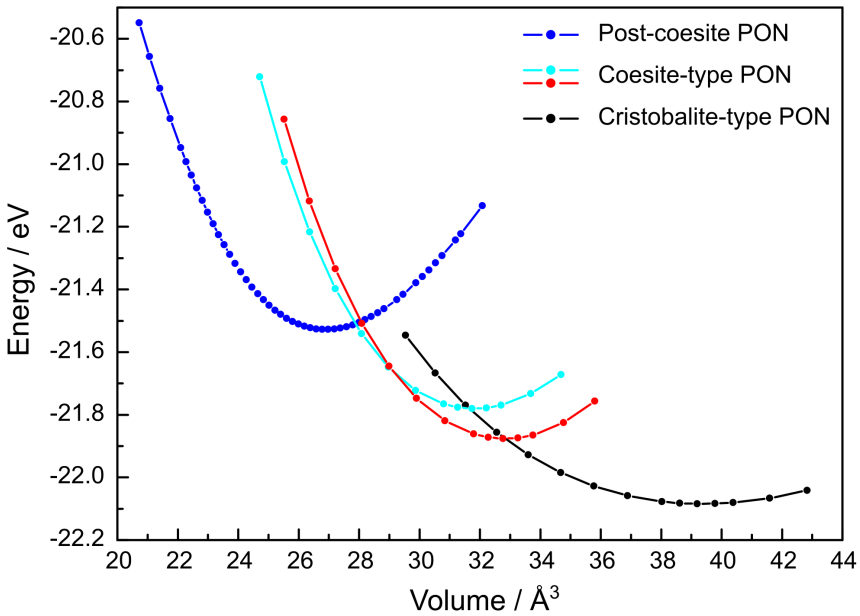

Figure C.17.: *E-V* curves of cri-, coe- and pc-PON from DFT calculations for one formula of PON.[38] The two curves of coe-PON correspond to two different N/O ordering models.

C.3. Author Contributions

S.V. Conceptualization: Supporting; Data curation: Lead; Formal analysis: Lead; Investigation: Lead; Validation: Equal; Visualization: Lead; Writing original draft: Lead; Writing review & editing: Equal

D.B. Conceptualization: Supporting; Formal analysis: Supporting; Investigation: Supporting; Validation: Supporting; Writing original draft: Supporting; Writing review & editing: Supporting

R.N. Formal analysis: Supporting; Investigation: Supporting; Validation: Supporting; Visualization: Supporting; Writing original draft: Supporting; Writing review & editing: Supporting

E.B. Data curation: Supporting; Formal analysis: Supporting; Investigation: Supporting; Validation: Supporting; Writing original draft: Supporting; Writing review & editing: Supporting

M.B. Data curation: Supporting; Formal analysis: Supporting; Investigation: Supporting; Validation: Supporting; Writing original draft: Supporting; Writing review & editing: Supporting

N.D. Funding acquisition: Equal; Investigation: Supporting; Methodology: Supporting; Project administration: Equal; Resources: Equal; Supervision: Equal; Validation: Equal; Writing original draft: Supporting; Writing review & editing: Supporting

L.D. Data curation: Supporting; Formal analysis: Supporting; Funding acquisition: Equal; Investigation: Supporting; Methodology: Supporting; Project administration: Equal; Resources: Equal; Supervision: Equal; Validation: Supporting; Writing original draft: Supporting; Writing review & editing: Supporting

W.S. Conceptualization: Lead; Funding acquisition: Lead; Project administration: Lead; Resources: Lead; Supervision: Lead; Validation: Equal; Writing original draft: Supporting; Writing review & editing: Equal

C.4. References

[1] A. Stock, B. Hoffmann, *"Die Einwirkung von Ammoniak auf Phosphorpentasulfid und der Phosphorstickstoff, P_3N_5"*, *Ber. Dtsch. Chem. Ges.* **1903**, *36*, 314.

[2] K. J. Kingma, R. E. G. Pacalo, P. F. McMillan, *"High-Pressure Stability of the Cristobalite Framework in PON and PN(NH)"*, *Eur. J. Solid State Inorg. Chem.* **1997**, *34*, 679.

[3] D. Walker, *"Lubrication, gasketing, and precision in multianvil experiments"*, *Am. Mineral.* **1991**, *76*, 1092.

[4] H. Huppertz, *"Multianvil high-pressure / high-temperature synthesis in solid state chemistry"*, *Z. Kristallogr.* **2004**, *219*, 330.

[5] A. A. Coelho, *"TOPAS-Academic Vers. 4.1"*, Brisbane, **2007**.

[6] A. A. Coelho, *"Indexing of powder diffraction patterns by iterative use of singular value decomposition"*, *J. Appl. Crystallogr.* **2003**, *36*, 86.

[7] G. S. Pawley, *"Unit-cell refinement from powder diffraction scans"*, *J. Appl. Crystallogr.* **1981**, *14*, 357.

[8] G. Oszlányi, A. Süto, *"The charge flipping algorithm"*, *Acta Crystallogr. A* **2008**, *64*, 123.

[9] G. Oszlányi, A. Süto, *"Ab initio structure solution by charge flipping. II. Use of weak reflections"*, *Acta Crystallogr. A* **2005**, *61*, 147.

[10] G. Oszlányi, A. Süto, *"Ab initio structure solution by charge flipping"*, *Acta Crystallogr. A* **2004**, *60*, 134.

[11] H. M. Rietveld, *"A profile refinement method for nuclear and magnetic structures"*, *J. Appl. Crystallogr.* **1969**, *2*, 65.

[12] R. W. Cheary, A. A. Coelho, J. P. Cline, *"Fundamental Parameters Line Profile Fitting in Laboratory Diffractometers"*, *J. Res. Natl. Inst. Stand. Technol.* **2004**, *109*, 1.

[13] Emispec Systems Inc., *"ES Vision, v4.0.164"*, Tempe, USA, **1994–2002**.

[14] Gatan Software Team, *"Digital Micrograph, v3.6.1: v3.6.1"*, Pleasanton, USA, **1999**.

[15] G. Kresse, J. Hafner, *"Ab initio molecular dynamics for liquid metals"*, *Phys. Rev. B: Condens. Matter Mater. Phys.* **1993**, *47*, 558.

[16] G. Kresse, J. Hafner, *"Ab initio molecular-dynamics simulation of the liquid-metal–amorphous-semiconductor transition in germanium"*, *Phys. Rev. B: Condens. Matter Mater. Phys.* **1994**, *49*, 14251.

[17] G. Kresse, J. Furthmüller, *"Efficiency of ab-initio total energy calculations for metals and semiconductors using a plane-wave basis set"*, *Comput. Mater. Sci.* **1996**, *6*, 15.

[18] J. P. Perdew, K. Burke, M. Ernzerhof, *"Generalized Gradient Approximation Made Simple"*, *Phys. Rev. Lett.* **1996**, *77*, 3865.

[19] J. P. Perdew, K. Burke, M. Ernzerhof, *"Generalized Gradient Approximation Made Simple"*, *Phys. Rev. Lett.* **1997**, *78*, 1396.

[20] P. E. Blöchl, *"Projector augmented-wave method"*, *Phys. Rev. B: Condens. Matter Mater. Phys.* **1994**, *50*, 17953.

[21] G. Kresse, Joubert, *"From ultrasoft pseudopotentials to the projector augmented-wave method"*, *Phys. Rev. B: Condens. Matter Mater. Phys.* **1999**, *59*, 1758.

[22] H. J. Monkhorst, J. d. Pack, *"Special points for Brillouin-zone integrations"*, *Phys. Rev. B: Condens. Matter Mater. Phys.* **1976**, *13*, 5188.

[23] I. Kantor, V. Prakapenka, A. Kantor, P. Dera, A. Kurnosov, S. Sinogeikin, N. Dubrovinskaia, L. Dubrovinsky, *"BX90: a new diamond anvil cell design for X-ray diffraction and optical measurements"*, *Rev. Sci. Instrum.* **2012**, *83*, 125102.

[24] H. P. Liermann, Z. Konôpková, W. Morgenroth, K. Glazyrin, J. Bednarčik, E. E. McBride, S. Petitgirard, J. T. Delitz, M. Wendt, Y. Bican, A. Ehnes, I. Schwark, A. Rothkirch, M. Tischer, J. Heuer, H. Schulte-Schrepping, T. Kracht, H. Franz, *"The Extreme Conditions Beamline P02.2 and the Extreme Conditions Science Infrastructure at PETRA III"*, *J. Synchrotron Radiat.* **2015**, *22*, 908.

[25] Rigaku Oxford Diffraction, *"CrysAlisPro Software system, version 1.171.37.35"*, Oxford, UK, **2014**.

[26] G. M. Sheldrick, *"SHELXT - integrated space-group and crystal-structure determination"*, *Acta Crystallogr. Sect. A: Found. Adv.* **2015**, *71*, 3.

[27] G. M. Sheldrick, *"A short history of SHELX"*, *Acta Crystallogr. Sect. A: Found. Adv.* **2008**, *64*, 112.

[28] H.-K. Mao, J. Xu, P. M. Bell, *"Calibration of the ruby pressure gauge to 800 kbar under quasi-hydrostatic conditions"*, *J. Geophys. Res.* **1986**, *91*, 4673.

[29] A. Dewaele, M. Torrent, P. Loubeyre, M. Mezouar, *"Compression curves of transition metals in the Mbar range: Experiments and projector augmented-wave calculations"*, *Phys. Rev. B: Condens. Matter Mater. Phys.* **2008**, *78*, 854.

[30] C. Prescher, V. B. Prakapenka, *"DIOPTAS: A program for reduction of two-dimensional X-ray diffraction data and data exploration"*, *High Pressure Res.* **2015**, *35*, 223.

[31] V. Petříček, M. Dušek, L. Palatinus, *"Crystallographic Computing System JANA2006: General features"*, *Z. Kristallogr. – Cryst. Mater.* **2014**, *229*, 345.

[32] F. D. Murnaghan, *"The compressibility of media under extreme pressures"*, *Proc. Natl. Acad. Sci. U.S.A.* **1944**, *30*, 244.

[33] F. Birch, *"Finite Elastic Strain of Cubic Crystals"*, *Phys. Rev.* **1947**, *71*, 809.

[34] J. Gonzalez-Platas, M. Alvaro, F. Nestola, R. Angel, *"EosFit7-GUI: A new graphical user interface for equation of state calculations, analyses and teaching"*, *J. Appl. Crystallogr.* **2016**, *49*, 1377.

[35] D. Baumann, W. Schnick, *"Pentacoordinate phosphorus in a high-pressure polymorph of phosphorus nitride imide $P_4N_6(NH)$"*, *Angew. Chem. Int. Ed.* **2014**, *53*, 14490; *Angew. Chem.* **2014**, *126*, 14718.

[36] L. Boukbir, R. Marchand, Y. Laurent, P. Bacher, G. Roult, *"Preparation and time-of-flight neutron diffraction study of the cristobalite-type PON phosphorus oxynitride"*, *Ann. Chim. Fr.* **1989**, *14*, 475.

[37] K. Landskron, H. Huppertz, J. Senker, W. Schnick, *"High-Pressure Synthesis of γ-P_3N_5 at 11 GPa and 1500 °C in a Multianvil Assembly: A Binary Phosphorus(V) Nitride with a Three-Dimensional Network Structure from PN_4 Tetrahedra and Tetragonal PN_5 Pyramids"*, *Angew. Chem. Int. Ed.* **2001**, *40*, 2643, *Angew. Chem.* **2001**, *113*, 2713.

[38] D. Baumann, R. Niklaus, W. Schnick, *"A high-pressure polymorph of phosphorus oxonitride with the coesite structure"*, *Angew. Chem. Int. Ed.* **2015**, *54*, 4388; *Angew. Chem.* **2015**, *127*, 4463.

[39] D. Baumann, S. J. Sedlmaier, W. Schnick, *"An unprecedented AB_2 tetrahedra network structure type in a high-pressure phase of phosphorus oxonitride (PON)"*, *Angew. Chem. Int. Ed.* **2012**, *51*, 4707; *Angew. Chem.* **2012**, *124*, 4784.

[40] T. Zoltai, M. J. Buerger, *"The crystal structure of coesite, the dense, high-pressure form of silica"*, *Z. Kristallogr.* **1959**, *111*, 129.

[41] H. Jacobs, R. Nymwegen, S. Doyle, T. Wroblewski, W. Kockelmann, *"Kristallines Phoshor(V)-nitrid-imid, HPN_2 bzw. DPN_2 - Strukturbestimmung mit Röntgen-, Synchrotron- und Neutronenstrahlung"*, *Z. Anorg. Allg. Chem.* **1997**, *623*, 1467.

[42] W. Sinclair, A. E. Ringwood, *"Single crystal analysis of the structure of stishovite"*, *Nature* **1978**, *272*, 714.

[43] W. Schnick, J. Lücke, *"Darstellung, Kristallstruktur und IR-spektroskopische Untersuchung von Phosphor(V)-nitrid-imid, HPN_2"*, *Z. Anorg. Allg. Chem.* **1992**, *610*, 121.

[44] S. Horstmann, E. Irran, W. Schnick, *"Phosphor(V)-nitrid α-P_3N_5: Synthese ausgehend von Tetraaminophosphoniumiodid und Kristallstrukturaufklärung mittels Synchrotron-Pulver-Röntgenbeugung"*, *Z. Anorg. Allg. Chem.* **1998**, *624*, 620.

[45] S. Horstmann, E. Irran, W. Schnick, *"Phosphorus(V) Nitride Imide HP_4N_7: Synthesis from a Molecular Precursor and Structure Determination with Synchrotron Powder diffraction"*, *Angew. Chem. Int. Ed. Engl.* **1997**, *36*, 1992; *Angew. Chem.* **1997**, *109*, 2085.

[46] D. Baumann, W. Schnick, *"High-pressure polymorph of phosphorus nitride imide HP_4N_7 representing a new framework topology"*, *Inorg. Chem.* **2014**, *53*, 7977.

[47] D. Andrault, R. J. Angel, J. L. Mosenfelder, T. Le Bihan, *"Equation of state of stishovite to lower mantle pressures"*, *Am. Mineral.* **2003**, *88*, 301.

[48] M. A. Carpenter, E. K. Salje, *"Elastic anomalies in minerals due to structural phase transitions"*, *Eur. J. Mineral.* **1998**, *10*, 693.

[49] M. A. Carpenter, R. J. Hemley, H.-K. Mao, *"High-pressure elasticity of stishovite and the $P4_2/mnm \rightleftharpoons Pnnm$ phase transition"*, *J. Geophys. Res. B: Solid Earth* **2000**, *105*, 10807.

D. Supporting Information for Chapter 6

Boron Phosphorus Nitride at Extremes: PN_6 Octahedra in the High-Pressure Polymorph β-BP_3N_6

Sebastian Vogel, Maxim Bykov, Elena Bykova, Sebastian Wendl, Simon D. Kloß, Anna Pakhomova, Stella Chariton, Egor Koemets, Natalia Dubrovinskaia, Leonid Dubrovinsky, and Wolfgang Schnick

Angew. Chem. Int. Ed. **2019**, *58*, 9060;

Angew. Chem. **2019**, *131*, 9158.

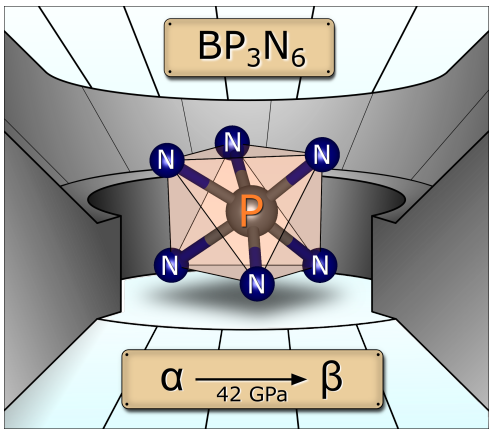

Abstract The high-pressure behavior of non-metal nitrides is of special interest for inorganic and theoretical chemistry as well as materials science, as these compounds feature intriguing elastic properties. The double nitride α-BP_3N_6 was investigated by in situ single-crystal X-ray diffraction (XRD) upon cold compression to a maximum pressure of about 42 GPa, and its isothermal bulk modulus at ambient conditions was determined to be 146(6) GPa. At maximum pressure the sample was laser-heated, which resulted in the formation of an unprecedented high-pressure polymorph, β-BP_3N_6. Its structure was elucidated by single-crystal XRD, and can be described as a decoration of a distorted hexagonal close packing of N with B in tetrahedral and P in octahedral voids. Hence, β-BP_3N_6 is the first nitride to contain PN_6 octahedra, representing the much sought-after proof of principle for sixfold N-coordinated P that has been predicted for numerous high-pressure phases of nitrides.

D.1. Experimental Procedures

Multianvil synthesis of α-BP_3N_6

Single-crystals of α-BP_3N_6 were synthesized according to Vogel et al., starting from $(PNCl_2)_3$, NH_4N_3 and h-BN in a high-pressure high-temperature reaction in a 1000 t hydraulic press (Voggenreiter, Mainleus) using the multianvil technique and a modified Walker-type module.[1–3] In a glovebox ($<$ 1 ppm O_2, H_2O; MBraun) stoichiometric amounts of the starting materials and an additional amount of NH_4Cl (25 wt-%) were ground and packed tightly into a crucible of h-BN (Henze, Kempten), which was closed with a lid of h-BN. The crucible was surrounded by two graphite furnaces and a ZrO_2 sleeve (Cesima Ceramics, Wust-Fischbeck) acting as a thermal insulator. The as-described sample was centered in a drilled through octahedron (5 % Cr_2O_3-doped MgO, 18 mm edge length, Ceramic Substrates & Components Ltd, Isle of Wight) using two MgO spacers (Cesima Ceramics, Wust-Fischbeck) and contacted using two Mo plates from both sides. The octahedron was placed in the center of eight Co-doped WC cubes with truncated edges (7 % Co, 11 mm edge length, Hawedia, Marklkofen), which were separated by pyrophyllite gaskets. The assembly was compressed to 8 GPa and the sample was heated to 1100 °C within 1 h. The temperature was kept constant for 5 h, before the sample was allowed to cool down to ambient temperature within 1 h. After subsequent slow decompression the recovered sample was washed with de-ionized water and α-BP_3N_6 was obtained as colorless, block-like single-crystals (Figure D.1). Energy-dispersive X-ray (EDX) spectroscopy was performed as chemical analysis (Table D.1).

Scanning electron microscopy and energy-dispersive X-ray spectroscopy

Scanning electron microscopy (SEM) and energy-dispersive X-ray (EDX) spectroscopy was performed on a Helios Nanolab G3 UC (FEI, Hillsboro), which was equipped with a X-Max 80 SDD detector (Oxford Instruments, Abingdon). For data collection and analysis the Aztec software was used.[4] To ensure electrical conductivity of the sample, it was coated with carbon using an electron beam evaporator (BAL-TEC MED 020, Bal Tec AG).

Synchrotron measurements and data analysis

In situ XRD measurements were carried out at the Extreme Conditions Beamline P02.2 (PETRA III) at the Deutsches Elektronen-Synchrotron (DESY, Hamburg).[5] The X-ray beam ($\lambda = 0.2894$ Å) was

focused to $1.4\times1.8\,\mu m^2$ ($V \times H$) by a Kirkpatrick-Baez mirror system and diffraction patterns were collected on a PerkinElmer XRD 1621 flat-panel detector. W served as an internal pressure standard. Powder X-ray diffraction patterns of W were obtained from wide scans ($\omega_{max} = \pm20°$; $t_{exposure} = 20\,s$) by masking diamond reflections and radial integration using the Dioptas software.[6] Lattice parameters of W were refined using the TOPAS Academic software (Pawley method) and pressures were determined on the basis of W equation of states.[7–9]

Single-crystal data of α- and β-BP_3N_6 were collected by ω scans ($\omega_{max} = \pm38°$; $\Delta\omega = 0.5°$; $t_{exposure} =$ 1–10 s), using 25/50 µm Pt filters for α-BP_3N_6 in the pressure range of $2.9(1)\,GPa \leq p \leq 42.4(1)\,GPa$ (Table D.2). The dataset of pressure-quenched β-BP_3N_6 was collected at ambient pressure without any filters. Due to the beam intensity varying temporality during data collection at ambient pressure (technical issue of the storage ring), datasets appear of poor quality as discussed in the manuscript and below. High-pressure data sets were not affected by this technical issue. Data analysis was performed using the CrysAlisPro software.[10] Due to fragmentation of the single-crystals, the laser heated sample showed multiple crystalline phases and domains as illustrated in Figure D.6. Using the reciprocal space viewer (Ewald Explorer, CrysAlisPro) reflections were grouped manually for separate indexing. As the indexed domains showed only few overlapped reflections, data sets were integrated independently. For integration of the ambient-pressure dataset of β-BP_3N_6 a filter for R_{int} (30 %) was applied. For instrument model calibration of CrysAlisPro (sample-to-detector distance, the detector's origin, offsets of the goniometer angles and rotation of the X-ray beam and the detector around the instrument axis) a single-crystal of an orthoenstatite ($(Mg_{1.93},Fe_{0.06})(Si_{1.93},Al_{0.06})O_6$, *Pbca*, $a = 8.8117(2)$, $b = 5.18320(10)$, $c = 18.2391(3)$ Å), was used.

Pressure-dependent XRD data of α-BP_3N_6 were solved independently at each pressure point using the SHELXT algorithm and structure refinement was performed with SHELXL in isotropic approximation against F^2 on all data by the full-matrix least squares algorithm.[11,12] The β-BP_3N_6 structure at 42.4(1) GPa was solved with SHELXT and refined in isotropic approximation against F^2 on all data by full-matrix least squares with SHELXL.[11,12] The structure model at ambient pressure was refined by full-matrix least squares using the high-pressure model as a starting point. Owing to a low number of observed reflections, the atomic displacement parameters of the P and N atoms were constrained to one common parameter, respectively. A refinement of the unknown monoclinic cell reported below (Figure D.6) was not feasible on the basis of the collected data.

Laser-heated diamond anvil cell

High-pressure experiments were carried out using a BX90 diamond anvil cell, which was equipped with two Boehler-Almax-type diamond anvils (250 µm culet) separated by a Re gasket.[13] The gasket was pre-indented to 30 µm and laser-drilled to an inner diameter of 100 µm. Ne was used as a pressure-transmitting medium and W served as an internal pressure standard. The cell was loaded with two single crystals of α-BP_3N_6 and compressed to an initial pressure of 2.9(1) GPa (Figure D.4). After cold compression to a maximum pressure of 42.4(1) GPa, the sample was heated from one side using a focused NIR fiber laser ($\lambda = 1070$ nm, $10\times10\,\mu m^2$). After a 3 s flash the laser was turned off and the sample was allowed to cool down to ambient temperature before single-crystal XRD data were collected (Figure D.5). Owing to a very short heating period, the maximum temperature was not measured.

Equation of state

The pressure-dependent evolution of the unit cell volume of α-BP_3N_6 ($2.9(1)\,\text{GPa} \leq p \leq 42.4(1)\,\text{GPa}$) was described by a second order Birch-Murnaghan equation of state (Equation D.1) using the EoSFit7 software.[14–16] Herein, the pressure p is described as a function of cell volume V with V_0 corresponding to the cell volume at a theoretical pressure of zero and K_0 representing the isothermal bulk modulus.

$$p(V) = \frac{3}{2}K_0\left[\left(\frac{V}{V_0}\right)^{-\frac{7}{3}} - \left(\frac{V}{V_0}\right)^{-\frac{5}{3}}\right] \tag{D.1}$$

Minimal bonding ellipsoids (MBE)

Each coordination polyhedra can be described as an ellipsoid with the ligands occupying its surface, when a displacement from the centre of the central atom is considered.[17] The so-called minimal bonding ellipsoid (MBE) is characterized by its radii $R1$, $R2$, and $R3$ with mean radius $\langle R\rangle$ and standard deviation $\sigma(R)$, the latter providing information on the distortion of the ellipsoid itself. The shape parameter S indicates oblate ($S < 0$), regular ($S \approx 0$) and prolate ($S > 0$) shape of the coordination polyhedra and the respective centre displacement of the central atom is given as a scalar. Herein, MBE analysis was used to quantify the distortions of the B/N and P/N polyhedra and fitting was performed using the PIEFACE software.[17]

D.2. Results and Discussion

Data on α-BP_3N_6

Table D.1.: From EDX measurements (atom-%) the atomic ratio B : P : N was calculated to 1.1(1) : 3.0(1) : 5.5(1), which is in good agreement with the nominal ratio of BP_3N_6.[1] Trace amounts of O were not considered, as they are most likely attributable to surface hydrolysis of the crystals.[1]

	C1	C2	C3	C4	C5	Average	Normalized ratio
B	11 %	11 %	12 %	11 %	11 %	11(1) %	1.1(1)
P	31 %	30 %	30 %	31 %	32 %	31(1) %	3.0(1)
N	57 %	57 %	56 %	56 %	57 %	57(1) %	5.5(1)
O	1 %	2 %	2 %	2 %	1 %	2(1) %	0.1(1)

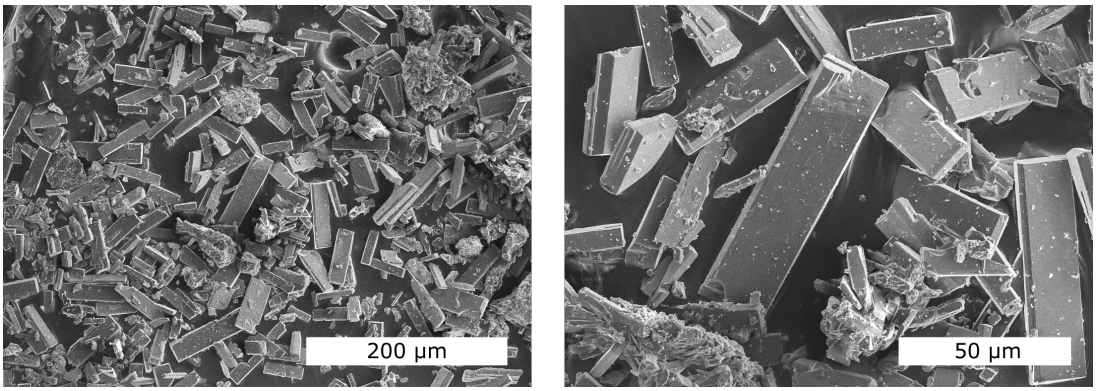

Figure D.1.: SEM images of a generic α-BP_3N_6 sample showing block-like single-crystals of α-BP_3N_6.[1]

Table D.2.: Crystallographic data of α-BP_3N_6 from single-crystal XRD refinements at ambient pressure[1] and $2.9(1)\,\text{GPa} \leq p \leq 42.4(1)\,\text{GPa}$.

Formula	**α-BP_3N_6**							
Pressure / GPa	0.00010(1)	2.9(1)	10.5(1)	11.3(1)	14.3(1)	26.1(1)	32.9(1)	42.4(1)
Crystal system	monoclinic							
Molecular weight / g·mol^{-1}	187.78							
Space group	$P2_1/c$ (no. 14)							
a / Å	5.0272(11)	5.0174(2)	4.9558(2)	4.9471(2)	4.9270(2)	4.8347(6)	4.7926(8)	4.7223(10)
b / Å	4.5306(12)	4.5192(1)	4.4602(1)	4.4513(1)	4.4319(1)	4.3484(2)	4.3145(3)	4.2614(4)
c / Å	17.332(3)	17.305(4)	17.076(4)	17.045(4)	16.971(3)	16.674(10)	16.545(14)	16.371(18)
β / °	106.387(9)	106.39(1)	106.49(2)	106.50(1)	106.53(1)	106.52(3)	106.51(5)	106.39(6)
Cell volume / Å^3	378.72(15)	376.45(9)	361.91(9)	359.89(8)	355.25(7)	336.1(2)	328.0(3)	316.1(4)
Formula units per cell	4							
Calculated X-ray density / g·cm^{-3}	3.293	3.313	3.446	3.466	3.511	3.711	3.802	3.946
Radiation	Mo-Kα ($\lambda = 0.71073$ Å)	Synchrotron ($\lambda = 0.28940$ Å)						
Device	Bruker D8 Venture	PETRA III, P02.2						
Filter / µm Pt	–	50	50	25	50	25	25	25
$F(000)$	368							
Observed reflections	7378	2254	2143	1960	1967	1868	1849	1777
Independent reflections ($> 2\sigma$)	1662 (1377)	1040 (972)	999 (967)	881 (853)	862 (821)	836 (792)	827 (772)	805 (755)
Number of parameters	91	42						
R_{int}	0.0482	0.0169	0.0227	0.0210	0.0202	0.0201	0.0218	0.0245
R_σ	0.0454	0.0227	0.0256	0.0239	0.0246	0.0221	0.0236	0.0261
$R1$ (all data)	0.0483	0.0328	0.0424	0.0372	0.0345	0.0431	0.0401	0.0460
$wR2$ (all data)	0.1001	0.0938	0.1137	0.1070	0.0993	0.1075	0.1016	0.1301
CSD	434784	1898720	1898716	1898723	1898724	1898717	1898721	1898718

Table D.3.: Interatomic T–N (T = B, P) distances (Å) occurring in α-BP_3N_6 from single-crystal XRD refinements at ambient pressure[1] and $2.9(1)\,\mathrm{GPa} \leq p \leq 42.4(1)\,\mathrm{GPa}$ as well as mean interatomic T–N distances for qualitative discussion. Standard deviations of mean interatomic T–N distances were calculated by averaging the respective standard deviations obtained from single-crystal XRD refinements.

Pressure / GPa	**0.00010(1)**	**2.9(1)**	**10.5(1)**	**11.3(1)**	**14.3(1)**	**26.1(1)**	**32.9(1)**	**42.4(1)**
P1–N6	1.5543(23)	1.5575(22)	1.5532(21)	1.5518(25)	1.5493(25)	1.5438(20)	1.5411(20)	1.5356(26)
N1	1.6564(18)	1.6566(18)	1.6405(19)	1.6408(22)	1.6348(20)	1.6166(21)	1.6089(23)	1.5986(32)
N3	1.6647(20)	1.6622(11)	1.6502(14)	1.6469(15)	1.6446(14)	1.6288(14)	1.6207(35)	1.6100(19)
N3	1.6658(20)	1.6665(32)	1.6515(32)	1.6501(34)	1.6462(34)	1.6323(35)	1.6223(14)	1.6135(51)
P2–N5	1.5676(18)	1.5706(27)	1.5628(27)	1.5686(28)	1.5678(27)	1.5540(28)	1.5523(29)	1.5517(42)
N6	1.5830(24)	1.5846(35)	1.5790(34)	1.5765(36)	1.5763(36)	1.5643(35)	1.5596(36)	1.5536(51)
N2	1.6719(20)	1.6685(13)	1.6527(16)	1.6516(17)	1.6487(16)	1.6310(16)	1.6259(15)	1.6160(21)
N1	1.6734(20)	1.6723(14)	1.6610(15)	1.6587(19)	1.6530(15)	1.6381(15)	1.6316(16)	1.6232(21)
P3–N5	1.5449(19)	1.5456(14)	1.5415(14)	1.5402(14)	1.5391(14)	1.5311(14)	1.5286(14)	1.5214(18)
N2	1.6558(18)	1.6548(17)	1.6408(18)	1.6401(21)	1.6353(19)	1.6188(19)	1.6107(21)	1.5997(29)
N4	1.6627(19)	1.6630(22)	1.6501(22)	1.6479(26)	1.6440(23)	1.6273(26)	1.6220(32)	1.6116(34)
N4	1.6747(18)	1.6703(28)	1.6544(29)	1.6557(31)	1.6505(31)	1.6308(31)	1.6232(25)	1.6164(46)
B1–N4	1.5473(34)	1.5376(44)	1.5209(55)	1.5160(57)	1.5090(56)	1.4855(56)	1.4698(55)	1.4597(75)
N3	1.5706(28)	1.5704(38)	1.5434(47)	1.5414(48)	1.5353(48)	1.5104(47)	1.5070(47)	1.4902(64)
N2	1.5735(30)	1.5714(23)	1.5553(23)	1.5529(29)	1.5460(26)	1.5231(26)	1.5150(26)	1.4978(25)
N1	1.5846(29)	1.5798(19)	1.5590(22)	1.5567(25)	1.5527(21)	1.5235(20)	1.5156(20)	1.5029(32)
Mean P–N	1.631(2)	1.631(2)	1.620(2)	1.619(3)	1.616(3)	1.601(3)	1.596(3)	1.588(4)
Mean B–N	1.569(3)	1.565(3)	1.545(4)	1.542(4)	1.536(4)	1.511(4)	1.502(4)	1.488(5)

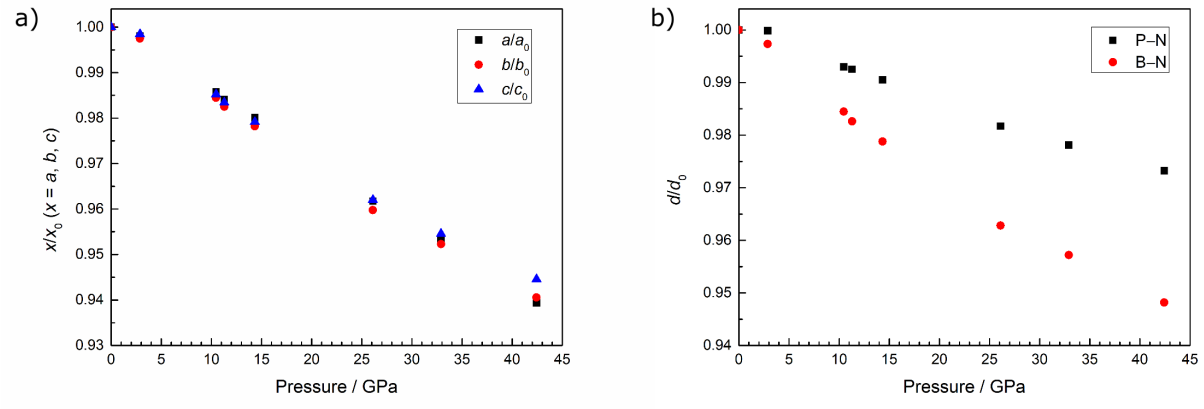

Figure D.2.: Uniform contraction of lattice parameters in α-BP_3N_6 upon pressure loading (a) and pressure-dependent evolution of mean interatomic P–N and B–N distances in α-BP_3N_6 as reported in Table D.3 (b).[1]

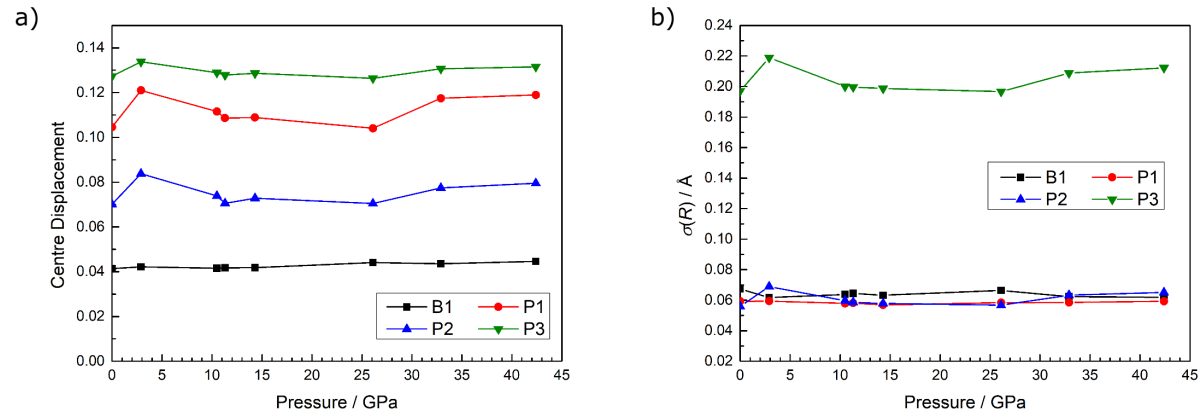

Figure D.3.: Pressure-dependent centre displacement (a) and $\sigma(R)$ (b) of the TN$_4$ tetrahedra (T = B, P) in α-BP_3N_6 obtained from MBE analysis.[1,17] Only small changes in centre displacement and $\sigma(R)$ indicate an isotropic contraction of the TN$_4$ tetrahedra upon pressure load without a significant change in distortion.

Table D.4.: Pressure-dependent ellipsoidal parameters of the MBE analyses of α-BP_3N_6 as partially illustrated in Figure D.3.[1,17]

	Pressure / GPa	$R1$	$R2$	$R3$	$\langle R \rangle$	σR	S	Centre Displacement	Coordination
B1	0.00010(1)	1.661	1.531	1.509	1.567	0.067	0.065	0.041	4
	2.9(1)	1.563	1.483	1.412	1.486	0.062	0.004	0.042	4
	10.5(1)	1.623	1.502	1.477	1.534	0.064	0.058	0.042	4
	11.3(1)	1.634	1.506	1.490	1.543	0.065	0.068	0.042	4
	14.3(1)	1.629	1.506	1.486	1.540	0.063	0.062	0.042	4
	26.1(1)	1.656	1.525	1.507	1.563	0.066	0.067	0.044	4
	32.9(1)	1.593	1.490	1.444	1.509	0.062	0.034	0.044	4
	42.4(1)	1.581	1.488	1.431	1.500	0.062	0.021	0.045	4
P1	0.00010(1)	1.705	1.630	1.560	1.632	0.059	0.002	0.105	4
	2.9(1)	1.668	1.545	1.539	1.584	0.059	0.070	0.121	4
	10.5(1)	1.692	1.598	1.553	1.614	0.058	0.028	0.112	4
	11.3(1)	1.696	1.607	1.555	1.620	0.058	0.020	0.109	4
	14.3(1)	1.694	1.605	1.556	1.618	0.057	0.022	0.109	4
	26.1(1)	1.706	1.628	1.563	1.632	0.058	0.006	0.104	4
	32.9(1)	1.682	1.569	1.549	1.600	0.058	0.054	0.117	4
	42.4(1)	1.677	1.558	1.545	1.593	0.059	0.062	0.119	4
P2	0.00010(1)	1.688	1.627	1.551	1.622	0.056	−0.010	0.070	4
	2.9(1)	1.674	1.566	1.508	1.583	0.069	0.029	0.084	4
	10.5(1)	1.685	1.602	1.540	1.609	0.060	0.010	0.074	4
	11.3(1)	1.685	1.608	1.542	1.612	0.059	0.005	0.071	4
	14.3(1)	1.684	1.608	1.543	1.612	0.058	0.005	0.073	4
	26.1(1)	1.690	1.625	1.551	1.622	0.057	−0.007	0.070	4
	32.9(1)	1.677	1.583	1.523	1.594	0.063	0.018	0.077	4
	42.4(1)	1.675	1.576	1.517	1.589	0.065	0.022	0.080	4
P3	0.00010(1)	0.187	1.593	1.391	1.618	0.197	0.022	0.127	4
	2.9(1)	1.829	1.579	1.293	1.567	0.219	−0.045	0.134	4
	10.5(1)	1.849	1.592	1.360	1.600	0.200	−0.007	0.129	4
	11.3(1)	1.856	1.591	1.368	1.605	0.200	0.003	0.128	4
	14.3(1)	1.853	1.594	1.366	1.604	0.199	−0.003	0.129	4
	26.1(1)	1.869	1.594	1.389	1.617	0.197	0.019	0.126	4
	32.9(1)	1.839	1.583	1.328	1.583	0.209	−0.022	0.131	4
	42.4(1)	1.835	1.581	1.315	1.577	0.212	−0.030	0.132	4

α-BP_3N_6 $\longrightarrow$ β-BP_3N_6 phase transition

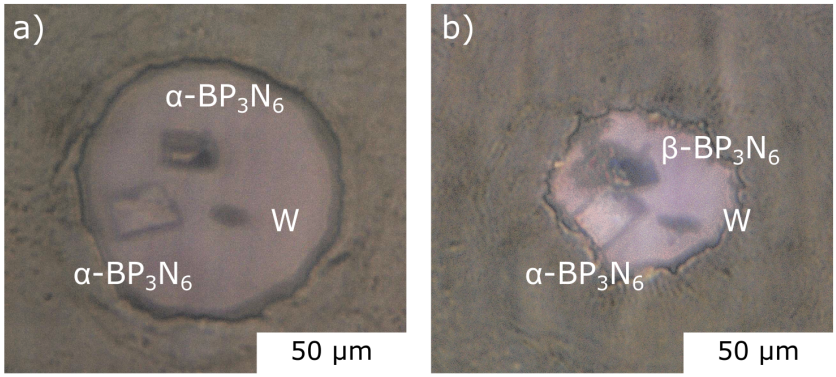

Figure D.4.: Microphotographs of BX90 DAC (250 µm culet, Re gasket) loaded with W and two crystals of α-BP_3N_6 at 2.9(1) GPa (a), and temperature- and pressure-quenched sample at ambient conditions, which had been laser heated at 42.4(1) GPa (b).

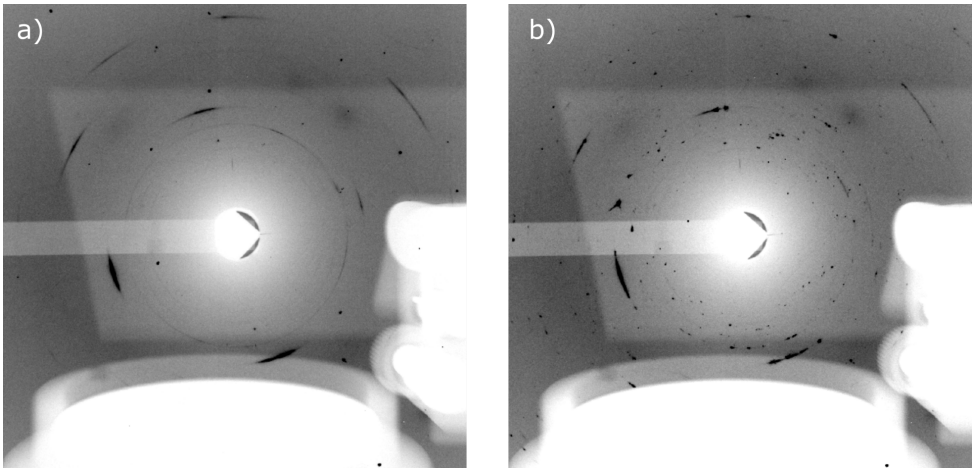

Figure D.5.: X-ray diffraction pattern ($\omega_{max} = 0$; $t_{exposure} = 2$ s) of the BP_3N_6 sample before (a, α-BP_3N_6, single-crystal), and after on-line laser heating at 42.4(1) GPa (b, crystalline multi-phase grains including domains of β-BP_3N_6).

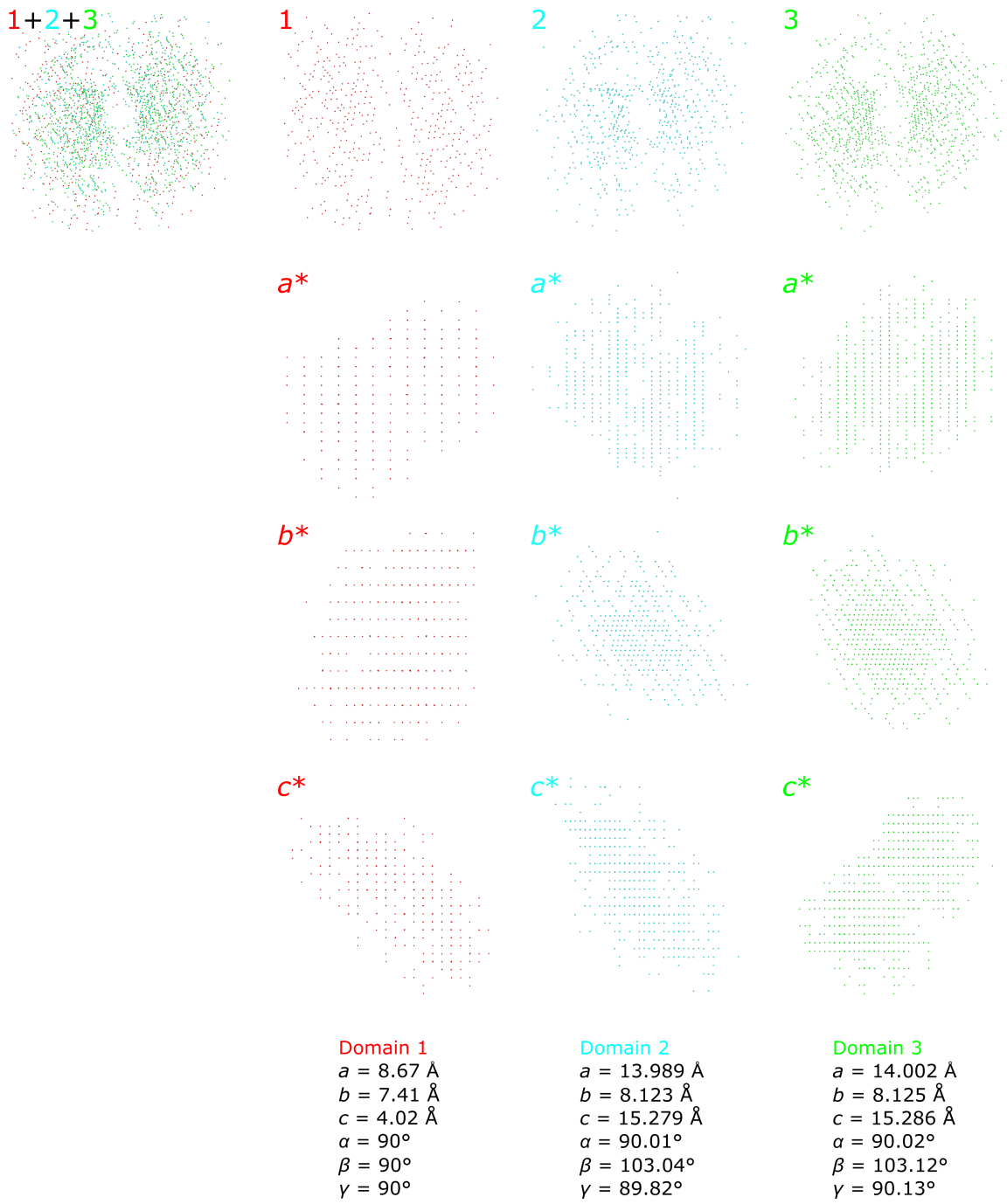

Figure D.6.: The screenshots of a generic indexed XRD data set (Ewald Explorer, CrysAlisPro) show the three major domains of a crystalline multi-phase grain, which formed upon laser heating at 42.4(1) GPa.[10] Analysis of several XRD data sets suggested the formation of two previously unknown phases with orthorhombic (domain 1; β-BP_3N_6) and monoclinic metrics (domain 2, 3), respectively. Datasets of the monoclinic cell, however, could not be refined and thus, this phase is not discussed within this manuscript.

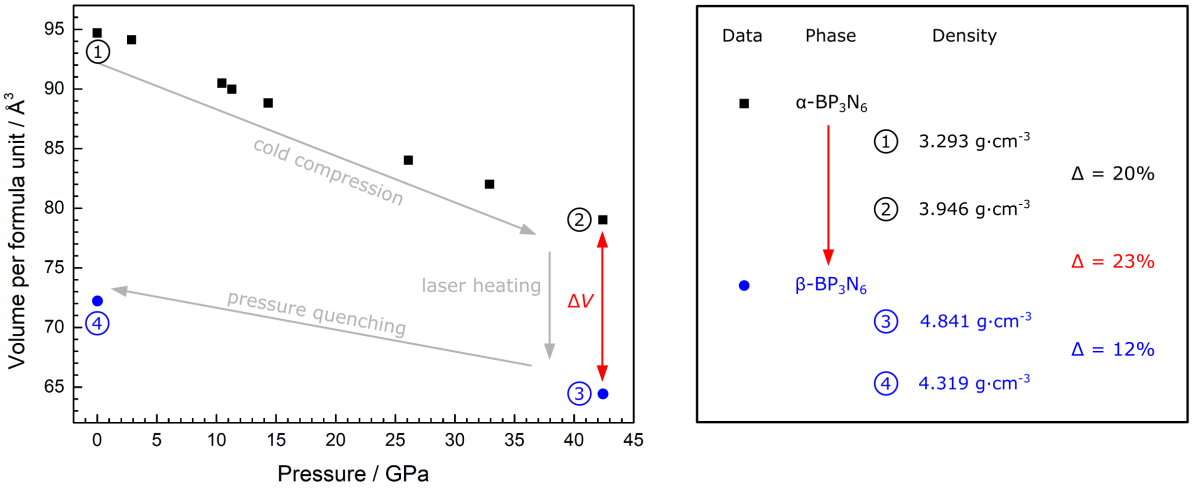

Figure D.7.: The α-$BP_3N_6 \longrightarrow \beta$-$BP_3N_6$ phase transition is characterized by a significant decrease in volume (23 %) and can be classified as a 1st order phase transition (reconstructive). Densities of selected pressure points are provided in the legend.

Data on β-BP_3N_6

Single-crystal XRD refinements

Table D.5.: Crystallographic data of β-BP_3N_6 at 42.4(1) GPa and ambient pressure from single-crystal XRD refinements. Owing to a low number of observed reflections at ambient pressure, the atomic displacement parameters of P and N were constrained to one common parameter, respectively.

Formula	**β-BP_3N_6**	
Pressure / GPa	42.4(1)	0.00010(1)
Crystal system	orthorhombic	
Molecular weight / g·mol^{-1}	187.78	
Space group	$Pna2_1$ (no. 33)	
Lattice parameters / Å	$a = 8.6666(10)$	$a = 8.992(2)$
	$b = 7.411(4)$	$b = 7.685(9)$
	$c = 4.0115(4)$	$c = 4.1787(11)$
Cell volume / Å^3	257.65(14)	288.8(4)
Formula units per cell	4	
Calculated X-ray density / g·cm^{-3}	4.841	4.319
Linear absorption coefficient / cm^{-1}	0.217	0.194
Radiation	Synchrotron ($\lambda = 0.28940$ Å)	
Device	PETRA III, P02.2	
θ-range / °	$1.91 < \theta < 18.36$	$1.84 < \theta < 9.24$
h,k,l range	$-14 \leq h \leq 14$	$-9 \leq h \leq 9$
	$-7 \leq k \leq 6$	$-5 \leq k \leq 3$
	$-6 \leq l \leq 6$	$-4 \leq l \leq 4$
$F(000)$	368	
Observed reflections	1265	217
Independent reflections ($> 2\sigma$)	771 (710)	162 (114)
Constraints	0	7
Number of parameters	41	34
R_{int}; R_σ	0.0653; 0.0617	0.0673; 0.0760
Final R indices ($I > 2\sigma(I)$)	$R1 = 0.0755$; $wR2 = 0.2026$	$R1 = 0.0767$; $wR2 = 0.1964$
Final R indices (all data)	$R1 = 0.0794$; $wR2 = 0.2114$	$R1 = 0.0878$; $wR2 = 0.2142$
Goodness of fit	1.121	1.003
Flack parameter x[a]	$-1.5(10)$	$-2.1(10)$
Residual electron density / eÅ^{-3}	1.614; -2.431	0.842; -0.825
CSD	1898722	1898719

[a]Owing to low Friedel pair coverage the Flack parameter could not be refined reliably.

Table D.6.: Fractional coordinates and isotropic atomic displacement parameters of β-BP_3N_6 at 42.4(1) GPa from single-crystal XRD refinement. All atoms occupy the general position with Wyckoff no. 4*a*.

Atom	***x***	***y***	***z***	U_{iso} / Å^2
P1	0.11000(13)	0.3881(4)	0.7550(4)	0.0045(3)
P2	0.37349(15)	0.2577(4)	0.2469(3)	0.0045(3)
P3	0.11308(13)	0.0672(4)	0.2372(4)	0.0043(3)
B1	0.2075(7)	0.5774(18)	0.1805(15)	0.0064(11)
N1	0.0523(5)	0.5808(12)	0.0090(13)	0.0051(8)
N2	0.2946(5)	0.0730(13)	0.0409(12)	0.0040(8)
N3	0.2088(5)	0.2308(14)	0.5109(12)	0.0056(8)
N4	0.2791(5)	0.4181(13)	0.0000(14)	0.0059(8)
N5	0.0345(5)	0.2385(13)	0.0151(13)	0.0061(8)
N6	0.4549(6)	0.4168(14)	0.4705(14)	0.0062(8)

Table D.7.: Fractional coordinates and isotropic atomic displacement parameters of β-BP_3N_6 at ambient pressure from single-crystal XRD refinement. All atoms occupy the general position with Wyckoff no. 4*a* and isotropic displacement parameters of P and N were constrained to one common parameter, respectively.

Atom	***x***	***y***	***z***	U_{iso} / Å^2
P1	0.1100(6)	0.389(2)	0.766(2)	0.010(2)
P2	0.3731(5)	0.258(2)	0.247(2)	0.010(2)
P3	0.1127(6)	0.066(2)	0.237(2)	0.010(2)
B1	0.211(3)	0.567(7)	0.205(10)	0.018(9)
N1	0.054(2)	0.591(6)	0.024(6)	0.010(3)
N2	0.291(2)	0.081(5)	0.057(6)	0.010(3)
N3	0.208(2)	0.234(7)	0.520(6)	0.010(3)
N4	0.279(2)	0.407(6)	0.002(6)	0.010(3)
N5	0.035(2)	0.246(7)	0.024(5)	0.010(3)
N6	0.453(2)	0.416(7)	0.461(5)	0.010(3)

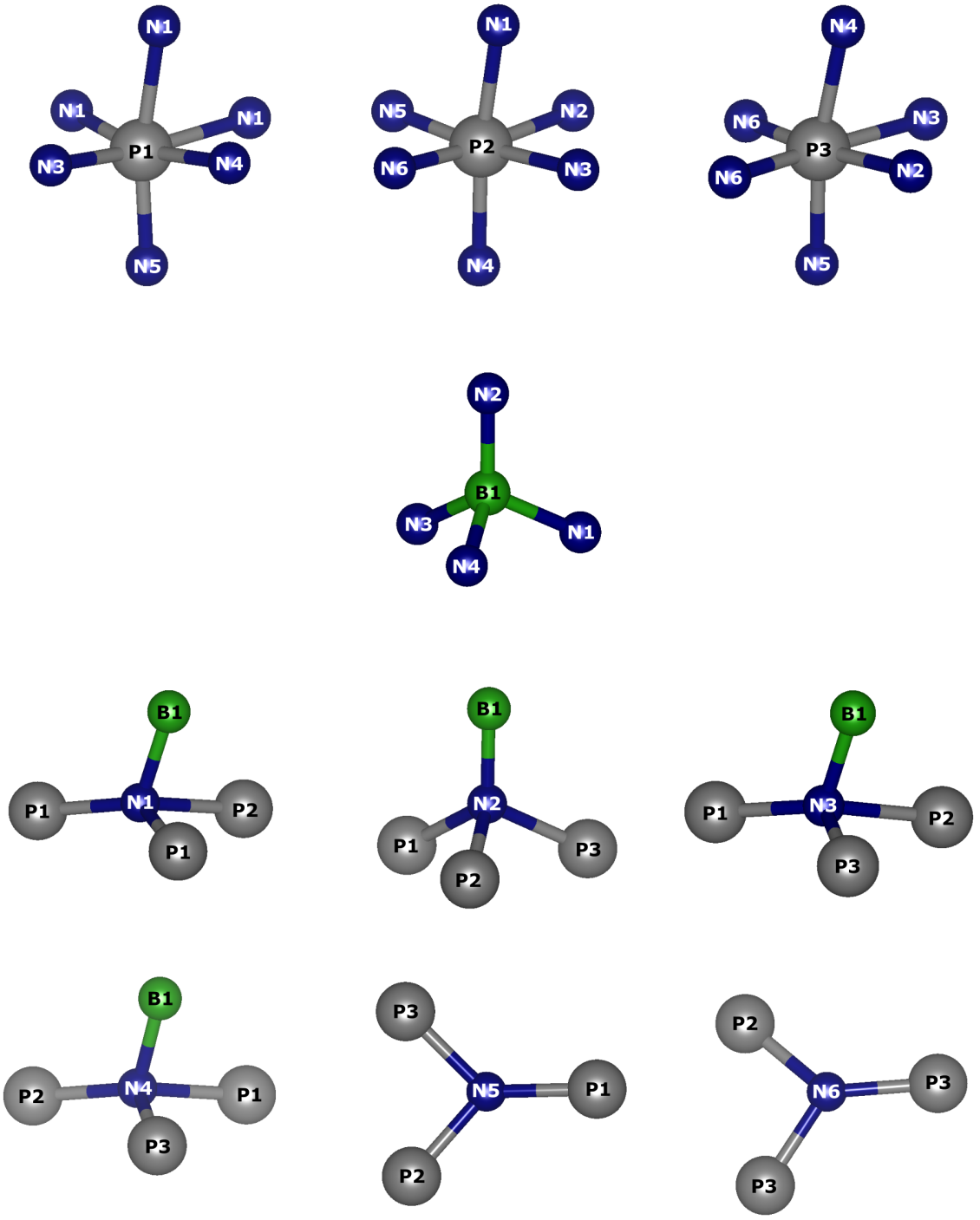

Figure D.8.: Coordination polyhedra of all atom sites in β-BP_3N_6 at 42.4(1) GPa. Phosphorus (gray) and boron (green) are in six- and fourfold N coordination, respectively. N (blue) is found in four- and threefold coordination of P and B as represented by the Niggli formula $^{3}_{\infty}\left[B^{[4]}P^{[6]}{}_3N^{[4]}{}_4N^{[3]}{}_2\right]$.

Table D.8.: Interatomic T–N (T = B, P) distances (Å) occurring in β-BP_3N_6 at 42.4(1) GPa and ambient pressure from single-crystal refinement with standard deviations given in brackets. High standard deviations at ambient pressure are attributable to the lack of high-quality single-crystal data at this pressure point. Standard deviations of mean interatomic T–N distances were calculated by averaging the respective standard deviations obtained from single-crystal XRD refinements.

Pressure / GPa	**42.4(1)**	**0.00010(1)**
P1–N5	1.657(8)	1.68(4)
N1	1.734(5)	1.79(2)
N3	1.747(8)	1.80(4)
N4	1.779(5)	1.82(2)
N2	1.816(8)	1.93(3)
N1	1.824(8)	1.95(4)
P2–N6	1.641(9)	1.67(4)
N5	1.677(5)	1.73(2)
N2	1.739(9)	1.74(4)
N4	1.750(8)	1.75(4)
N3	1.788(5)	1.88(2)
N1	1.799(8)	1.85(4)
P3–N6	1.654(8)	1.72(2)
N6	1.664(6)	1.73(4)
N5	1.694(8)	1.79(5)
N2	1.760(5)	1.78(2)
N4	1.790(8)	1.91(4)
N3	1.834(8)	1.95(4)
B1–N2	1.446(8)	1.47(5)
N3	1.511(14)	1.67(7)
N1	1.511(8)	1.61(4)
N4	1.518(14)	1.61(6)
Mean P–N	1.74(1)	1.81(4)
Mean B–N	1.50(1)	1.59(6)

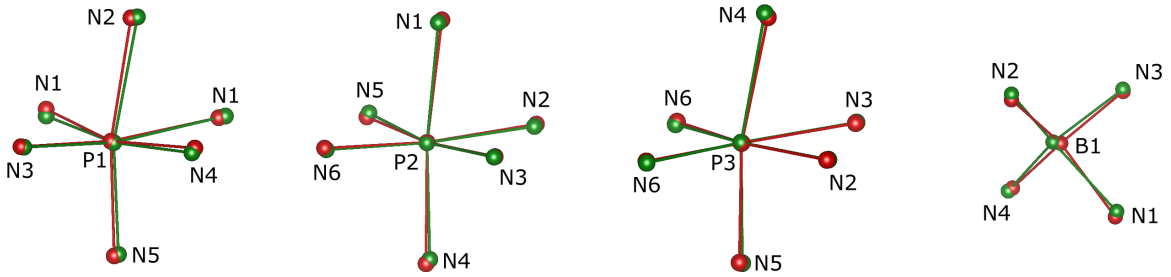

Figure D.9.: The overlay of the coordination polyhedra in β-BP_3N_6 at 42.4(1) GPa (red) and ambient pressure (green) show no significant changes upon pressurequenching. Elongated interatomic distances are not apparent from this illustration, as the unit cell parameters were normalized to those at 42.4(1) GPa to visualize relative distortions. B, P and N atoms are displayed as spheres 0.6 Å in diameter.

Table D.9.: Interatomic angles (°) occurring in β-BP_3N_6 obtained from single-crystal refinement at 42.4(1) GPa.

N5–P1–N1	97.3(3)	N6–P2–N5	86.2(3)	N6–P3–N6	96.8(3)	N2–B1–N3	118.2(5)
N5–P1–N3	95.7(3)	N6–P2–N2	173.9(3)	N6–P3–N5	91.2(4)	N2–B1–N1	116.4(5)
N5–P1–N4	93.5(3)	N6–P2–N4	91.3(3)	N6–P3–N2	92.6(3)	N2–B1–N4	117.7(5)
N5–P1–N2	169.2(3)	N6–P2–N3	95.7(3)	N6–P3–N4	98.7(3)	N3–B1–N1	102.1(5)
N5–P1–N1	93.7(3)	N6–P2–N1	92.9(4)	N6–P3–N3	173.8(3)	N3–B1–N4	100.0(9)
N1–P1–N3	99.6(3)	N5–P2–N2	94.4(3)	N6–P3–N5	84.9(3)	N1–B1–N4	99.2(5)
N1–P1–N4	165.1(2)	N5–P2–N4	93.7(3)	N6–P3–N2	170.5(3)		
N1–P1–N2	90.0(3)	N5–P2–N3	173.8(2)	N6–P3–N4	98.2(3)		
N1–P1–N1	89.5(3)	N5–P2–N1	92.2(3)	N6–P3–N3	89.4(3)		
N3–P1–N4	89.4(3)	N2–P2–N4	94.7(4)	N5–P3–N2	96.1(3)		
N3–P1–N2	90.9(3)	N2–P2–N3	83.1(3)	N5–P3–N4	169.1(3)		
N3–P1–N1	165.9(3)	N2–P2–N1	81.1(3)	N5–P3–N3	90.1(3)		
N4–P1–N2	78.0(3)	N4–P2–N3	92.2(3)	N2–P3–N4	79.2(2)		
N4–P1–N1	79.6(3)	N4–P2–N1	173.0(3)	N2–P3–N3	81.2(2)		
N2–P1–N1	78.4(3)	N3–P2–N1	81.8(3)	N4–P3–N3	79.6(3)		

Table D.10.: Interatomic angles (°) occurring in β-BP_3N_6 obtained from single-crystal refinement at ambient pressure. High uncertainties are attributable to the lack of high-quality single-crystal data at this pressure point.

N5–P1–N1	95(1)	N6–P2–N5	87(1)	N6–P3–N6	98(1)	N2–B1–N1	117(3)
N5–P1–N3	97(1)	N6–P2–N2	174(2)	N6–P3–N2	169(1)	N2–B1–N4	126(3)
N5–P1–N4	92(1)	N6–P2–N4	93(2)	N6–P3–N5	83(1)	N2–B1–N3	114(3)
N5–P1–N2	167(2)	N6–P2–N1	91(2)	N6–P3–N4	99(1)	N1–B1–N4	100(2)
N5–P1–N1	93(2)	N6–P2–N3	95(1)	N6–P3–N3	89(1)	N1–B1–N3	94(2)
N1–P1–N3	97(1)	N5–P2–N2	95(1)	N6–P3–N2	94(1)	N4–B1–N3	100(4)
N1–P1–N4	170(1)	N5–P2–N4	96(1)	N6–P3–N5	93(2)		
N1–P1–N2	93(1)	N5–P2–N1	91(1)	N6–P3–N4	98(1)		
N1–P1–N1	92(2)	N5–P2–N3	172(1)	N6–P3–N3	173(2)		
N3–P1–N4	87(1)	N2–P2–N4	92(2)	N2–P3–N5	95(1)		
N3–P1–N2	91(2)	N2–P2–N1	84(2)	N2–P3–N4	80(1)		
N3–P1–N1	165(2)	N2–P2–N3	82(1)	N2–P3–N3	80(1)		
N4–P1–N2	79(1)	N4–P2–N1	172(2)	N5–P3–N4	169(2)		
N4–P1–N1	82(2)	N4–P2–N3	92(1)	N5–P3–N3	88(2)		
N2–P1–N1	76(2)	N1–P2–N3	80(1)	N4–P3–N3	81(1)		

Minimal bonding ellipsoids (MBE)

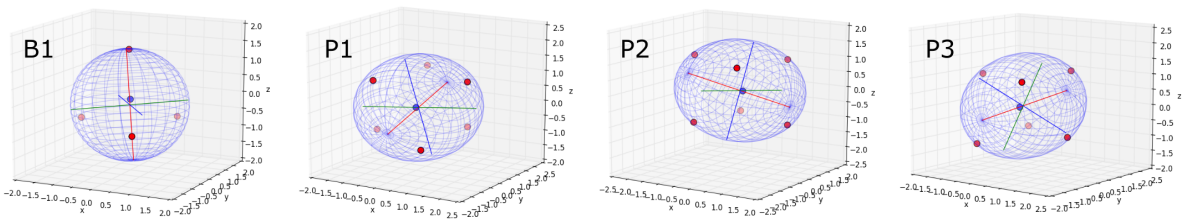

Figure D.10.: Minimal bonding ellipsoids (MBEs) of BN_4 and PN_6 polyhedra in β-BP_3N_6 at 42.4(1) GPa fitted with the PIEFACE software.[17] B/P: blue, N: red.

Table D.11.: Ellipsoidal parameters of MBEs of the in β-BP_3N_6 structure at 42.4(1) GPa.[17]

	***R*1**	***R*2**	***R*3**	$\langle R \rangle$	**σ(R)**	***S***	**Center Disp.**	**CN**
B1	1.608	1.440	1.408	1.485	0.088	0.083	0.162	4
P1	1.801	1.763	1.695	1.753	0.044	−0.017	0.083	6
P2	1.843	1.722	1.622	1.729	0.090	0.007	0.072	6
P3	1.866	1.717	1.590	1.725	0.112	0.006	0.106	6

CHARDI analysis

Table D.12.: CHARDI analysis of the β-BP_3N_6 structure at 42.4(1) GPa revealed mean effective coordination numbers of 3.93 and 5.68 for B and P and mean total charges of +3.07, +4.98 and −3.00 for B, P and N, in line with formal oxidation states (+III, +V, −III).[18]

Polyhedra	**P1N$_6$**	**P2N$_6$**	**P3N$_6$**	**B1N$_4$**
Average bond length / Å	1.7594	1.7325	1.7326	1.4963
Polyhedral volume / Å^3	7.0984	6.8473	6.7847	1.6726
Distortion index (bond length)	0.02667	0.02828	0.03585	0.01674
Quadratic elongation	1.0163	1.0095	1.0162	1.0189
Bond angle variance / $^{\circ 2}$	54.0037	28.7111	51.2013	88.2130
Effective coordination number	5.6999	5.6998	5.6306	3.9360
Total charges				
P/B	5.099	4.967	4.860	3.074
N1	−2.890	−2.890		−2.890
N2	−3.125	−3.125	−3.125	−3.125
N3	−2.775	−2.775	−2.775	−2.775
N4	−2.891	−2.891	−2.891	−2.891
N5	−3.090	−3.090	−3.090	
N6		−3.230	−3.230	

MAPLE analysis

Table D.13.: The Madelung part of lattice energy (MAPLE) of the β-BP_3N_6 structure was determined to 92 631 kJ·mol^{-1} at 42.4(1) GPa, which is in fair agreement with values for α-BP_3N_6 and the sum of respective binary nitrides.[19–24]

Phase(s)	**MAPLE / kJ·mol^{-1}**	**Difference**
β-BP_3N_6 (42.4(1) GPa)	92631	
α-P_3N_5 + c-BN	91 732	1.0 %
α-P_3N_5 + h-BN	91 877	0.8 %
γ-P_3N_5 + c-BN	90 049	2.9 %
γ-P_3N_5 + h-BN	90 194	2.7 %
α-BP_3N_6	90 556	2.3 %

D.3. Author Contributions

S.V. Conceptualization: Equal; Formal analysis: Lead; Investigation: Equal; Validation: Equal; Visualization: Lead; Writing-Original Draft: Lead; Writing Review & Editing: Equal

M.B. Formal analysis: Equal; Investigation: Equal; Validation: Equal; Writing Review & Editing: Supporting

E.B. Formal analysis: Equal; Investigation: Equal; Validation: Equal; Writing Review & Editing: Supporting

S.W. Investigation: Supporting; Writing Review & Editing: Supporting

S.K. Investigation: Supporting; Writing Review & Editing: Equal

A.P. Investigation: Equal; Writing Review & Editing: Supporting

S.C. Methodology: Supporting; Writing Review & Editing: Supporting

E.K. Methodology: Supporting; Writing Review & Editing: Supporting

N.D. Funding acquisition: Equal; Project administration: Equal; Resources: Equal; Supervision: Equal; Validation: Equal; Writing Review & Editing: Supporting

L.D. Funding acquisition: Equal; Methodology: Lead; Project administration: Equal; Resources: Equal; Supervision: Equal; Writing Review & Editing: Supporting

W.S. Conceptualization: Equal; Funding acquisition: Lead; Project administration: Lead; Resources: Lead; Supervision: Lead; Validation: Equal; Writing Original Draft: Equal; Writing Review & Editing: Equal

D.4. References

[1] S. Vogel, A. T. Buda, W. Schnick, *"United in Nitride: The Highly Condensed Boron Phosphorus Nitride BP_3N_6"*, *Angew. Chem. Int. Ed.* **2018**, *57*, 13202; *Angew. Chem.* **2018**, *130*, 13386.

[2] H. Huppertz, *"Multianvil high-pressure / high-temperature synthesis in solid state chemistry"*, *Z. Kristallogr.* **2004**, *219*, 330.

[3] D. Walker, *"Lubrication, gasketing, and precision in multianvil experiments"*, *Am. Mineral.* **1991**, *76*, 1092.

[4] Oxford Instruments, *"AZtecEnergy Vers. 3.1"*, Abington, **2016**.

[5] H. P. Liermann, Z. Konôpková, W. Morgenroth, K. Glazyrin, J. Bednarčik, E. E. McBride, S. Petitgirard, J. T. Delitz, M. Wendt, Y. Bican, A. Ehnes, I. Schwark, A. Rothkirch, M. Tischer, J. Heuer, H. Schulte-Schrepping, T. Kracht, H. Franz, *"The Extreme Conditions Beamline P02.2 and the Extreme Conditions Science Infrastructure at PETRA III"*, *J. Synchrotron Radiat.* **2015**, *22*, 908.

[6] C. Prescher, V. B. Prakapenka, *"DIOPTAS: A program for reduction of two-dimensional X-ray diffraction data and data exploration"*, *High Pressure Res.* **2015**, *35*, 223.

[7] A. A. Coelho, *"TOPAS-Academic Vers. 4.1"*, Brisbane, **2007**.

[8] G. S. Pawley, *"Unit-cell refinement from powder diffraction scans"*, *J. Appl. Crystallogr.* **1981**, *14*, 357.

[9] A. Dewaele, P. Loubeyre, M. Mezouar, *"Equations of state of six metals above 94 GPa"*, *Phys. Rev. B: Condens. Matter Mater. Phys.* **2004**, *70*, 515.

[10] Rigaku Oxford Diffraction, *"CrysAlisPro Software system, version 1.171.37.35"*, Oxford, UK, **2014**.

[11] G. M. Sheldrick, *"SHELXT - integrated space-group and crystal-structure determination"*, *Acta Crystallogr. Sect. A: Found. Adv.* **2015**, *71*, 3.

[12] G. M. Sheldrick, *"A short history of SHELX"*, *Acta Crystallogr. Sect. A: Found. Adv.* **2008**, *64*, 112.

[13] I. Kantor, V. Prakapenka, A. Kantor, P. Dera, A. Kurnosov, S. Sinogeikin, N. Dubrovinskaia, L. Dubrovinsky, *"BX90: a new diamond anvil cell design for X-ray diffraction and optical measurements"*, *Rev. Sci. Instrum.* **2012**, *83*, 125102.

[14] F. D. Murnaghan, *"The compressibility of media under extreme pressures"*, *Proc. Natl. Acad. Sci. U.S.A.* **1944**, *30*, 244.

[15] F. Birch, *"Finite Elastic Strain of Cubic Crystals"*, *Phys. Rev.* **1947**, *71*, 809.

[16] J. Gonzalez-Platas, M. Alvaro, F. Nestola, R. Angel, *"EosFit7-GUI: A new graphical user interface for equation of state calculations, analyses and teaching"*, *J. Appl. Crystallogr.* **2016**, *49*, 1377.

[17] J. Cumby, J. P. Attfield, *"Ellipsoidal analysis of coordination polyhedra"*, *Nat. Commun.* **2017**, *8*, 14235.

[18] R. Hoppe, S. Voigt, H. Glaum, J. Kissel, H. P. Müller, K. Bernet, *"A new route to charge distributions in ionic solids"*, *J. Less-Common Met.* **1989**, *156*, 105.

[19] R. Hoppe, *"On the Madelung Part of Lattice Energy"*, *Z. Naturforsch. A: Phys. Sci.* **1995**, *50*, 555.

[20] R. S. Pease, *"Crystal Structure of Boron Nitride"*, *Nature* **1950**, *165*, 722.

[21] R. H. Wentorf, *"Cubic Form of Boron Nitride"*, *J. Chem. Phys.* **1957**, *26*, 956.

[22] R. H. Wentorf, *"Synthesis of the Cubic Form of Boron Nitride"*, *J. Chem. Phys.* **1961**, *34*, 809.

[23] S. Horstmann, E. Irran, W. Schnick, *"Synthesis and Crystal Structure of Phosphorus(V) Nitride α-P_3N_5"*, *Angew. Chem. Int. Ed. Engl.* **1997**, *36*, 1873; *Angew. Chem.* **1997**, *109*, 1938.

[24] K. Landskron, H. Huppertz, J. Senker, W. Schnick, *"High-Pressure Synthesis of γ-P_3N_5 at 11 GPa and 1500 °C in a Multianvil Assembly: A Binary Phosphorus(V) Nitride with a Three-Dimensional Network Structure from PN_4 Tetrahedra and Tetragonal PN_5 Pyramids"*, *Angew. Chem. Int. Ed.* **2001**, *40*, 2643, *Angew. Chem.* **2001**, *113*, 2713.

E. Supporting Information for Chapter 7

Nitride Spinel: An Ultraincompressible High-Pressure Form of BeP_2N_4

Sebastian Vogel, Maxim Bykov, Elena Bykova, Sebastian Wendl, Simon D. Kloß, Anna Pakhomova, Natalia Dubrovinskaia, Leonid Dubrovinsky, and Wolfgang Schnick

Angew. Chem. Int. Ed. **2019** (accepted);

Angew. Chem. **2019** (accepted).

DOI: 10.1002/anie.201910998

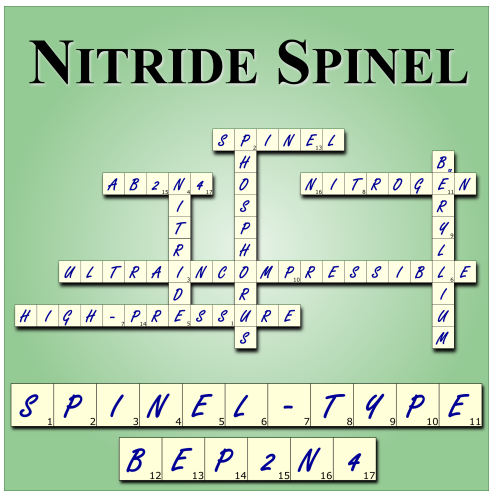

Abstract Owing to its outstanding elastic properties, the nitride spinel γ-Si_3N_4 is of considered interest for materials scientists and chemists. DFT calculations suggest that Si_3N_4-analog beryllium phosphorus nitride BeP_2N_4 adopts the spinel structure at elevated pressures as well and shows outstanding elastic properties. Herein, we investigate phenakite-type BeP_2N_4 by single-crystal synchrotron X-ray diffraction and report the phase transition into the spinel-type phase at 47 GPa and 1800 K in a laser-heated diamond anvil cell. The structure of spinel-type BeP_2N_4 was refined from pressure-dependent in situ synchrotron powder X-ray diffraction measurements down to ambient pressure, which proves spinel-type BeP_2N_4 a quenchable and metastable phase at ambient conditions. Its isothermal bulk modulus was determined to 325(8) GPa from equation of state, which indicates that spinel-type BeP_2N_4 is an ultraincompressible material.

E.1. Experimental Procedures

Safety instructions

Owing to the toxicity of beryllium and its compounds, handling and preparations were carried out carefully and with proper safety arrangements.[1] The sample size was chosen to the smallest possible amount in each step and starting materials (Be, Be_3N_2) have only been handled either in a separate glovebox with fine particulate air filter, or in sealed containers. All contaminated materials were properly purged or disposed.

Preparation of starting materials

Beryllium nitride Be_3N_2 was synthesized by heating Be (abcr, 99 %) in N_2 atmosphere at 1400 °C for 5 h in a radio-frequency furnace.[2] The reaction product contained up to 5 wt-% Be as a minor side phase as determined by powder X-ray diffraction and Rietveld refinement. An additional purification for the high-pressure high-temperature reaction towards BeP_2N_4, however, was not necessary.[3,4]

Phosphorus nitride P_3N_5 was obtained by ammonolysis of P_4S_{10} (Acros Organics, > 98 %).[5] P_4S_{10} was loaded in a fused silica tube and saturated in a flow of dry ammonia (Air Liquide, 5.0) for 4 h at ambient temperature. Subsequently, the reaction mixture was heated to 850 °C for 4 h in a flow of dry ammonia. The reaction product was yielded as an orange powder and its purity was confirmed by powder X-ray diffraction, FTIR spectroscopy and CHNS analysis.[6]

Multianvil synthesis of phenakite-type BeP_2N_4

phe-BeP_2N_4 was synthesized following the description of Pucher et al. from Be_3N_2 and P_3N_5 in a high-pressure high-temperature reaction, using a hydraulic 1000 t press and a modified Walker module.[7,8] In a glovebox (MBraun, Garching, Germany; < 1 ppm O_2, H_2O; fine particulate air filter) stoichiometric amounts of Be_3N_2 and P_3N_5 were ground in a tungsten carbide (WC) mortar and packed tightly in a crucible made of h-BN (Henze, Kempten, Germany), which was sealed with a h-BN cap. The crucible, enveloped by two graphite sleeves acting as the resistance heating and a ZrO_2 sleeve acting as a heat shield, was placed in a drilled octahedron (5 % Cr_2O_3 doped MgO, 18 mm edge length, Ceramic Substrates & Components Ltd, Isle of Wight, United Kingdom). The sample was centered in the octahedron using two MgO spacers and two Mo discs, which served as an electric contact to the graphite furnaces.

The as-prepared octahedron was placed in the center of eight Co-doped WC cubes with truncated edges (7 % Co, 11 mm edge length, Hawedia, Marklkofen, Germany), which were separated by pyrophyllite gaskets (Ceramic Substrates & Components Ltd, Isle of Wight, United Kingdom). A more detailed description of the octahedron-within-cubes payload can be found in literature.[9] The assembly was compressed to 7 GPa within 200 min and heated subsequently to 1500 °C within 40 min . The temperature was kept constant for another 30 min before the sample was allowed to cool down to ambient temperature within 30 min . The assembly was decompressed within 600 min and the reaction product was obtained as an air and moisture resistant gray powder owing to minor amounts of black phosphorus, which appears as a side phase of phe-BeP_2N_4, as was confirmed by powder X-ray diffraction (Figure E.1).[7,10]

Powder X-ray diffraction (PXRD)

Powder X-ray diffraction patterns of the starting materials and phe-BeP_2N_4 were collected on a STOE Stadi P (STOE & Cie GmbH, Darmstadt, Germany, Mo-Kα_1 radiation, $\lambda = 0.71073$ Å, Ge(111) monochromator) equipped with a MYTHEN 1K Si strip detector in modified Debye-Scherrer geometry. For this purpose, the samples were sealed in glass capillaries with an outer diameter of 0.3 mm (Hilgenberg, Malsfeld, Germany).

Synchrotron measurements

Pressure-dependent X-ray diffraction (XRD) measurements were performed at the Extreme Conditions Beamline P02.2 (PETRA III) at the Deutsches Elektronen-Synchrotron (DESY, Hamburg, Germany).[11] The X-ray beam ($\lambda = 0.2894$ Å) was focused to $1.4 \times 1.8\ \mu m^2$ ($V \times H$) by a Kirkpatrick-Baez mirror system and diffraction patterns were collected on a PerkinElmer XRD 1621 flat-panel detector. Internal pressures were determined using the ruby fluorescence method and a relative error of 2 % was assumed.[12,13]

To find a suitable particle of phe-BeP_2N_4, several grains of the as-obtained sample from the multianvil syntheses were loaded on a diamond anvil and tested by XRD (Figure E.2). Subsequently, an ω step scan ($\omega_{max} = \pm 33°$; $\Delta\omega = 0.5°$; $t_{exposure} = 1$ s) of a suitable multi-domain grain of phe-BeP_2N_4 was collected and data analysis was performed using the CrysAlisPro software.[14] Several domains could be indexed using the reciprocal space viewer (Ewald Explorer, CrysAlisPro, Figure E.3), of which the most intense

domain was integrated independently (low number of overlapping reflections) to yield a single-crystal dataset of phe-BeP_2N_4 (Table E.1–E.11).

A single-crystal of an ortho-enstatite ($(Mg_{1.93},Fe_{0.06})(Si_{1.93},Al_{0.06})O_6$, *Pbca*, $a = 8.8117(2)$, $b = 5.18320(10)$, $c = 18.2391(3)$ Å) was used for instrument model calibration of CrysAlisPro (sample-to-detector distance, the detector's origin, offsets of the goniometer angles and rotation of the X-ray beam and the detector around the instrument axis).

Powder X-ray diffraction patterns of spinel-type sp-BeP_2N_4 were obtained from wide scans ($\omega_{max} = \pm 20°$; $t_{exposure} = 20$ s) by radial integration with masked diamond reflections using the Dioptas software.[15]

Laser-heated diamond anvil cell and synthesis of sp-BeP_2N_4

Synthesis and cold decompression of sp-BeP_2N_4 were performed in a symmetrical diamond anvil cell, using two Boehler-Almax-type diamond anvils (200 µm culet, DESY supply) separated by a Re gasket that had been pre-indented to 30 µm and laser-drilled to an inner diameter of about 80 µm. Ne was used as a pressure-transmitting medium and ruby spheres served as an internal pressure standard. The cell was loaded with a pre-selected polycrystalline particle of phe-BeP_2N_4 and compressed to an initial pressure of 0.2 GPa after pressure loading.

The sample was cold-compressed to approximately 20 GPa and a step scan was collected, before the pressure was increased to 47.3(9) GPa. At maximum pressure another step scan was collected and subsequently the sample was heated from both sides to 1800(200) K using a focused NIR fiber laser ($\lambda = 1070$ nm, 10×10 µm^2). After 5 s of heating the appearance of non-indexed reflections indicated the formation of the predicted spinel-type BeP_2N_4 phase (Figure E.5). To ensure a full conversion of phe- into sp-BeP_2N_4 within the heated area, the sample was heated for another 60 s (Figure E.5). The sample was allowed to cool down to ambient temperature before pressure-dependent PXRD patterns were collected upon cold decompression.

Single-crystal X-ray diffraction refinement

The structure of phe-BeP_2N_4 was solved using the SHELXT algorithm and refined with SHELXL against F^2 on all data by the full-matrix least squares algorithm.[16,17] All atoms were refined anisotropically and

without any restraints or constraints. Solution and refinement was performed using the WinGX software package and the resulting structure model was visualized using VESTA.[18,19]

Rietveld refinements

Rietveld refinements were performed with the TOPAS Academic software.[20,21] All atoms were refined isotropically and the values of B_{iso} were fixed to 0.8. The background was described by a shifted Chebyshev polynomial. Peak profiles were modeled with to the fundamental parameters approach in the case of STOE measurements and by Pseudo-Voigt functions in the case of synchrotron measurements.[22,23] The emission profile of the synchrotron radiation was refined from a CeO_2 standard and kept constant for the pressure-dependent Rietveld refinements of sp-BeP_2N_4.

Equation of state

The pressure-volume data from cold decompression of sp-BeP_2N_4 were described by a second (Equation E.1) and third order Birch-Murnaghan equation of state (Equation E.2) using the EoSFit7 software.[24–26] The pressure p is described as a function of cell volume V with V_0 corresponding to the cell volume at a theoretical pressure of zero and K_0 representing the isothermal bulk modulus with its derivation K_0', which is fixed to 4 in the case of a second order Birch-Murnaghan equation of state.

$$p(V) = \frac{3}{2}K_0\left[\left(\frac{V}{V_0}\right)^{-\frac{7}{3}} - \left(\frac{V}{V_0}\right)^{-\frac{5}{3}}\right] \tag{E.1}$$

$$p(V) = \frac{3}{2}K_0\left[\left(\frac{V}{V_0}\right)^{-\frac{7}{3}} - \left(\frac{V}{V_0}\right)^{-\frac{5}{3}}\right]\cdot\left[1+\frac{3}{4}\left(K_0'-4\right)\cdot\left(\left(\frac{V}{V_0}\right)^{-\frac{2}{3}}-1\right)\right] \tag{E.2}$$

E.2. Results and Discussion

Powder X-ray diffraction of phe-BeP_2N_4

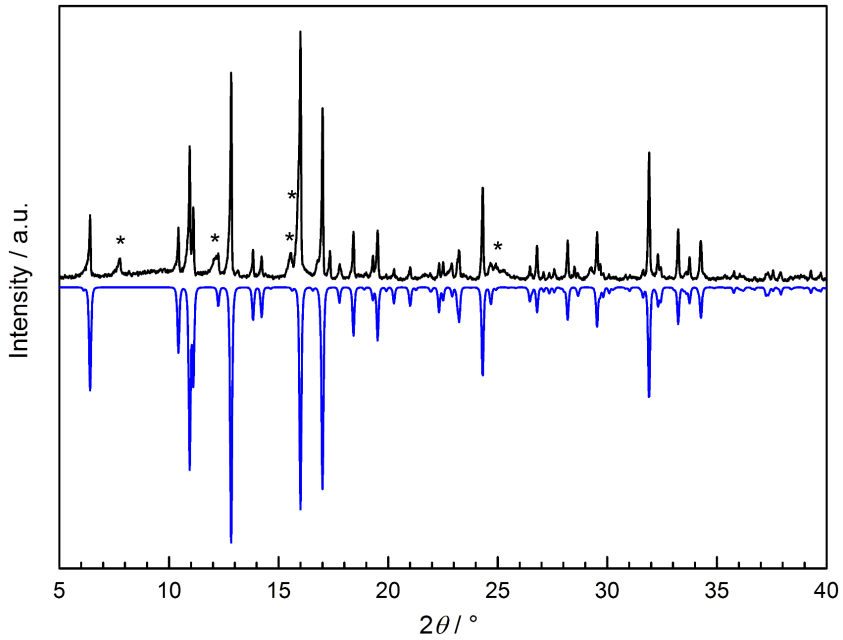

Figure E.1.: Experimental PXRD pattern of the sample obtained from the multianvil synthesis (black, Mo-Kα_1, $\lambda = 0.71073$ Å) confirming that phe-BeP_2N_4 is the majority phase (simulated blue pattern) next to some minor amounts of black phosphorus (Bragg reflections marked by asterisks).[7,10]

Single-crystal X-ray diffraction of phe-BeP_2N_4

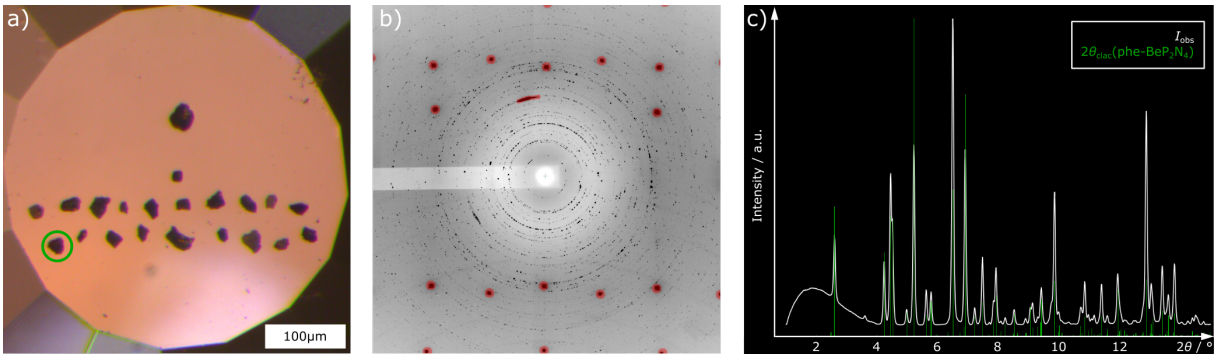

Figure E.2.: Microphotograph of a diamond anvil, which was loaded with particles of the phe-BeP_2N_4 containing sample (a). The green highlighted particle appeared as a suitable multi-domain grain for high-pressure investigations, as indicated by synchrotron XRD measurements (b, c). Processing of the single-crystal XRD data is visualized in Figure E.3.

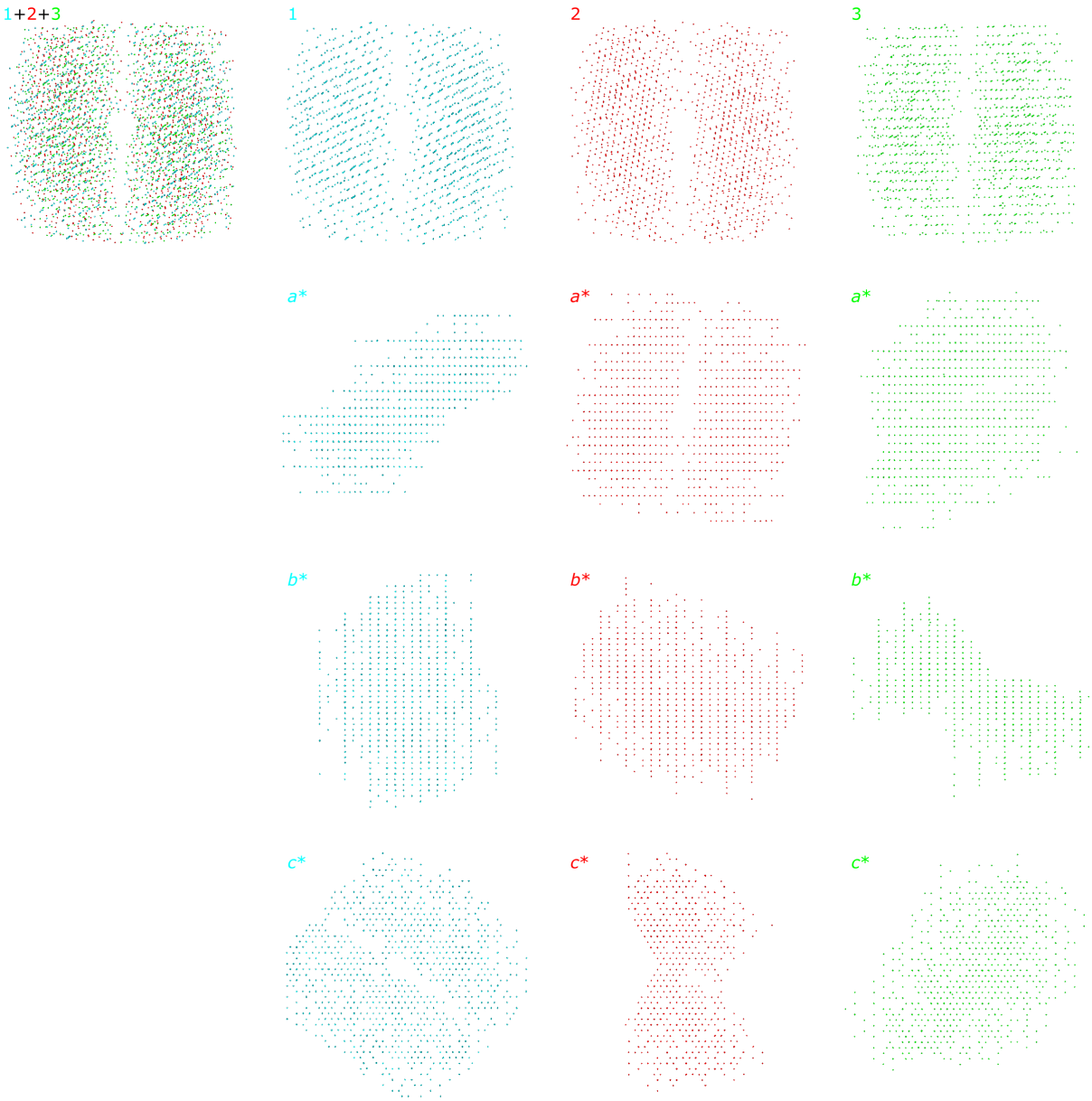

Figure E.3.: From the XRD measurement of the pre-selected phe-BeP_2N_4 particle (Figure E.2) three major domains (1, 2, 3) were indexed (Ewald Explorer, CrysAlisPro), of which domain 2 appeared as the most intense.[14] Its diffraction intensities were integrated independently, as there was only a minor and random overlap with the other domains.

Table E.1.: Crystallographic data on phe-BeP_2N_4 from single-crystal XRD at ambient conditions.

Formula	**phe-BeP_2N_4**
Crystal system	hexagonal
Molecular weight / g·mol^{-1}	126.99
Space group (no.)	$R\bar{3}$ (148)
Lattice parameters / Å	$a = 12.6979(15)$
	$c = 8.3595(10)$
Cell volume / Å^3	1167.3(5)
Formula units per cell	18
Calculated X-ray density / g·cm^{-3}	3.252
Linear absorption coefficient / cm^{-1}	0.144
Radiation	Synchrotron ($\lambda = 0.28940$ Å)
Device	P02.2, PETRA III, DESY
θ-range / °	$1.8 < \theta < 13.95$
$F(000)$	1116
Observed reflections	2856
Independent reflections ($> 2\sigma$)	1241 (979)
Number of parameters	64
R_{int}; R_σ	0.0656; 0.0763
Final R indices ($I > 2\sigma(I)$)	$R1 = 0.0546$; $wR2 = 0.1297$
Final R indices (all data)	$R1 = 0.0668$; $wR2 = 0.1403$
Goodness of fit	1.015
Residual electron density / e·Å^{-3}	1.145; -1.078
CSD	1946333

Table E.2.: Fractional coordinates and isotropic atomic displacement parameters of phe-BeP_2N_4 from single-crystal XRD refinement at ambient conditions. All atoms occupy the general Wyckoff position $18f$.

Atom	x	y	z	U_{eq} / Å^2
Be1	0.1932(3)	0.2116(3)	0.2498(3)	0.0040(1)
P1	0.21293(5)	0.01881(5)	0.41728(6)	0.0040(1)
P2	0.20947(5)	0.01369(5)	0.08278(6)	0.0054(4)
N1	0.2042(2)	0.0807(2)	0.2482(2)	0.0047(4)
N2	0.0036(2)	0.3325(2)	0.0845(2)	0.0050(4)
N3	0.1221(2)	0.2116(2)	0.0746(2)	0.0052(4)
N4	0.1182(2)	0.2131(2)	0.4252(2)	0.0058(7)

Table E.3.: Anisotropic atomic displacement parameters (Å^2) of phe-BeP_2N_4 from single-crystal XRD refinement at ambient conditions.

Atom	U_{11}	U_{22}	U_{33}	U_{23}	U_{13}	U_{12}
Be1	0.005(1)	0.006(1)	0.008(1)	0.0012(7)	0.0007(7)	0.0031(9)
P1	0.0041(2)	0.0038(3)	0.0044(2)	−0.0001(1)	0.0000(2)	0.0023(2)
P2	0.0036(2)	0.0037(2)	0.0046(2)	0.0001(2)	0.0002(1)	0.0017(2)
N1	0.0067(7)	0.0037(7)	0.0050(6)	−0.0001(5)	0.0003(5)	0.0020(6)
N2	0.0048(7)	0.0048(7)	0.0043(6)	−0.0009(4)	0.0003(4)	0.0023(6)
N3	0.0047(7)	0.0066(7)	0.0044(6)	−0.0004(5)	0.0008(5)	0.0033(6)
N4	0.0042(7)	0.0065(7)	0.0052(6)	−0.0006(5)	−0.0007(5)	0.0028(6)

Table E.4.: Comparison of the crystallographic data of phe-BeP_2N_4 reported in this work (single-crystal XRD) and those published by Pucher et al. (PXRD).[7]

Formula	**phe-BeP_2N_4**	
Crystal system	hexagonal	
Space group (no.)	$R\bar{3}$ (148)	
Lattice parameters / Å	$a = 12.6979(15)$	$a = 12.6897(2)$
	$c = 8.3595(10)$	$c = 8.3469(2)$
Cell volume / Å^3	1167.3(5)	1164.01(4)
Formula units per cell	18	
Calc. X-ray density / g·cm^{-3}	3.252	3.258
Be1(x,y,z)	0.1932(3), 0.2116(3), 0.2498(3)	0.2080(20), 0.2223(20), 0.249(4)
P1(x,y,z)	0.21293(5), 0.01881(5), 0.41728(6)	0.2127(5), 0.0208(4), 0.4165(7)
P2(x,y,z)	0.20947(5), 0.01369(5), 0.08278(6)	0.2011(5), 0.0061(5), 0.0770(7)
N1(x,y,z)	0.20419(17), 0.08070(17), 0.2482(2)	0.1936(10), 0.0730(8), 0.2486(15)
N2(x,y,z)	0.00355(15), 0.33250(15), 0.0845(2)	0.3318(11), 0.3297(11), 0.2611(16)
N3(x,y,z)	0.12209(17), 0.21155(16), 0.0746(2)	0.1293(10), 0.2158(10), 0.0805(15)
N4(x,y,z)	0.11817(16), 0.21305(17), 0.4252(2)	0.1297(13), 0.2275(10), 0.4192(15)
Reference	this work	Pucher et al.[7]
Method	single-crystal XRD, synchrotron	powder XRD, Cu-Kα_1

Figure E.4.: phe-BeP_2N_4 was cold-compressed to an intermediate pressure of 19.3(4) GPa, at which a XRD step scan was collected before the pressure was increased to 47.3(9) GPa and another XRD step scan was collected. At both datasets were indexed with the cell metrics of phe-BeP_2N_4 as illustrated with the CrysAlisPro Ewald Explorer (19.3(4) GPa: red, 47.3(9) GPa: blue).[14] Corresponding cell metrics are listed in Table E.5.

Table E.5.: Pressure evolution of the lattice parameters of phe-BeP_2N_4, which were obtained from synchrotron XRD step scans.

Pressure / GPa	***a* / Å**	***c* / Å**	***V* / Å^3**
0.00010(1)	12.698(2)	8.360(1)	1167.3(5)
19.3(4)	12.437(2)	8.14(3)	1090(1)
47.3(9)	12.087(5)	7.931(3)	1003.4(7)

phe-BeP_2N_4 $\longrightarrow$ sp-BeP_2N_4 phase transition

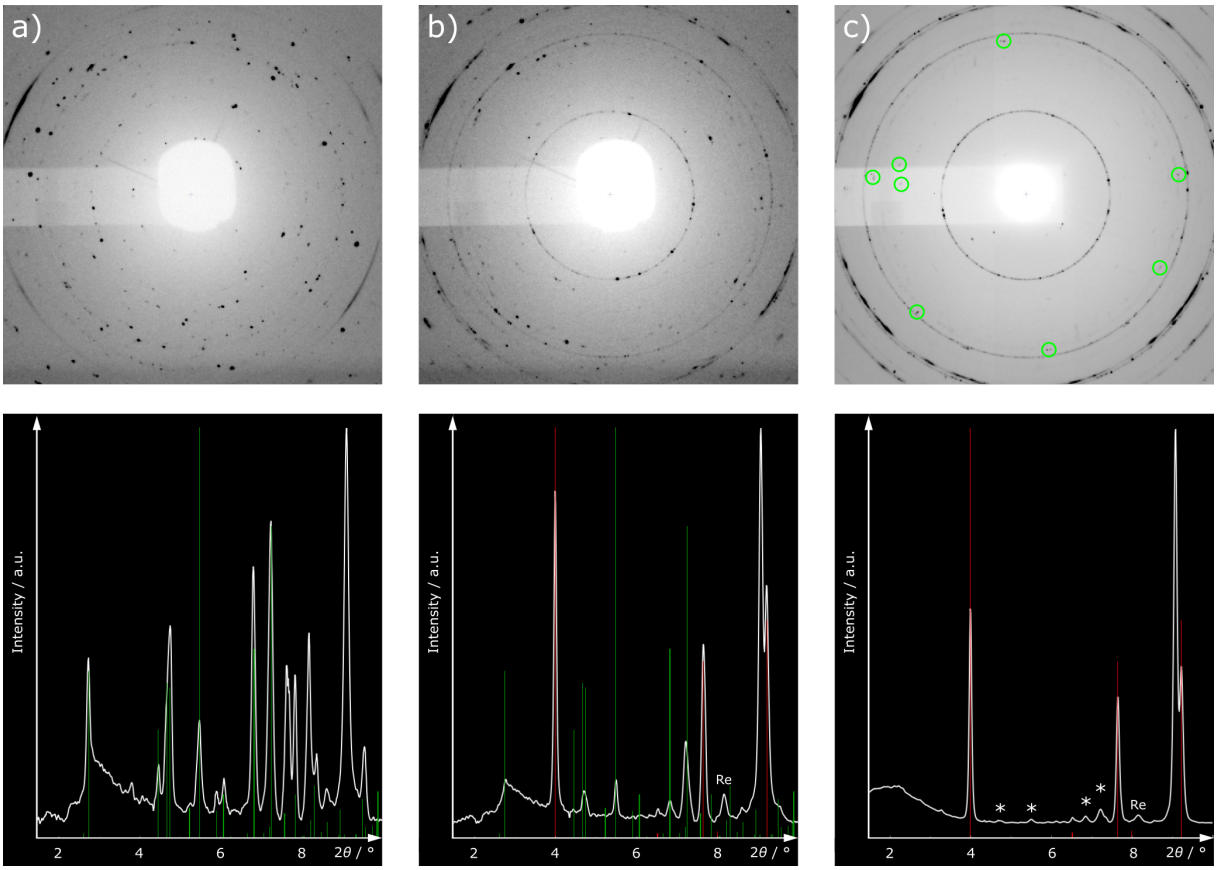

Figure E.5.: XRD patterns of the BeP_2N_4 sample before (a, phe-BeP_2N_4), during (b, phe- and sp-BeP_2N_4) and after laser heating at 47.3(9) GPa (c, sp-BeP_2N_4). Calculated Bragg reflections of phe- and sp-BeP_2N_4 are visualized in green and red. The intense reflection at $2\theta \approx 9°$ corresponds to Ne, which served as a pressure transmitting medium. Minor amounts of phe-BeP_2N_4 in c are marked with green circles (top) and white asterisks (bottom). Weak scattering of the Re gasket is labelled in b and c.

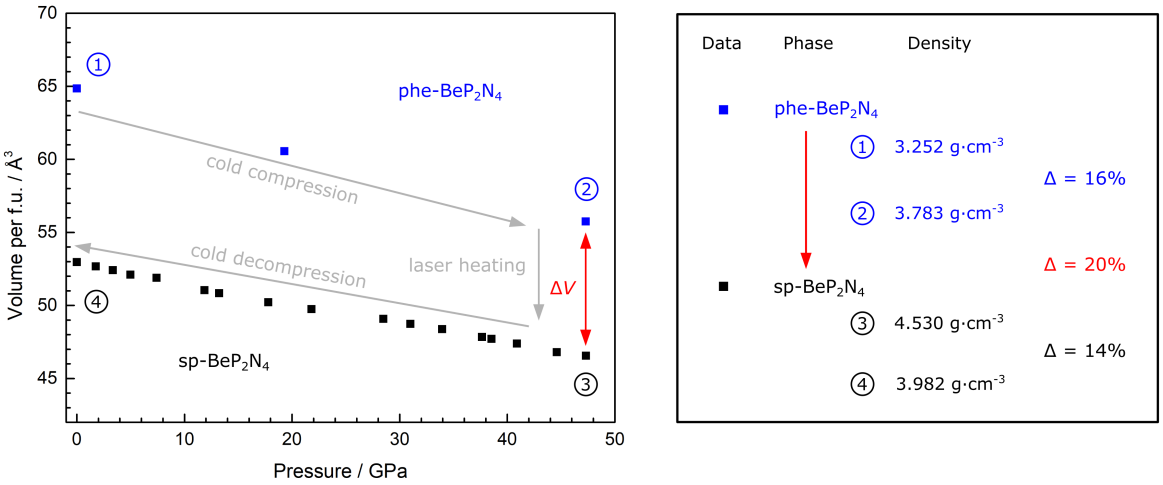

Figure E.6.: Scheme summarizing the synchrotron experiments performed within this work. The pre-selected particle (Figure E.2) of phe-BeP_2N_4 (1) was cold compressed to 19.3(4) GPa, before the pressure was increased to 47.3(9) GPa (2, Figure E.4, Table E.5). Upon laser heating at maximum pressure, phe-BeP_2N_4 transformed into the predicted sp-BeP_2N_4 (3, Figure E.5). This phase transition is characterized by a significant decrease in volume (20 %) and thus can be classified as a first order phase transition. At ambient temperature sp-BeP_2N_4 was stepwise decompressed to ambient pressure (4) to probe its elastic properties (Table E.9).

Rietveld refinements of sp-BeP_2N_4

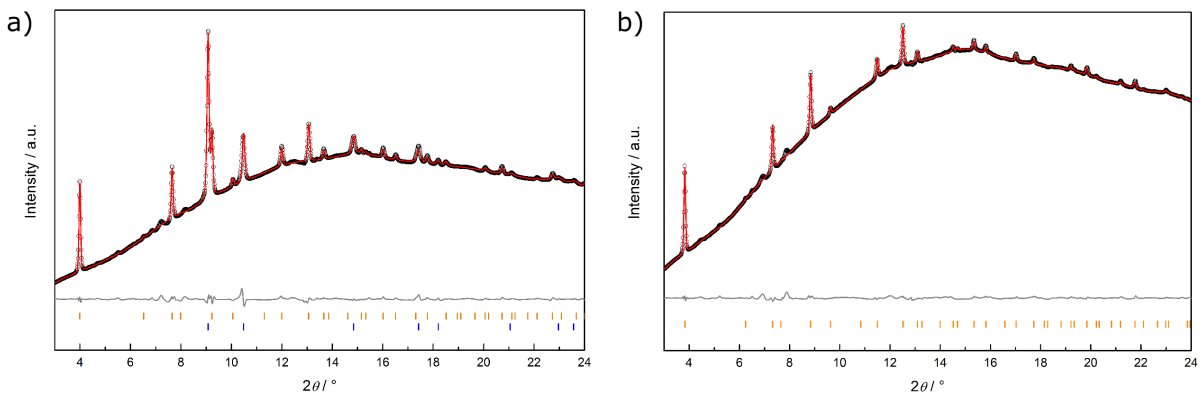

Figure E.7.: Rietveld plots of the refinement of sp-BeP_2N_4 at 47.3(9) GPa (a) and ambient pressure (b). Observed and calculated intensities are displayed in black and red, respectively. The difference plot ($I_{obs} - I_{calc}$) is drawn in gray and calculated Bragg reflections of sp-BeP_2N_4 (orange) and Ne (blue) are marked by vertical lines.

Table E.6.: Crystallographic data on sp-BeP_2N_4 from Rietveld refinements at 47.3(9) GPa and ambient pressure.

Formula	**sp-BeP_2N_4**	
Crystal system	cubic	
Space group (no.)	$Fd\bar{3}m$ (227)	
Pressure / GPa	47.3(9)	0.00010(1)
Lattice parameter a / Å	7.1948(2)	7.5107(2)
Cell volume / Å^3	372.44(3)	423.68(3)
Formula units per cell	8	
Calc. X-ray density / g·cm^{-3}	4.530	3.982
Device	P02.2, PETRA III, DESY	
Radiation	Synchrotron ($\lambda = 0.289\,40$ Å)	
θ-range / °	$1.5 < \theta < 12$	
Temperature / K	293(2)	
Data points	1677	
Number of observed reflections	41	47
Number of parameters (thereof background)	35(28)	
R_p (background corrected) / %[a]	0.266 (17.7)	0.134 (30.5)
R_{wp} (background corrected) / %[a]	0.444 (9.40)	0.205 (12.8)
R_{Bragg} / %[a]	0.254	0.174
CSD	1946347	1946345

[a] Owing to a very high background of the synchrotron PXRD measurements, the reported R values are very low and may not serve as the most suitable quality criteria in this case. The background corrected indices, however, indicate that the peak profiles that have been modelled with Pseudo-Voigt functions in the first approximation differ from the observed profiles. The comparison of the integral observed and calculated intensities, in turn, shows only marginal deviations, as represented by low values of R_{Bragg}. In conclusion, the graphical plots in Figure E.7 in combination with the respective values of R_{Bragg} may serve as the most appropriate indicators of quality for the Rietveld refinements performed within this work.

Table E.7.: Fractional coordinates and isotropic atomic displacement parameters of sp-BeP_2N_4 from Rietveld refinement at 47.3(9) GPa.

Atom	**Wyck.**	***x***	***y***	***z***	B_{iso} **/ Å^2**
Be1	8*b*	3/8	3/8	3/8	0.8 (fixed)
P1	16*c*	0	0	0	0.8 (fixed)
N1	32*e*	0.2438(3)	0.2438(3)	0.2438(3)	0.8 (fixed)

Table E.8.: Fractional coordinates and isotropic atomic displacement parameters of sp-BeP_2N_4 from Rietveld refinement at ambient pressure.

Atom	**Wyck.**	***x***	***y***	***z***	B_{iso} **/ Å^2**
Be1	8*b*	3/8	3/8	3/8	0.8 (fixed)
P1	16*c*	0	0	0	0.8 (fixed)
N1	32*e*	0.2403(3)	0.2403(3)	0.2403(3)	0.8 (fixed)

Table E.9.: Pressure evolution of the lattice parameter a, the unit cell volume V, the calculated X-ray density ρ_{calc}, the fractional coordinate of N1 ($x = y = z$) and the interatomic Be–N and P–N distances for sp-BeP_2N_4. The provided CSD numbers contain the supplementary crystallographic data to those phases. These data can be obtained free of charge from The Cambridge Crystallographic Data Centre.

Pressure / GPa	***a* / Å**	***V* / Å^3**	**ρ_{calc} / g·cm^{-3}**	**N1(*x, y, z*)**	**Be–N / Å**	**P–N / Å**	**CSD**
47.3(9)	7.1948(2)	372.44(3)	4.530	0.2438(3)	1.635(2)	1.755(2)	1946347
44.6(9)	7.2076(2)	374.43(3)	4.505	0.2434(3)	1.643(2)	1.756(2)	1946344
40.9(8)	7.2371(3)	379.05(5)	4.451	0.2445(4)	1.636(3)	1.770(3)	1946343
38.5(8)	7.2536(3)	381.65(5)	4.421	0.2444(4)	1.641(3)	1.774(3)	1946342
37.7(8)	7.2602(4)	382.69(6)	4.408	0.2440(5)	1.647(4)	1.773(4)	1946340
34.0(7)	7.2877(2)	387.05(3)	4.359	0.2425(3)	1.673(2)	1.769(2)	1946339
31.0(6)	7.3054(3)	389.88(5)	4.327	0.2437(4)	1.661(3)	1.782(3)	1946338
28.5(6)	7.3221(3)	392.56(5)	4.297	0.2430(4)	1.674(3)	1.781(3)	1946337
21.8(4)	7.3557(3)	397.99(5)	4.239	0.2411(4)	1.706(3)	1.776(3)	1946336
17.8(4)	7.3786(2)	401.72(3)	4.199	0.2410(3)	1.713(2)	1.781(2)	1946335
13.2(3)	7.4088(2)	406.67(3)	4.148	0.2402(2)	1.730(2)	1.783(2)	1946334
11.9(2)	7.4191(1)	408.37(2)	4.131	0.2395(2)	1.741(2)	1.780(2)	1946346
7.4(1)	7.4598(2)	415.13(3)	4.064	0.2411(2)	1.730(2)	1.801(2)	1946349
5.0(1)	7.4702(2)	416.87(3)	4.047	0.2421(3)	1.720(2)	1.811(2)	1946341
3.3(1)	7.4846(1)	419.28(2)	4.023	0.2400(2)	1.750(2)	1.799(2)	1946348
1.8(1)	7.4969(2)	421.35(3)	4.004	0.2411(3)	1.739(2)	1.810(2)	1946332
0.00010(1)	7.5107(2)	423.68(3)	3.982	0.2403(3)	1.752(2)	1.808(2)	1946345

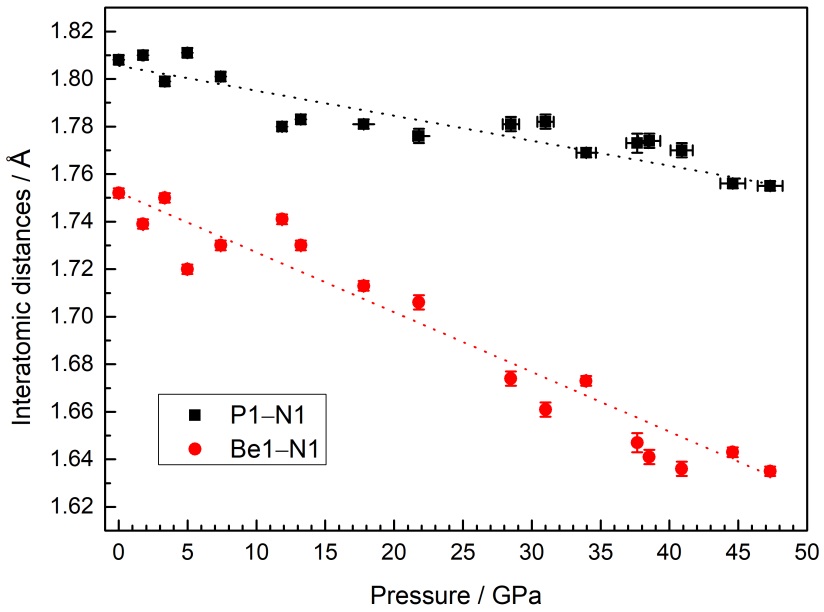

Figure E.8.: Pressure evolution of the interatomic P–N and Be–N distances that were obtained from pressure-dependent Rietveld refinements.

Table E.10.: The Madelung part of lattice energy (MAPLE) of sp-BeP_2N_4 is 58 140 kJ·mol^{-1} at 47.3(9) GPa, which is in line with the calculated values for phe-BeP_2N_4 and the weighted sum of binary nitrides P_3N_5 and Be_3N_2.[3,6,27]

Phase(s)	**MAPLE / kJ·mol^{-1}**	**Difference**
sp-BeP_2N_4 (47.3(9) GPa)	58 140	
phe-BeP_2N_4	58 542	0.7 %
$^1/_3$ (2 P_3N_5 + Be_3N_2) = „BeP_2N_4“	58 992	1.4 %

Table E.11.: Comparison of the experimental and calculated crystallographic data on sp-BeP_2N_4.[7]

Formula	**sp-BeP_2N_4**		
Method	PXRD, Rietveld	DFT (LDA)	DFT (GGA)
Crystal system		cubic	
Space group (no.)		$Fd\bar{3}m$ (227)	
Lattice parameter a / Å	7.5107(2)	7.4654	7.5648
Cell volume / Å^3	423.68(3)	416.06	432.9
Formula units per cell		8	
Calculated density / g·cm^{-3}	3.982	4.055	3.897
Be1(x,y,z)	$^3/_8$, $^3/_8$, $^3/_8$	$^3/_8$, $^3/_8$, $^3/_8$	$^3/_8$, $^3/_8$, $^3/_8$
P1(x,y,z)	0, 0, 0	0, 0, 0	0, 0, 0
N1(x,y,z)	0.2403(3), 0.2403(3), 0.2403(3)	0.24062, 0.24062, 0.24062	0.24053, 0.24053, 0.24053
Reference	this work	Pucher et al.[7]	

Equation of state of sp-BeP_2N_4

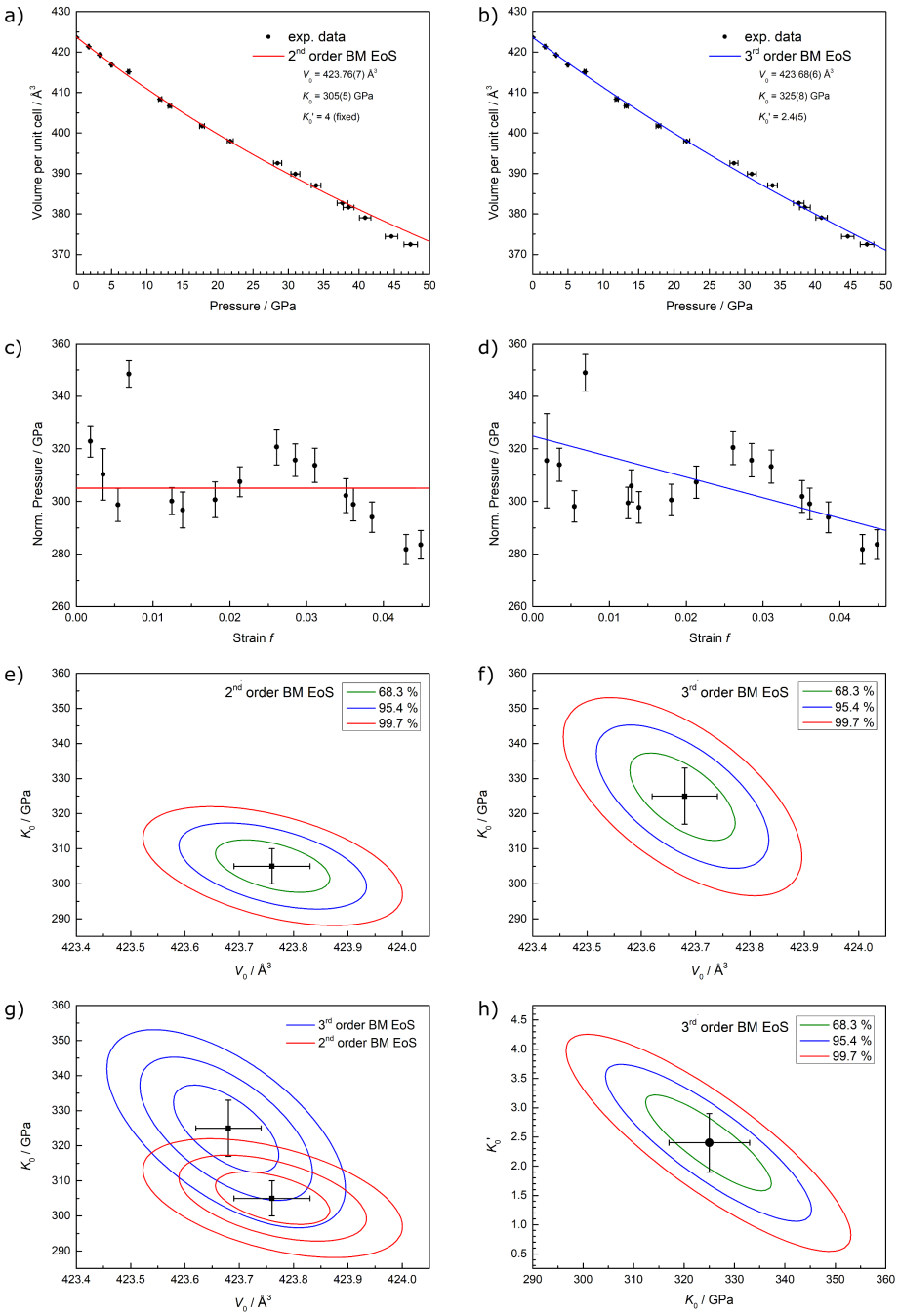

Figure E.9.: The pressure-volume data from pressure-dependent Rietveld refinements of sp-BeP_2N_4 were fitted by a 2nd (a) and 3rd order Birch-Murnaghan equation of state (b).[24,25] Respective plots of the normalized pressure as a function of strain f are provided (c, d), as well as an illustration of the 1σ (68.3 %), 2σ (95.4 %, and 3σ (99.7 %) level of confidence for V_0, K_0 and K_0' (e–h). The experimental data are best described by the 3rd order Birch-Murnaghan equation of state on a sufficient level of accuracy (fit parameters: $V_0 = 423.68(6)$ Å^3, $K_0 = 325(8)$ GPa, $K_0' = 2.4(5)$).

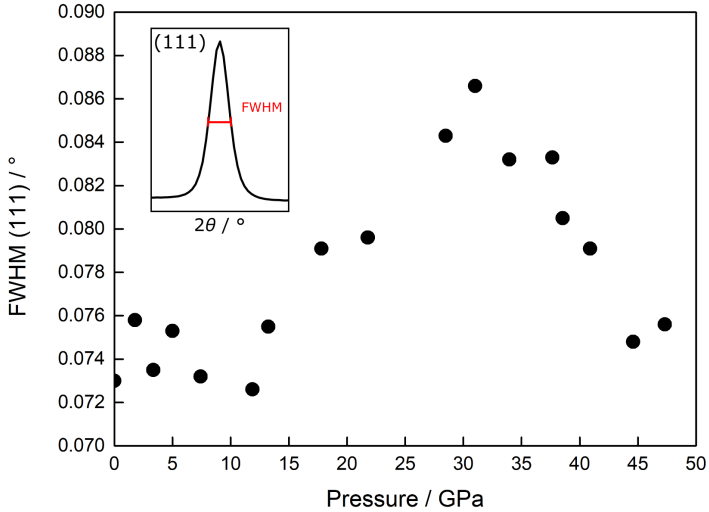

Figure E.10.: The full width at half maximum (FWHM) of the reflection (111) of sp-BeP_2N_4 appears increased between 18 and 44 GPa, which may be owed to a non-hydrostatic sample environment that may also affected the experimental *p*-*V* data, as discussed below.

Discussion of the elastic properties of sp-BeP_2N_4

sp-BeP_2N_4 was investigated by pressure-dependent powder synchrotron XRD measurements and Rietveld refinements. The as-obtained experimental pressure-volume data are suitable for the examination of the elastic properties of sp-BeP_2N_4 (Table E.5), when errors of both, pressure and volume are considered.

The pressure-volume data was initially fitted by a 2nd order Birch-Murnaghan equation of state (Equation E.1, Figure E.9a, c, e) with fitting parameters $V_0 = 423.76(7)$ Å^3, $K_0 = 305(5)$ GPa, and $K_0' = 4$ (fixed). This model was suggested to be suitable for sp-BeP_2N_4 as K_0' was proposed to be approximately 4 from DFT calculations.[28,29] However, as illustrated in Figure E.9a, a significant mismatch of the experimental data at high pressures is observed. Therefore, the *p*-*V* data was fitted by a 3rd order Birch-Murnaghan equation of state (Equation E.2, Figure E.9b, d, f, h) with fitting parameters $V_0 = 423.68(6)$ Å^3, $K_0 = 325(8)$ GPa, $K_0' = 2.4(5)$, which fits the experimental data quite well. Remaining minor deviations of the experimental data and the fitted curve at $p > 25$ GPa may be owed to non-hydrostatic conditions in the DAC, as is indicated by a slightly increased full width at half maximum (FWHM) of the title compound's (111) reflection at high pressures (Figure E.10). Summarizing, the experimental *p*-*V* data may be best described by the 3rd order Birch-Murnaghan equation of state ($V_0 = 423.68(6)$ Å^3, $K_0 = 325(8)$ GPa, K_0' = 2.4(5)), however, a possibly non-hydrostatic sample environment at high pressures may have affected the experimental *p*-*V* data systematically.

The as-obtained bulk modulus K_0(sp-BeP_2N_4) = 325(8) GPa appears higher than values that were proposed by DFT calculations ($K_{0,calc}$ = 263–291 GPa, Table E.12), whereas its derivation K_0' = 2.4(5) turns out to be lower than calculated previously ($K_{0,calc}'$ = 3.990–4.036).[7,28–30] These significant deviations may be related to errors in the experimental data, as discussed above, but may be also attributable to systematical errors within the DFT calculations. It was demonstrated for PBE-based DFT calculations, for instance, that the bulk modulus K_0 is systematically underestimated by about 4.9 %, whereas its derivation K_0' is overestimated by about 4.8 %.[31] sp-BeP_2N_4 may further feature a more covalent character than has been assumed from the theoretical studies, as the covalency can be correlated with a compound's elastic properties.[32]

Moreover, the presented experimental data suggest sp-BeP_2N_4 to be even less compressible than spinel-type Si_3N_4 (γ-Si_3N_4),[33] for which a bulk modulus of K_0 = 290–317 GPa was reported.[33–36] This effect, however small, may be owed to a higher degree of covalency in sp-BeP_2N_4, as both, the Be–N and P–N bonds may be considered more covalent than the Si–N bond, referring to theoretical examinations[30] and the energies of the constituting valence orbitals in a first approximation.[37] Moreover, the unit cell volume of sp-BeP_2N_4 at ambient pressure is about 10 % smaller as compared with γ-Si_3N_4.[33] Therefore, sp-BeP_2N_4 features a higher valence electron density than γ-Si_3N_4, which likely affects its compressibility, as well.[32] A rather significant difference between sp-BeP_2N_4 and γ-Si_3N_4 is observed for the derivation of the bulk modulus K_0', which was determined to 2.4(4) and 6.0(8) for sp-BeP_2N_4 and γ-Si_3N_4, respectively.[35] This may be attributable to the different elemental composition of the nitride spinels. The BeN_4 and PN_6 polyhedra, therefore, likely affect the compressibility of sp-BeP_2N_4 in a different way, than the omnipresent Si–N bonds in γ-Si_3N_4.

In contrast to its compressibility, the hardness of sp-BeP_2N_4 is of considerable conjecture. The Vickers hardness of sp-BeP_2N_4 was proposed to H_V = 45 GPa from (semi)empirical calculations,[28] but first-principle calculations propose a significant lower hardness for sp-BeP_2N_4, considering its low shear strength.[29] Latest calculations on the hardness of group 14 nitride spinels showed that their hardness can be correlated with their electronic structure (e. g. band gap).[38] Within the scope of future examinations, therefore, hardness measurements of sp-BeP_2N_4 may be supported by experimental and theoretical investigations on its electronic structure, as exemplarily shown for solid solutions within the $(Ge_xSi_{1-x})_3N_4$ system.[39]

Table E.12.: Comparison of certain experimental and calculated values of sp-BeP_2N_4 at ambient pressure.

Reference	Method	a / Å	V / Å^3	ρ / g·cm^{-3}	Be–N / Å	P–N / Å	V_0 / Å^3	K_0 / GPa	K_0'
Pucher et al.[7]	LDA	7.4654	416.1	4.05	1.7376	1.7619	416.1	291	-
Pucher et al.[7]	GGA	7.5648	432.9	3.90	1.7991	1.8224	432.9	263	-
Ching et al.[30]	OLCAO (LDA)	7.4654	416.1	4.05	1.762	1.822	432.9	279	-
Ding et al.[28]	LDA	7.4470	413.0	4.05	1.7855	1.8288	-	280	3.997
Ding et al.[28]	GGA	7.4710	417.0	4.09	1.7855	1.8288	-	268	4.036
Zhang et al.[29]	GGA	7.5530	430.9	4.19	1.759	1.819	-	268	3.990
this work	exp., DAC	7.5107(2)	423.68(3)	3.982	1.752(2)	1.808(2)	423.7(1)	325(8)	2.4(5)

E.3. Author Contributions

S.V. Conceptualization: Equal; Data curation: Lead; Formal analysis: Lead; Investigation: Lead; Validation: Lead; Visualization: Lead; Writing original draft: Lead; Writing review & editing: Lead

M.B. Formal analysis: Supporting; Investigation: Equal; Writing original draft: Supporting; Writing review & editing: Supporting

E.B. Formal analysis: Supporting; Investigation: Equal; Writing original draft: Supporting; Writing review & editing: Supporting

S.W. Formal analysis: Supporting; Investigation: Equal; Writing original draft: Supporting; Writing review & editing: Supporting

S.K. Formal analysis: Supporting; Investigation: Supporting; Writing original draft: Equal; Writing review & editing: Supporting

A.P. Investigation: Supporting; Methodology: Equal; Writing review & editing: Supporting

N.D. Funding acquisition: Equal; Project administration: Equal; Resources: Equal; Supervision: Supporting; Writing review & editing: Supporting

L.D. Funding acquisition: Equal; Project administration: Equal; Resources: Equal; Supervision: Supporting; Writing review & editing: Supporting

W.S. Conceptualization: Lead; Funding acquisition: Lead; Project administration: Lead; Resources: Equal; Supervision: Lead; Validation: Equal; Writing original draft: Supporting; Writinq review & editing: Equal

E.4. References

[1] D. Naglav, M. R. Buchner, G. Bendt, F. Kraus, S. Schulz, *"Off the Beaten Track-A Hitchhiker's Guide to Beryllium Chemistry"*, *Angew. Chem. Int. Ed.* **2016**, *55*, 10562; *Angew. Chem.* **2016**, *128*, 10718.

[2] O. Reckeweg, C. Lind, A. Simon, F. J. DiSalvo, *"Rietveld Refinement of the Crystal Structure of α-Be_3N_2 and the Experimental Determination of Optical Band Gaps for Mg_3N_2, Ca_3N_2 and $CaMg_2N_2$"*, *Z. Naturforsch. B: J. Chem Sci.* **2003**, *58*, 159.

[3] M. v. Stackelberg, R. Paulus, *"Untersuchungen über die Kristallstruktur der Nitride und Phosphide zweiwertiger Metalle"*, *Z. Phys. Chem.* **1933**, *22B*, 305.

[4] P. Eckerlin, A. Rabenau, *"Die Struktur einer neuen Modifikation von Be_3N_2"*, *Z. Anorg. Allg. Chem.* **1960**, *304*, 218.

[5] A. Stock, B. Hoffmann, *"Die Einwirkung von Ammoniak auf Phosphorpentasulfid und der Phosphorstickstoff, P_3N_5"*, *Ber. Dtsch. Chem. Ges.* **1903**, *36*, 314.

[6] S. Horstmann, E. Irran, W. Schnick, *"Synthesis and Crystal Structure of Phosphorus(V) Nitride α-P_3N_5"*, *Angew. Chem. Int. Ed. Engl.* **1997**, *36*, 1873; *Angew. Chem.* **1997**, *109*, 1938.

[7] F. J. Pucher, S. R. Römer, F. W. Karau, W. Schnick, *"Phenakite-type BeP_2N_4 – a possible precursor for a new hard spinel-type material"*, *Chem. – Eur. J.* **2010**, *16*, 7208.

[8] D. Walker, *"Lubrication, gasketing, and precision in multianvil experiments"*, *Am. Mineral.* **1991**, *76*, 1092.

[9] H. Huppertz, *"Multianvil high-pressure / high-temperature synthesis in solid state chemistry"*, *Z. Kristallogr.* **2004**, *219*, 330.

[10] P. W. Bridgman, *"Two New Modifications of Phosphorus"*, *J. Am. Chem. Soc.* **1914**, *36*, 1344.

[11] H. P. Liermann, Z. Konôpková, W. Morgenroth, K. Glazyrin, J. Bednarčik, E. E. McBride, S. Petitgirard, J. T. Delitz, M. Wendt, Y. Bican, A. Ehnes, I. Schwark, A. Rothkirch, M. Tischer, J. Heuer, H. Schulte-Schrepping, T. Kracht, H. Franz, *"The Extreme Conditions Beamline P02.2 and the Extreme Conditions Science Infrastructure at PETRA III"*, *J. Synchrotron Radiat.* **2015**, *22*, 908.

[12] H.-K. Mao, J. Xu, P. M. Bell, *"Calibration of the ruby pressure gauge to 800 kbar under quasi-hydrostatic conditions"*, *J. Geophys. Res.* **1986**, *91*, 4673.

[13] A. Dewaele, M. Torrent, P. Loubeyre, M. Mezouar, *"Compression curves of transition metals in the Mbar range: Experiments and projector augmented-wave calculations"*, *Phys. Rev. B: Condens. Matter Mater. Phys.* **2008**, *78*, 854.

[14] Rigaku Oxford Diffraction, *"CrysAlisPro Software system, version 1.171.37.35"*, Oxford, UK, **2014**.

[15] C. Prescher, V. B. Prakapenka, *"DIOPTAS: A program for reduction of two-dimensional X-ray diffraction data and data exploration"*, *High Pressure Res.* **2015**, *35*, 223.

[16] G. M. Sheldrick, *"SHELXT - integrated space-group and crystal-structure determination"*, *Acta Crystallogr. Sect. A: Found. Adv.* **2015**, *71*, 3.

[17] G. M. Sheldrick, *"A short history of SHELX"*, *Acta Crystallogr. Sect. A: Found. Adv.* **2008**, *64*, 112.

[18] L. J. Farrugia, *"WinGX suite for small-molecule single-crystal crystallography"*, *J. Appl. Crystallogr.* **1999**, *32*, 837.

[19] K. Momma, F. Izumi, *"VESTA 3 for three-dimensional visualization of crystal, volumetric and morphology data"*, *J. Appl. Crystallogr.* **2011**, *44*, 1272.

[20] H. M. Rietveld, *"A profile refinement method for nuclear and magnetic structures"*, *J. Appl. Crystallogr.* **1969**, *2*, 65.

[21] A. A. Coelho, *"TOPAS-Academic Vers. 4.1"*, Brisbane, **2007**.

[22] R. W. Cheary, A. Coelho, *"A fundamental parameters approach to X-ray line-profile fitting"*, *J. Appl. Crystallogr.* **1992**, *25*, 109.

[23] R. W. Cheary, A. A. Coelho, J. P. Cline, *"Fundamental Parameters Line Profile Fitting in Laboratory Diffractometers"*, *J. Res. Natl. Inst. Stand. Technol.* **2004**, *109*, 1.

[24] F. D. Murnaghan, *"The compressibility of media under extreme pressures"*, *Proc. Natl. Acad. Sci. U.S.A.* **1944**, *30*, 244.

[25] F. Birch, *"Finite Elastic Strain of Cubic Crystals"*, *Phys. Rev.* **1947**, *71*, 809.

[26] J. Gonzalez-Platas, M. Alvaro, F. Nestola, R. Angel, *"EosFit7-GUI: A new graphical user interface for equation of state calculations, analyses and teaching"*, *J. Appl. Crystallogr.* **2016**, *49*, 1377.

[27] R. Hoppe, S. Voigt, H. Glaum, J. Kissel, H. P. Müller, K. Bernet, *"A new route to charge distributions in ionic solids"*, *J. Less-Common Met.* **1989**, *156*, 105.

[28] Y.-C. Ding, B. Xiao, *"Electronic Structure, Mechanical Properties and Intrinsic Hardness of a New Superhard Material BeP_2N_4"*, *Acta Phys.-Chim. Sin.* **2011**, *27*, 1621.

[29] M. Zhang, H. Yan, Y. Zhao, Q. Wei, *"Mechanical properties and atomistic deformation mechanism of spinel-type BeP_2N_4"*, *Comput. Mater. Sci.* **2014**, *83*, 457.

[30] W. Y. Ching, S. Aryal, P. Rulis, W. Schnick, *"Electronic structure and physical properties of the spinel-type phase of BeP_2N_4 from all-electron density functional calculations"*, *Phys. Rev. B* **2011**, *83*, 155109.

[31] K. Lejaeghere, V. van Speybroeck, G. van Oost, S. Cottenier, *"Error Estimates for Solid-State Density-Functional Theory Predictions: An Overview by Means of the Ground-State Elemental Crystals"*, *Crit. Rev. Solid State Mater. Sci.* **2014**, *39*, 1.

[32] M. T. Yeung, R. Mohammadi, R. B. Kaner, *"Ultraincompressible, Superhard Materials"*, *Annu. Rev. Mater. Res.* **2016**, *46*, 465.

[33] A. Zerr, R. Riedel, G. Miehe, G. Serghiou, M. Schwarz, E. Kroke, H. Fueß, P. Kroll, R. Boehler, *"Synthesis of cubic silicon nitride"*, *Nature* **1999**, *400*, 340.

[34] N. Nishiyama, R. Ishikawa, H. Ohfuji, H. Marquardt, A. Kurnosov, T. Taniguchi, B.-N. Kim, H. Yoshida, A. Masuno, J. Bednarcik, E. Kulik, Y. Ikuhara, F. Wakai, T. Irifune, *"Transparent polycrystalline cubic silicon nitride"*, *Sci. Rep.* **2017**, *7*, 44755.

[35] N. Nishiyama, J. Langer, T. Sakai, Y. Kojima, A. Holzheid, N. A. Gaida, E. Kulik, N. Hirao, S. I. Kawaguchi, T. Irifune, Y. Ohishi, *"Phase relations in silicon and germanium nitrides up to 98 GPa and 2400 °C"*, *J. Am. Ceram. Soc.* **2019**, *102*, 2195.

[36] A. Zerr, M. Kempf, M. Schwarz, E. Kroke, M. Göken, R. Riedel, *"Elastic Moduli and Hardness of Cubic Silicon Nitride"*, *J. Am. Ceram. Soc.* **2002**, *85*, 86.

[37] J. B. Mann, T. L. Meek, L. C. Allen, *"Configuration Energies of the Main Group Elements"*, *J. Am. Chem. Soc.* **2000**, *122*, 2780.

[38] T. D. Boyko, A. Moewes, *"The hardness of group 14 spinel nitrides revisited"*, *J. Ceram. Soc. Japan* **2016**, *124*, 1063.

[39] T. D. Boyko, E. Bailey, A. Moewes, P. F. McMillan, *"Class of tunable wide band gap semiconductors γ-$(Ge_xSi_{1-x})_3N_4$"*, *Phys. Rev. B: Condens. Matter Mater. Phys.* **2010**, *81*, 86.

F. Miscellaneous

F.1. List of Publications within this Thesis

The following enumeration lists all publications within this thesis in chronological order, including title, authors, citation, and author contributions.

1. **Stishovite's Relative: A Post-Coesite Form of Phosphorus Oxonitride**

   Sebastian Vogel, Dominik Baumann, Robin Niklaus, Elena Bykova, Maxim Bykov, Natalia Dubrovinskaia, Leonid Dubrovinsky, and Wolfgang Schnick

   Published in: *Angew. Chem. Int. Ed.* **2018**, *57*, 6691;
   Angew. Chem. **2018**, *130*, 6801.

   Access via: DOI: 10.1002/anie.201803610

   The syntheses and formal analyses were done by Sebastian Vogel and Dominik Baumann. DFT calculations were performed by Robin Niklaus. In situ experiments in diamond anvil cells and data processing were performed by Sebastian Vogel, Maxim Bykov, and Elena Bykova under the supervision of Leonid Dubrovinsky and Natalia Dubrovinskaia. Sebastian Vogel wrote the major part of the manuscript and Wolfgang Schnick, Natalia Dubrovinskaia, and Leonid Dubrovinsky supervised the project. All authors contributed to the discussion of the results and revised the manuscript.

2. United in Nitride: The Highly Condensed Boron Phosphorus Nitride BP_3N_6

Sebastian Vogel, Amalina T. Buda, and Wolfgang Schnick

Published in: *Angew. Chem. Int. Ed.* **2018**, *57*, 13202;
Angew. Chem. **2018**, *130*, 13386.
Access via: DOI: 10.1002/anie.201808111

Syntheses and formal analyses were performed by Sebastian Vogel and Amalina T. Buda over the course of her Bachelor thesis that was supervised by Sebastian Vogel and Wolfgang Schnick. Structural analysis and data evaluation was performed by Sebastian Vogel. Sebastian Vogel wrote the manuscript and Wolfgang Schnick supervised the project. All authors contributed to the discussion of the results and revised the manuscript.

3. Rivalry under Pressure: The Coexistence of Ambient-Pressure Motifs and Close-Packing in Silicon Phosphorus Nitride Imide SiP_2N_4NH

Sebastian Vogel, Amalina T. Buda, and Wolfgang Schnick

Published in: *Angew. Chem. Int. Ed.* **2019**, *58*, 3398;
Angew. Chem. **2019**, *131*, 3436.
Access via: DOI: 10.1002/anie.201813789

Synthesis and formal analyses were performed by Sebastian Vogel and Amalina T. Buda over the course of her Bachelor thesis that was supervised by Sebastian Vogel and Wolfgang Schnick. Sebastian Vogel evaluated the data and wrote the manuscript. The project was supervised by Wolfgang Schnick. All authors contributed to the discussion of the results and revised the manuscript.

4. Boron Phosphorus Nitride at Extremes: PN_6 Octahedra in the High-Pressure Polymorph β-BP_3N_6

Sebastian Vogel, Maxim Bykov, Elena Bykova, Sebastian Wendl, Simon D. Kloß, Anna Pakhomova, Stella Chariton, Egor Koemets, Natalia Dubrovinskaia, Leonid Dubrovinsky, and Wolfgang Schnick

Published in: *Angew. Chem. Int. Ed.* **2019**, *58*, 9060;
Angew. Chem. **2019**, *131*, 9158.
Access via: DOI: 10.1002/anie.201902845

Sebastian Vogel performed the precursor synthesis and conceptualized the project with Wolfgang Schnick. Prearrangements of the diamond anvil cells were done by Sebastian Vogel, Stella Chariton, and Egor Koemets. Sebastian Vogel, Maxim Bykov, Elena Bykova, Sebastian Wendl, Simon D. Kloß, and Anna Pakhomova performed synchrotron X-ray diffraction measurements and data processing was done by Sebastian Vogel, Maxim Bykov, and Elena Bykova. Sebastian Vogel wrote the manuscript and Wolfgang Schnick, Natalia Dubrovinskaia, and Leonid Dubrovinsky supervised the project. All authors contributed to the discussion of the results and revised the manuscript.

5. Nitride Spinel: An Ultraincompressible High-Pressure Form of BeP_2N_4

Sebastian Vogel, Maxim Bykov, Elena Bykova, Sebastian Wendl, Simon D. Kloß, Anna Pakhomova, Natalia Dubrovinskaia, Leonid Dubrovinsky, and Wolfgang Schnick

Published in: *Angew. Chem. Int. Ed.* **2019** (accepted);
Angew. Chem. **2019** (accepted).
Access via: DOI: 10.1002/anie.201910998

Precursor synthesis was done by Sebastian Vogel, who conceptualized the project together with Wolfgang Schnick. Elena Bykova, Anna Pakhomova and Sebastian Vogel performed the prearrangements of the diamond anvil cell. Synchrotron X-ray diffraction experiments were performed by Sebastian Vogel, Maxim Bykov, Elena Bykova, Sebastian Wendl, Simon D. Kloß, and Anna Pakhomova. Sebastian Vogel evaluated the data and wrote the manuscript. Wolfgang Schnick, Natalia Dubrovinskaia, and Leonid Dubrovinsky supervised the project. All authors contributed to the discussion of the results and revised the manuscript.

F.2. List of Publications beyond this Thesis

The following list contains the publications beyond this thesis in chronological order, including title, authors, citation, and author contributions.

1. **SrP_3N_5NH – A Framework-type Imidonitridophosphate Featuring Structure-Directing Hydrogen Bonds**

   Sebastian Vogel, and Wolfgang Schnick

   Published in: *Chem. Eur. J.* **2018**, *24*, 14275.
   Access via: DOI: 10.1002/chem.201803210

   Synthesis, characterization, and data processing as well as writing the manuscript was done by Sebastian Vogel. Wolfgang Schnick supervised the project. All authors contributed to the discussion of the results and revised the manuscript.

2. **High-pressure Synthesis of Ultraincompressible Hard Rhenium Nitride Pernitride $Re_2(N_2)(N)_2$ Stable at Ambient Conditions**

   Maxim Bykov, Stella Chariton, Hongzhan Fei, Timofey Fedotenko, Georgios Aprilis, Alena V. Ponomareva, Ferenc Tasnádi, Igor A. Abrikosov, Benoit Merle, Patrick Feldner, Sebastian Vogel, Wolfgang Schnick, Vitali B. Prakapenka, Eran Greenberg, Michael Hanfland, Anna Pakhomova, Hanns-Peter Liermann, Tomoo Katsura, Natalia Dubrovinskaia, and Leonid Dubrovinsky

   Published in: *Nat. Commun.* **2019**, *10*, 2994.
   Access via: DOI: 10.1038/s41467-019-10995-3

   Maxim Bykov, Leonid Dubrovinsky and Natalia Dubrovinskaia desinged the research project and Maxim Bykov, Leonid Dubrovinsky, Natalia Dubrovinskaia, and Igor A. Abrikosov wrote the manuscript. X-ray diffraction experiments were performed by Maxim Bykov, Leonid Dubrovinsky, Stella Chariton, Timofey Fedotenko, Georgios Aprilis, Vitali B. Prakapenka, Eran Greenberg, Michael Hanfland, Anna Pakhomova, and Hanns-Peter Liermann, and X-ray diffraction data was analyzed by Maxim Bykov. Alena V. Ponomareva, Ferenc Tasnádi, Igor A. Abrikosov performed the theoretical calculations.

Hongzhan Fei, Maxim Bykov, Tomoo Katsura, Sebastian Vogel, and Wolfgang Schnick performed synthesis in the large volume press and the synthesis of precursors. Nanoindentation measurements were done by Benoit Merle and Patrick Feldner. Leonid Dubrovinsky performed the electrical resistance measurements. All authors contributed to the discussion of the results and revised the manuscript.

F.3. Fundings

The research presented within this thesis and related work was funded by the Deutsche Forschungsgemeinschaft (DFG; SCHN 377/18-1, Projekt Nitridische Phosphat-Netzwerke), the Verband der Chemischen Industrie e.V. (VCI; PhD fellowship for Sebastian Vogel), the Deutsches Elektronen Synchrotron (DESY; I-20180016), the European Synchrotron Radiation Facility (ESRF; CH-5609), and the Ludwig-Maximilians-Universität München (LMU). Travel awards by the Gesellschaft Deutscher Chemiker e.V. and the International Union of Crystallography are gratefully appreciated.

F.4. Conference Contributions and Presentations

Nitrides for Future

Sebastian Vogel, Wolfgang Schnick

Talk, Tage der AC, **2019**, Munich, Germany

Accessing Mixed Non-Metal Nitrides via an Innovative High-Pressure High-Temperature Reaction

Sebastian Vogel, Wolfgang Schnick

Talk, 10th International Symposium on Nitrides, **2019**, Barcelona, Spain

Arbeiten unter Hochdruck – Ein Einblick in die moderne Hochdruckchemie

Sebastian Vogel

Talk, Ehemalige berichten, **2019**, Michelstadt, Germany

Von Diamanten und Legenden

Sebastian Vogel, Wolfgang Schnick

Talk, Seminar Schnick Group, **2019**, Munich, Germany

BP_3N_6 – ein innovativer Zugang zu gemischten Nichtmetallnitriden

Sebastian Vogel, Amalina T. Buda, Wolfgang Schnick

Poster, 19. Vortragstagung für Anorganische Chemie der Fachgruppen Wöhler-Vereinigung und Festkörperchemie und Materialforschung, **2018**, Regensburg, Germany

Phosphorus on the Brink of Sixfold Coordination in Nitride Compounds

Sebastian Vogel, Wolfgang Schnick

Talk, Workshop of the IUCr Commission on High Pressure, **2018**, Honolulu, Hawai'i, USA

Under Pressure

Sebastian Vogel, Wolfgang Schnick

Talk, FCI Stipendiatentreffen, **2018**, Munich, Germany

Ein Hauch von Nichts

Sebastian Vogel, Wolfgang Schnick

Talk, 3. Obergurgl-Seminar Festkörperchemie, **2018**, Obergurgl, Austria

Under Pressure

Sebastian Vogel, Wolfgang Schnick

Talk, Seminar Schnick Group, **2017**, Munich, Germany

Post-Coesit-Modifikation von PON

Sebastian Vogel, Wolfgang Schnick

Talk, 43. Hirschegg-Seminar Festkörperchemie, **2017**, Hirschegg, Austria

Hochdruck-Hochtemperatur-Synthese und Charakterisierung neuartiger Imidonitridophosphate

Sebastian Vogel, Wolfgang Schnick

Talk, Seminar Schnick Group, **2017**, Munich, Germany

Nitrogen Rich Covalent Organic Frameworks for Photocatalytic Hydrogen Evolution

Sebastian Vogel, Vijay Vyas, Frederik Haase, Bettina Lotsch

Poster, Undergraduate Research Conference on Molecular Sciences (URCUP), **2014**, Wildbad Kreuth, Germany

F.5. Deposited Crystal Structures

The Crystallographic Information Files (CIFs) of the compounds that are discussed within this thesis are cataloged at the Fachinformationszentrum (FIZ) Karlsruhe, Germany and/or the Cambridge Crystallographic Data Centre (CDCC), Cambridge, United Kingdom. These data can be downloaded free of charge quoting the respective depository number.

Table F.1.: List of the compounds that are discussed within this thesis with corresponding depository numbers.

Compound	Pressure / GPa	CSD	Compound	Pressure / GPa	CSD
pc-PON	0.00010(1)	433717	phe-BeP_2N_4	0.00010(1)	1946333
pc-PON	1.8(1)	434035			
			sp-BeP_2N_4	0.00010(1)	1946345
SiP_2N_4NH	0.00010(1)	1880683	sp-BeP_2N_4	1.8(1)	1946332
			sp-BeP_2N_4	3.3(1)	1946348
α-BP_3N_6	0.00010(1)	434784	sp-BeP_2N_4	5.0(1)	1946341
α-BP_3N_6	2.9(1)	1898720	sp-BeP_2N_4	7.4(1)	1946349
α-BP_3N_6	10.5(1)	1898716	sp-BeP_2N_4	11.9(2)	1946346
α-BP_3N_6	11.3(1)	1898723	sp-BeP_2N_4	13.2(3)	1946334
α-BP_3N_6	14.3(1)	1898724	sp-BeP_2N_4	17.8(4)	1946335
α-BP_3N_6	26.1(1)	1898717	sp-BeP_2N_4	21.8(4)	1946336
α-BP_3N_6	32.9(1)	1898721	sp-BeP_2N_4	28.5(6)	1946337
α-BP_3N_6	42.4(1)	1898718	sp-BeP_2N_4	31.0(6)	1946338
			sp-BeP_2N_4	34.0(7)	1946339
β-BP_3N_6	0.00010(1)	1898719	sp-BeP_2N_4	37.7(8)	1946340
β-BP_3N_6	42.4(1)	1898722	sp-BeP_2N_4	38.5(8)	1946342
			sp-BeP_2N_4	40.9(8)	1946343
			sp-BeP_2N_4	44.6(9)	1946344